UNIVERSITY OF ASTON IN BIRMINGHAM

THE WEAR OF ALUMINIUM BRONZE ON STEEL IN AVIATION KEROSENE

Thesis submitted for the degree

of

Doctor of Philosophy

by

William Poole, B.Sc., M.Sc.

Supervisor: J.L.Sullivan

Physics Department March 1979

SUMMARY

THE WEAR OF ALUMINIUM BRONZE ON STEEL IN AVIATION KEROSENE

by WILLIAM POOLE

Submitted for the Degree of Doctor of Philosophy - 1979

The ability of lubricants of the same viscosity to provide adequate lubrication for surfaces in relative motion (lubricity), can widely vary. Under boundary lubrication conditions fluid films of poor lubricity, can break down giving rise to contact. Contact results in wear, which under severe conditions, can damage the moving components beyond repair. The special case of an aircraft, axial-piston, fuel pump has been studied for this project.

The pump consists of steel pistons running in cadmium plated aluminium bronze bores lubricated by aviation kerosene of variable lubricity. Seizure occurs in the pump if the fuel lubricity is poor but protection is afforded by the inclusion of an additive in the fuel. The latter is not universally accepted by the operating companies so the project not only aims to determine the mechanism of failure of the pump but also the mechanism of protection by the additive.

Boundary lubricated wear was simulated using a flat-faced pin-on-disk machine and friction and wear rate measured for bronze sliding against steel for various fuels. Wear rates of between 10^{-9} and 10^{-6} mm^3 mm^{-1} were found and, although the additive has an initial pro-wear effect, very low wear could be obtained when the additive was present.

The wear pins and disks, samples from a pump simulation rig (the Lucas two-piston rig) and from 'in service' pumps were analysed. The physical analytical techniques used, in this part of the work, included scanning and transmission electron microscopy, X-ray powder diffraction, electron probe microanalysis and Auger spectroscopy. This analysis has shown that the aluminium content, of the bronze, plays an important role, in the seizure mechanism, by diffusion to the steel surface. The additive prevents seizure by preferential corrosion of aluminium from the bronze, thus preventing its transfer to the steel. Similarities between laboratory, intermediate test rig and 'in service' experience have been found by using this analytical approach.

Finally a new theory has been instigated to predict wear rates under conditions of boundary lubrication where oxidation is occurring.

/Lubrication/Wear/Lubricity/Bronze/Physical techniques/

ACKNOWLEDGMENTS

The Author would like to thank Professor S.E. Hunt, Head of the Department of Physics and Dr. T.F.J. Quinn, Reader in Tribology, in whose laboratories the majority of work was carried out.

Advice, guidance and encouragement has been given to me by my Supervisors, namely, Mr. J.L. Sullivan (Physics Department, Aston University) and Mr. K.P. Palmer (Lucas Aerospace, Birmingham). I am very grateful for all the valuable time, and for the efforts, they have made to assist me during the course of the project.

Thanks are also due to Professor Smallman, Dr. H.N. Southworth, Dr. J.F. Smith and Mr. D.D. Hall with whose permission and assistance the Auger spectrometer, at the University of Birmingham, was used for part of the analysis carried out in this work.

I am grateful to the technicians of the Physics and Metallurgy Departments at Aston for their help with various aspects of the project and also to Mr. Lane and his colleagues in the Physics Department Workshops. Special thanks to Mr. R. Howell and Mr. S. Fuggle (Metallurgy) for their instructions in the use of the electron probe and scanning electron microscope.

Mr. C.J.S. Chapman is acknowledged for his advice and help with the electronics and the colour photography.

Financial assistance for the project was provided by the Science Research Council and by the University of Aston in Birmingham. The latter and Lucas Aerospace also provided travelling expenses, in particular for a Conference in Kansas City, Missouri, for which I am very grateful.

Finally, but certainly by no means least, I am indebted to Mrs. B. Fitch who has typed the manuscript into a very acceptable form.

TO MY MOTHER AND FATHER

CONTENTS

CHAPTER 1

INTRODUCTION

Lubrication is a means of reducing friction and wear in the moving components of machinery. It is not always the case that these moving components can be lubricated by a lubricant specifically designed for that purpose. In these situations the lubrication afforded by the fluid is of secondary importance.

A variety of lubricants have been used in bearings other than oil. Molasses have been used in sugar mill bearings, liquid sodium in nuclear reactor pumps and water for bearings in electric power generators. Avoiding contamination of the product being manufactured, environmental conditions and reduction in firerisk are factors which have determined the use of these fluids as lubricants.

Problems arise from using the process fluid as the lubricant. For example, the liquid sodium used in reactor pumps is highly corrosive. Another example is the pumping of low viscosity aviation fuels to jet engines which can result in failure of the pump due to the poor lubricating properties of some fuels. The latter problem is the subject studied for this dissertation.

1.1 The Lucas Axial Piston Pump

A description of the design and running conditions of a Lucas Aerospace aircraft fuel pump will serve to illustrate the different types of lubrication regimes which can exist between surfaces in relative motion and problems that can arise from the composition of the lubricant.

The main features of an axial piston pump are shown in the diagrammatic section on plate I (courtesy of Lucas Aerospace). The

PLATE I - LUCAS AXIAL PISTON PUMP

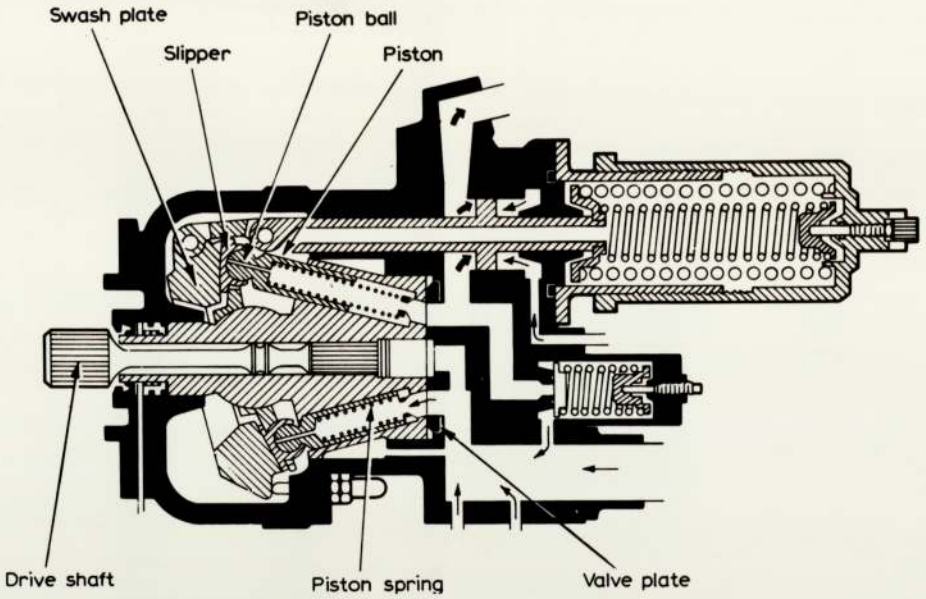

Diagrammatic view of piston pump.

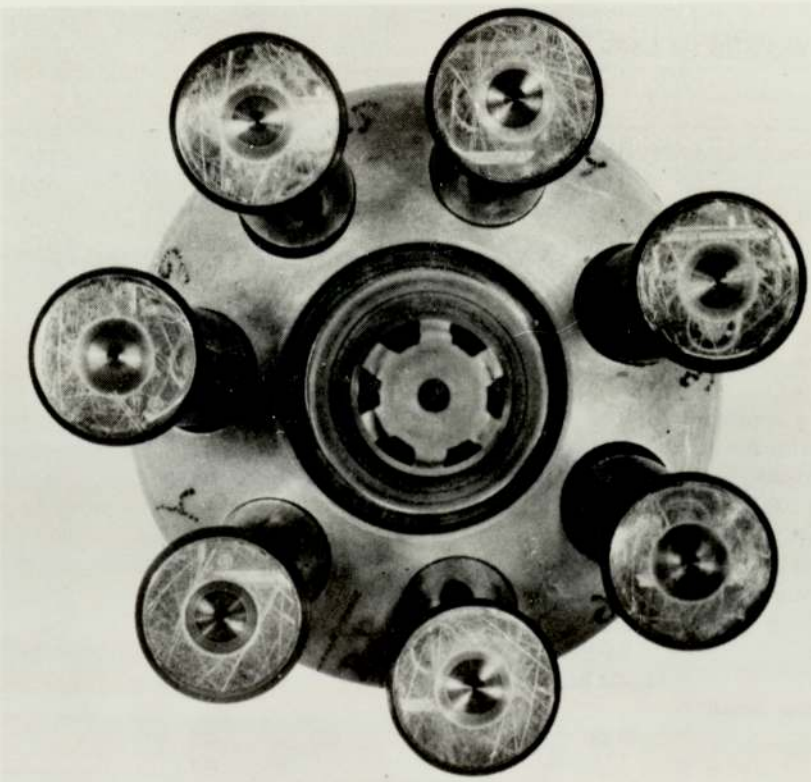

Pump rotor following a failure typical of those due to poor lubricity fuel.

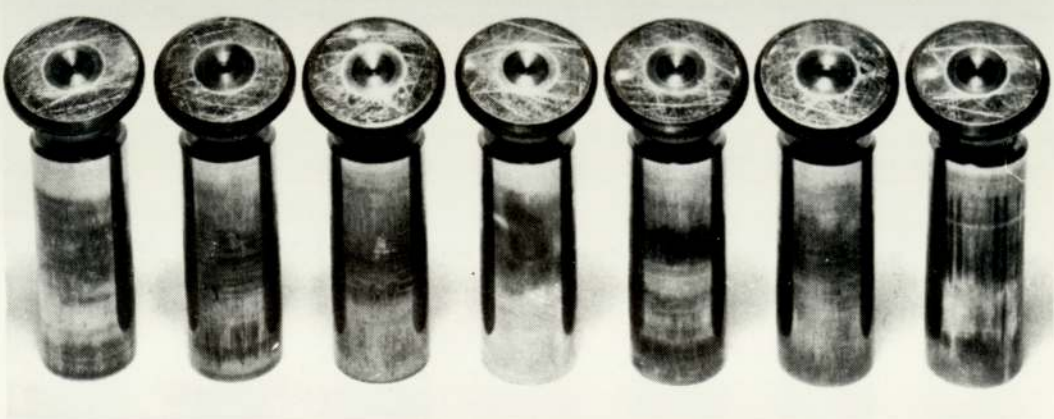

Pistons showing damage typical of a poor lubricity failure.

pump has a swashplate, the angle of which can be adjusted, to vary the stroke of the pistons. Pistons are manufactured from KE961 steel which is a high carbon (1.45-1.65%), 13% chromium steel. The piston slippers push against the swashplate and are lubricated by fuel oil. As the rotor is rotated the pistons are successively driven down into the cadmium plated aluminium bronze bores. The bronze (DTD 197A aluminium bronze) consists of 10% aluminium, 5% nickel, 5% iron with the remainder copper. On the return stroke the pistons are forced back against the swashplate by a spring and the pressure of the incoming fuel. The surfaces between the pistons and bores are obviously in relative motion and, during this motion, they are lubricated by the fuel which is being pumped. Simple harmonic motion is performed by the pistons relative to the bores while the pump is running. The pistons reach a maximum velocity when half way through the stroke and will be instantaneously at zero velocity at each end of the stroke. This range of speeds can produce various lubrication conditions between the pistons and bores.

1.2 Lubrication Regimes

1.2.1 Fluid Film Conditions

This condition is produced when the sliding velocity is relatively high and the load relatively light. In the case of the fuel pump it might be expected to prevail when the piston is at its maximum velocity (figure 1.1a) which is at mid stroke. The precise conditions under which fluid film conditions occur will also depend on temperature and pressure, because of the dependence of viscosity on these parameters, on the geometry of the sliding system (a wedge shape being necessary for the production of a hydrodynamic film) and on surface topography. The film thickness normally exceeds 10^{-6} M and is many times thicker than the surface roughness.

1.2.2 Elastohydrodynamic Conditions

These conditions arise because of high pressures when the surfaces may deform (figure 1.1b) in order to maintain a complete fluid film between the surfaces. The lubricant viscosity rises considerably in the high contact pressures and further assists the formation of effective fluid films. Film thickness is between 10^{-7}M and 10^{-6} M in this case.

1.2.3 Mixed Lubrication

Mixed lubrication arises when the film thickness is between 5×10^{-8} and 10^{-6} M. Fluid film and elastohydrodynamics represent situations where the surface are kept apart by the lubricant and so no wear can occur from contact. In the mixed lubrication regime (figure 1.1c) intermittent contact can occur between the surfaces resulting in wear. In this case some fluid film is always maintained between the surfaces and this will arise, for example, as the piston slows towards the end of the stroke. Film thickness is about 5×10^{-8} to 10^{-6} M for the mixed lubrication regime.

1.2.4 Boundary Lubrication

This type of lubrication occurs under conditions of low speed and high loads. If, in the pump, high side loads are experienced at the end of the stroke, where the speed is low, then boundary lubrication conditions will occur. Good boundary lubrication arises when metal-to-metal contact is prevented by the adsorption of polar molecules onto the surfaces (figure 1.1d). The effectiveness of a boundary lubricant is dependent on the manner in which the molecules are attached to the metal surface. This can occur in three ways namely i) physical adsorption in which a weak electrostatic interaction occurs between the electrons of the adsorbing molecule

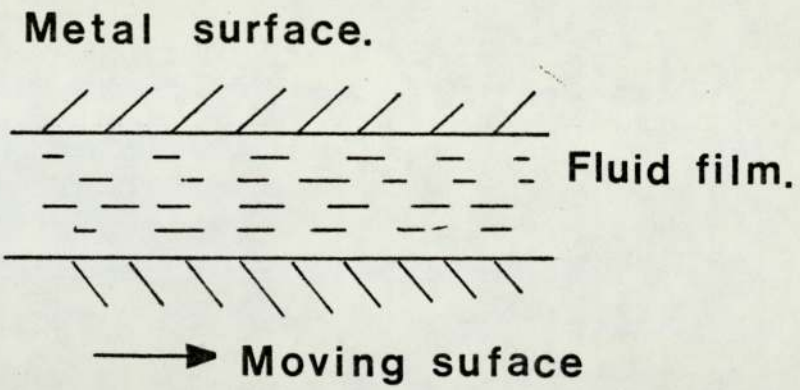

a) Fluid film lubrication.

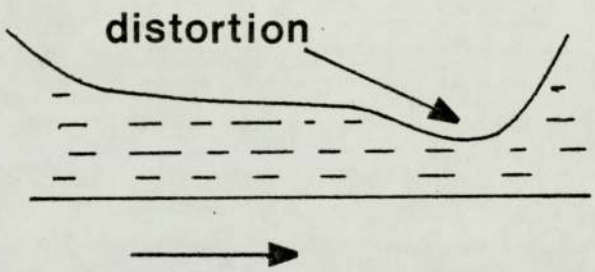

b) Elastohydrodynamic.

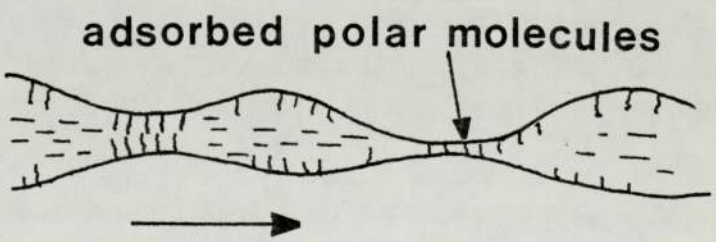

c) Mixed lubrication.

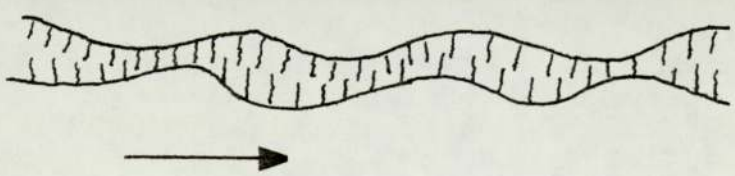

d) Boundary lubrication.

Figure 1.1, Lubrication Regimes.

and the metal nucleus, ii) chemical adsorption in which the outer shell electrons of the metal and adsorbing atoms interact, and iii) chemical reaction occurs above some reaction temperature and involves elements such as sulphur, chlorine, phosphorus and zinc. The latter elements are often compounded into mixtures which are called extreme pressure additives. The surface films formed by these elements are of the order of 5×10^{-9} to 10^{-8} M thick.

Variation of coefficient of friction with a dimensionless parameter, which is a function of load, speed and lubricant viscosity, is shown in figure 1.2. The various lubrication regimes can be identified with different parts of this Stribeck curve as shown in the diagram and given by Dowson (1).

1.3 Lubricity

The term lubricity applied to fluids has been used throughout the thesis, this has been defined by Dukek and Vere (2) in the following way. "If two liquids, A and B, have the same viscosity but under the same operating conditions A gives less friction or wear than B, then A is said to have better lubricity".

The questions now arise as to what components of an aviation fuel impart good lubricity characteristics and how fuels of poor lubricity are produced. Good lubricity was thought, by Appeldoorn and Dukek (3), to be imparted by high molecular weight aromatics in the case of steel-on-steel test equipment. Vere (4) suggests that the fully saturated hetrocylic sulphur compounds impart good lubricity properties and that they are more active than the heavy aromatics.

Modern jet engines require fuel of high thermal stability, to quote Johnson and Shamblin (5), "thermal instability of present day jet fuels is primarily a problem in gum and sediment formation. Gums and sediment arise from hot compounds of sulphur being

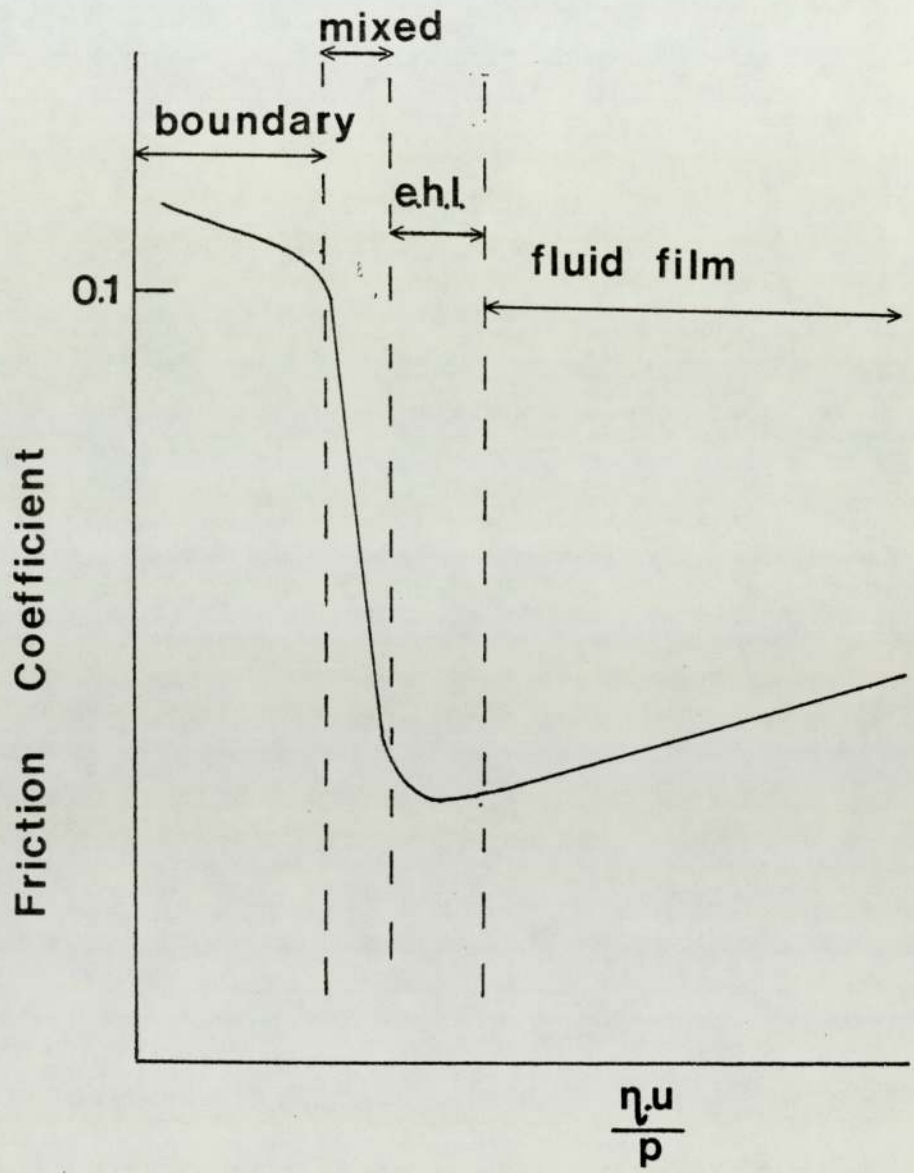

Figure 1.2 Typical Stribeck Curve.
(Ref. 1)

deposited and this causes problems with orifices and narrow tubes." Stability is obtained during refining and consequently new methods were introduced so that the fuel specifications could be achieved. Originally fuels were produced by acid treating and by copper sweetening, the former uses sulphuric acid, and the latter oxygen and copper chloride, to reduce sulphur content. Hydrotreating was introduced to produce the high thermally stable fuels required by modern aircraft. This process leads to the production of what are commonly called hydrofined fuels. Another process currently being used to produce stable fuels involves oxidation of mercaptans (sulphur compounds) and is called the "Merox" process but the hydrotreating method is more efficient and economical. All these processes are more fully described in the petroleum processing handbook (6).

Hydrotreatment resulted in many of the good lubricity components of fuels being removed during refining, in particular the mercaptan and aromatic content was reduced (3). Since most of the compounds removed are polar in nature there will be little remaining in the fuel to protect the surfaces when operating under boundary lubricating conditions. These compounds are removed so that only very low concentrations remain but the addition of quantities up to about 15 parts per million (p.p.m.) by volume of polar compounds have been found sufficient to restore lubricity to fuels (4). The addition of the corrosion inhibitor Hitec E515 (Edwin Cooper Ltd.) was found to be of particular benefit (4).

At this stage it will be advantageous to describe a little of the aviation fuel specification terminology. Figure 1.3 shows the various types of aviation fuels as given by the Royal Aeronautic Society and Institute of Petroleum (7). The fuel types, AVCAT, AVTUR, AVTAG and AVGAS (with the American equivalents JP5, JETA,

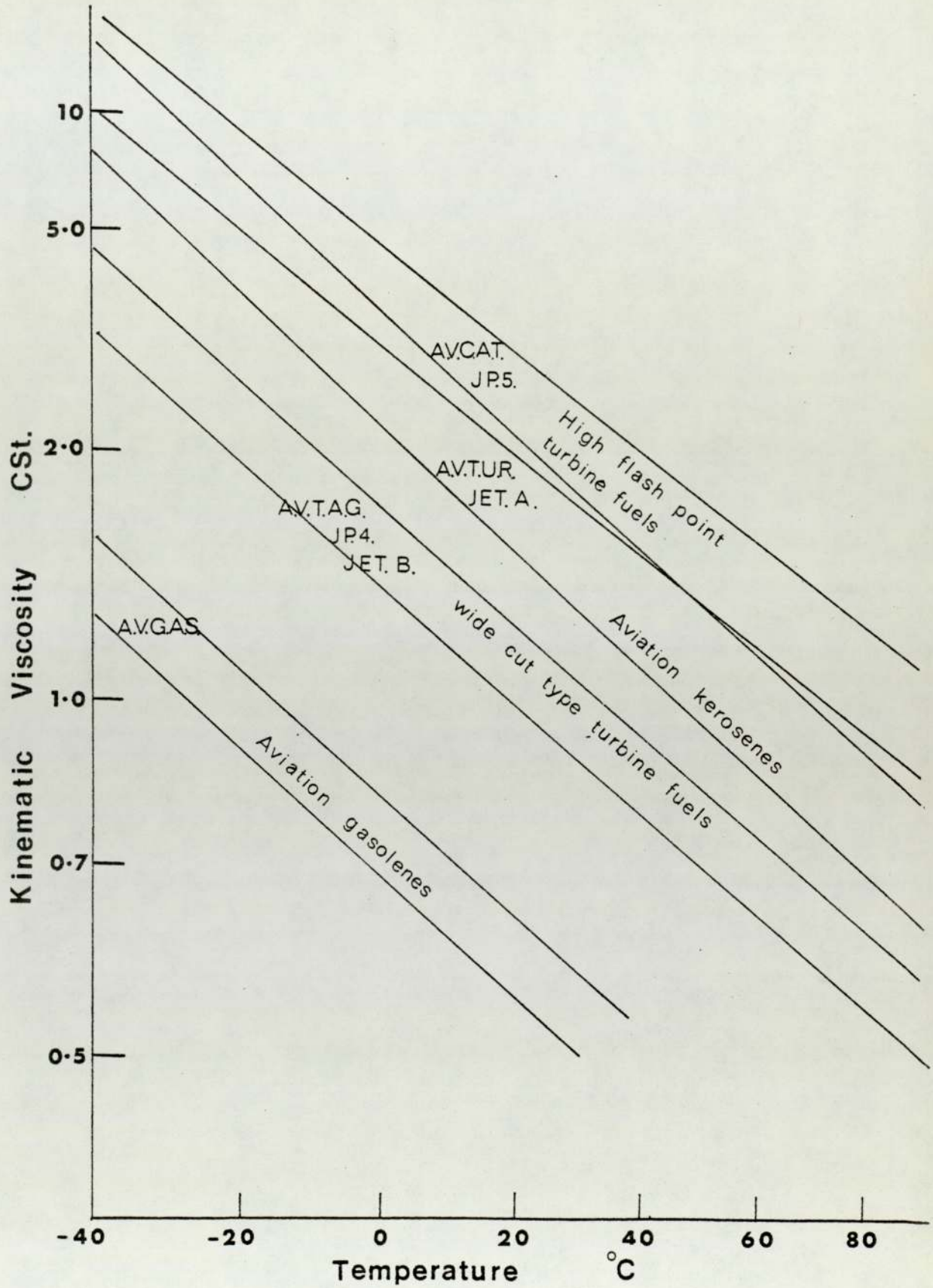

Figure 1.3. (Ref.7).

JP4 and JET B) are the joint service designations for the particular fuel specifications (8) as given by the procurement executive of the Ministry of Defence.

1.4 The Lubricity Problem

The problem of poor lubricity was first experienced in 1965 when test pump failures were experienced (9). Effects of poor lubricity were not confined to piston pumps or the particular, cadmium plated, aluminium bronze - steel metallurgy of that pump. Sticking of fuel system control valves was in fact the first recorded field problem and that involved a steel-on-steel metallurgy (10).

Aird and Forgham (9) describe the first fuel pump failure which occurred in 1966 and then deal with a number of incidents which took place in the period from 1966 to 1969 inclusive. In most cases the failures involved hydrofined AVTAG and AVTUR fuels apart from one occasion in 1969 when an acid treated fuel was involved. The failures which occurred during 1968 involved some pumps with a silver plated bronze-steel metallurgy but in general failures over the period were cadmium plated bronze-steel systems.

A later report (11) states that three pump failures occurred during 1972 and that this had risen to eleven during the first quarter of 1973, all of which occurred on commercial aircraft. Finally Vere et al (10) report that the original problem of control valve sticking re-occurred in 1974.

Typical lubricity failures of piston pumps are shown in Plates I and II (courtesy of Lucas Aerospace). These pumps are of the cadmium plated bronze-steel metallurgy. A number of steps were taken to alleviate the problem, but there has been no general acceptance, by the operating companies, of any particular solution. Some operators opted for a change in metallurgy from camium plated bronze to carbon lined steel rotors. Conversion of all pumps to this

PLATE II - AXIAL PUMP LUBRICITY FAILURE

TOP: PISTON

BOTTOM: ROTOR

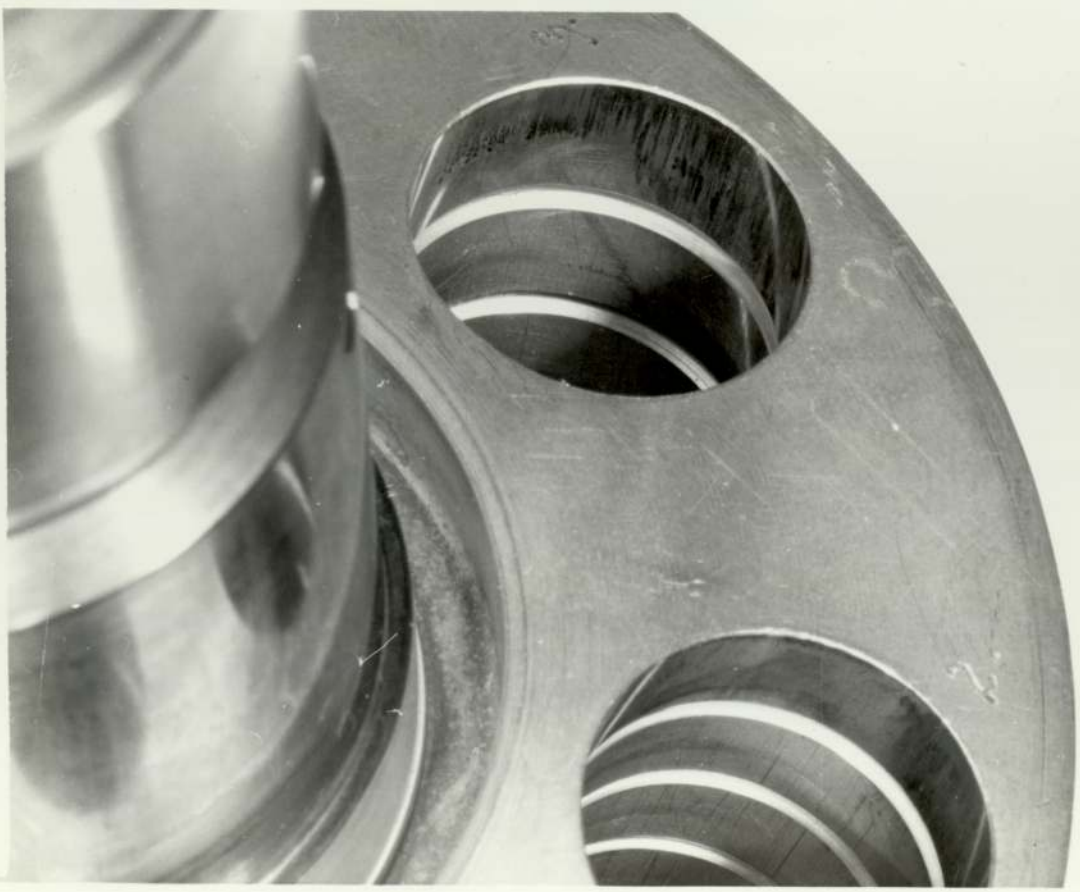

ABOVE: A PISTON AFTER 1ST. 50 HOUR ENDURANCE (60333)
BELOW: No. 3 BORE AFTER 1ST. 50 HOUR ENDURANCE (60334)

metallurgy, however takes time considering the number of pumps in service. An alternative was found in the use of the corrosion inhibitor Hitec E515 (formerly Santolene C) to improve the lubricity of fuels (12). The additive is used in fuel at the rate of 12 p.p.m. (10) and consists basically of dilinoleic acid (a polar compound) and an ester of orthophosphoric acid (13). Although approved for use, Hitec E515 is not mandatory for use in fuels used by civil aircraft operators. Some operators have been concerned about the possible deleterious side effects. The phosphorus component may induce a high temperature corrosion phenomenon on engine turbine blades. The additive may also effect electrical conductivity, water separating characteristics and thermal stability of fuels (14). Finally some of the fuel manufacturers have introduced a new refining process called the "Merox" process in which mercaptans are removed or converted to the disulphide state (6). Vos (14) expects the development of a hydrogen cracking process to be used to revalidate heavier fractions of the crude oil distillation and that this will produce fuels of very poor lubricity. Consequently although the "Merox" process has been introduced hydrotreating plants are still in operation and so fuels of poor lubricity are still being produced by the oil companies. Published data suggests that changing the refining process may in fact not be a solution to the lubricity problem (9, 15).

1.5 Research, and Monitoring of, Fuel Lubricity

The main aims of the companies associated with the production and use of aviation fuels has been to rank fuels according to their lubricating ability, to detect Hitec E 515 in fuels and to determine chemical compounds which impart good lubricity properties to the fuel.

1.5.1 The Lucas Dwell test

Most workers interested in fuel lubricity have, at one time or another, used the dwell test to try and rank fuels (10, 16). The method measures friction between a flat-faced aluminium bronze pin rubbing against a steel disk. The dwell number is the number of revolutions of the disk required for the coefficient of friction to attain a value of 0.4 when a fixed amount of the test fuel is evenly distributed over the disk to a thickness of 0.166 μm. A high dwell number indicates a fuel with good lubricity properties and a low dwell number a poor lubricity fuel.

Between the testing of each fuel sample a stringent cleaning of the disk is carried out and the cleanliness of the disk is checked by use of a reference fuel (generally Shell sol.T). If the disk does not meet the required clealiness (indicated by a dwell number less than 50 for the reference fuel) then relapping is carried out using diamond paste.

Aird and Forgham (9) claimed that the dwell test was suitable for inclusion in a fuel specification but Bishop and Howells (17) object to this on the grounds of poor repeatability. In reply Aird and Forgham (18) say that the results fall to within $\pm$ 50% of the mean which is acceptable for differentiating between fuels of good and bad lubricity since the dwell numbers lie in the range 50 to 1000.

A large number of factors have been attributed by various workers (10) to the variations found with dwell number. These include final boiling point of the fuel and naphthalene, alkalene and high molecular weight compound content of the fuels. Humidity, polishing and cleaning techniques also have been found to influence the results.

The numerical value of the dwell number has been found to be

independent of load and contact area but dependent on the test procedure and on the origin and history of the test rig.

Generally the test has been observed to give a poor response to the additive Hitec E515 and in some cases could only be detected relative to the base fuel (a sample of which is not always available for this type of testing).

1.5.2 Ball-on-cylinder tests

In 1967 Appeldoorn and Dukek (3) carried out tests using a ball-on-cylinder machine in which they measured friction, wear and metallic contact. The system used was steel on steel with a roughness of 0.254 to 0.3 μM (10-12 μ inches) c.l.a. compared to 0.0254 μM c.l.a. of the steel pistons in the pump considered in this work. Viscosity, volatility and hydrocarbon type along with trace components of organic acids, sulphur and nitrogen compounds were investigated to determine their effect on lubricity. They found that lubricity was dependent on polar compounds and this was substantiated by work with additives. Emphasis was placed on the role of aromatics in improving lubricity. The claim that aromatics improved lubricity was questioned by Johnston (19). He cites work by Kirchkin et al (20) in which it was shown that anti-oxidant and metal deactivating additives may be important. Further he suggests that sulphur and nitrogen compounds are important.

The benefits of using a ball-on-cylinder machine for evaluating jet fuel lubricity was shown by Tao and Appeldoorn in 1968 (21). Their tests were claimed to detect as little as 5 p.p.m. of additive and effects due to atmosphere. The exclusion of oxygen and water greatly reduced wear and scuffing. The ability to work at high temperatures with small fuel samples and a good correlation between the wear measurements and field experience were

aspects claimed to favour the use of this type of machine. The ball and disk are submerged in a bath of the fluid under test so that only a small sample of fuel is required for the test. Shayeson (22) points out that debris in the fuel may affect the results obtained from the tests.

Results from a more detailed investigation, into the role of aromatics and atmospheric conditions, have been given by Appeldoorn and Tao in 1968 (23). This work shows that paraffins exhibit low wear in dry inert atmospheres with high wear in wet oxygenated conditions. Aromatics scuff easily in dry inert atmospheres but improve with additions of oxygen and water. The best lubricity characteristics were shown to occur with a mixture of 30% aromatics (1 - methyl naphthalene) in 70% paraffin (white oil). Essentially the aromatics have a synergistic effect with the paraffins but have poor lubricity characteristics when tested alone. This behaviour of aromatics could not be explained and it was concluded that the metal surfaces nor the atmosphere was directly involved. As pointed out by Podolsky (24) this last statement conflicts with the data produced. He also disagrees with another of their conclusions, that "the heavy aromatics are the most probable lubricity agents", on the grounds that extreme pressure properties of the oils and the structural-group fraction (naphthene-paraffin and aromatic) separated from them, is very similar. In reply to these criticisms (25), Appeldoorn and Tao cite their earlier work (3) and restate their finding of improved lubricity with aromatic content.

Further work has been carried out in 1970 by Suresh et al (26) using a ball-on-cylinder device. Steel disks were used with a surface finish of 0.2 to 0.254 μM c.l.a. (8-10 μ inches) with what appears to be a "once through" fuel supply system. They concluded

that the anti wear properties of fuels was not directly related to viscosity, volatility or aromatic content which is in contradiction with the work of Appeldoorn et al (3, 21, 23, 25). Work at Shell Research (10) did "not disagree" with that of Suresh et al (26). Nandy et al (27) showed the difference in lubricity between fuels produced from different crude oils. A crude, heavy in sulphur and sulphur compounds was found to produce a very poor lubricity fuel, presumably from excessive hydrotreatment (the process used on these crudes). The addition of stearic or oleic acids, recognised boundary lubricants (28), and Hitec E515 were all found to improve lubricity.

In 1974 Anitotri et al (29) used a ball-on-cylinder machine to show that dilution of poor lubricity hydrotreated fuels with conventionally refined fuels is not sufficient to restore lubricity. This result is in direct contradiction to Vere (30) who found that the addition of ten percent of chemically treated fuel to hydrofined fuel restored lubricity to a satisfactory level. "In service" experience would tend to support this view.

Several lubricity improving corrosion inhibitors were tested by workers at the Air Force Wright Aeronautical Laboratories in the United States. All the additives were found to be effective in JP-4 and JP-5 fuels. No correlation could be found for the effectiveness of the additives at 24°C with the effectiveness at 65°C. It was suggested that Hitec E515 may function as an extreme pressure additive at high temperatures. Finally they conclude that "although the relative lubricity of fuels can be examined with the ball-on-cylinder, the relationship between wear scar diameter and fuel lubricity has not been firmly established". This was substantiated by the use of statistical analysis.

1.5.3 Pin-on-disk and Pin-on-cylinder Tests

Vere (4, 10, 30, 31) used a omforming pin-on-steel cylinder machine to investigate lubricity. The pins were phosphor bronze plated with either silver or cadmium apparently to simulate fuel pump metallurgy although the pump is in fact cadmium plated aluminium bronze. Problems were found with plating in that it tended to peel off the pin rather than wear in the expected manner. This was particularly true with the cadmium plating. The work showed the increase in wear due to hydrotreatment and Vere's graph comparing fuels is reproduced here in figure (1.4). Additive influence on lubricity was also investigated and metal deactivators and anti oxidants appeared to have no effect on lubricity in contradiction to Kirchkin et al (20). Improvements in lubricity were observed when a corrosion inhibitor was used at the 2000 p.p.m. level. This concentration was calculated to give a monolayer coverage of the apparatus and tubing.

An attempt to isolate and identify lubricity agents, with the aid of thin layer chromatography and mass spectrometry, was made so that the problem could be understood. Polynuclear aromatics and fully saturated sulphur compounds (e.g. thiahydrindane and thiadecalin) were extracted and identified. The latter seemed to be the more active lubricity agents and thiahydrindane was synthesised so that it could be added to a severely hydrotreated fuel (4). A significant increase in lubricity was found with the addition of 150 p.p.m. to the fuel.

Work carried out in industry (10) produced a test which could differentiate between fuels of different lubricity. Aluminium bronze was worn against steel and the wear scar measured every twelve minutes for a load of 0.1 kg.

Sulphur compounds of the type found in jet fuels were shown to

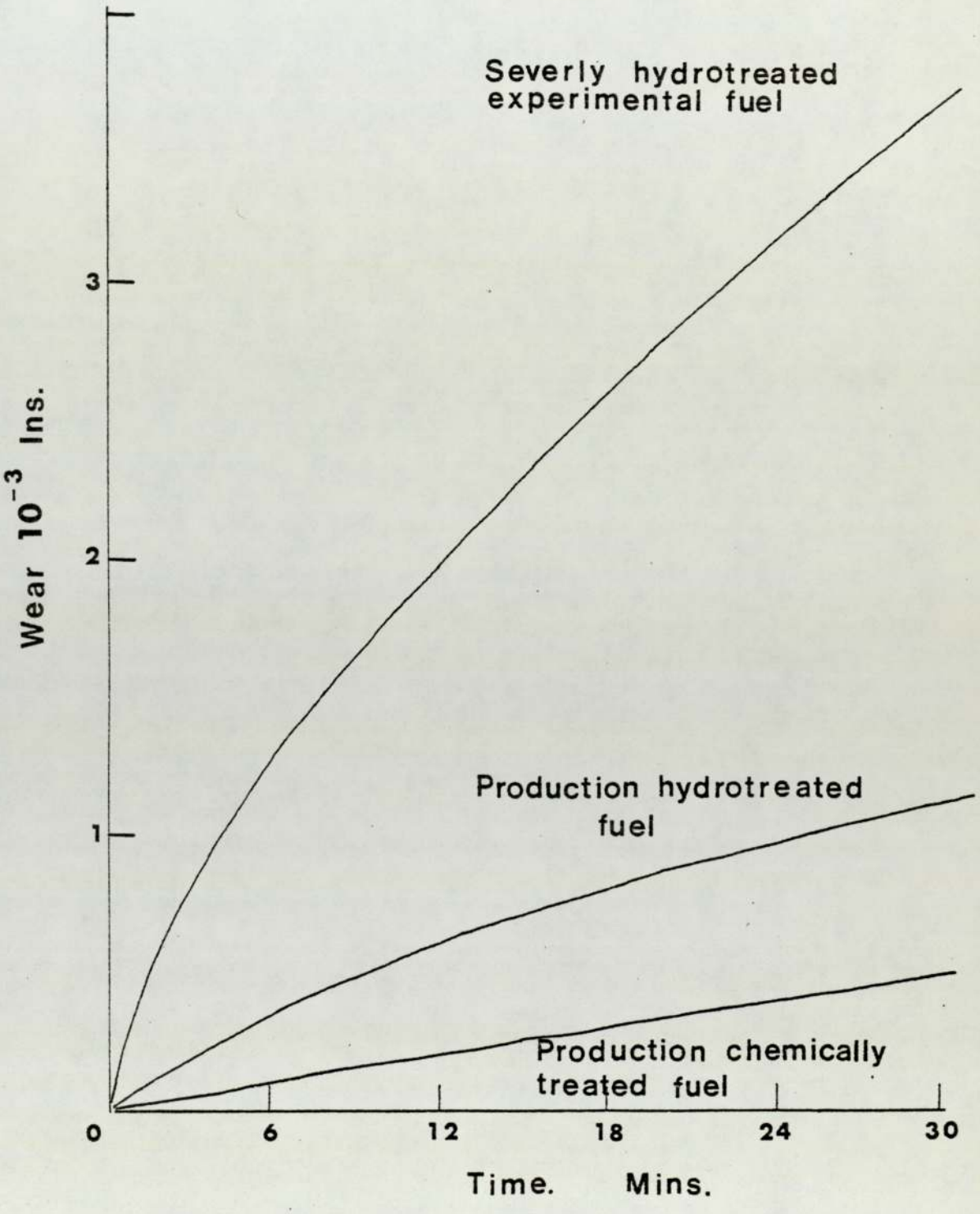

Figure 1.4. Comparison of wear between fuels.
Ref. 10.

be pro-wear with a good extreme pressure action. Polynuclear aromatics, aromatic nitrogen compounds and oxygen compounds, especially carboxylic acids improve lubricity.

An oil company (10) found that Hitec E515 was pro-wear with some fuels and did not improve the anti-seizure properties significantly.

1.5.4 Other mechanical tests

The four-ball machine has been used by a number of workers to investigate lubricity (3, 21, 23, 26). Generally it has been found too severe to descriminate the anti-wear properties of jet fuels. This is particularly true at elevated temperatures and in humid air scuffing occurs at 0.5 kg load. Appeldoorn and Tao (23) used a 4-ball machine to find seizure loads and concluded that scuffing was not the result of a reaction between the fuel aromatic content and the metal surface.

A comparison between the results obtained from the four ball and the ball on cylinder machines, under different atmospheres was made by Appeldoorn et al (32). They found that oxygen and water vapour increased wear and that for steel on steel an oxidative wear process was occurring. A phosphate ester was tested and the wear rate was then found to be independent of the atmosphere. This is of particular interest when considering the wear properties of Hitec E515 which contains an ester of orthophosphoric acid. These results were also found using ball-on-cylinder, micro-Ryder and vane pump tests.

Fuel volatility appeared to have an important influence on the results obtained from the 4-ball machine, with wear increasing with volatility. In this work Klaus and Bieber also showed that low volatility (high boiling point) polar impurities reduce wear when added to a volatile hydrocarbon fuel (33). The presence of oxygen

in the lubricant molecules was found to reduce the pro-wear influence of dissolved oxygen.

Ryder gear tests have been found satisfactory for testing aviation fuel lubricity (3, 21). Problems arise from contamination of the test fuel with oil from the non-test gears. A micro-Ryder rig, loaded with air pressure, to avoid the above problems was found to be unable to differentiate between fuels of differing lubricity and repeatability was poor.

Vane pump tests showed the effect of the aromatic concentration very strikingly (23) and results obtained from this pump agree with those from the four-ball and ball-on-cylinder (3). The device was also sensitive to additives. McHugh (34) points out, however, that the vane and ring do not give the same wear pattern.

1.6 The detection of Hitec in Hydrotreated Fuels

None of the mechanical tests apart from actual pumps, give a satisfactory indication of the presence of Hitec E515 at the concentration specified for fuels. A result of this is that some effort has been used to try and find alternative methods of detecting this, and other similar, additives.

One technique which comes to mind is chromatography of which there are several variations. Thin layer chromatography has already been mentioned in the review of Vere's work (4). The large number of components making up a kerosene fraction has been shown by Mitra et al (35). Some ninety-one components eluted from the column some of which were not identified.

A technique of extracting the dimeric acid component of Hitec E515 from aviation fuel was developed by Hillman et al (36). The extract was then analysed using gel permeation chromatography for identification. A method was developed that allowed an acceptably

precise quantification with a relatively short period (about 1 hour) using a simple bench top gel permeation chromatography instrument.

Another method for the determination of Hitec E515 was developed by Blok et al (37). Note that they refer to Hitec as Santolene C. The dilinoleic acid is extracted chemically from the fuels to give a sufficient sample size for analysis. This process tends to extract naphthenic acids as well as the dimer acid so the two are separated by liquid chromatography which must be carried out with care.

Potentiometric tritation identification of the low concentration of Hitec in jet fuels requires an initial sample size of 3 kg which is quite large. An alternative to this is to react the extract with methylene-blue which can then be compared to a set of standard colours or analysed using an absorptiometer. The latter technique requires only 200 ml of fuel but takes some 4 to 5 hours to carry out.

A flow microcalorimeter similar to that used by Groszek (38) has been adapted by Smith (39) in an enthalpimetric approach to the lubricity of aviation fuels. The heat evolved when polar components, present in a fuel, were adsorbed or desorbed from a solid-liquid interface was measured. This was achieved by measuring temperature with thermistors. Alumino-silicate was used as the adsorbent.

It was found that the amount of heat evolved was dependent on the type of refining process. This heat arose from oxygen and sulphur compounds and aromatics and olefins. Although some correlation was found with wear tests, as far as ranking fuels with respect to lubricity is concerned, the method was found to be relatively insensitive to low concentrations (14 p.p.m.) of Hitec E515.

1.7 Additives

It has already been pointed out that one possible solution to the lubricity problem is the addition of certain types of compound to jet fuel in order to restore lubricity. Normally this type of additive is included with a package of other additives which have various functions such as anti-oxidation, anti-sludging, anti-wear and anti-icing (8, 40). Often these additives are manufactured as a 'package' and then added to the fuel.

Hitec E515 is not the only additive capable of improving lubricity. During the course of this work a number of other corrosion inhibitors were approved for use but Hitec E515 has in the past been the only approved additive (8) and remains widely in use in the industry. A detailed study of these additives (and others not yet approved) has been attempted (11).

Some work is currently being carried out by Dacre et al (41) to determine the effectiveness of various components of Hitec E515 in improving lubricity. They have used radioactive tracer techniques to plot adsorption-desorption isotherms for fatty acid components on iron, steel, cadmium and aluminium bronze. Dimer acid is considered to be the most important component and adsorbs in multilayers onto the surfaces. A synergistic effect was found to arise between the dimer acid and the base solvent (n-hexadecane in this case). Further the dimer acid was shown to be very tenacious even at high temperatures (80 and 100°C) where little desorption occurred.

Finally a new addive, Hitec E580, has been recently introduced in which there is no phosphate ester component. Little is yet known about this additive but it appears to be as effective as Hitec E515 in the role of lubricity improvement and as a corrosion inhibitor.

1.8 Theoretical Considerations

Wear can be described as "abrasive", adhesive ("severe") or "corrosive" (or "mild" or oxidational). Theory for boundary lubricated adhesive wear has been developed by Kingsbury (42, 43) and later by Rowe (44) based on the wear equation developed for adhesive wear under dry sliding conditions.

An expression for adhesive wear under dry conditions has been developed by a number of researchers. Holm (45) determined that the wear rate might be related to the real area of contact when considered on an atomic scale. Aggregates of atoms forming wear particles were introduced by Burwell and Strang (46) in a development of the law to account for wear debris size. The idea of interacting asperities, as a cause of large fluctuations in friction (termed stick-slip), was proposed by Bowden and Laben and related to adhesion (47). Subsequently Bowden and Tabor (48) reported that adhesion was largely responsible for friction.

Archard (49) considered a hemispherical asperity rubbing against a flat plane and then used the same argument to develop a wear equation for multiple asperity contacts. The equation showed that wear rate was proportional to the real area of contact when measured as volume of material removed per unit sliding distance. The constant of proportionality was termed the 'K' factor. Archard interpreted the 'K-factor' in the following way. If $K = 10^{-3}$ then one in every 10^{3} contacts produces a wear particle, so K is in fact the probability of producing a wear particle (50). In 1956 Archard and Hirst (51) had carried out a large number of wear tests, with various metallic combinations, to demonstrate that the wear equation could be obtained empirically and apply over a wide range of metals.

Most metals will undergo oxidation and so Quinn (52) obtained an expression for the K-factor in terms of oxidational parameters

resulting in a form of Archards wear equation applicable to oxidational wear.

Kingsbury (42, 43) introduced the concept of the fractional film defect to take into account the action of a lubricant. This parameter represents the fraction of the real area of contact which is prevented from coming into contact by the presence of a lubricant. Starting with the wear equation proposed by Burwell and Strang (46) and Archard (49), Rowe (44) used Kingsbury's fractional film defect to obtain a wear equation for a boundary lubricated system. Boundary molecule size, the fundamental time of vibration of the boundary molecule and the heat of adsorption of the particular type of boundary molecule were found to be factors on which wear depended. The theory, as such, took no account of the lubricant in which the boundary type molecule was dissolved, so Rowe attempted to account for this by the introduction of two fractional film defects, one for the boundary molecule, the other for the base solvent (53).

Another theory, by Sakurai et al (54), is based on the critical pressure of hydrodynamic lubrication and the probability that a metal-to-metal contact will occur and result in a wear particle. Gupta et al (55) presented an equation relating wear scar diameter to carbon number from an empirical approach to the wear of aviation fuels.

It has been suggested by Beerbower (56) that most of the above models (and others) are consistent but that their coverage is often limited to specific conditions or systems.

1.9 Program of Research carried out in this investigation

Work carried out by the companies and interested parties has been directly concerned with finding a rapid solution to the original problem and then an attempt to monitor fuel lubricity.

The effects of the components of the fuel and atmospheric conditions have been studied in some depth. Little attention has been paid to the manner in which the metals wear. This would seem to be a serious gap in the knowledge of the problem since the metals are an integral part of the system and, in the final analysis, it is they which cause the failure. Consequently an understanding of how the metals wear in the presence of hydrofined fuel and a similar fuel containing a corrosion inhibitor would be beneficial.

In view of the fact that the ranking of fuels, according to their lubricating ability, has been deemed important most of the tests have been carried out under specific conditions of load and speed. No data is available about the variation of wear rate with load for the aluminium bronze-steel system. Further, in the tests carried out there have been problems with detecting the presence of Hitec E515 and, even when it has been detected, its effect has appeared to function in a manner diametrically opposite to the fuel pump experience.

Emphasis has also been placed on producing a rapid test (15 to 20 minutes) which could be included in a fuel specification. This has meant that with such short tests the wear mode has probably had insufficient time to become established. The particular case of the dwell test ignores wear altogether and is based on friction measurements. However the fact that wear measurements correlate with pump experience better than friction measurements has been shown by a number of workers.

Consideration of these points led to the basic program of wear tests and analysis. The aims were thus: 1) to obtain wear rate against load curves for hydrofined fuel with and without Hitec E515, 2) to run the tests for a sufficient duration in order to establish wear under conditions of boundary lubrication (or otherwise in the

case of fuel without additive) and 3) to analyse the worn surfaces and wear debris from selected tests once the wear pattern was known. Surface finish and fuel type were to be monitored and friction and temperature measurements were also to be made although less emphasis was to be placed on these parameters.

This approach to research is favoured by Wilson and Eyre (57) who reason that metallographic changes should be analysed by physical techniques in order to obtain a better understanding of the mechanisms involved with the wear process in a given situation. Consequently it was hoped that in this way mechanisms for the failure of the fuel pump and for its protection by Hitec E515 could be elucidated.

Phillips et al (58) have demonstrated the usefulness of Auger electron spectroscopy in Tribological work and this technique was thought to be applicable in this case. The technique is surface sensitive (order of a few angströms) and so is ideal for the study of the thin 'boundary' films expected to be present on the surfaces. Combining this with electron probe microanalysis and scanning and transmission electron microscopy would, it was hoped, give good insight to the processes occurring on the surfaces during wear.

To ensure that the surface analysis results, obtained from the laboratory specimens, were consistent with those obtained from aircraft fuel pumps samples from a pump simulation rig, and actual fuel pumps, were to be analysed with the same techniques.

Finally a theory, based on the experimental evidence, will be developed. It was hoped that this would be a firm basis which could be modified to account for future experimental results thus leading to a theory which could be used to predict wear rates when aluminium bronze wears against steel in the presence of aviation fuels under boundary lubricated conditions.

CHAPTER 2

EXPERIMENTAL DETAILS

2.1 Introduction

The experiments can be divided into two main sections. Experiments were carried out to measure parameters which might indicate the lubricating ability of the fuels studied. This involved measuring friction, wear rate, contact resistance and temperature. These tests provided samples for analysis in the second group.

The second group of experiments was to analyse the worn surfaces, the wear debris and fuels. The emphasis was placed on the analysis of the worn surfaces for which techniques such as Auger electron spectroscopy, electron probe microanalysis and scanning electron microscopy were used for this purpose. Samples for analysis came from three main sources (i) failed aircraft fuel pumps, (ii) a piston pump simulation rig and (iii) a Denison wear test machine.

2.2 The Lucas Two-Piston Rig

The failed aircraft pump samples had been stored for some years. Consequently it was necessary to produce lubricity failures which could be analysed, as soon as possible, after the failure to be certain that there were no storage effects. Running a pump to failure would have been expensive and it would have been difficult to obtain bore samples suitable for analysis. To overcome these problems Lucas Aerospace designed, built and operated a pump simulation rig, the main features of which are shown in figure 2.1. The rig consisted of a rotor having to extractable bores diametrically

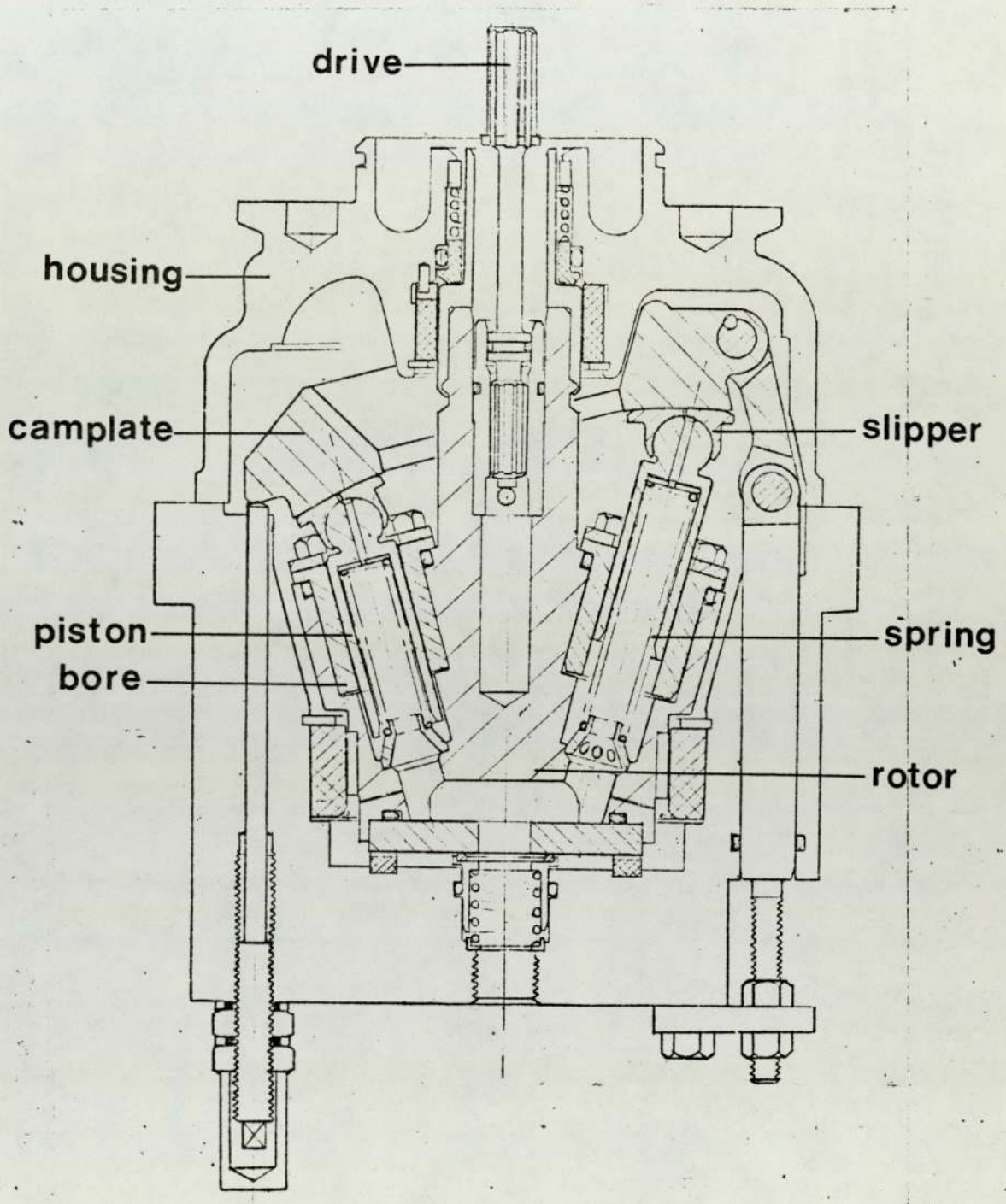

Figure 2.1. Lucas Two-Piston Rig.
Courtesy - Lucas Aerospace.

opposite. These bores were made from the standard production metallurgy of cadmium plated aluminium bronze and the pistons were production KE 961 steel.

Tests were carried out with hydrofined 2494 aviation kerosene of expected low lubricity. It was this type of fuel which had produced the aircraft fuel pump failures so the two-piston rig would be expected to seize. After these tests a similar fuel with a standard addition of 15 p.p.m. of the corrosion inhibitor, Hitec E515, was tested in the rig with the expectation of no failure. These fuels were re-circulated to reduce the quantity required for a particular test to about 68 dm^3. Piping used for the rig was stainless steel. Prior to starting a test the system was flushed out with hydrofined kerosene for cleaning purposes.

Operating conditions were chosen to simulate aircraft take off conditions and so give an accelerated test and reduced the running time. Take off conditions would be the most severe conditions experienced by the service pump and so would be the most likely to produce a failure. This involved using the maximum camplate angle which represents the maximum stroke, and hangout from the bores, of the pistons resulting in the maximum side loads on the pistons. The maximum camplate angle of 15.5° could be manually preset. A further feature of the rig was that fuel was pumped into the test pump, at a pressure which could be varied, by a slave pump. This pressure was selected to be about 12.5 MN M^{-2} which is the approximate maximum pressure experienced in this type of aircraft fuel pump on take off. To prevent excess damage to the rig if seizure occurred the drive shaft was fitted with a shear pin.

The parameters measured during each test were the inlet and outlet fuel temperatures (to the test pump), pressure, main fuel flow rate and cooling flow rate. The temperatures were measured with

copper-constantan thermocouples. It was hoped that by measuring these parameters some change might indicate imminent failure of the test pump, for example increased outlet temperature. Piston and bore dimensions were monitored before and after testing.

2.3 Denison wear tests

A Denison T62 Tribotester was used for laboratory experiments. This machine (see Plate III) consists of a flat faced pin-on-disk configuration. The disk can be rotated, with speeds in the range 100 r.p.m. to 6000 r.p.m., by a continuously variable d.c. motor. A boundary lubricated mode of wear was to be simulated on this machine and to obtain this simulation, reciprocating motion (as found in the fuel pumps) was not necessary. Loads of between 0.5 Kg and 20 Kg could be applied to the wear pin by using a sprung loaded weight pan. The latter was used to prevent shock loading of the wear pin. Again, since boundary lubricated wear conditions were to be simulated, no attempt was made to simulate the pump loadings (see appendix I for the calculation of loadings in a fuel pump). The wear pin was held in a brass holder which was electrically isolated from the lever type load arm by a tufnol insert. The 2:1 ratio load arm was then counter balanced. The complete load arm assembly could be moved so that a number of wear track positions could be used on the disk.

A recirculation system was used to apply fuel to the disk. Glassware was used for the majority of the system but Vinescol 23 6 mm diameter rubber tubing was used where flexible connections were required. This type of tubing was selected because it does not contain plasticisors. Consequently nothing would leak out from this tubing and contaminate the fuel. Actual pumping was by a Watson-Marlow peristaltic pump, through one micron filter paper into a constant head tank above the disk. This enabled a steady and constant

flow to be maintained at a rate of 20 ml Min^{-1}. Fuel was pumped from, and returned to, a two litre storage tank. Note that for the above flow rate a two hour test would require 3.6 litres for the fuel to be circulated once.

Table 2.1 gives a materials specification for the DTD 197 aluminium bronze and HE 15W duralumin used for the wear pins and the KE 961 steel equivalent, KE 180, used for the disk. The only difference between these two steel materials is that KE 180 does not

TABLE 2.1 MATERIALS SPECIFICATION

DTD 197A	HE 15W	KE 180
Copper	Aluminium	Iron
Nickel 4-6%	Copper 4.5%	Carbon 1.45-1.65%
Aluminium 8-11%	Manganese 1.5%	Silicate 0.4-0.65%
Iron 4-6%		Manganese 0.3-0.5%
Zinc 0.5% Max.		Chromium 12.5-13.5%
Manganese 0.25% Max.		Sulphur 0.04% Max.
Silicate 0.25% Max.		Phosphorus 0.03% Max.

contain the 0.5 to 0.75% Tungsten that KE 961 contains. The use of KE 180 was enforced because of the size requirements of the disk (KE 961 is not manufactured in sufficiently large diameter bars). Two disks were manufactured by Lucas Aerospace in a manner similar to piston production. This involved stress relieving and hardening and tempering with demagnetization. The disk face was then lapped to a flatness of two light bands (0.635 μM) with a surface finish better than 0.0254 μM the latter being equivalent to the piston surface finish. In one case the roughness was increased to 0.0635 μM. The dimensions and tolerances on the disk are shown in figure 2.2 (a).

PLATE III DENISON WEAR TEST MACHINE

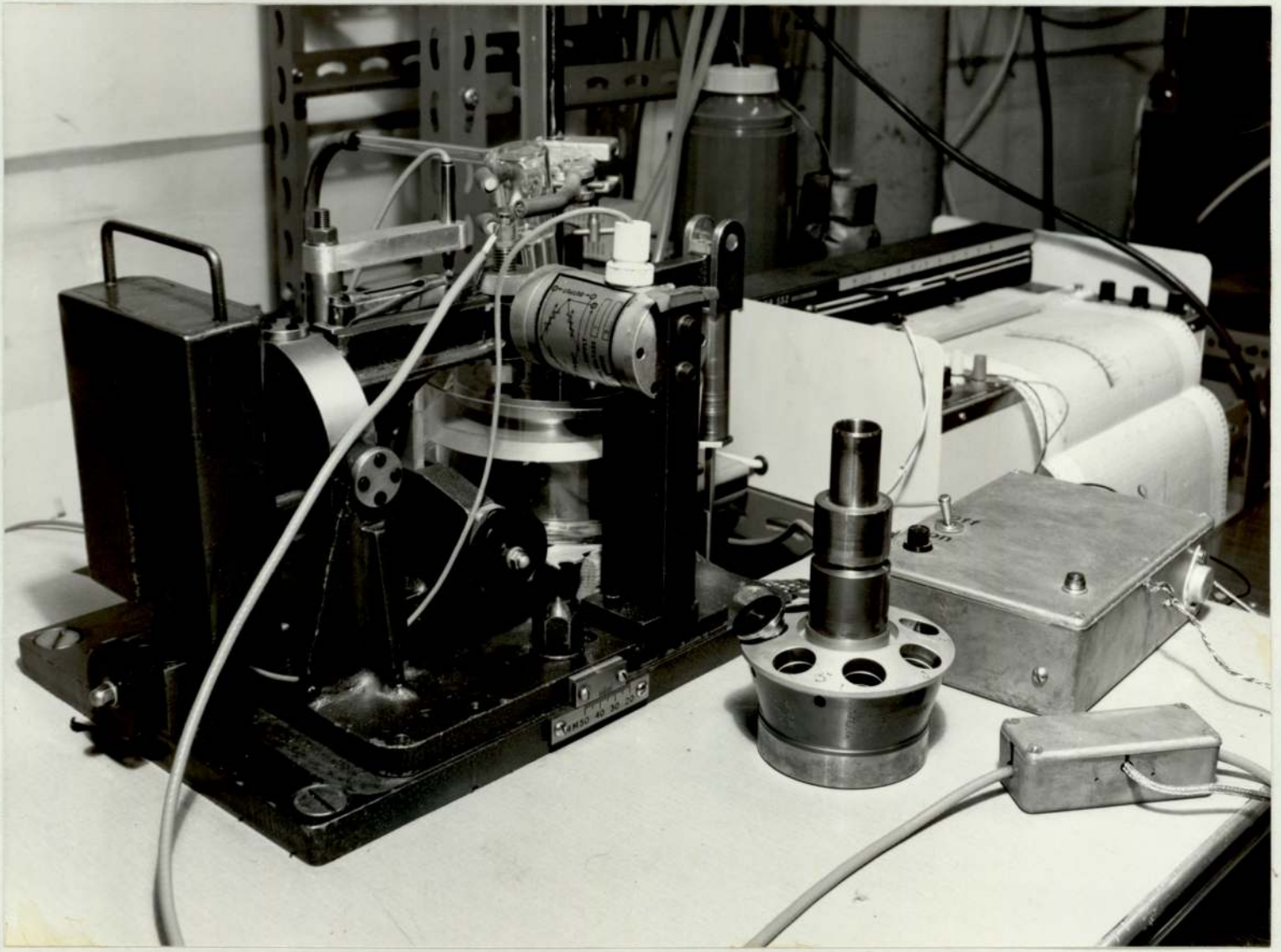

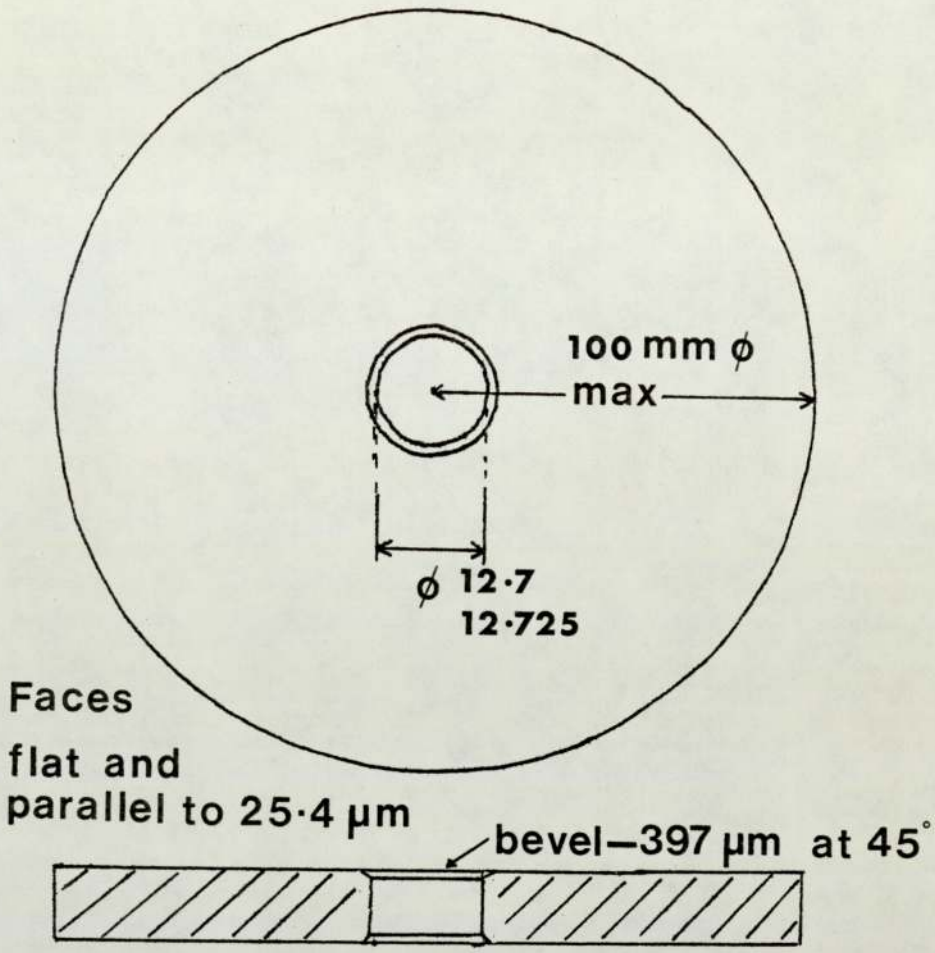

a) Wear test disk

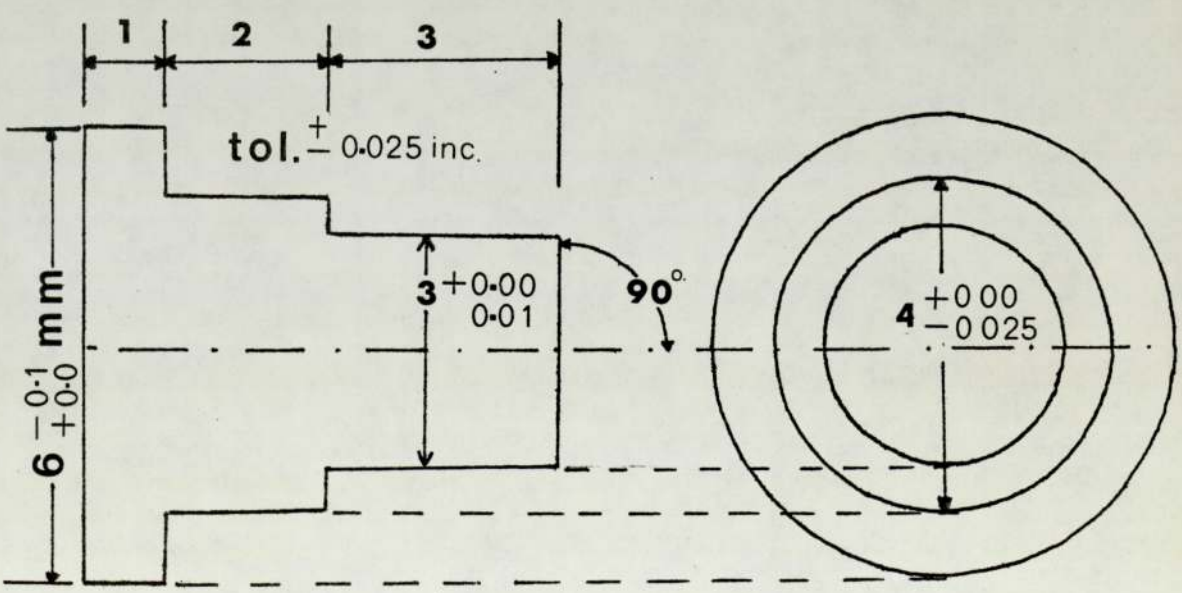

dimensions in mm where not given.

b) Wear pins

Figure 2.2

Lapping was generally carried out with diamond paste and shellsol T (a paraffinic oil unlikely to contaminate hydrofined kerosene with any lubricity improving compounds). Some later lapping of the disks was carried out with diamond dust and shellsol T to avoid introducing lubricity improving compounds from the diamond paste.

Generally the pins were used with the surface finish as turned on the lathe. However some pins were used after polishing the wear surface with various grades of silica-carbide wet or dry paper. For polishing purposes these pins were mounted in a quick, cold setting, acrylic resin mounting plastic (Northill Plastics Ltds., London N16 6BP). All the duralumin pins were used without polishing. The details of the dimensions and tolerances for the pins are shown in figure 2.2 (b). Most of the pins were made with a 3mm diameter flat wear surface, which was considered a reasonable dimension to give suitable wear rates and sufficient area for surface analysis. A small number of pins were made with a 2 mm diameter in order to increase the load per unit area for one series of wear tests.

2.4 Test Fuels

In this work four main groups of lubricant were used namely 2, 2, 4 trimethylpentane, shellsol T, Hydrofined 2494 Kerosene and Hydrofined 2494 Kerosene with additions of the corrosion inhibitor Hitec E515. The first of these lubricants, 2, 2, 4 trimethylpentane (iso-octane) was used as a reference fuel since it contains no aromatics, sulphur, phosphorous or nitrogen compounds. Hence one would expect this fluid to be of low lubricity. The main problem with using trimethylpentane was its difference in viscosity, about 4×10^{-4} NSM^{-2} compared with about 10^{-3} NSM^{-2} for kerosene at room temperature.

A replacement reference fluid used was shellsol T which was the

reference fluid used in the Lucas Dwell test. This again was expected to have poor lubricity properties.

Obviously the best reference fuel would be a highly refined kerosene from which the lubricity agents had been removed. One of the best methods of ensuring that one such fuel was available, was to filter some hydrofined kerosene through a column of 13% alumina catalyst (synclyst brand 3A). This catalyst removed lubricity improving compounds from the fuel . In a few cases dry nitrogen was bubbled through the fuel to try and reduce any effects which might arise from water.

Finally tests were carried out using fuels containing various concentrations of the additive Hitec E515. This included a commercial sample of hydrofined 2494 fuel with 15 p.p.m. of Hitec E515 added by the suppliers as for aircraft usage. Other test fuels were made up in the laboratory by mixing 7.5, 15, 30 and 50 p.p.m. of Hitec, by weight, with alumina catalyst filtered hydrofined kerosene.

2.5 Friction and wear measurements

Wear measurements were made by using a linear displacement voltage transducer of 0.5 mm stroke (sangmo Weston Controls Ltd., N6 BR Minature A.C. gauging transducer with in line oscillator/ demodulator unit). The transducer was held against a flat plate attached to the load arm so that as the pin wore, and the load arm moved, the displacement was continuously recorded on a chart recorder along with the frictional force. The wear transducer calibration was checked, using a Universal measuring instrument which can be set to an accuracy of 0.25 μM. The transducer power supply voltage was set at 12.5 volts for this calibration which is shown in figure 2.3.

Friction measurements were made by using a resistance bridge type strain gauge load cell (Pye-Ether Dynamometer type UF2) with

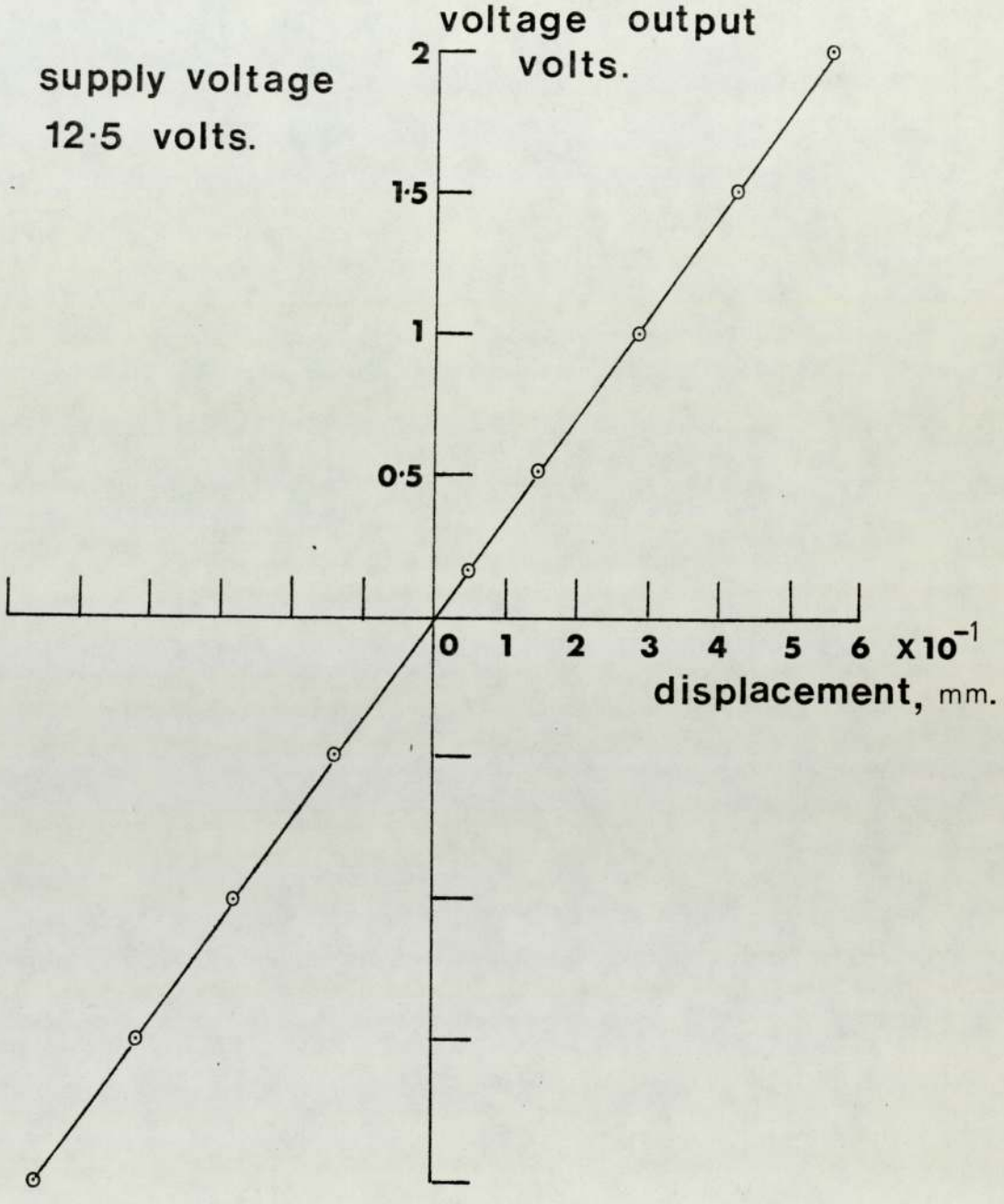

Figure 2·3 wear transducer calibration.

ranges of 0.5 to 5 Kgf full scale deflection. The sensitivity of the amplifier was adjusted when the load cell was statically loaded by the use of a pulley and weights. In this way the chart recorder could be calibrated to give a direct reading of coefficient of friction.

A check on the drift of the friction and wear transducers showed that it was negligible after an initial warm up period as shown in figure 2.4. Assuming that once the pin had run-in there were no errors in measuring wear from misalignment then the speed of the disk could be held to within $\pm$ 5 r.p.m. Further the radius where the pin contacts the disk was measured to the centre of the pin so this gave an error or $\pm$ 1.5 mm for the edge of the pin. However it could be set to an accuracy of 0.1 mm itself.

2.6 Measurement of Thermal E.M.F.'s, Contact Resistance and Capacitance

The system of aluminium bronze sliding against steel provided the opportunity of measuring thermal e.m.f.'s generated between the copper and iron in these materials. The dynamical thermocouple method developed by Furey (59) was consequently adopted for this system. Electrical connections were taken from the pin holder, and through a carbon brush connection from the disk to the load arm. The contact resistance between the pin and disk was measured using a universal bridge type TF2700 (Marconi Instruments) and found to be 3.8 Ω under static conditions and about 1.5 Ω under dynamic conditions for a dry contact. Applying kerosene to the disk increased the dynamic resistance to 12 Ω with a capacitance of 600 PF at 300 r.p.m. The leakage resistance and capacitance between the pin holder and load arm were found to be 5.3×10^9 and 53 PF respectively. Furey found, in his work, that short duration high

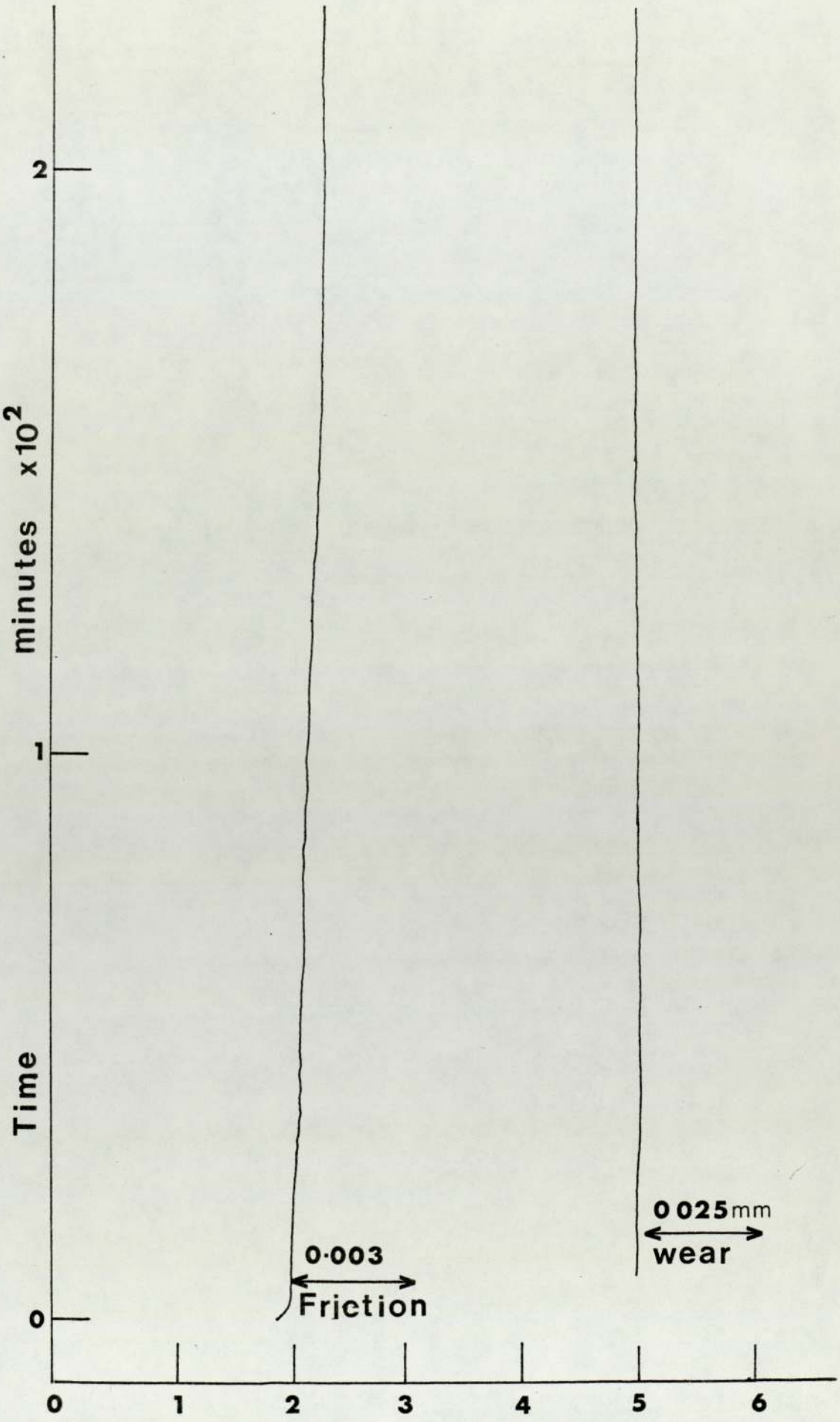

Figure 2·4, drift characteristics.

temperature spikes could be detected. Assuming that these spikes last for the period during which asperities are in contact then $t = 2a/v$ where 'a' is the radius of an asperity and v the linear speed of the disk. Taking 'a' to be about 10^{-2} mm and the maximum speed to be about 2.5 MS^{-1}, t would be about 4×10^{-6} seconds. Consequently any amplifier design had to detect 20 μV signals at a frequency of 1mHz from a low impedance source. Czichos et al (60) suggest that the pulse rise time for a contact is about 0.1 μ seconds for boundary lubricated conditions.

A suitable amplifier for this purpose was found to be an F.E.T. input device (R.C.A. CA3140E operational amplifier) with a full power badnwidth of about 1 mHz, slow rate of 9V/μS and input noise of 12 to 40 nV $(Hz)^{-\frac{1}{2}}$.

The input was expected to be of the order of 20 μ V per degree centigrade so a gain of 30 would give an amplifier output of 0.6 mV $^{o}C^{-1}$. For a temperature of 200°C this would give an output of 120 mV which is sufficient for detection with the oscilloscope. The complete circuit, with standard frequency compensation and null offset, is shown in figure 2.5 (a). Note that metal oxide resistors and cermets were used to reduce noise from the passive components. The frequency gain for this amplifier circuit is shown in figure 2.6 for a gain of 30 and a 10mV sine wave input from a 600 Ω source.

The amount of drift with time on the scope for the output of this circuit is shown in figure 2.7. The oscilloscope was triggered externally so that a single shot of the output of the thermocouple amplifier, for one revolution of the disk, could be displayed. This was done using a magnet, mounted on the drive shaft, passing a magnetic tape head the output of which was amplified before passing into the single shot circuit. These circuits are shown in figure 2.5 (b).

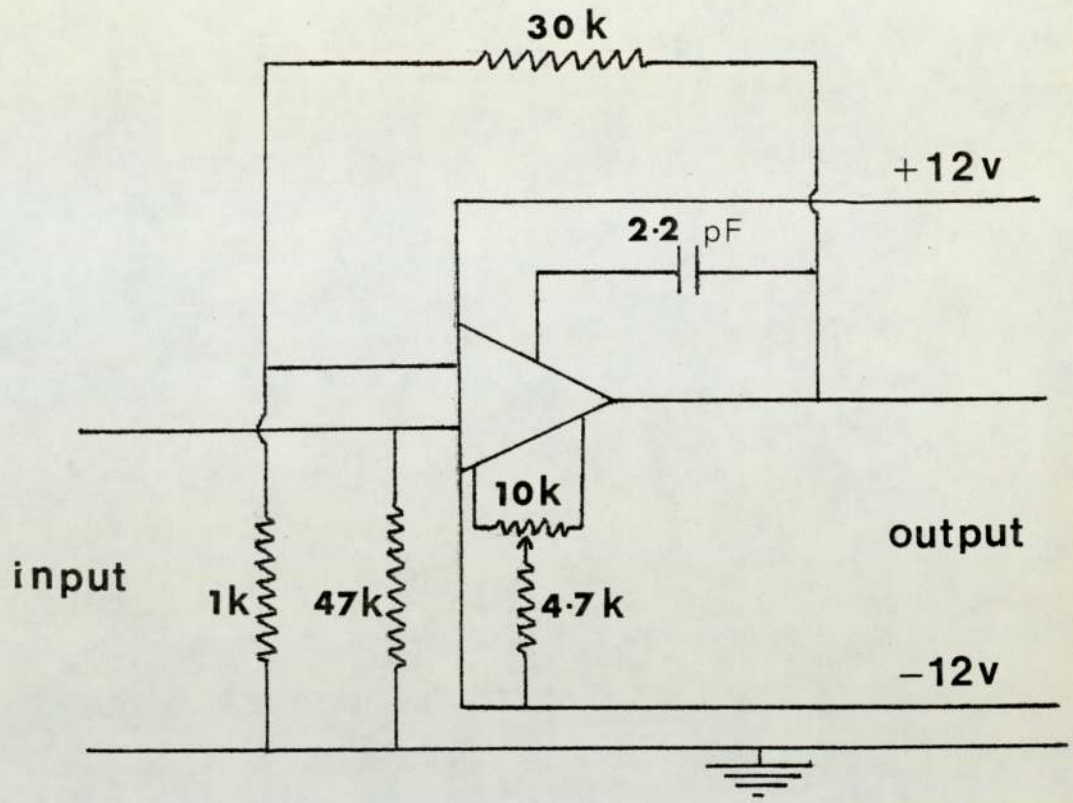

a) cA3140E, x30 gain, amplifier.

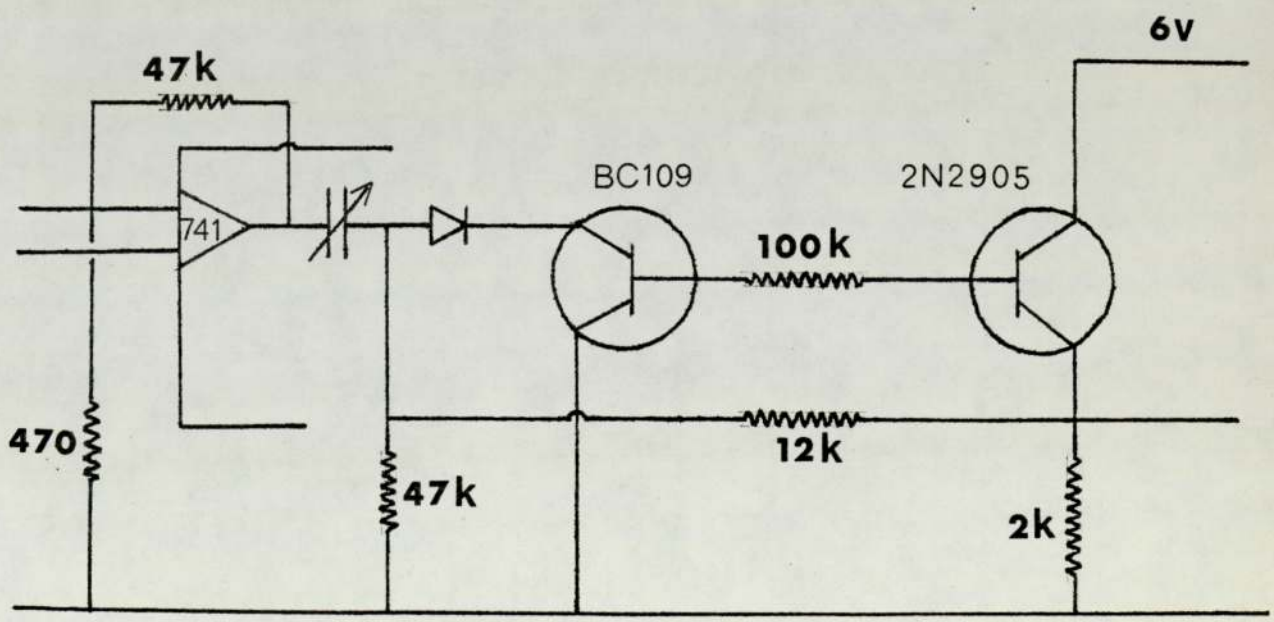

b) single shot trigger circuit.

Figure 2.5

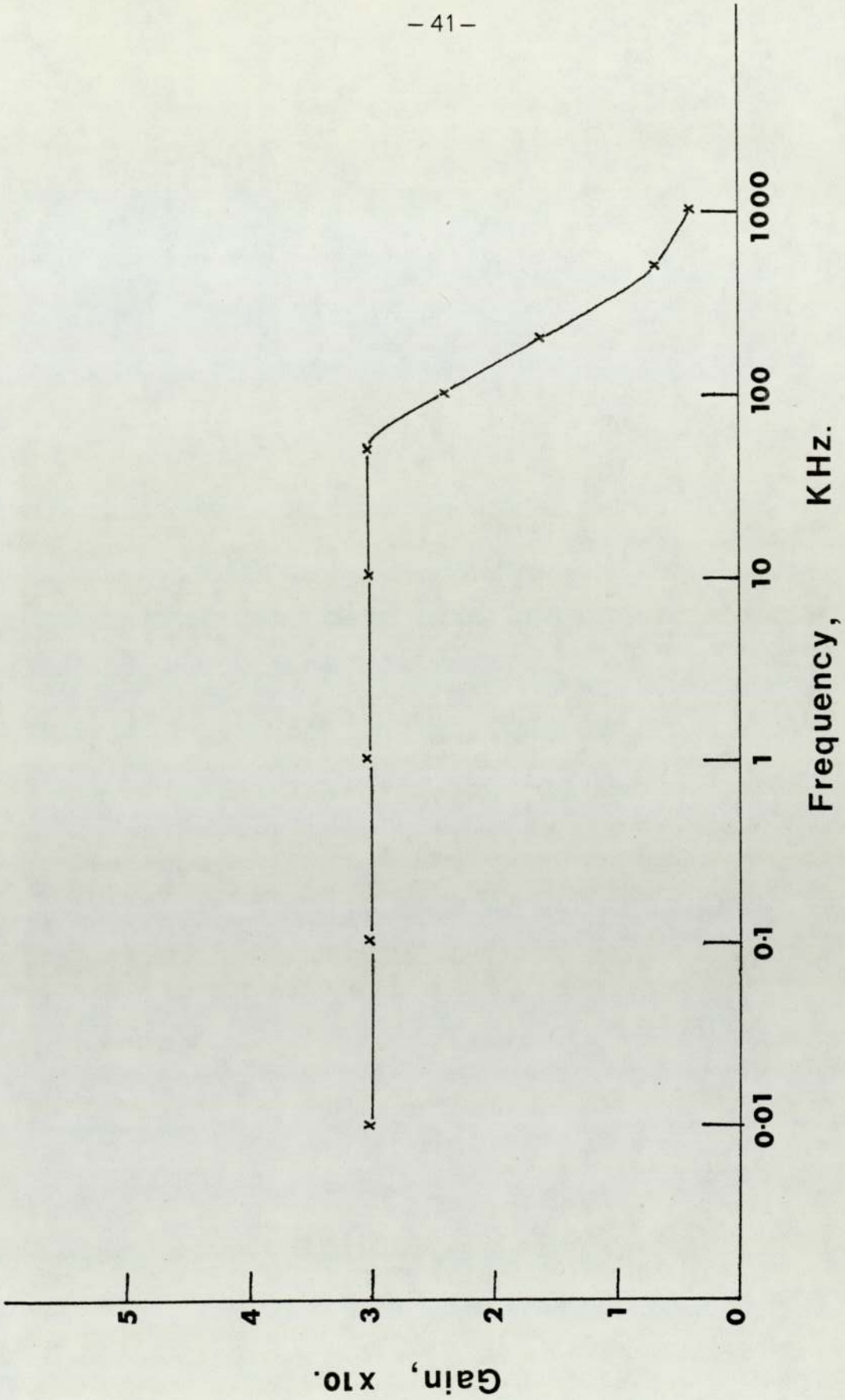

Figure 2.6, CA3410E frequency response.

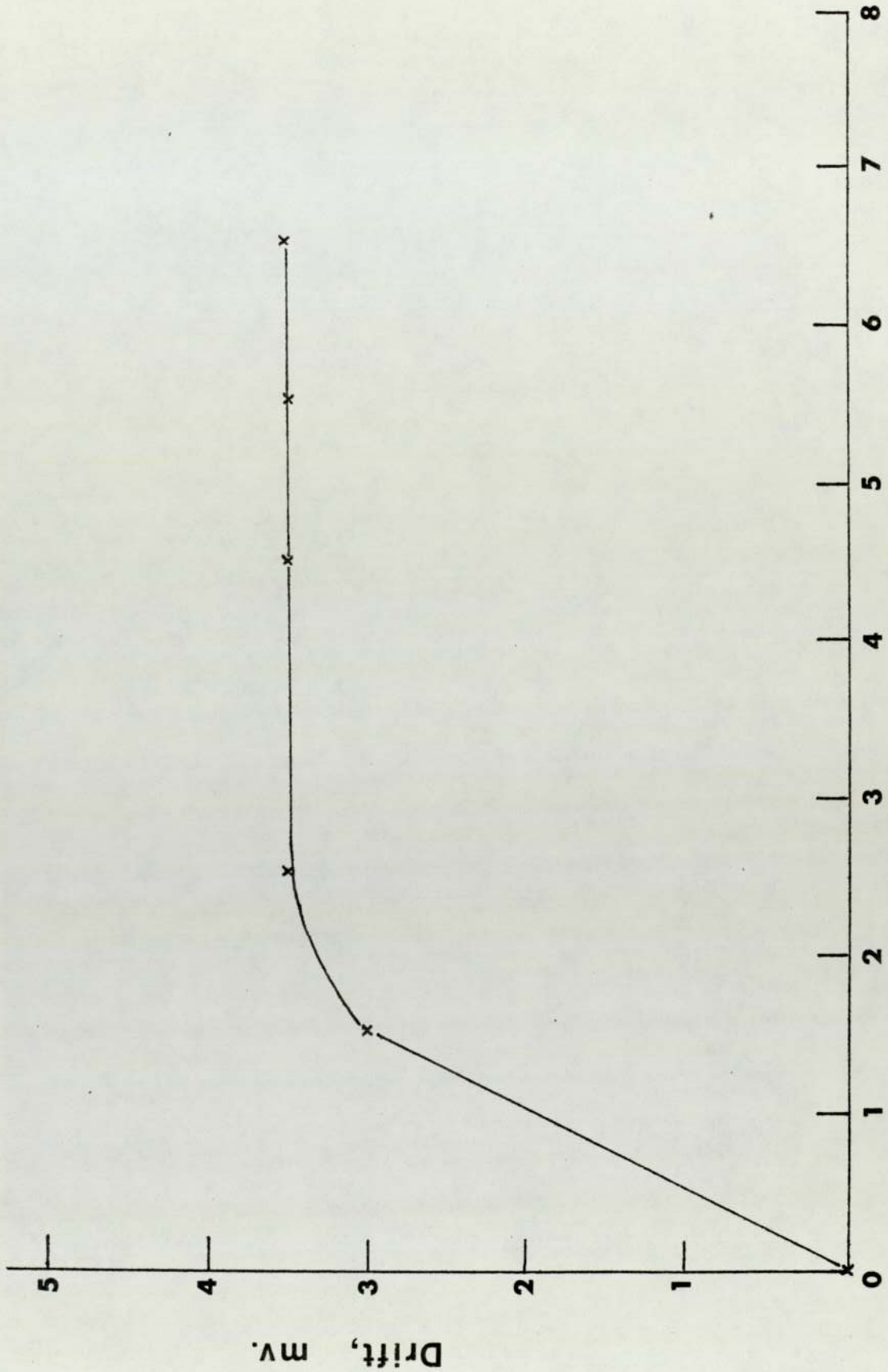

Figure 2.7, CA3104E drift – oscilloscope output.

The thermocouple amplifier was nulled with the zero off-set and the output set to zero for the input open and short circuit conditions. Temperature calibration was obtained from a junction formed by aluminium bronze and KE 961 steel. Since wires of these materials were not commercially available strips had to be turned off rods. This was not an easy task since the bronze tends to be brittle. The junction was heated and the temperature monitored along with the output from the amplifier. The temperature was measured with a cambridge portable potentiometer bridge type 4422A with an accuracy better than $\pm$ 1%. The calibration curve is given in figure 2.8.

The TF2700 bridge was also used to measure contact resistance. The bridge was connected across the pin and disk and an oscilloscope used to detect its output. The bridge output was an 0.4V peak-to-peak sine wave which was fully displayed when no contact occurred. If there was contact then a truncated form of sine wave was displayed.

2.7 The wear test procedure

The procedure for each series of wear testing will now be described. Prior to starting each test it was important to ensure that the wearing components and all other surfaces which came into contact with the test fluid were thoroughly cleaned. Typical cleaning procedures used by other workers are listed in Table 2.2. In this work the pins and disks were given an initial clean in a vapour bath using shell SBP2 petroleum ether. After this they were given a short ultrasonic clean in shellsol T. Further before the actual test a sample of the test fluid was circulated around the rig and then thrown away. The glass ware was cleaned with concentrated nitric acid and also in the vapour bath. Note that the components put in the vapour bath reached the desorption

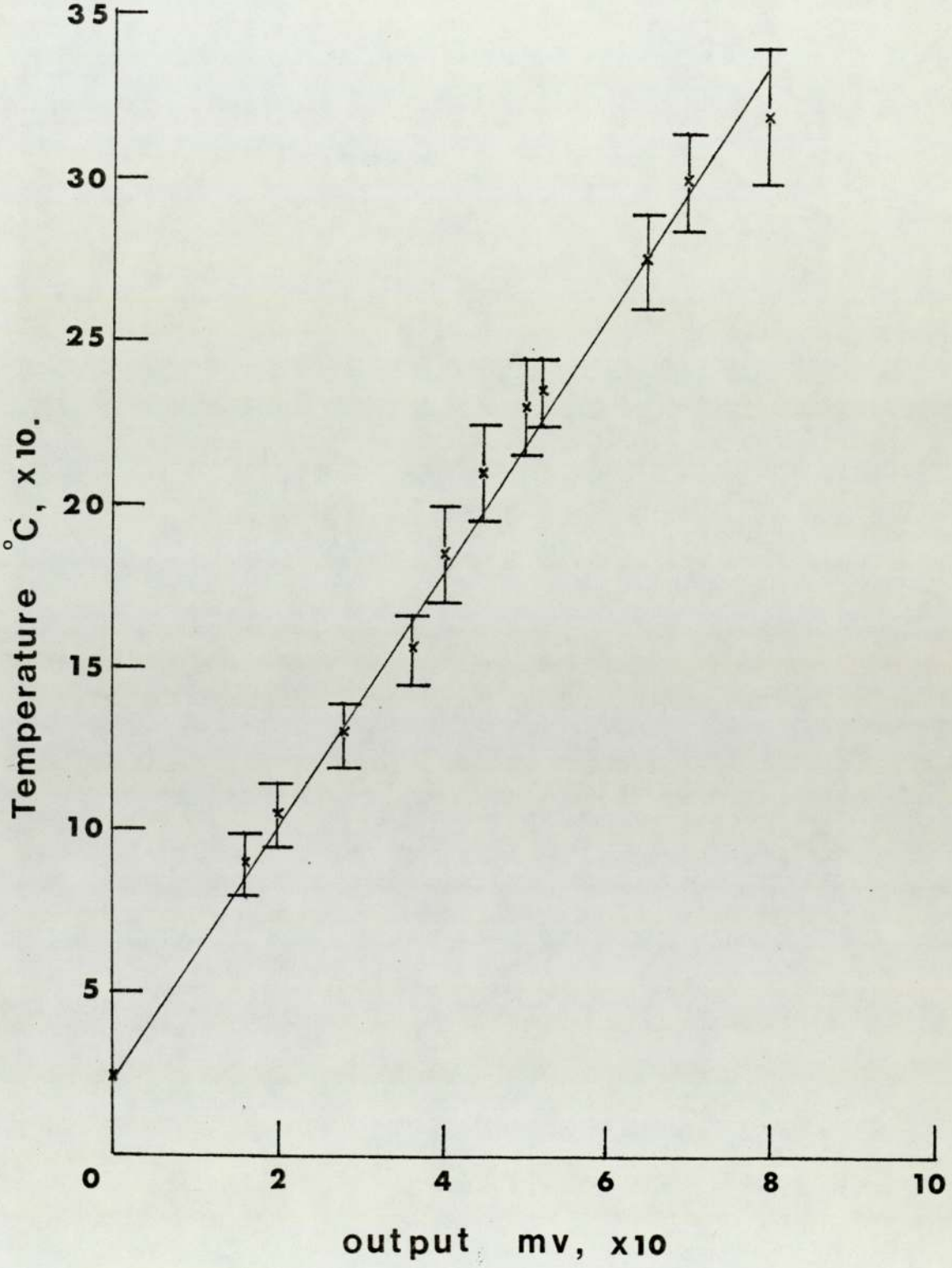

Figure 2.8, Amplifier calibration.

temperature of Hitec E515. Wherever possible tubing was replaced between series of tests with additive and tests without additive, also two constant head tanks were available.

TABLE 2.2 OF CLEANING TECHNIQUES USED IN THE STUDY OF THE LUBRICITY OF AVIATION FUELS

CLEANING AGENT	RESEARCH GROUP	REF. NO.	COMMENTS
Acetone-Propanol	USAF Wright	11	
Petroleum Ether	Pattinson		
Isopropyl Alcohol (IPA) (Anular Grade)+Carbon	Edwin-Cooper	10	Not satisfactory
Ultrasonics + Organic	"		Improved
Solvents + Decon	"		Results
Heated Disk (150°C) in Hydrotreated Fuel	"		Unsuccessful
IPA + Ultrasonics (1hr)	"		Reasonable
Hot IPA (150°C)	"		Poor Results
Methyl IsoButyl Ketone + Ultrasonics	"		Much Better than I.P.A.
Etch in Nitol	"		
IPA + Carbon	Lucas	10	
Acetone-Methanol-Toluene	Leeds University	10	Poor with Additives
Disk Polish with Aqueous Suspension of Alumina	"		Improvement

Care was taken in the assembly of the test pieces so that no contamination was introduced at this stage.

Alignment of the pin and disk was achieved by means of a spirit level on the load arm. After a run-in period of about 20 minutes initial experiments were carried out with the test fuel to determine operating conditions for the wear tests. This involved plotting a

Strikbeck type curve, which was done by using a single load and measuring the friction force for a number of speeds. Fein (61) has objected to this type of plot and suggested that the whole curve could be generated from elasto-hydrodynamic conditions. To check that this was not so the contact resistance, between the pin and disk, was monitored during these tests.

Having obtained information on the best operating conditions to achieve boundary lubrication wear tests were carried out under these conditions. Each test was run with a new wear pin on a new wear track on the disk. Most tests were carried out at a constant linear velocity of 0.62 MS^{-1} although one series of test was done by changing the velocity with constant loads of 5, 10 and 12.5 Kg. Again the initial wear-in period was between 20 and 30 minutes. The wear tests lasted on average 60 to 120 minutes depending on the amount of wear occurring.

Some short duration wear tests of about 20 minutes were carried out for loads of 2.5 Kg to 15 Kg, in steps of 2.5 Kg, at a constant speed. For these tests one pin was used and one wear track the load being periodically increased. These tests were carried out for the poor lubricity fuels and in cases where the disk roughness was higher than normal. This was possible since under these conditions a reasonable wear rate could be measured in these time intervals.

The weight of the wear pins was measured before and after each test so that the wear rate could be calculated from weight loss.

Eight tests were carried out on each disk after which they were relapped to remove the wear tracks. Various lapping compounds were tried, the best being either diamond paste in shellsol T or diamond dust in shellsol T. After each lapping a centre line average (c.l.a) talysurf was carried out to check that the required surface finish had been obtained. Examples of the talysurfs for different

polishings carried out are shown in figure 2.9.

Other wear tests were carried out whilst bubbling dry nitrogen through the fuel to see if there were any effects due to water. However since nitrogen compounds may form lubricity improvers this was only done for a limited number of tests.

Tests were also carried out to find the variation in wear with concentration of additive. Starting with a hydrofined fuel a test was run and then 5 p.p.m. Hitec added and the test continued. The concentration was then made up to 15, 30 and 40 p.p.m. This was repeated for 15, 20 and 40 p.p.m.

Finally some dry wear tests were carried out during which temperature measurements were taken as in the case of fuel samples.

In the wear tests the wear rate was calculated from the equations.

$$\text{Wear Rate} = \frac{0.0141\,\Delta X}{R\,\Omega\,\Delta t} \quad mm^3 mm^{-1}$$

Where ΔX is the displacement measured directly from the chart recorder output of the displacement transducer, R the disk radius at which the test is carried out Ω the disk speed in r.p.m. and Δt the duration of the experiment.

$$\text{Also wear rate} = \frac{\Delta M}{120\,\pi\,\rho\,v\,\Delta t} \quad mm^3 mm^{-1}$$

where ΔM is the pin weight loss, ρ the pin material density, v the linear speed of the disk and Δt again is the test duration.

2.8 Sample Analysis

A study of boundary lubricated wear can be divided into three main sections, namely, the two rubbing surfaces, the wear debris and the lubricant. Most of the analysis in this work was carried out on

c.l.a.
μm.

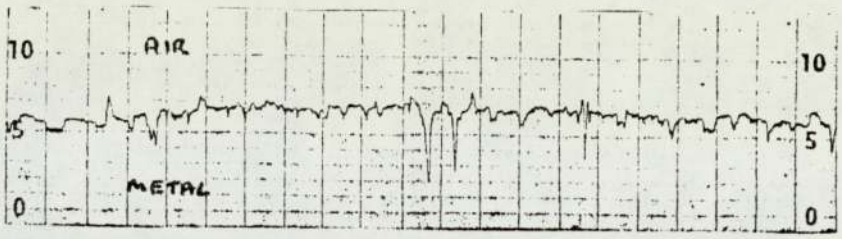

0·02

diamond dust and shellsol T

0·05

diamond paste and kerosene

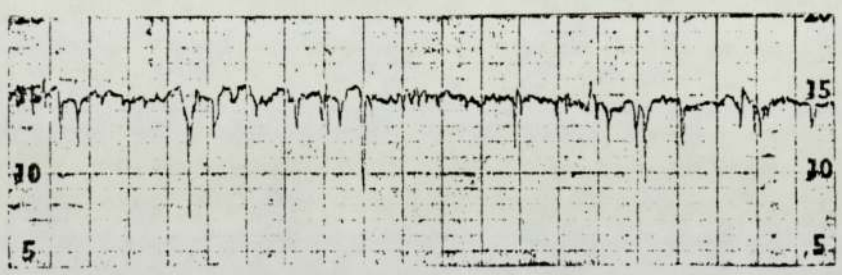

003

diamond paste and oil

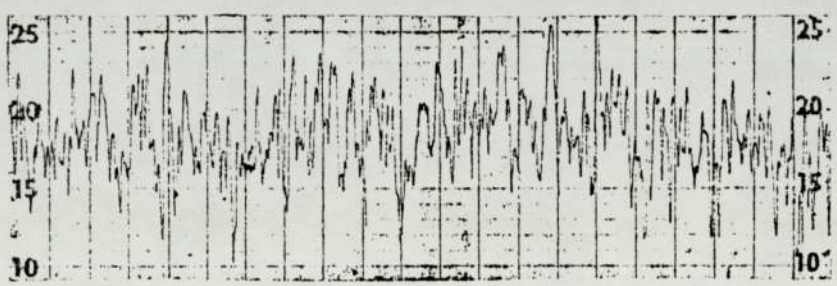

009

alumina and water

vertical x 5.10^4 ; horizontal x 100

Figure 2.9 Talysurfs of disk surfaces.

the two rubbing surfaces and in particular on the aluminium bronze wear pins.

2.9 Auger Electron Spectroscopy

Two things suggest that a surface sensitive technique would be useful for studying the surfaces worn under these boundary lubricated conditions. The first is that the active components of the additives in lubricants form protective layers as shown by Allen and Drauglis (62). Secondly the pistons from pumps run on hydrofined fuels show thin layer deposits exist on them in the early stages of a lubricity failure.

Auger electron spectroscopy (A.E.S) is a surface sensitive technique and was used in this case. A low energy electron beam is used in this technique to ionize surface atoms, subsequent relaxation of the atom gives rise to Auger electron emission. The process can be illustrated by the use of the electron shell model of the atom. The incident beam removes an inner core K-shell electron (fig. 2.10 (a)).

This results in ionisation of the atom with the K shell being one electron defficient. Relaxation to a stable state can then occur by say, an L shell electron falling to the K shell. This means that the L shell will now be unstable and, consequently an electron may be emitted from this shell. This emitted electron is termed an Auger electron and the transitions occurring to produce it is called a K.L.L. Auger transition (see figure 2.10 (b)).

Many other transitions can occur with other shells being involved. The energy at which these transitions occur will be specific to the atom which has been ionised, consequently that particular atom can be identified by the energy of the Auger electrons that it emits. Charts have now been produced which show

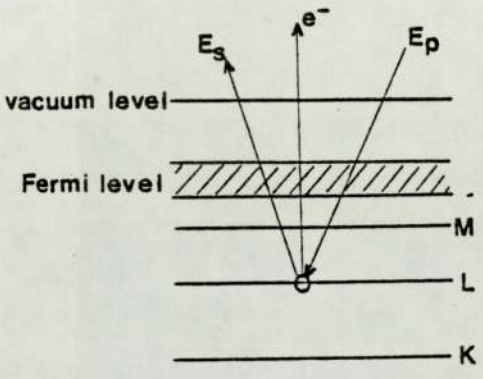

a) Ionization of a surface atom.

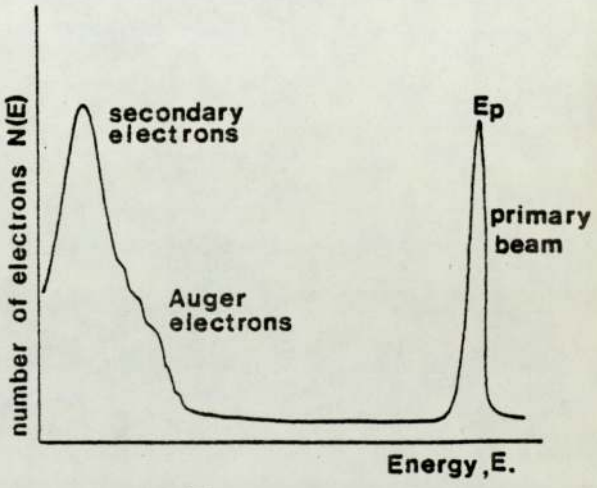

c) Energy spectrum

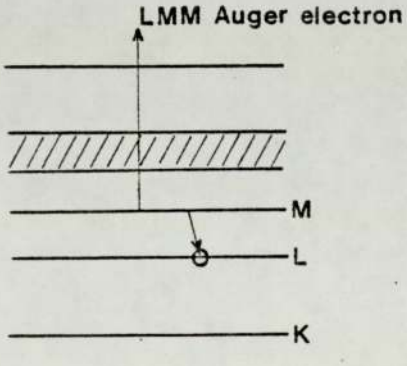

b) Relaxation of the atom with Auger emission.

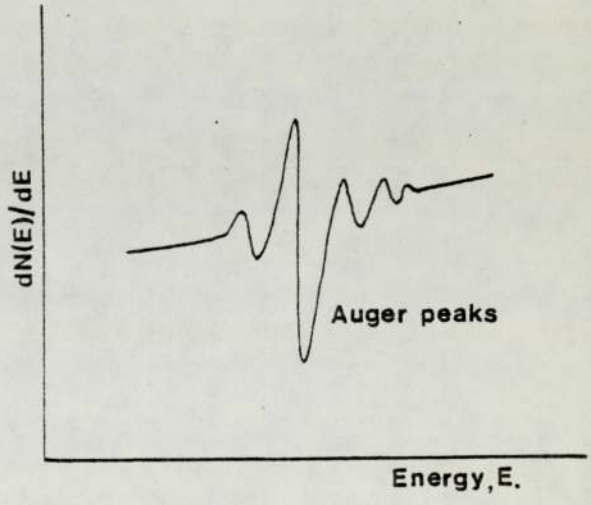

d) differentiated spectrum

Figure 2.10, The Auger process.

the principal Auger electron energies for most atoms. Auger electrons being emitted from a surface may interact with other atoms as they escape. This means that they may loose or gain a small amount of energy (a few electron volts) which results in plasmon loss and plasmon gain peaks. These peaks can be useful in identifying oxides as shown by Suleman and Pattinson (63).

If the electrons, coming off the surface irradiated with a low energy electron beam, are counted, and a plot of number of electrons collected against energy is made, then the Auger electrons appear as small deviations on the secondary electron peak-figure 2.10 (c). However, if a plot of the differential of the number of electrons collected with respect to energy is made then the Auger peaks are well resolved as shown in figure 2.10 (d). This technique then permits the identification of surface layer atoms.

The usefulness of the technique is increased by ion beam etching the surface. The surface is bombarded by heavy ions of Argon or Xenon and in this way surface atoms are removed. A consequence of this is that depth profiles of the atoms present on the surface can be obtained. Depth profiles can be plotted as Auger peak-to-peak heights against depth or some function of depth. Such a plot can be misleading since it does not take into account the relative cross-section for the particular Auger transition plotted. Thus there may appear to be more of a particular element present than actually exists. Some progress has been made by Chang (64) towards a quantitative analysis for this relatively modern technique. The concentrations have been plotted against the product of sputter depth and time of sputtering. The details of the quantification carried out to determine relative concentrations and the relationship between the product of sputtering current and sputter time are given in Appendix II.

2.10 (Operating procedure and sample preparation)

Some of the earlier samples analysed were removed from the wear test machines and stored in hydrofined fuel or the test fuel. As soon as the spectrometer was available these samples were given a brief clean in the vapour bath. The samples were kept below the desorption temperature of the additive during this cleaning. The main purpose of the cleaning was to remove any weakly bound surface contamination which may have resulted from storage. Later samples were stored dry in a dessicator and given a cold wash with acetone before mounting. The spectrometer design and operation was such that it was preferable if all workers mounted samples at a radius of 95.25 mm. A mounting was designed to hold the wear pins as shown in figure 2.11(a). Three of these were made to fit onto an existing holder and were etched in a solution of 65% concentrated nitric acid, 30% distilled water and 5% hydrofloric acid to avoid contamination of the vacuum system. These holders were mounted onto an existing main frame which could then be bolted into the system (Plate IV). The system used for this work was a vacuum generators model shown in plate V. Once the samples had been mounted the system was pumped down to a vacuum of better than 10^{-10} Torr. The ultra high vacuum was required to keep the samples clean during sputtering and a vacuum of better than 10^{-9} Torr greatly reduces the formation of carbonaceous deposits on the sample. Out gasing of the electron gun, ion gun, titanium sublimation pump and pressure gauge filaments before starting the experiments was also necessary to avoid contamination of the surfaces.

A 2KeV beam energy with an emission current of 0.4mA (0.2 mA on some later samples) was used as a compromise between a higher beam energy, to obtain the high energy transitions, and a

lower beam energy, to prevent damaging the surface films. This produced a beam spot of about 1 mm diameter at the sample and a beam current of approximately 10 μA. The modulation voltage used for detection was 3v peak-to-peak.

The initial setting up procedure involved the optimisation of the differentiated peak of the elastically scattered electrons - to be referred to as the "elastic" peak. To obtain the optimum elastic peak the angular position of the sample relative to the hemi-cylindrical voltage analyser was adjusted. The electron beam was then checked for focus and alignment to give the maximum "elastic" peak. The Auger spectrum was then quickly recorded on a storage oscilloscope and any further adjustment made to the above parameters to obtain a balance between the low and high energy resolution on the spectrum. An initial spectrum was then output on an X-Y plotter. Energy calibration was by assuming that the copper 920 eV and 940 eV peaks were in the correct position. It was assumed that there would be an error μ in the starting voltage and that there were M eV mm^{-1} on the chart recording. For a starting voltage of 30 eV and 700 eV the energies were scanned over a "window" of 700 eV. The position of the two copper peaks then gives

$$700 \pm \mu + 109.25\ M = 920$$
$$700 \pm \mu + 119.5M = 940$$

assuming μ is a constant gives

$$M = 1.95\ eV\ mm^{-1}$$

In fact the approximation of M = 2eV/mm^{-1} gave reasonable results when identifying peaks from their energy.

Having taken the initial spectrum depth profiling was carried

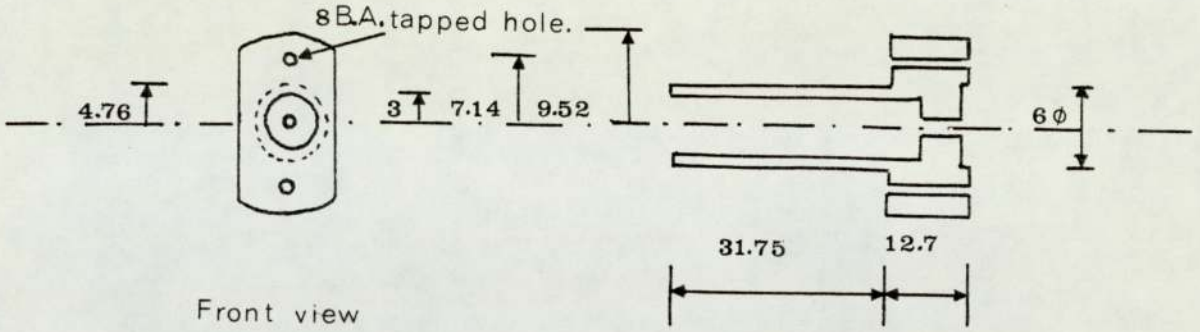

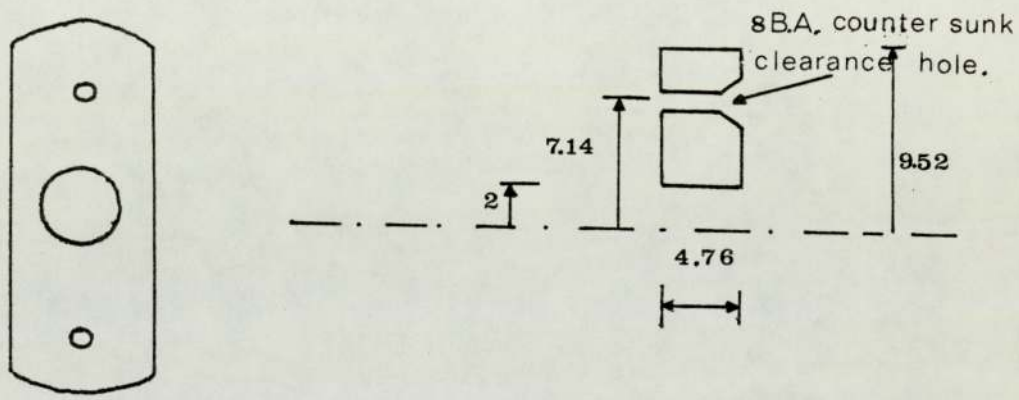

a) Auger holder. steel.

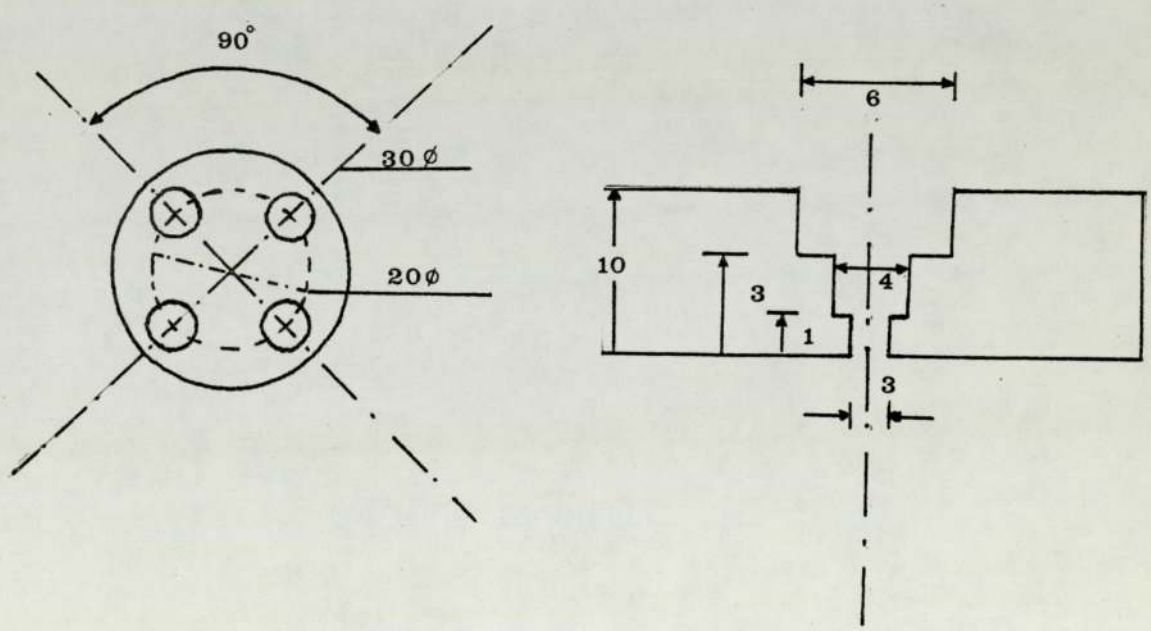

b) E.P.M.A. holder. brass.

all dimensions in mm

Figure 2.11, Wear pin holders.

PLATE IV AUGER SAMPLE HOLDER

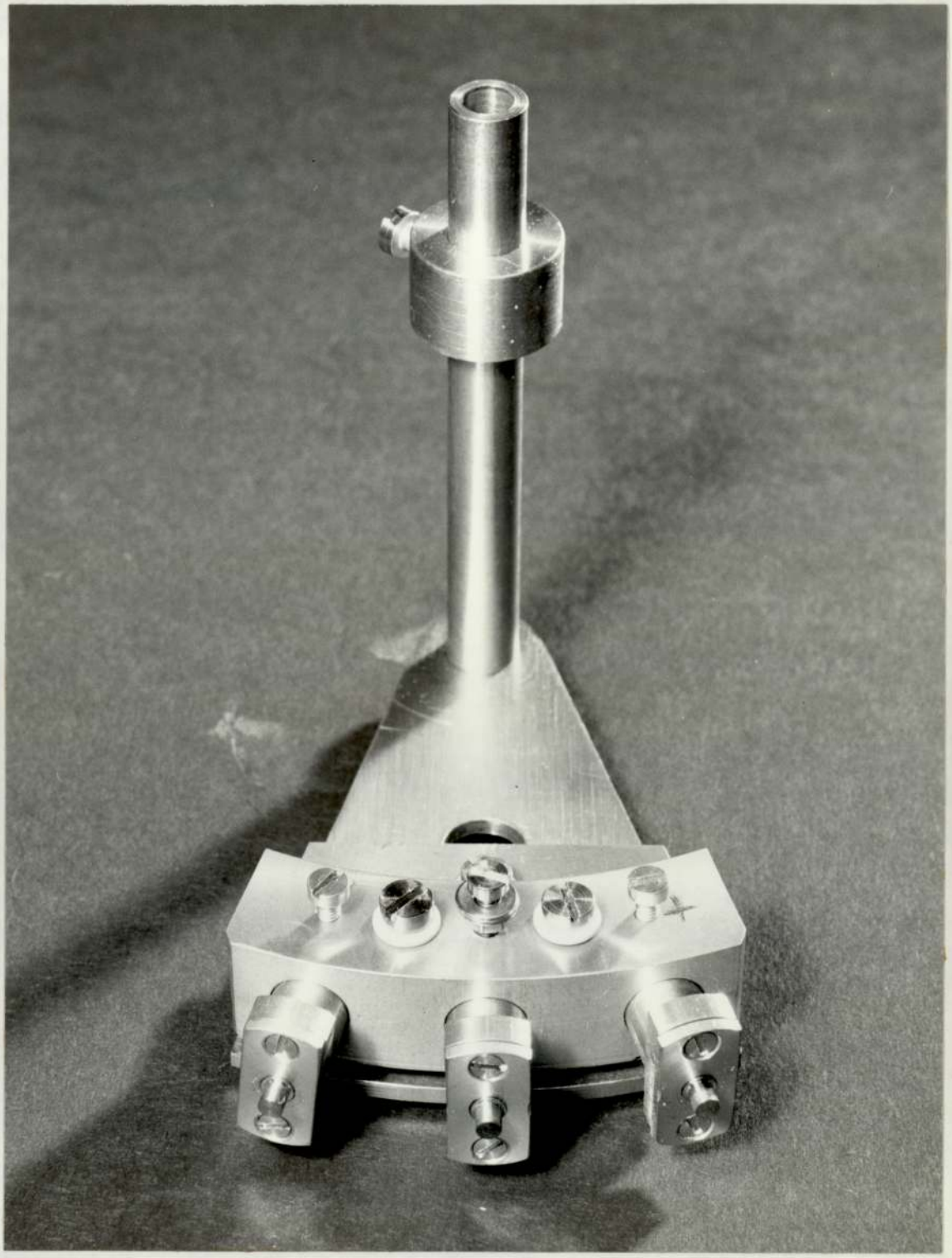

PLATE V AUGER SPECTROMETER

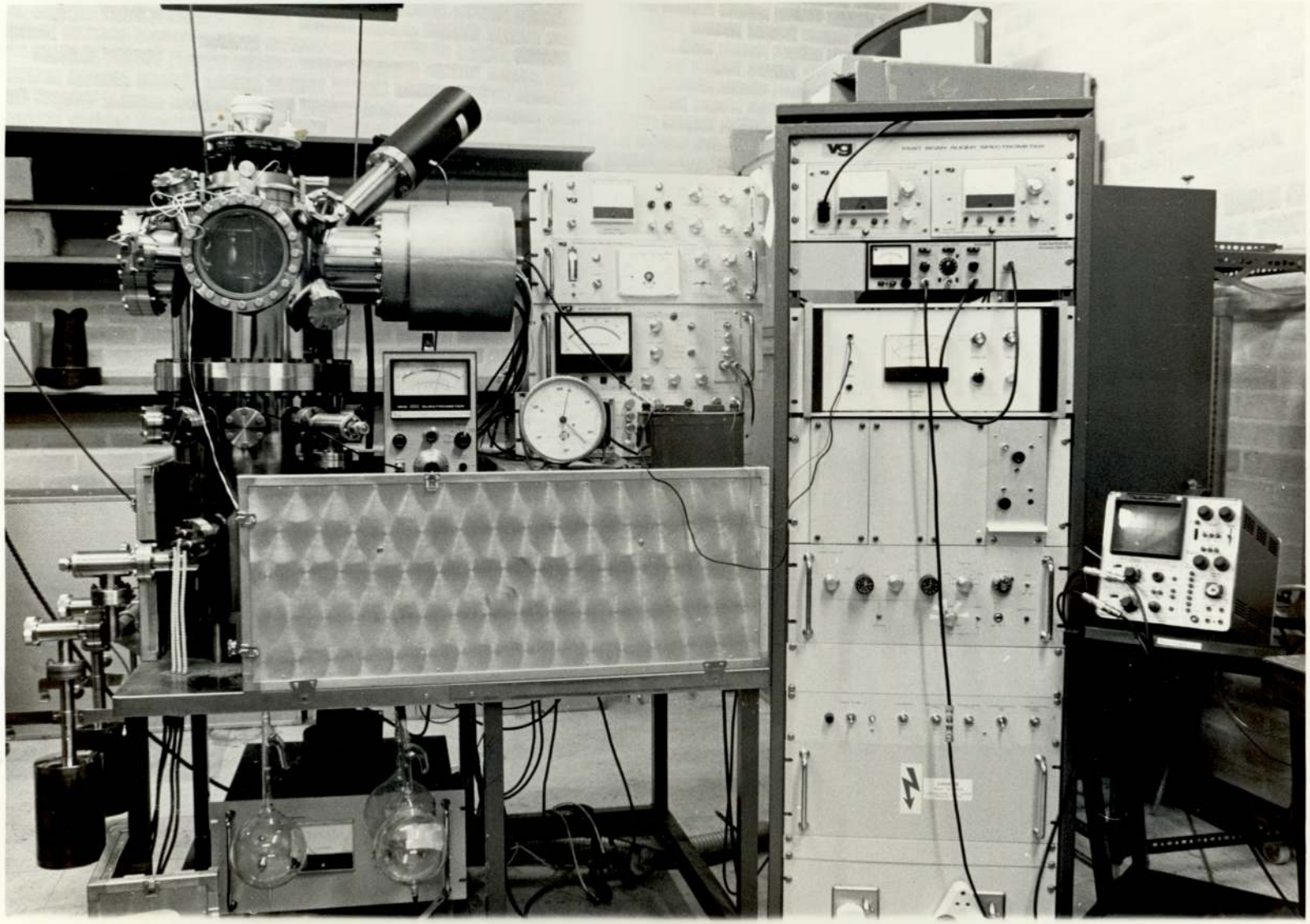
VG

out using mainly Xenon ion sputtering but, on a few occasions due to system operation for other workers, argon was used as the sputtering ion. Xenon was preferred for sputtering since no difficulty is experienced with surface layer formation.

A low background was thus required during sputtering to prevent surface reactions with reactive background species. Xenon was allowed into the vacuum chamber through a bleed valve and sputtering carried out at a Xenon pressure of 10^{-4} Torr. The ion beam size was of the order of 10^{-2}M at the sample. After sputtering, during which the ion current at the sample and the time of sputtering were noted, the Xenon was pumped out and a spectrum immediately taken. Providing the sputtering time was short all three samples were sputtered and then a spectrum taken from each. For longer times each sample was analysed individually to prevent background contamination occurring whilst the other samples were being sputtered.

Experiments were also carried out to determine the effect of changing the focus by defocusing the beam, changing the primary beam energy by $\pm$ 150 eV and also investigating different areas of one sample. Changes in the shape of the "elastic" peak were also observed.

2.11 Electron Probe Microanalysis

The technique of Auger spectroscopy analyses only surface layers. Sputtering increases the thickness analysed by depth profiling. However, even after long periods of sputtering, on the present system, the total depth analysed was only of the order of typically 5×10^{-10}M. The Auger electrons themselves come from a depth given by:

$$t = 6.65 \times 10^{-11} \times \sqrt{E}$$

where E is the energy of the escaping Auger electrons. For the 60 and 920 eV copper Auger electrons the escape depths are 5×10^{-10}M and 20×10^{-10}M respectively. Thick oxide films can be more easily analysed by the use of the electron probe. This technique has been described fully elsewhere. Birks (65) presented a graph of effective range against beam energy which is reproduced here in figure 2.12. For the 10^{-7}A current and 15KeV beam energy used in this work the effective depth from which x-rays are detected can be estimated using this graph. The depth works out to be 5×10^{-7}M which results in a relatively large volume being analysed compared to the Auger system. Note that the 2KeV beam used for the Auger analysis results in a beam penetration of up to 2×10^{-8}M but only Auger electrons produced in the very thin layer at the surface escape, as illustrated previously. The use of the electron probe also enabled x-ray distribution photographs to be taken of elements present on the surface. The one micrometer spot could also be rastered along a distance of 100 μM to give line profiles of elements present. The crystal type x-ray spectrometer allowed scans of Bragg angle to be made hence permitting element identification. This type of detector requires that the samples be accurately set in position (to within $\pm$ 0.25 mm) for analysis. Since the wear pins were a difficult shape for mounting in the standard holder a special holder was made for them as shown in figure 2.11(b). The samples were degreased in acetone before mounting in the instrument. A small number of samples were taper sectioned with a 10° angle so that the difference between the surface layer and underlying aluminium bronze could be observed.

2.12 Microscopy

Three forms of microscopy have been used to monitor the surface topography of wear samples.

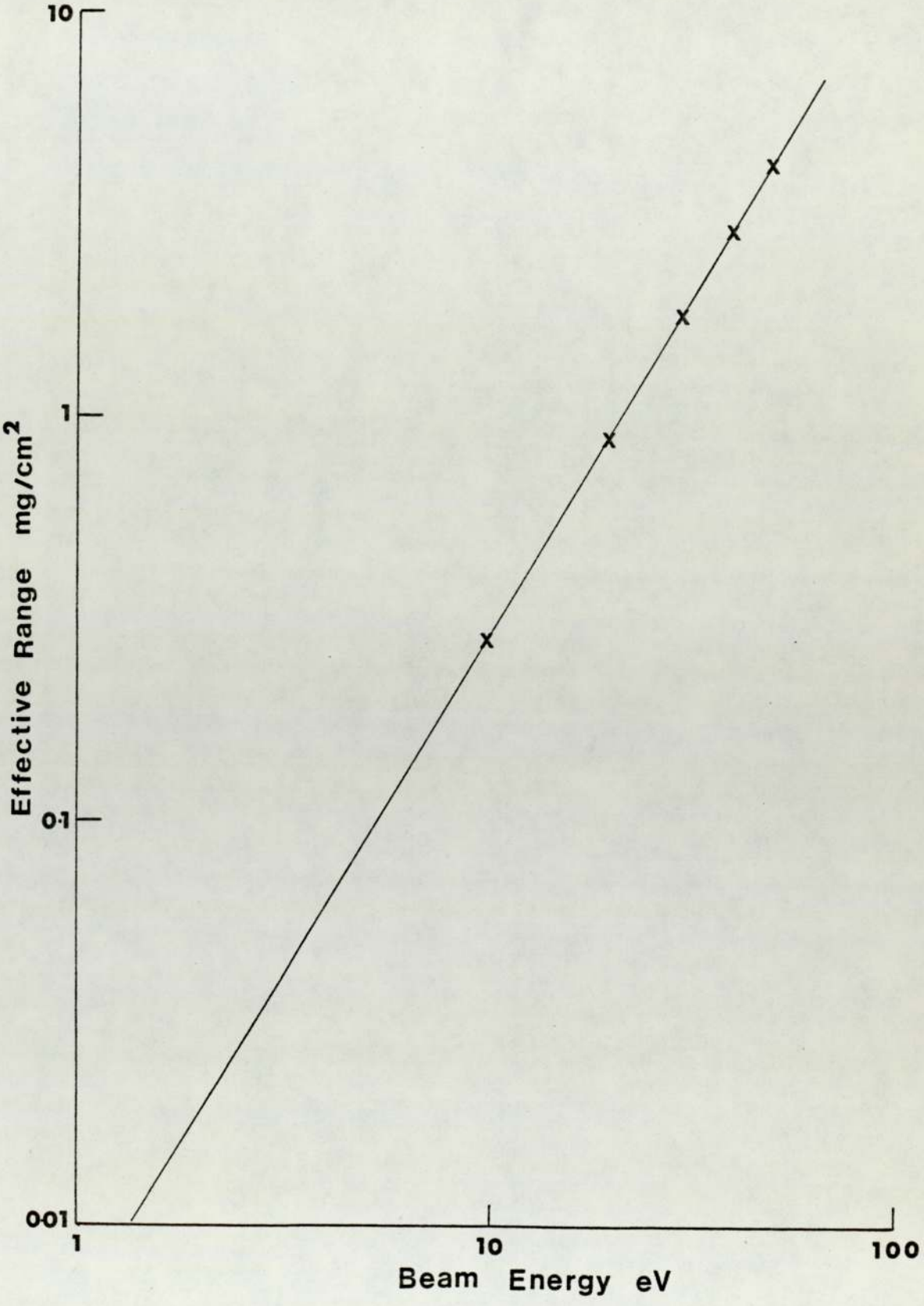

Figure 2.12 see Ref. 65.

All the wear pins were analysed using a light reflection microscope as soon as the wear test was completed. The appearance and colour of each pin was noted. Samples from the two piston rig were also observed.

Transmission electron microscopy was found useful for determining the surface topography of the disks and wear tracks. Since the disks were too large to go into the scanning electron microscope carbon replicas were made from the surface of the disk. Shadowing was carried out with gold-palladium wire at an angle of 60°. Quinn (66) has illustrated the use of this technique, for the analysis of wear surfaces in some detail so the diagrams in figure 2.13 are included here as a brief summary of the technique.

Scanning electron microscopy was also used to look at samples from all the wear surfaces. In the case of the two piston rig pistons and bores, and the Denison wear machine disks, samples of approximately 10^{-4} M^2 were taken from these specimens. Note that at the end of the major series of wear tests some further tests were carried out, with hydrofined fuel and fuel with additive, to produce a disk with wear tracks which could be sectioned for analysis in the scanning microscope. This microscope also had a solid state detector for x-ray analysis. X-ray distribution photographs, of selected elements could be obtained along with an energy scan to determine the elements present on the surfaces. Most of the analysis was carried out using a 20 KeV beam and emission current of about 100 μA. The samples were generally set at an angle of 45° to the beam. However sharper angles were investigated for the x-ray analysis to see if the contribution from the bulk could be reduced.

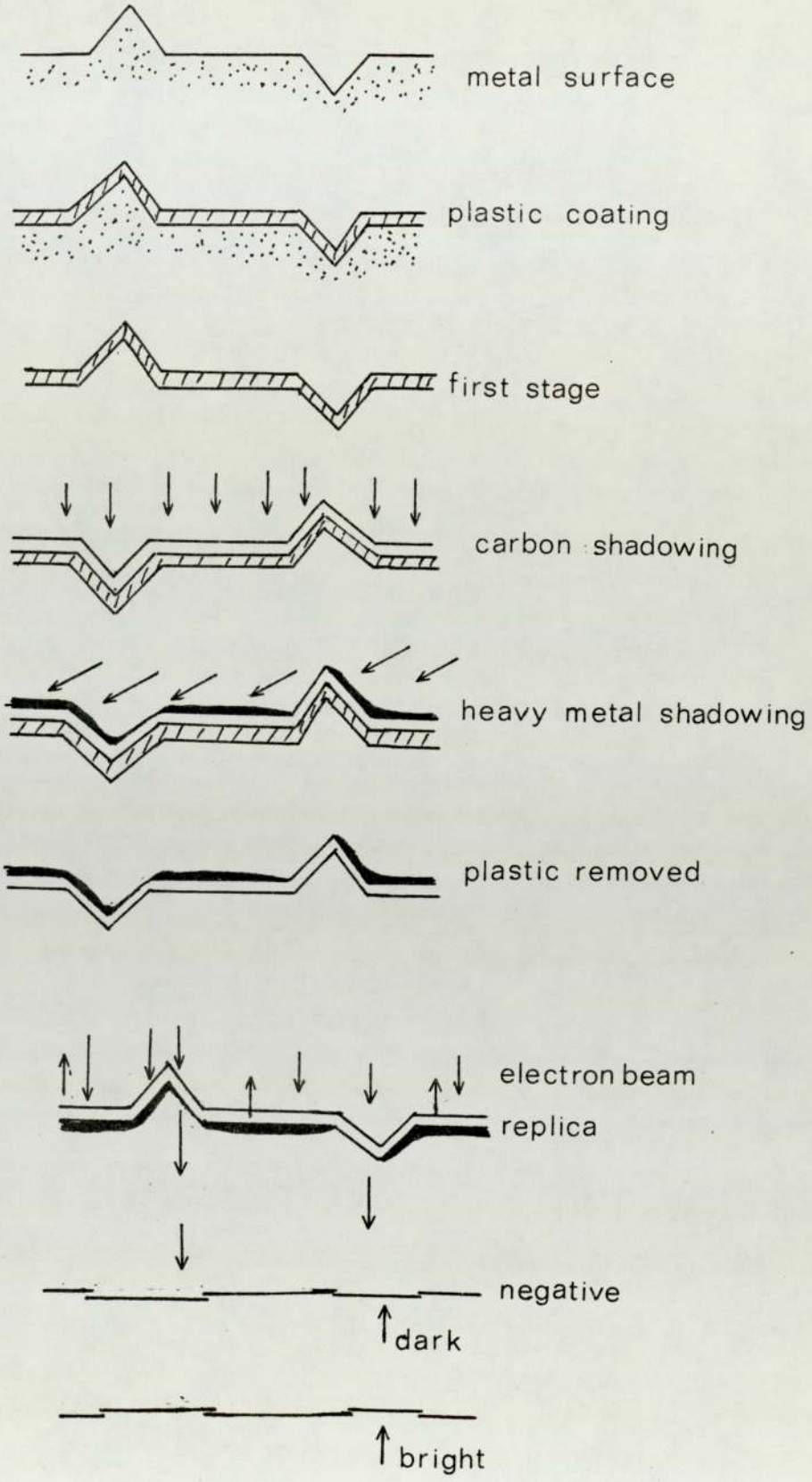

Figure 2.13 Carbon Replicas

2.13 Analysis of wear debris

Wear debris from the pin-on-disk machine was in the form of a very fine powder. A useful technique for analysis of this debris is an x-ray powder method. The debris was collected and then washed and separated from the kerosene by the use of acetone and an ultracentrifuge. It was then packed into a thin walled capillary of 0.3 mm diameter which was then mounted at the centre of a 114.6 mm diameter powder camera.

Cobalt radiation provided a suitable wavelength, for sample analysis, at 30 ma and 40 KeV for 15 minutes. An iron filter was used to produce an adsorption edge for the radiation.

Samples from tests with 2, 2, 4 Trimethyl-pentane, hydrofined kerosene and a reference aluminium bronze sample were analysed. One sample was also taken from the bore of a lubricity failed two-piston rig test.

2.14 Analysis of fuels

A small amount of work was carried out on the analysis some of the fuel samples used in the Denison wear test experiments.

First of all gas-liquid chromatography was used to analyse selected samples. A 1.524 M by 6.35 x 10^{-3}M column of Apezon was used at a temperature of 127°C (400°K). After 26 minutes the temperature was programmed at 5°C/min until a temperature of 195°C was reached. The sample size used was 1 μ litre. Three samples were analysed, under instruction, at Lucas Aerospace. These were a hydrofined fuel which was thought to be free from additives, hydrofined fuel containing 15 p.p.m. of Hitec E515, and a fuel which had become discoloured due to storage.

Mass spectroscopy was also used to look at samples of hydrofined fuel, hydrofined fuel with 15 p.p.m. of Hitec and a

sample Hitec E515. The test conditions using a vacuum generators M.S.9 system were a 4 kV beam voltage, electron energy of 70 eV, a trap current of 100 μA and trap pressure of 10^{-6} Torr. A number of tests were carried out at temperatures of 50°C, 150°C, 250°C and 300°C to see if the additive would distill off at higher inlet temperatures. A few tests were also carried out using an M.S.10 instrument with a mass range up to 200 (compared to 400 for the M.S.9). Operating conditions in this case was 50 μA trap current and impeller voltage -0.1V. The trap pressure in this case was 2.1×10^{-1} Torr and the inlet was initially pumped down to 5×10^{-1} Torr. Sample was admitted to the inlet system until the pressure rose to 2.2 Torr. Final inlet was through a bleed valve.

Finally some experiments were carried out using the optical technique of ellipsometry. A typical instrument arrangement is shown in figure 2.14. This method is more fully described in Appendix III. Three sets of samples were prepared for analysis namely a hydrofined fuel, a hydrofined fuel with additions of Hitec E515 at room temperature and between 80 and 85°C and various concentrations of this additive in hydrofined fuel. Most of this work was carried out using silver plated slides of dimensions 10 x 20 x 2 mm. Silver was selected because it has good reflectivity, does not form oxides easily and has easily obtainable optical constants. Further tests were carried out by forming films on KE 961 steel, DTD 197A aluminium bronze and aluminium. All samples were throughly decreased in a vapour bath with petrol before use in the experiments. The steel and bronze slides were manufactured to the same surface finish as found in the fuel pumps. These samples were left immersed in Hitec E515 for a period of one week, at room temperature, to allow surface reactions to take place.

Silver plated slides were used to find the effect of temperature

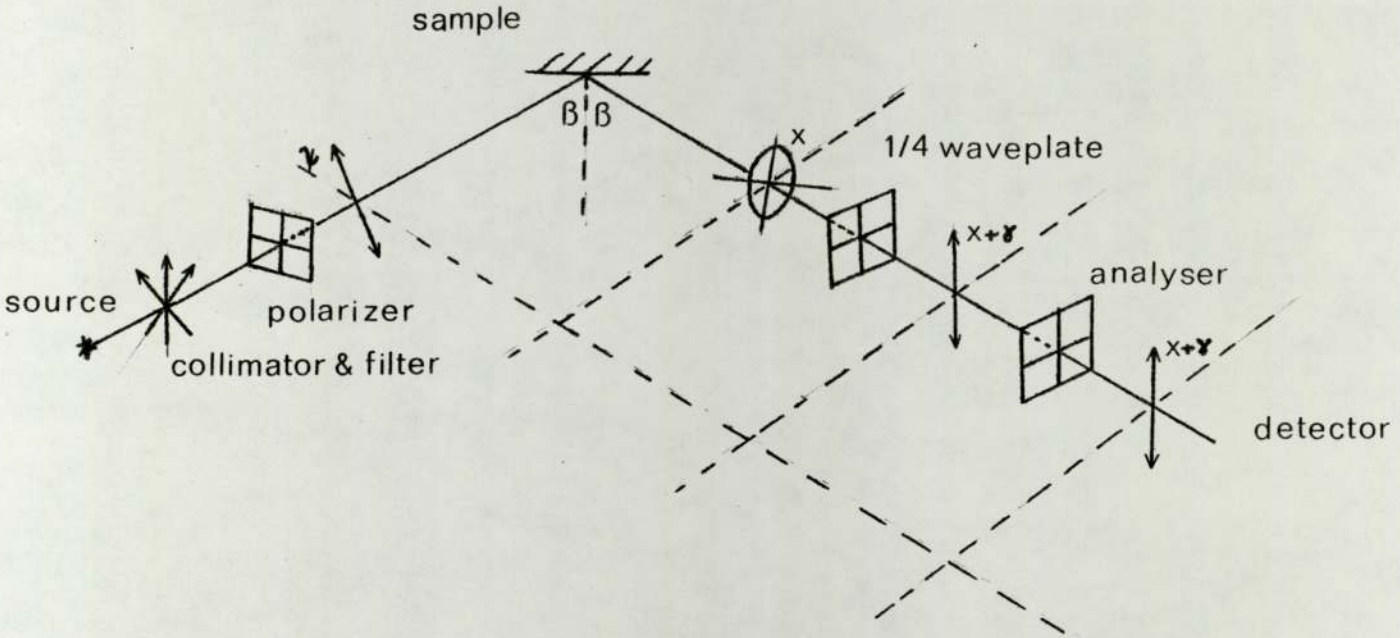

$$\Delta = 2x - 90 = 2\gamma$$

$$\frac{r_p}{r_s} = \tan\psi e^{i\Delta}$$

Figure 2.14, Ellipsometry.

on the adsorption of the additive. Polariser and analyser readings were taken for the clean slide which was then dipped into the additive at 20°C. The slide was then withdrawn at right angles to the surface so that a uniform film formed and excess fluid allowed to drain off the surface. The polariser and analyser readings were then retaken. One of these samples was then allowed to dry and the readings were taken again. Similar measurements were then made for slides heated to about 85°C in isopropyl alcohol.

Measurements were also made on silver plated slides for fuels containing 100, 10, 1, 0.1 and 0.01% by weight of additive to see if a 15 p.p.m. concentration could be detected.

Similar measurements were attempted with the various metallurgies mentioned above. Two different ellipsometers were used to make these measurements. The reference azimiths were 4°, 94°, 184° and 274° for the polariser, 32°, 122°, 212° and 302° for the analyser and 108° and 198° for the quarter wave plate. The quater wave plate was set at 153° and green light of wavelength 5894$\mathring{A}$ at an angle of incidence of 61.5° was used for the measurements. The reference azimiths for the ellipsometer used to make the concentration variation measurements were 46.4°, 136.06°, 227.23° and 316.43° for the polariser, 41.45°, 133.03°, 220.65° and 312.73° for the analyser and the reference axes of the quater wave plate were 73.5°, 163.2°, 253.4° and 343.45°. The quater wave plate was set at 118° for these measurements.

CHAPTER 3

EXPERIMENTAL RESULTS

The experimental results presented here will be divided up into sections similar to those used for the description of the experiments. The results of the mechanical tests will be given followed by the analysis. The latter will commence with the results of the optical microscopy which was used to select samples for detailed analysis with the more sensitive analytical techniques.

3.1 The Lucas Two Piston Rig

Measurement of pressure, flow rates and temperatures did not give any indication of immediate failure. Wear debris, however, was observed in the flow meter on the outlet side of the test pump. A lubricity failure was produced using hydrofined fuel after 10 hours running at 4000 r.p.m. and 12.41 MN m^{-2} pressure. Testing with hydrofined kerosene with 15 mg. $litre^{-1}$ of Hitec E515 greatly reduced the wear. The failure test produced an increase in bore size of up to 0.254 mm whilst testing with fuel and additive produced 0.046 mm increase in bore size after twice the running time. Pistons and sleeves from the rig are shown in Plates VI, VII, VIII illustrating failure and unfailed cases.

3.2 Denison wear tests

3.2.1 Stribeck curves

The stribeck curves suggested that boundary lubrication conditions occurred in the speed range 150 to about 600 r.p.m. with loads of 2.5 Kg to 15 Kg which would be suitable test conditions. The curves were dependent on the surface finish of the discs. This

PLATE VI: TWO PISTON RIG PISTONS

(LEFT: FAILURE)

PLATE VII: TWO PISTON RIG BORE

(GOOD CONDITION)

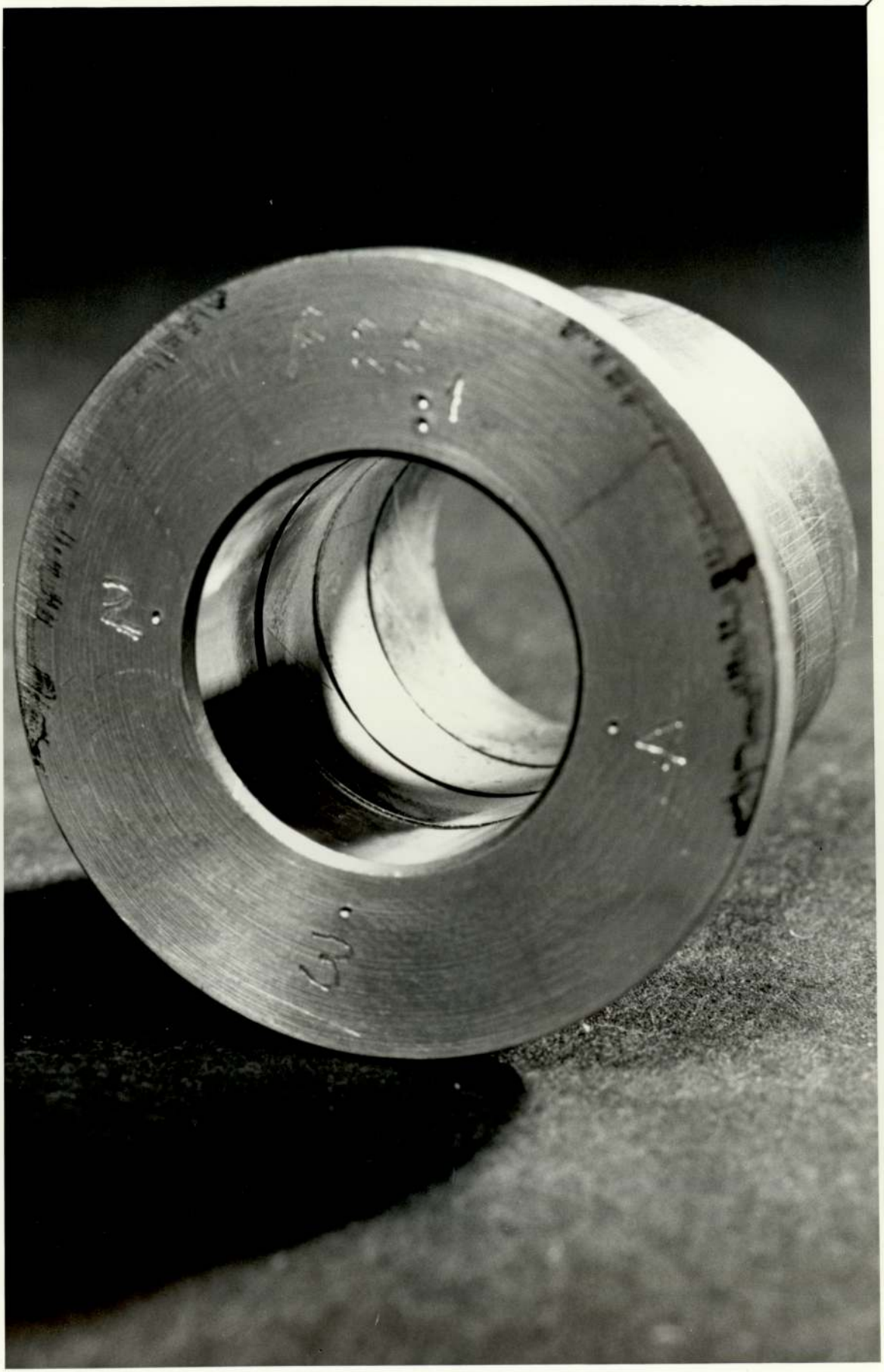

PLATE VIII: TWO PISTON RIG BORE

(FAILURE)


R 2

is expected since an alternative plot of the Stribeck curve is coefficient of friction against film thickness ratio which is defined as the ratio of effective film thickness to the sum of the c.l.a. surface roughnesses. This effect is shown in figure 3.1 for a hydrofined fuel containing 15 p.p.m. of Hitec. This curve also shows that a very sharp transition, from mixed or boundary conditions to full fluid film conditions, existed for the normal piston surface roughness of better than 0.0254μM (figure 3.1(a)). For the higher surface roughness disk the coefficient of friction did not fall to the full fluid film value (figure 3.1(b)). Contact resistance measurements confirmed that the curve represented different lubrication regimes. A plot of contact resistance and friction force against load shows this in figure 3.2. The curves for the two reference fuels and for alumina filtered hydrofined kerosene are shown in figure 3.3. The 2, 2, 4 trimethylpentane curve has been corrected for the viscosity difference and shows no tendency to fluid film conditions over the range considered. At a speed of 2000 r.p.m. seizure occurred between the pin and disk. A repeat of the measurements at the lower speeds again shows the effect of surface roughness, the coefficient of friction being increased. The Shellsol T curve shows a large amount of scatter particularly at the onset of fluid film lubrication. Finally, the curve for alumina catalyst filtered fuel shows a steady decrease in friction coefficient, to a value of about 0.03, until at 2000 R.P.M. seizure occurred. A similar fuel with the addition of 15 p.p.m. of Hitec E515 showed a similar result with a seizure occurring at 2500 R.P.M. Increasing the concentration of additive to 50 p.p.m. produced a sharp fall in coefficient of friction, to about 0.001, at a speed of 2000 R.P.M. The results for 0, 15 and 50 p.p.m. concentration of additive in hydrofined 2494 kerosene are shown in figure 3.4.

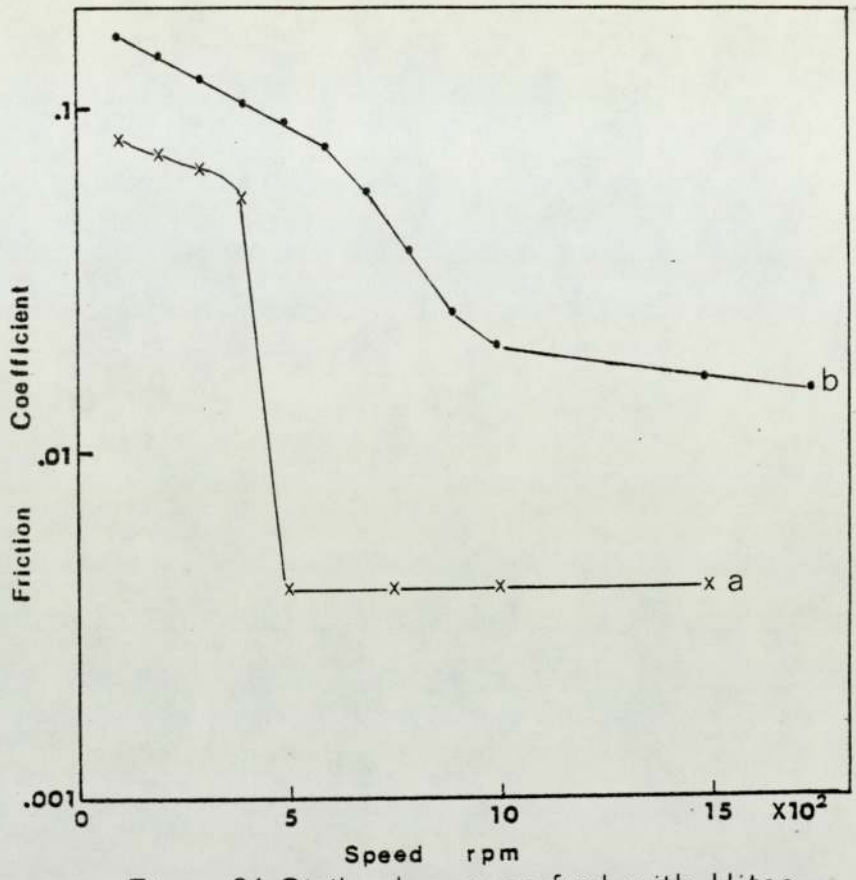

Figure 3.1 Stribeck curves fuel with Hitec
a) 0·0254 μm cla b) 0 06 μm

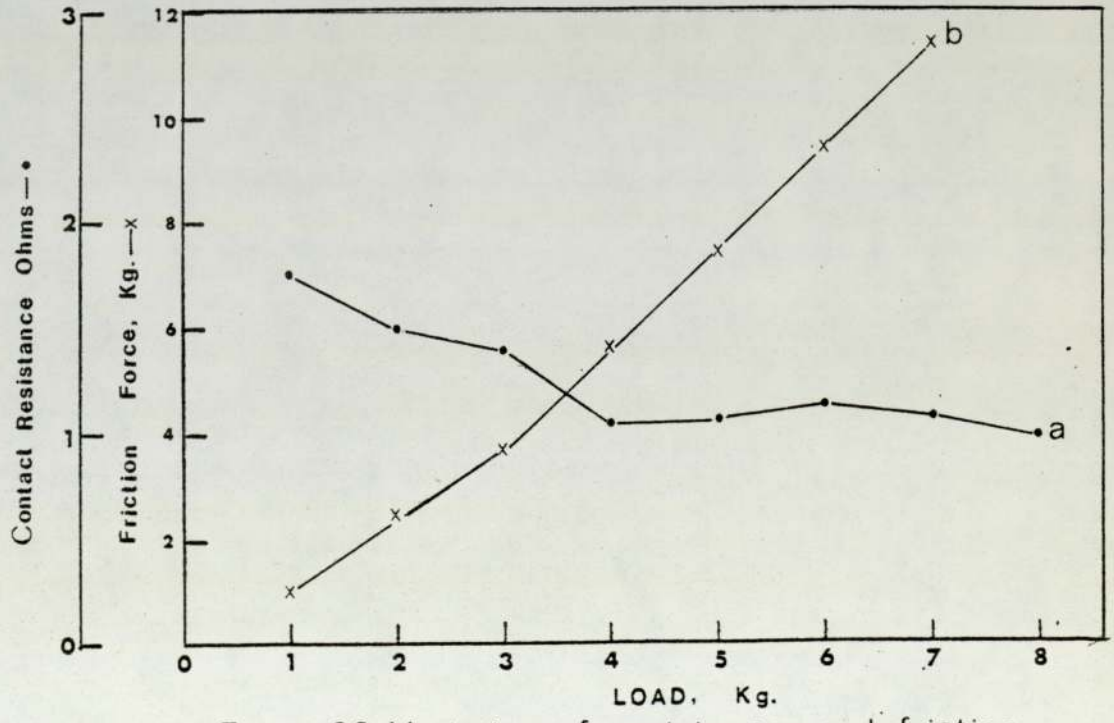

Figure 3.2 Variation of resistance,a,and friction force,b, with load

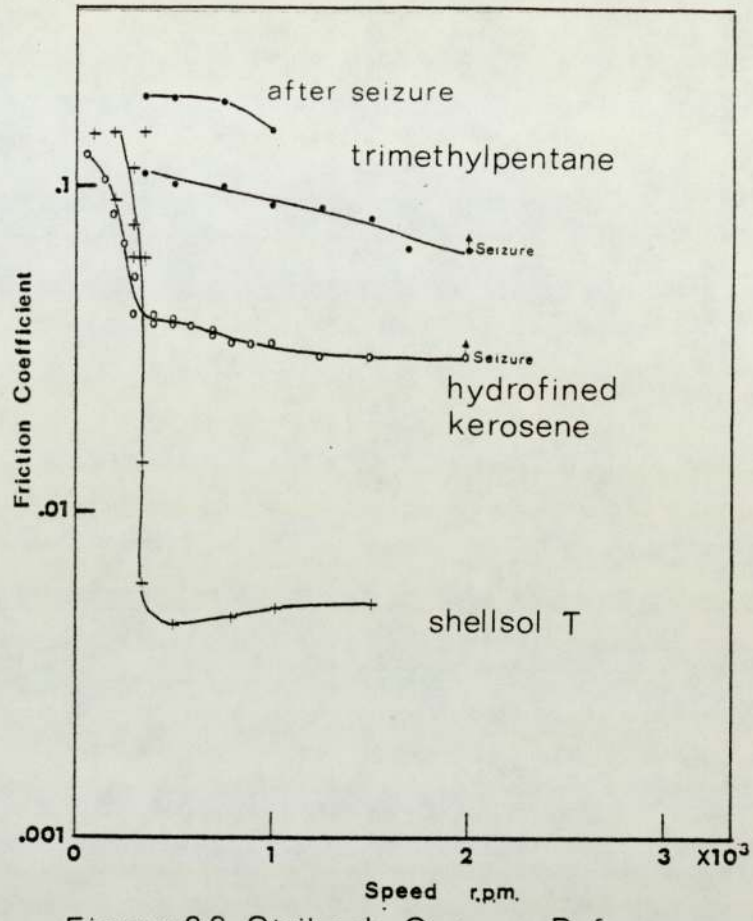

Figure 3.3, Stribeck Curves – Reference Fuels.

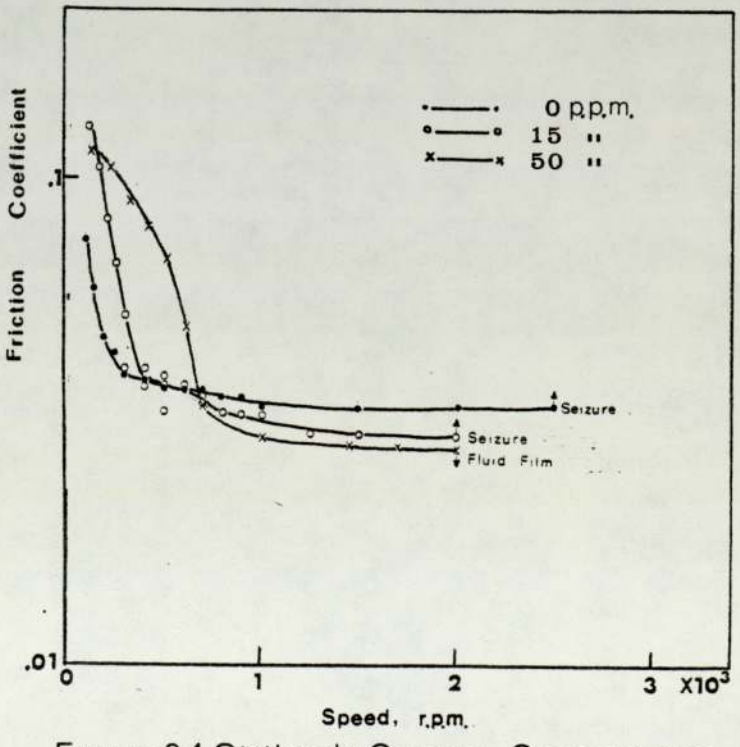

Figure 3.4, Stribeck Curves – Concentrations of Hitec.

These results show a difference between two samples of hydrofined kerosene with a nominal addition of 15 p.p.m. of Hitec E515. This may be attributed to surface roughness effects, additive concentration or to metallurgical effects as will be shown later. However, it must be remembered that these tests were only carried out to give an indication of the operating conditions. Consequently too much importance need not be given to the differences between samples in these tests.

3.2.2 Reference fuel wear tests

Tests with 2, 2, 4 trimethylpentane reference fluid produced quite a large amount of scatter. At 1.3 ms^{-1} separate tests gave values of 10^{-7} mm^3 mm^{-1} and 2 x 10^{-8} mm^3 mm^{-1} respectively for the wear rate. For this fluid the wear rate was found to increase with increasing speed, as shown in figure 3.5(a), for a 2 Kg load. Friction was found to be reasonably constant and wear linear with time except for the higher speed tests (2.67 ms^{-1}) where some sharp changes were found in the friction force and in the wear rate. In this case the wear rate was found to be approximately linear over the period of the test. At higher speeds seizure occurred between the pin and disk.

A very large amount of scatter was found with the tests using Shellsol T as shown by figure 3.5(b). The friction and wear were found to be very irregular with large friction 'spikes' occurring as shown in figure 3.6. Typically these 'spikes' lasted about 30 seconds with the maximum coefficient of friction being about 0.17 and the minimum at less than 0.02. Note that for dry wear the coefficient of friction was about 0.4. During the periods of high friction the speed was seen to fall and in some cases seizure occurred. Figure 3.6. also shows that, superimposed on the spike,

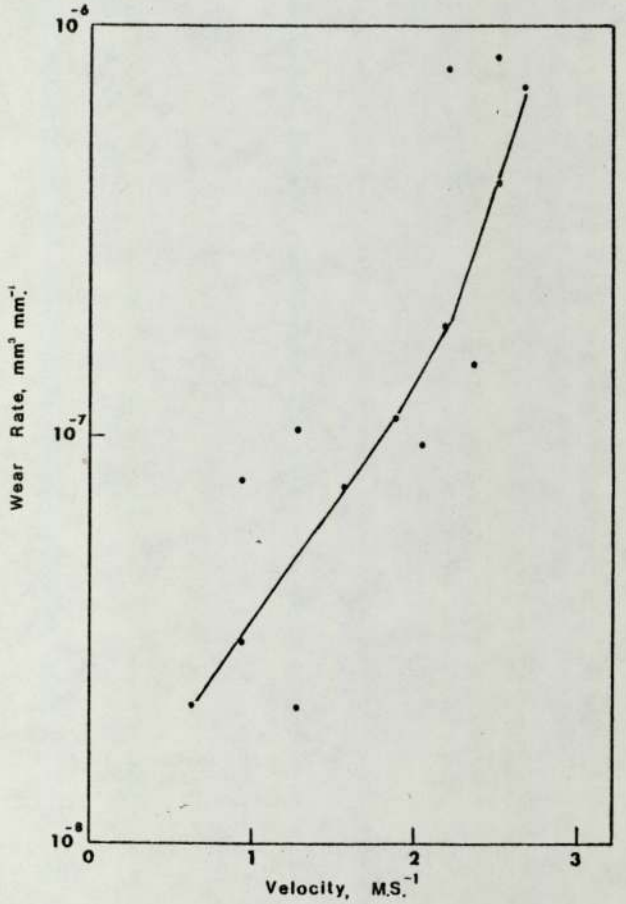

a)Trimethylpentane

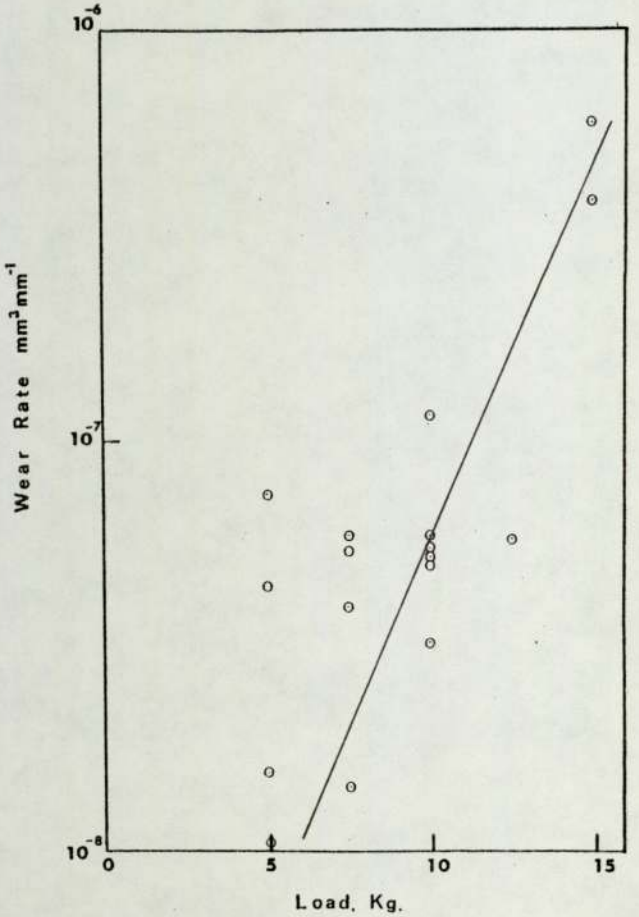

b)Shellsol T

Figure 3.5 Wear Test Results for Reference Fuels

there were oscillations which varied in amplitude. This amplitude variation was particularly large as the friction was falling to the lower value. Note also that there was a period of very steady friction (about 8 seconds in figure 3.6) at the high value friction. Once the coefficient of friction rose above a value of 0.06 the maximum value was rapidly reached in about 7 seconds. The fall to a low value occurred equally as quickly in about 5 seconds. The period between spikes varied but after the run-in time it was normally between twenty and thirty minutes.

Not all tests followed this mode of wear, in fact about 40% had high friction spikes while 35% had periods of steady friction ($\mu \doteqdot .1$) with periods of low friction and no wear. A further 21% had steady friction ending in seizure with the remainder only showing a wear-in phase followed by no wear. Bubbling dry nitrogen through the test fluid before and during the tests had no observable effect.

The alumina catalyst filtered hydrofined kerosene produced steady friction and wear. The wear rate against load curve for 0.62 ms^{-1} is shown in figure 3.7(a). During the tests there was some severe stick-slip with loss of speed in some cases. A similar series of tests with 2 x 10^{-3} M diameter pins produced a similar curve (figure 3.7(b)) and a seizure at 12.5 kg load. Again stick-slip was found to occur.

3.2.3 Wear tests with fuels containing Hitec E515

Figure 3.8(a) shows the variation in wear rate against linear velocity for hydrofined 2494 fuel containing 15 p.p.m. of Hitec E515. The wear rate is expressed in volume removed per unit sliding distance. This graph shows that the wear rates, as calculated from transducer and weight loss measurements, have good agreement. For a constant load the wear rate was found to decrease

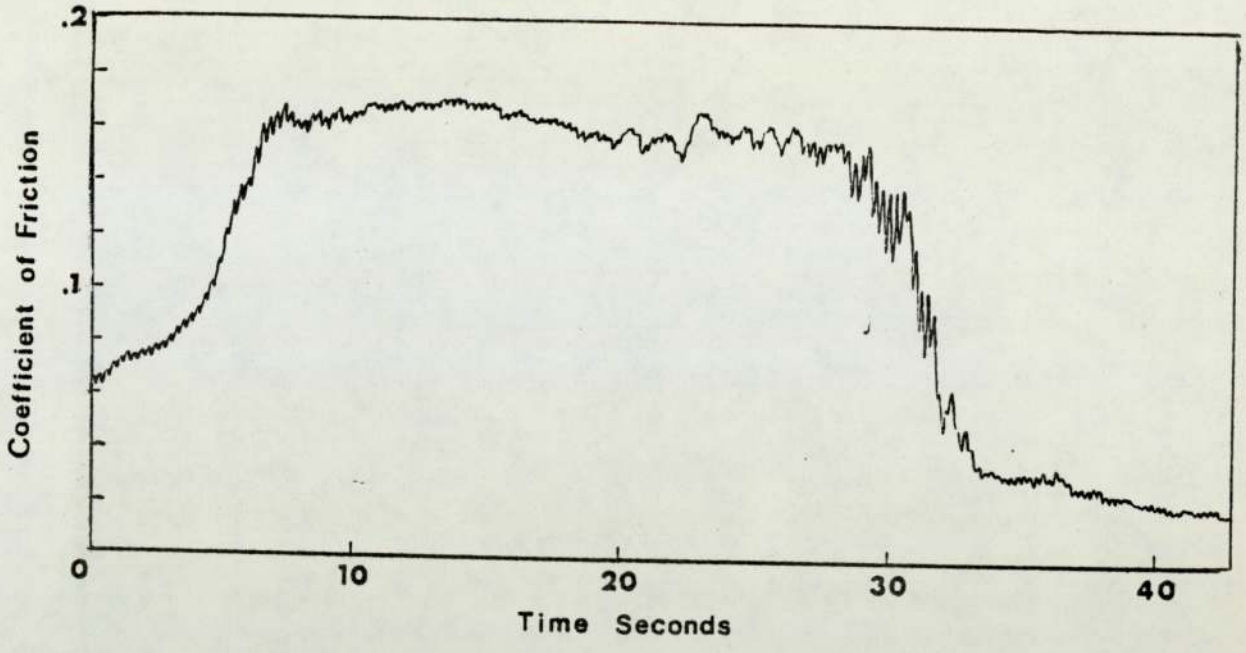

Figure 3.6, Friction Trace for Shellsol T.

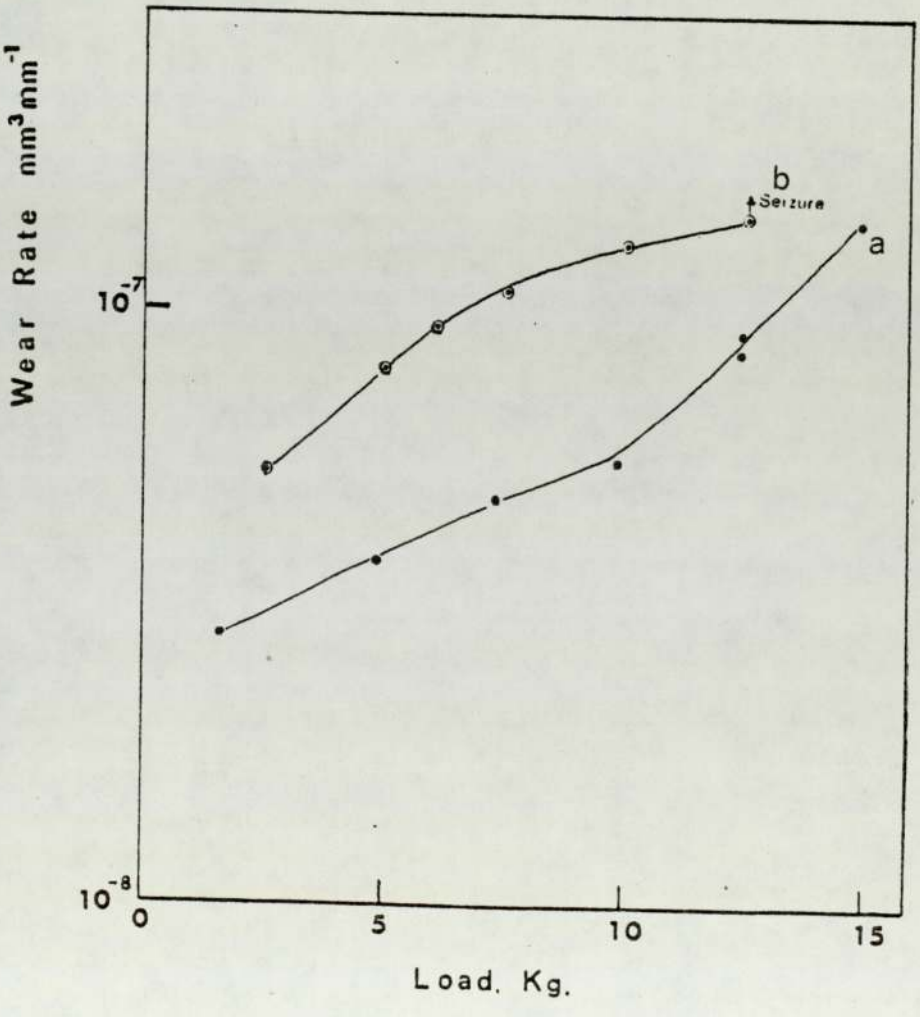

Figure 3.7, Wear Results for Alumina Catalyst filtered fuel a) 3 mm and b) 2 mm pins.

with increasing speed until at some speed zero wear resulted. The point at which zero wear occurred correlated with the fall in friction to a fluid film value on the Stribeck curves. The change in slope between the 5, 10 and 12.5 kg curves indicate a transition point on the wear rate against load curve. The results of a series of tests using loads from 2.5 kg to 15 kg at a speed of 0.62 ms^{-1} illustrate this last point and are shown in figure 3.8(b). It was generally found that the friction remained at a constant value for these tests and that the displacement was linear with time. In a few cases there were periods of low friction (the coefficient of friction being about 0.003 indicative of fluid film conditions) and no wear. The wear followed the same pattern of linearity with time in these cases. Wear rate was calculated from the time of contact and wear, and not from the total wear test time, in these cases. A similar series of wear tests were carried out on a disk of 0.06 μm roughness (compared to 0.02 μm c.l.a.) and in both cases a reduction in wear rate occurred at the higher loads (figure 3.8(c)). For the higher roughness disk the wear rate is a maximum at a load of 8 kg and for the lower roughness 12.5 kg. Some of the tests which were carried out on the higher roughness disk were of short duration (15 to 20 minutes) but the results from these tests were found to be similar to the standard tests. In all cases the frictional force remains steady but some non linearity was observed in the wear. Note that at the higher loads with increased roughness the scatter in results became quite large. Reasons for this will be discussed later.

The addition of 15 p.p.m. of Hitec to alumina filtered fuel prevented seizure occurring at 12.5 kg load on a 2 x 10^{-3} M wear pin. In this case the transition point was not obvious, the wear rate being similar over the entire range of loads. At the lower

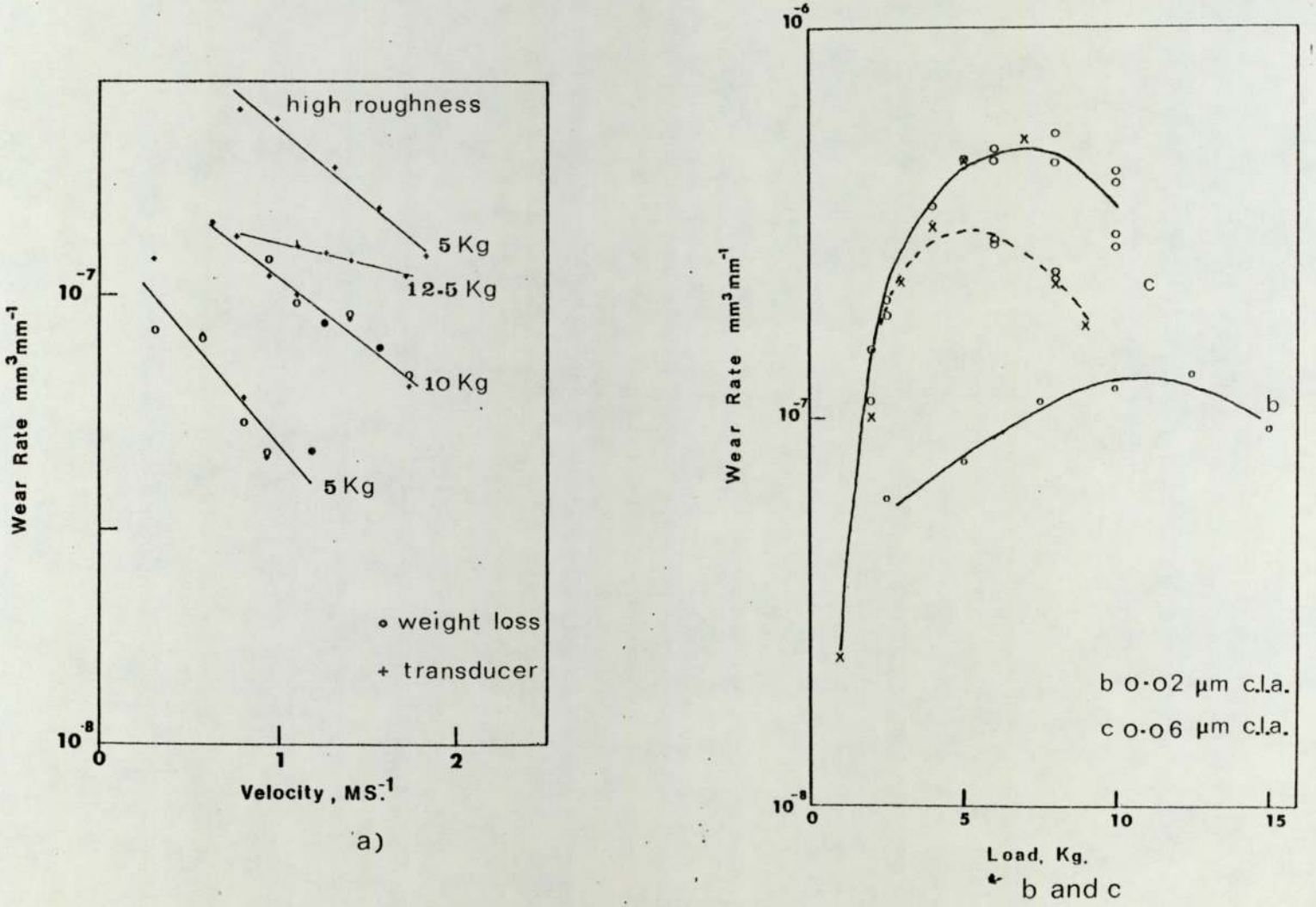

Figure 3.8 Wear Results for Hydrofined Kerosene plus Hitec.

loads the effect of the additive appears to have been pro-wear compared to the hydrofined fuel tests. Figure 3.9 shows this comparison between the fuel with and without the additive for these small diameter wear pins. More will be said about these differences in the discussion chapter.

Table 3.1 shows the results of adding various concentrations of additive to the fuel. Test 1 was the original zero concentration

Table 3.1 Concentration effects of Hitec E515

Test	Concentration p.p.m.	Wear Rate $mm^3\ mm^{-1}$
1	0	5.5×10^{-8}
2	15	$9.9 \times 10^{-8}/0$
3	30	0
4	15	0
5	7.5	0
6	0	7.03×10^{-8}
7	0	5.1×10^{-8}

LOAD = 10 kg SPEED 0.62 ms^{-1}

wear test with alumina filtered hydrofined kerosene. After the addition of 15 p.p.m. of Hitec the wear rate was observed to increase (test 2). After a period of 90 minutes the wear rate then dropped to zero. Increasing the concentration produced a zero wear condition as shown by test 3. On dilution of the test 3 fuel to 15 and 7.5 p.p.m. it can be seen that zero wear still existed in test 4 and test 5 showing a memory effect of the additive. The use of additive free hydrofined fuel produced wear again (tests 6 and 7)

with test 6 giving a result close to the original zero concentration test.

3.2.4 Statistical Analysis

The results which have been presented graphically have more meaning when some idea of the spread of results is known. Table 3.2 shows the results of a statistical analysis on wear rate measurements from 10 kg load, 0.2 ms^{-1} tests with hydrofined fuel with and without Hitec E515.

Table 3.2 Statistical analysis of wear results

Sample	Mean $\bar{x}$	Sample σ_n	Population σ_n
Alumina filtered hydrofined kerosene + Hitec	1.22×10^{-7}	6.9×10^{-8}	7.32×10^{-8}
Same without Hitec	9.95×10^{-8}	4.04×10^{-8}	4.29×10^{-8}

This analysis was based on 13 results from each sample and assumes a normal distribution. Strictly this assumption cannot be made with such a small sample size and so non-parametric statistics should be used for the analysis. The results from this type of statistic indicate that the distribution was in fact normal. The result from this comparative type of statistic suggest that there is little difference between the mean wear rates measured for the two samples under the same conditions. Table 3.3 shows the ranking of the results for the Wilcoxon test for the paired case.

Table 3.3 Results for Non-parametric statistical analysis

Wear Rate $mm^3\ mm^{-1}$

15 p.p.m.Hitec	0 Hitec		
X	Y	$D = X-Y(x10^{-8})$	Rank
9.9×10^{-8}	7.03×10^{-8}	2.88	5
1.42×10^{-7}	5.09×10^{-8}	9.16	7
7.63×10^{-8}	9.3×10^{-8}	-1.67	4
7.5×10^{-8}	6.29×10^{-8}	1.21	2
7.5×10^{-8}	8.79×10^{-8}	-1.29	3
7.0×10^{-8}	1.71×10^{-8}	-10.1	8
7.3×10^{-8}	7.34×10^{-8}	-0.04	1
2.4×10^{-7}	1.57×10^{-7}	8.3	6
2.5×10^{-7}	1.29×10^{-7}	12.1	9

From this Table the probability of finding a sum of ranks among all sums of negative D value ranks ≤ 16 was found to be, for a two tailed test, $2P = 2.34$. This is then a measure of the significance of the different wear rates measured for the two samples.

3.2.5 Subsidiary wear tests

The results of varying the initial surface roughness of the wear pins are shown in figure 3.10. These results lie within the scatter predicted by the statistical analysis on previous samples. Consequently no firm conclusions could be drawn from these results.

Some tests carried out on a commercial hydrofined fuel not containing Hitec produced a large amount of scatter and a friction mode similar to the spikes found with the Shellsol T wear tests.

The wear rate against load curves for two speeds, 0.62 and 1.24 ms^{-1} are shown in figure 3.11.

Figure 3.12 shows the results for dry wear tests carried out with aluminium bronze wear pins. Even in these tests quite a large amount of scatter was observed, as shown, but the general trend was for the wear rate to increase with load until seizure occurred at 5 kg.

Finally the results for tests using duralumin wear pins are shown in figures 3.13 and 3.14. Shellsol T and hydrofined 2494 both produced seizure at a load of 12.5 kg. Addition of 15 p.p.m. Hitec E515 prevented seizure occurring and, at a load of 2 kg the wear rate dropped to zero after a short period. A fall in wear rate was also observed for Shellsol T and hydrofined fuel at,or below,this load. For loads between 2 and 12.5 kg the wear rates were similar for all three fuels, (see figure 3.13). Figure 3.14 shows the effect of varying the concentration. Consecutive tests with 0, 7.5, 15 and 30 produced a steady fall in wear rate with concentration but at 40 p.p.m. there was an increase in wear rate. A repeat of the 15 p.p.m. concentration then produced a higher wear rate and a test at 20 p.p.m. concentration also produced a wear rate above what might have been expected. This then again indicates a pro-wear effect with aluminium present.

3.2.6 Temperature measurements

Measurements made under lubricated conditions showed no signs of any high temperature spikes. In general the output was in the range of 5 mV to about 20 mV representing temperatures of between 50 and 100°C. A reasonable average for these tests is about 75°C. The temperature profile generally remained constant over one revolution of the disk but in some cases there were hot spots on the disk.

The dry wear situation was found to show high voltage spikes

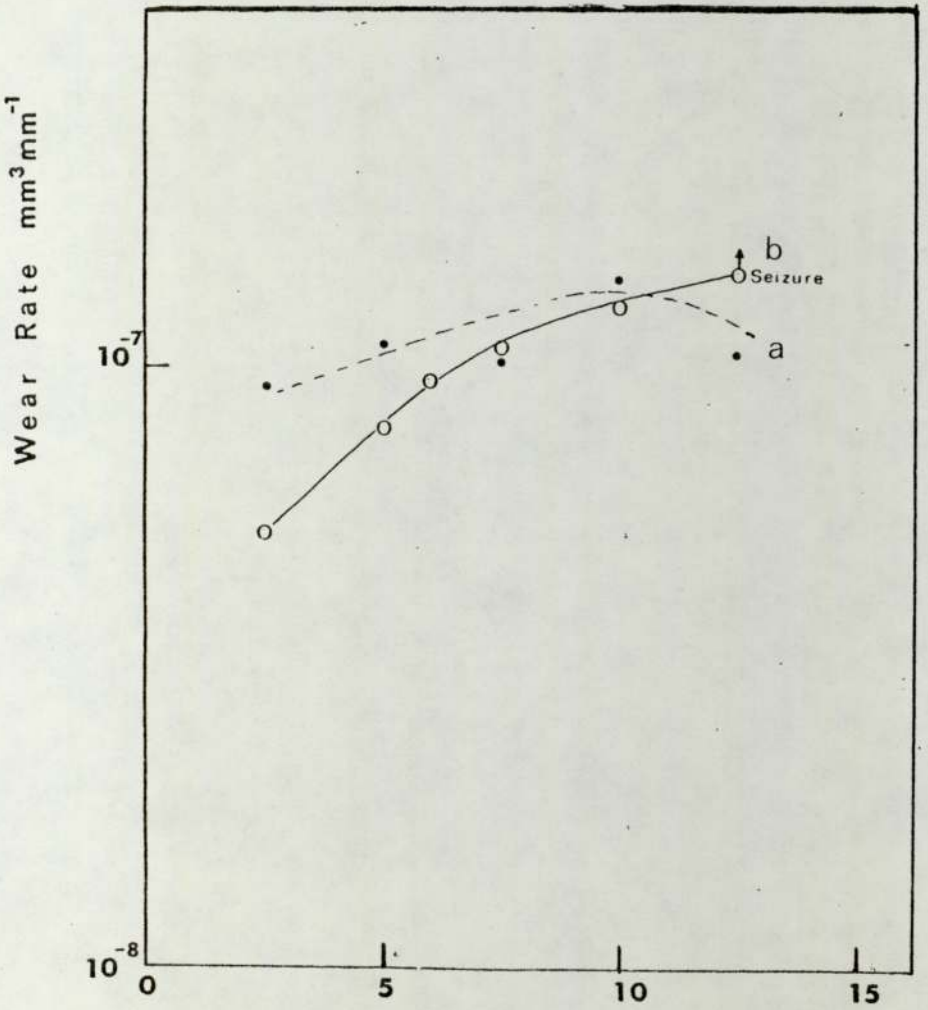

Figure 3.9, Comparison between fuel a) with and b) without Hitec - 2 mm ∅ pins.

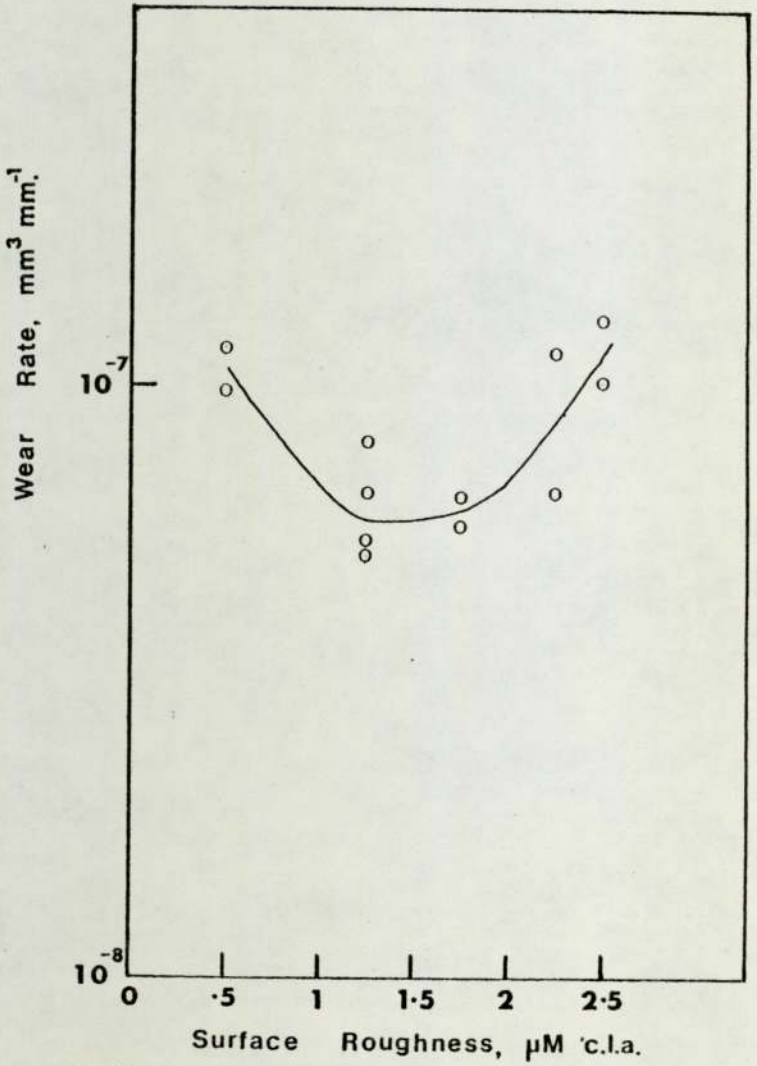

Figure 3.10 Effect of pin roughness on wear.

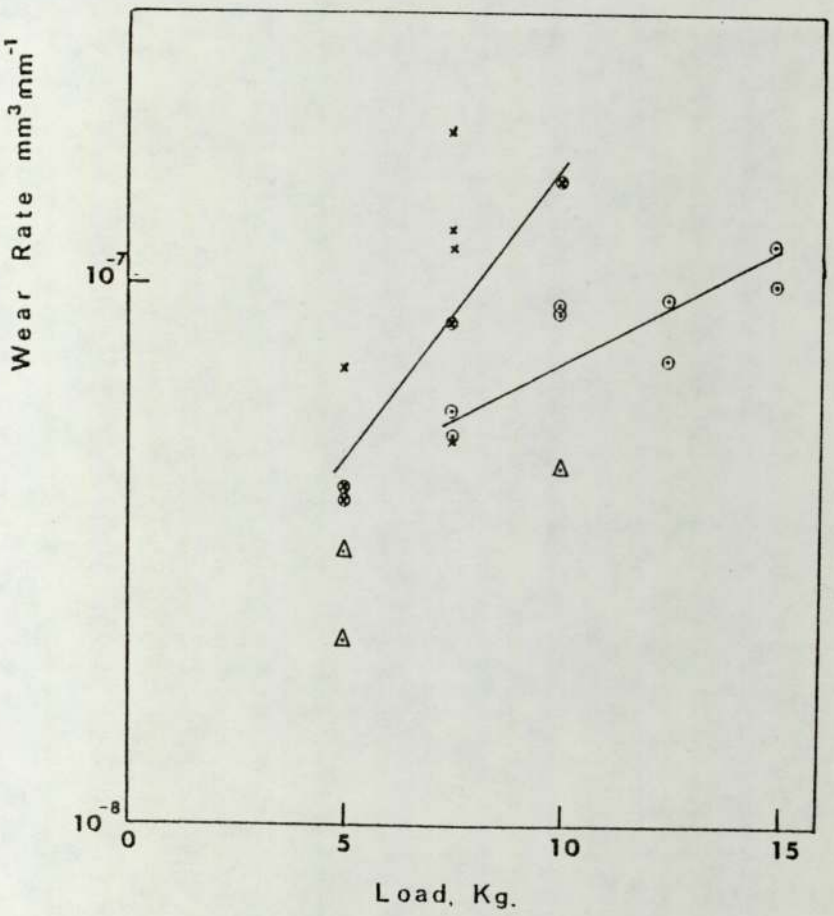

Figure 3.11, Hydrofined kerosene Wear Results

⊗1·24 M S^{-1} – ⊙ 0·62 MS^{-1}

x, △ Insufficient wear to be reliable.

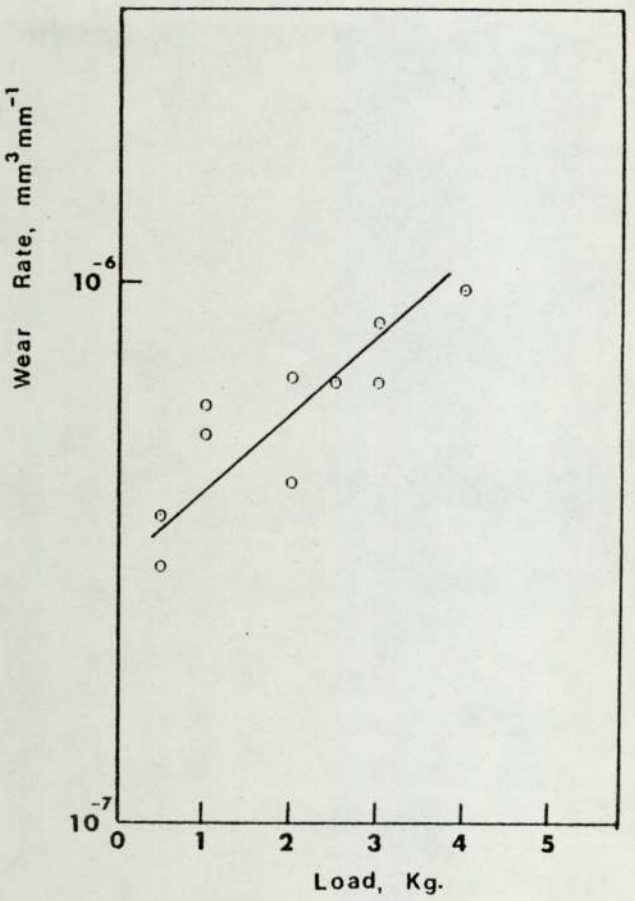

Figure 3·12 Dry Wear Results.

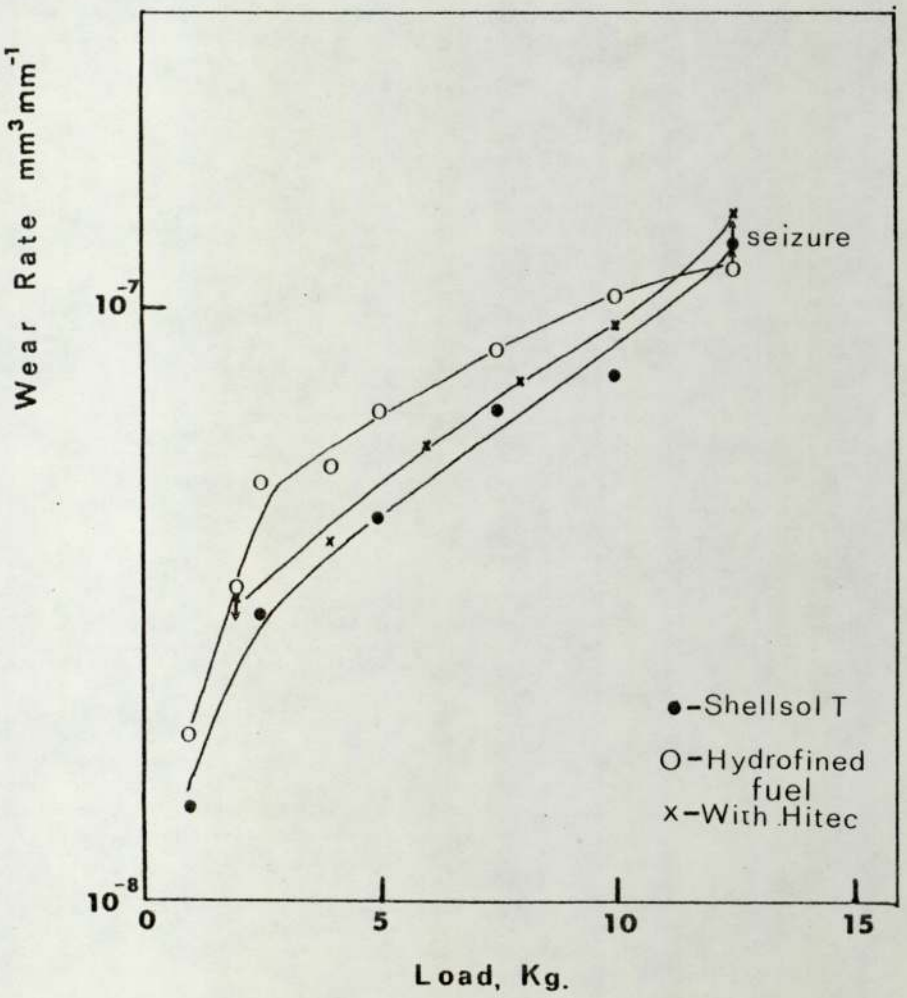

Figure 3.13, Wear Rates for Duralumin Wear pins.

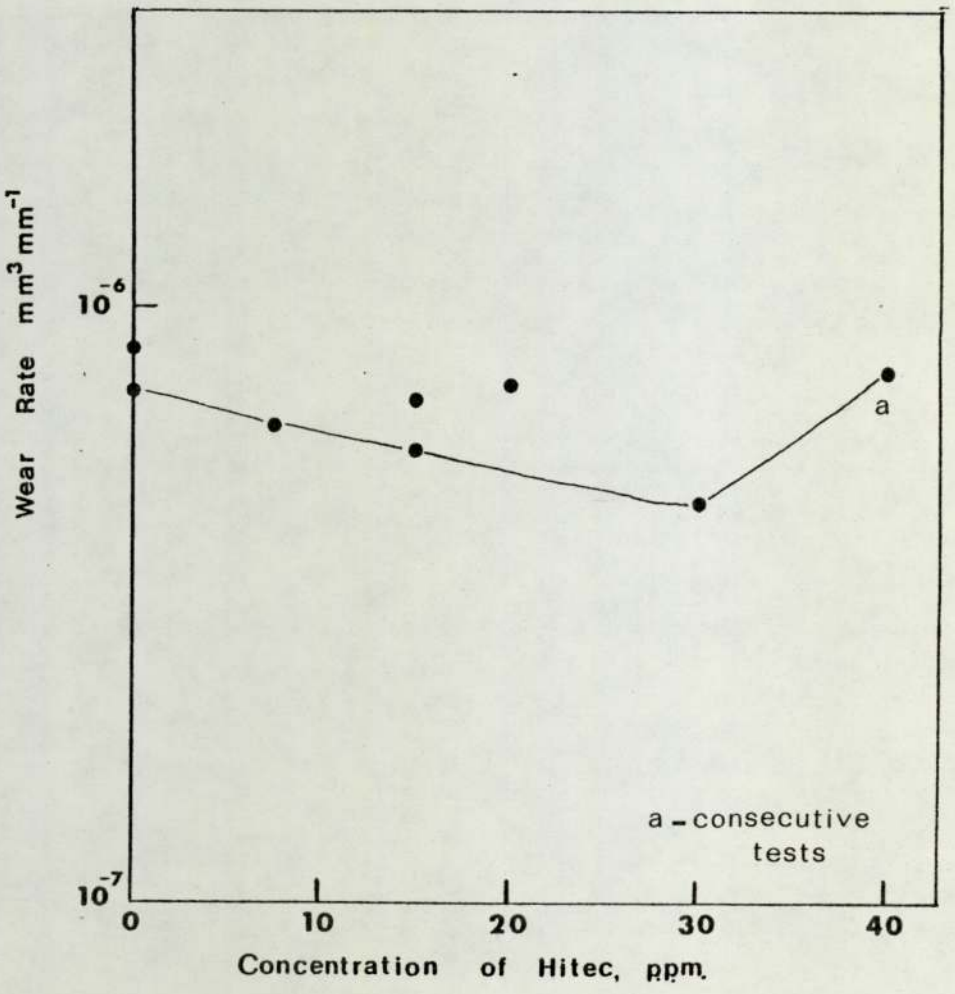

Figure 3.14, Effect of Hitec on the Wear of Duralumin.

on the output. Figure 3.15 shows three typical outputs under dry wear conditions. These traces represent the temperature profile over one revolution of the disk at a speed of 0.62 ms^{-1} and 1.5 kg load. The maximum output was found to be approximately 100 mV with a 'bulk' temperature output voltage of about 40 mV. These values represent a temperature range of 185 °C to approximately 400°C if one assumes a linear extrapolation of the calibration curve. The temperature coefficient, assuming a linear relationship to 100°C was 6.5 μV/°C for this basic iron-copper junction compared to 54 μV/°C for iron constantan and 46.5/μV/°C for copper constantan.

3.3 Analysis of Samples

3.3.1 Optical microscopy

Inspection of the wear pins indicated very strongly that if additive was present then the surface was copper rich in colour. Hydrofined fuels produced wear pins which were a bright clean aluminium bronze colour. In some cases pins were found to be in an intermediate state between regions of copper rich material surrounded by the normal aluminium bronze colour. Some examples are illustrated in Plate IX.

It was found that this appearance was related to the friction value in some way. For the tests which finished with a low coefficient of friction 17% were aluminium bronze colour in appearance, 29% were of an intermediate appearance and 54% were copper rich.

On the basis of these results and the wear tests samples were selected for analysis using the physical analytical techniques the results of which will now be presented.

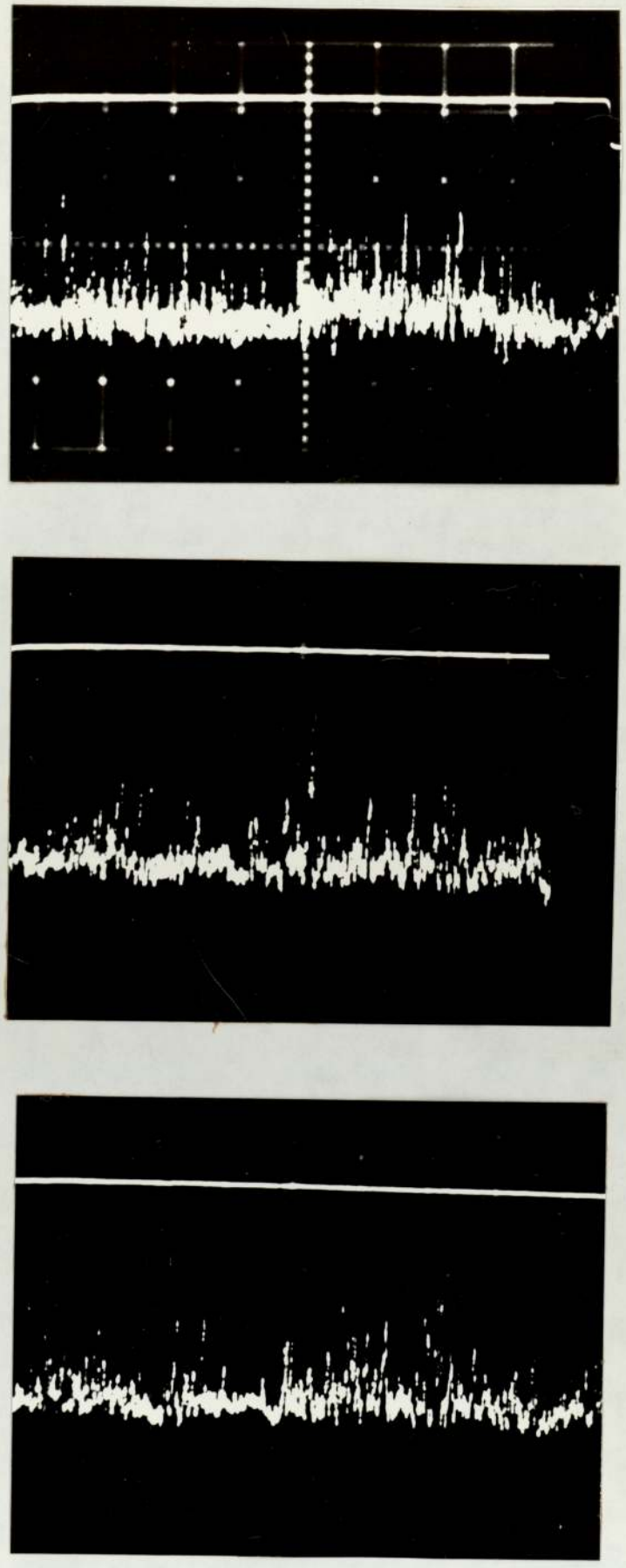

Figure 3.15 Examples of the average pin-disk interface temperatures over 1 revolution of the disk; at 0.62 MS^{-1} and 1.5 Kg load.

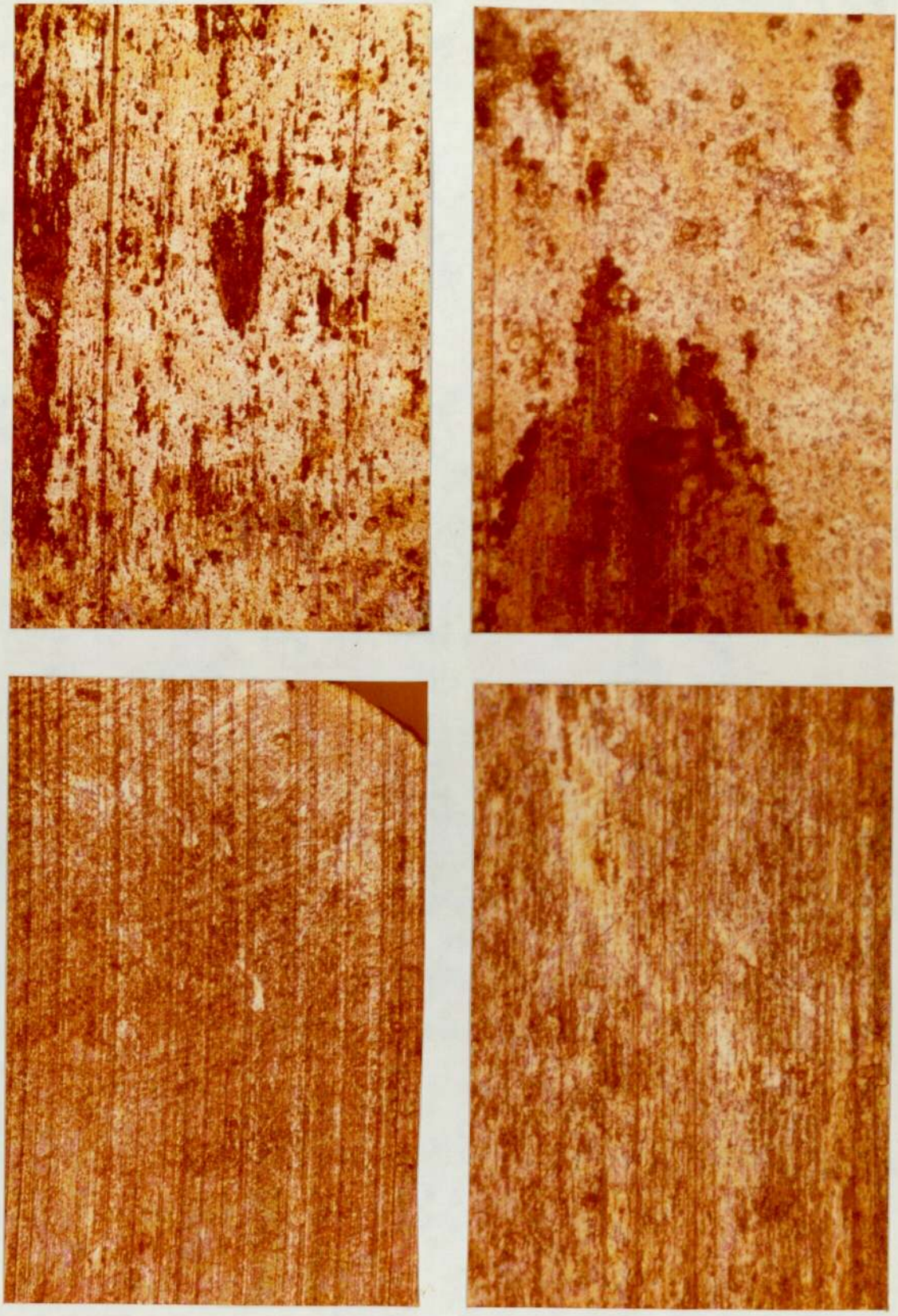

PLATE IX: WEAR PIN SURFACES:
(a) and (b) From tests with fuel plus Hitec,
(c) and (d) From tests with fuel without Hitec.

3.3.2 Auger Spectroscopy

Qualitative differences can be seen between the various samples analysed, using Auger spectroscopy, in the spectra produced.

Most of the samples produced with hydrofined fuel, containing 15 p.p.m. of Hitec E515, did not show any phosphorus to be present on the surface (figure 3.16(a)). The initial spectrum, before sputtering shows sulphur, carbon, nitrogen, oxygen, copper to be present with indications of nickel and iron. After about 800 μA minutes of sputtering iron was clearly resolved. The presence of aluminium will be discussed later. A similar result was found for a wear pin which had been used on a disk of higher surface roughness (0.06μm c.l.a.) but phosphorus was noted on the surface after about 10 μA minutes sputtering (figure 3.16(b)). It was also noted that some chlorine was present in this case.

The origin of the phosphorus was expected to be the phosphate ester component of Hitec E515. Figure 3.17 shows phosphorus present on the surface of unworn aluminium bronze which had been submerged in additive which was at a temperature greater than 100°C. The spectra at zero and about 10 μA minutes sputtering time both show phosphorus, sulphur and chlorine along with carbon, oxygen, nitrogen and copper.

The spectra for aluminium bronze worn in the presence of hydrofined alumina catalyst filtered kerosene and 2, 2, 4 trimethylpentane were very similar (figures 3.18(a), (b)). Obviously no phosphorus was observed on the surfaces in these cases. Again iron became more easily observed after sputtering and, in the case of the hydrofined fuel sample, there was a suggestion of aluminium at the higher energies (about 1400 eV).

Finally spectra for a KE961 steel sample run in hydrofined fuel containing 15 p.p.m. Hitec E515 are shown in figure 3.19. The main

elements observed here were iron, carbon, oxygen and sulphur. Small amounts of chlorine and nitrogen were observed along with indications of chromium.

Aluminium oxide was identified on the bronze wear pin surfaces as plasmon loss and plasmon gain peaks at low energy. Changing the beam energy by $\pm$ 150 eV, about the primary energy of 2KeV, enabled these peaks to have slightly improved resolution. These effects can be observed in figure 3.20 for a number of different sputtering times. The last of this set of spectra shows the effect of defocussing the electron beam. The small unresolved peaks can be seen more clearly in figure 3.21 which is for the 278 μA minute sputter time spectra. Peaks are found at 41 eV, 47 eV, 54 eV, 58 eV, 60 eV and about 67 eV. The peak at 47 eV can be assigned to iron. Peaks at 58 eV and 60 eV are copper peaks, the 58 eV peak being distinct but poorly resolved. In fact the 58 eV appears more as a shoulder on the spectra. The peak at 105 eV is also a copper peak. This leaves us with peaks at 41 eV, 54 eV and 67 eV. The 'shoulder' at 67 eV is a result of the main aluminium peak. The peaks present at about 42 eV and also 54 eV would appear to be the aluminium oxide plasmon loss peaks. Peaks at between 36 and 39 eV were observed on some samples. Consequently this evidence points to the presence of aluminium oxide near, or at, the surface. Note that during sputtering the 54 eV peak has emerged whilst the 67 eV peak diminishes in size (see figure 3.20). Evidence of the unresolved peaks between 60 and 105 eV is shown by the changes of slope of the spectra as the beam energy is increased. This is particularly noticeable at between 67 eV and 80 eV for a beam energy of 1.85 KeV (Figure 3.21).

Sulphur was often resolved as a doublet or triplet when present on the surface of aluminium bronze. A typical resolved

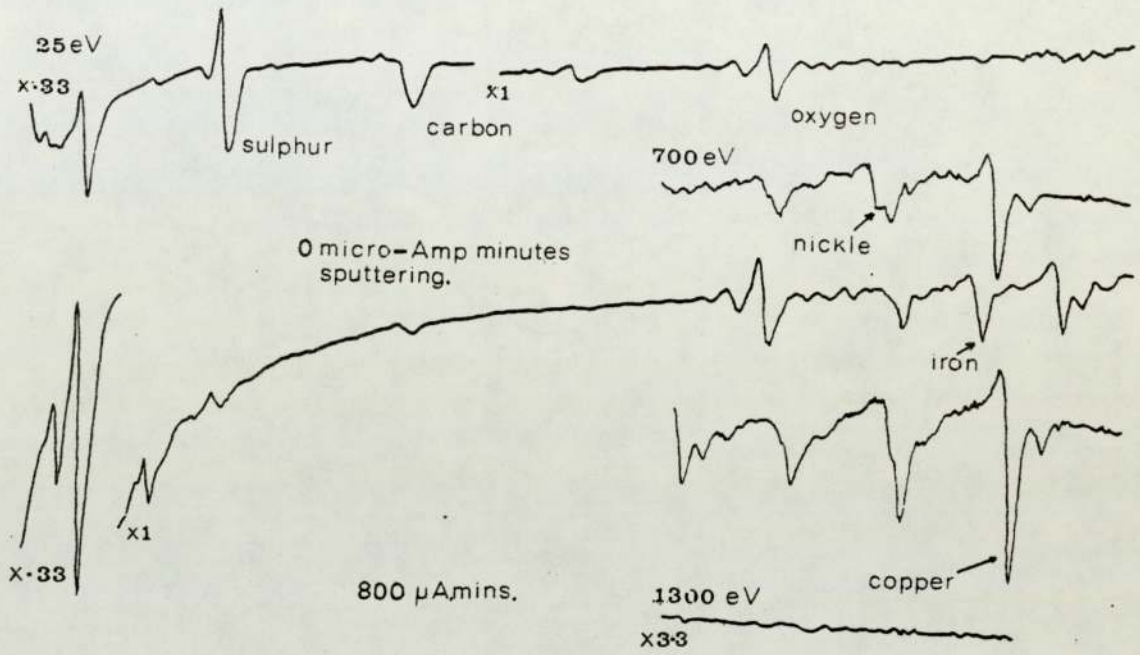

a) Auger spectra for hydrofined fuel plus Hitec bronze wear pin.

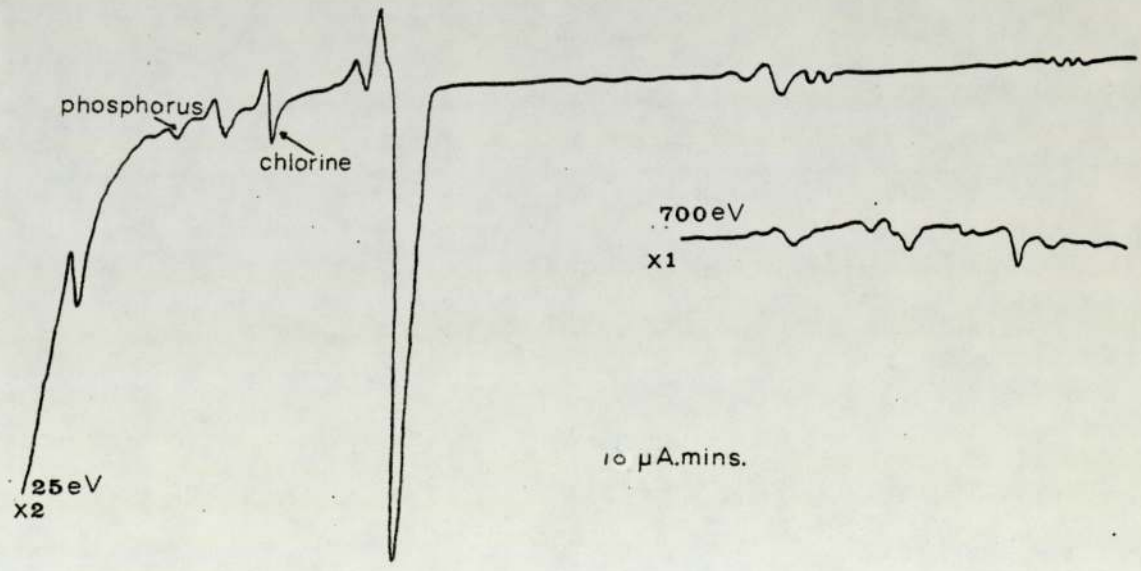

b) as above but 0·06 μm c.l.a.

Figure 3.16

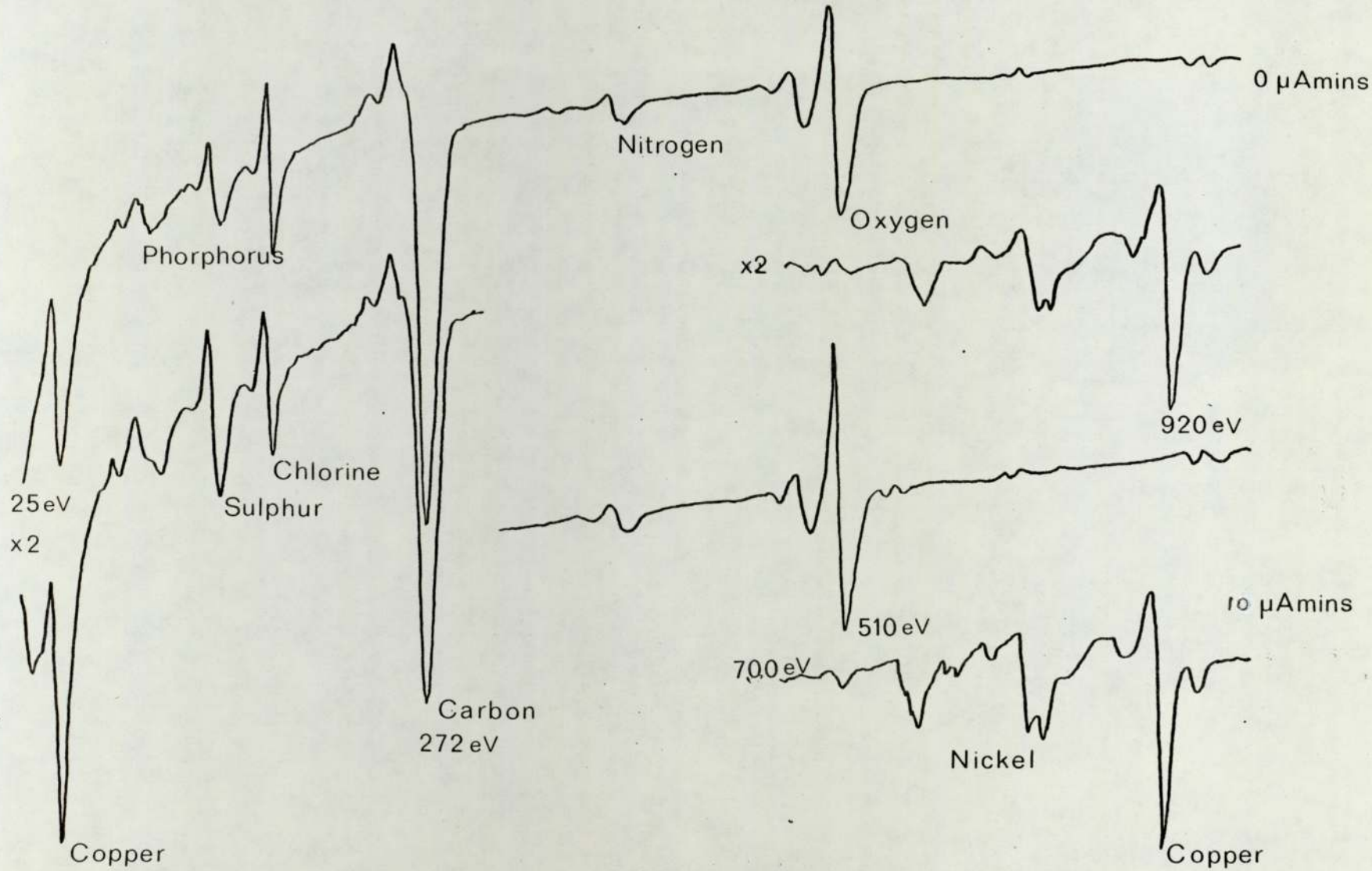

Figure 3.17, Auger Spectra for bronze soaked in Hitec at 150°C.

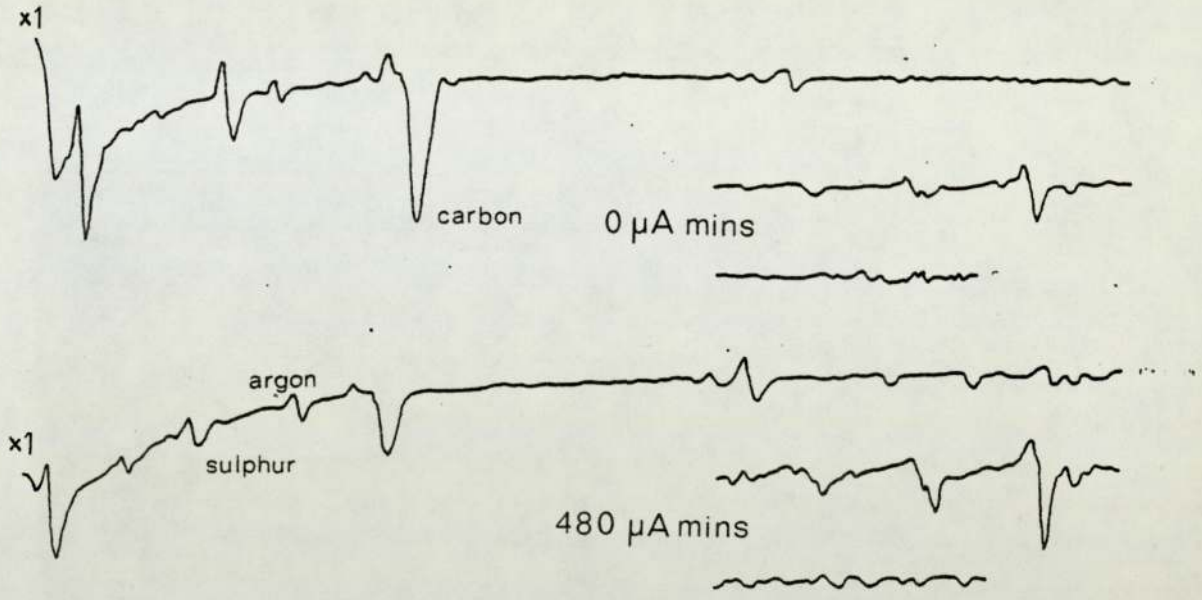

a)Hydrofined kerosene-Auger Spectra.

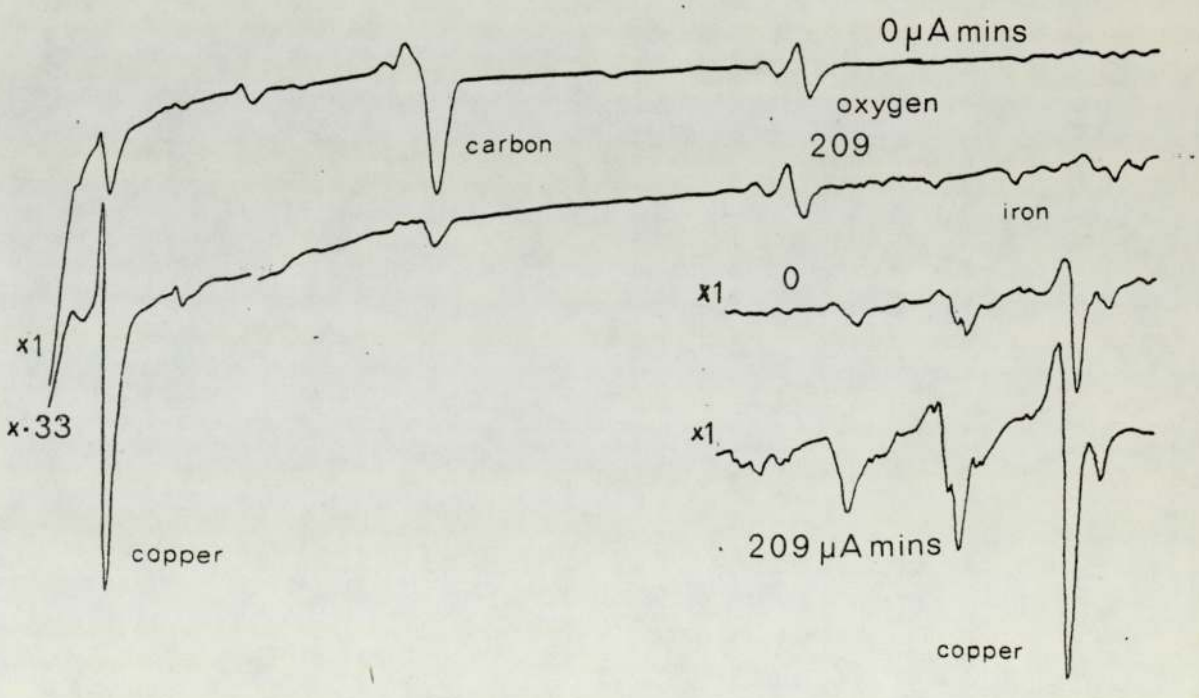

b) 2,2,4 Trimethylpentane - Auger Spectra.

Figure 3.18

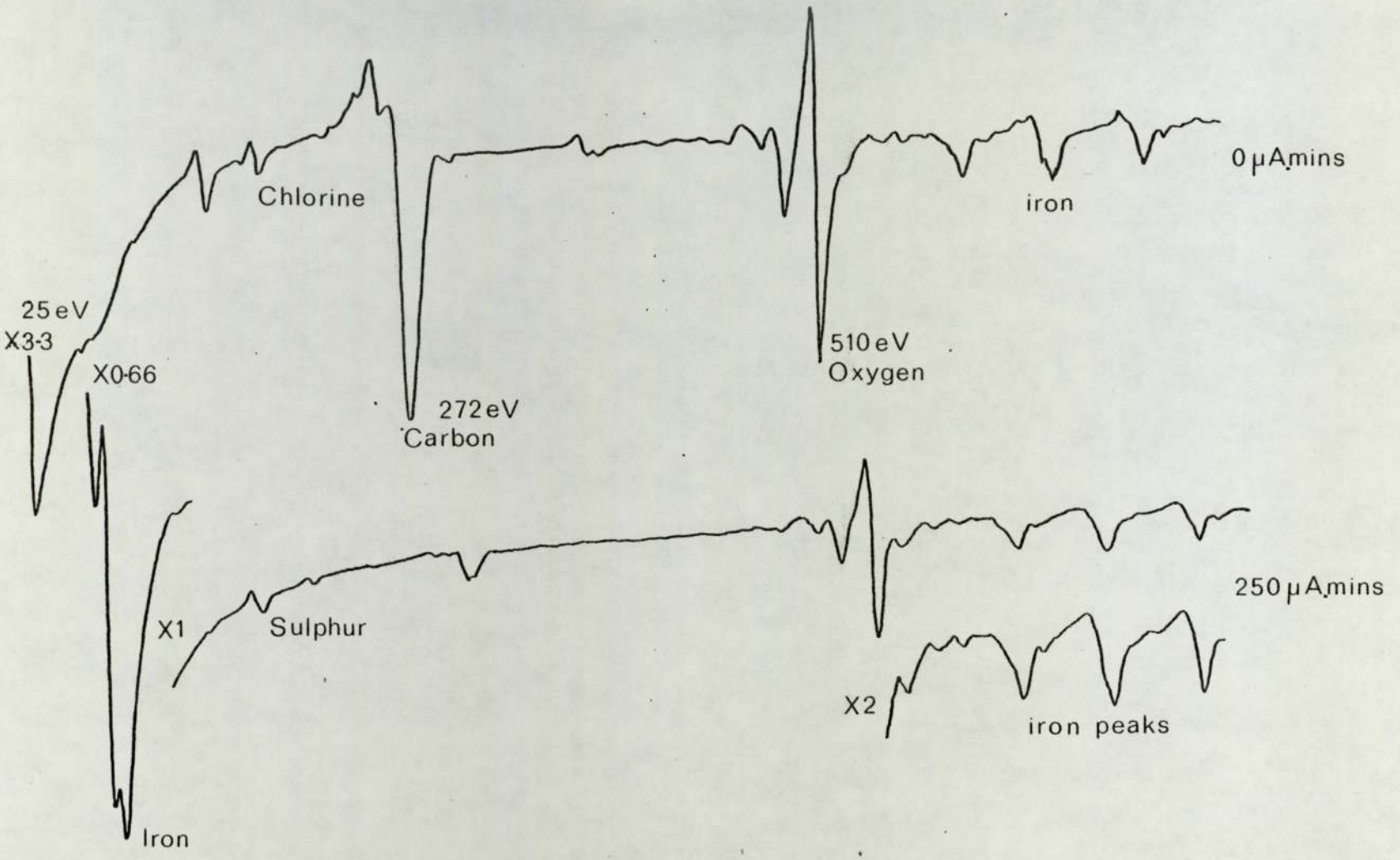

Figure 3.19, Auger Spectra for K.E.961 Steel run in kerosene plus Hitec.

triplet sulphur peak is shown in figure 3.22(a). This suggests that sulphur was present on the surface as a compound. The triplet was not so distinct for the hydrofined fuel, and there was only a trace amount of sulphur on the pin worn in trimethylpentane, as for the fuel and additive wear pins.

It will be shown later that a carbon layer existed on the bronze and steel surfaces which were worn in the presence of additive. Above this layer there was carbon picked up from the laboratory atmosphere. Slight differences can be seen between the carbon peaks from these two layers. The carbon peak from the atmospheric contamination is not as symmetric as the carbon in the underlying layer. This contaminant type peak is also seen on the wear pin from the trimethylpentane test which was to be expected. The sample from hydrofined fuel tests shows a similar result with only a slight difference in the initial part of the peak. These differences are shown in figure 3.22(b).

The oxygen present in the samples from hydrofined kerosene and trimethylpentane tests gave similar shaped oxygen peaks. The fuel and Hitec sample also gave a similar peak at the surface but after sputtering the characteristic oxide oxygen peaks emerged (figure 3.22(c)).

Finally the presence of nickel was observed through the change in shape of the copper 840 and 848 eV peaks. Figure 3.23 shows these peaks for aluminium bronze and also the pure copper and pure nickel peaks as given in the handbook of Auger electron spectroscopy. Note that the peak at 848/849 eV in aluminium bronze is larger than the 848 peak for pure copper showing the contribution from the nickel 849 eV peak.

Changes were observed in the elastic peak before and after sputtering and with position on the sample. Most samples which had

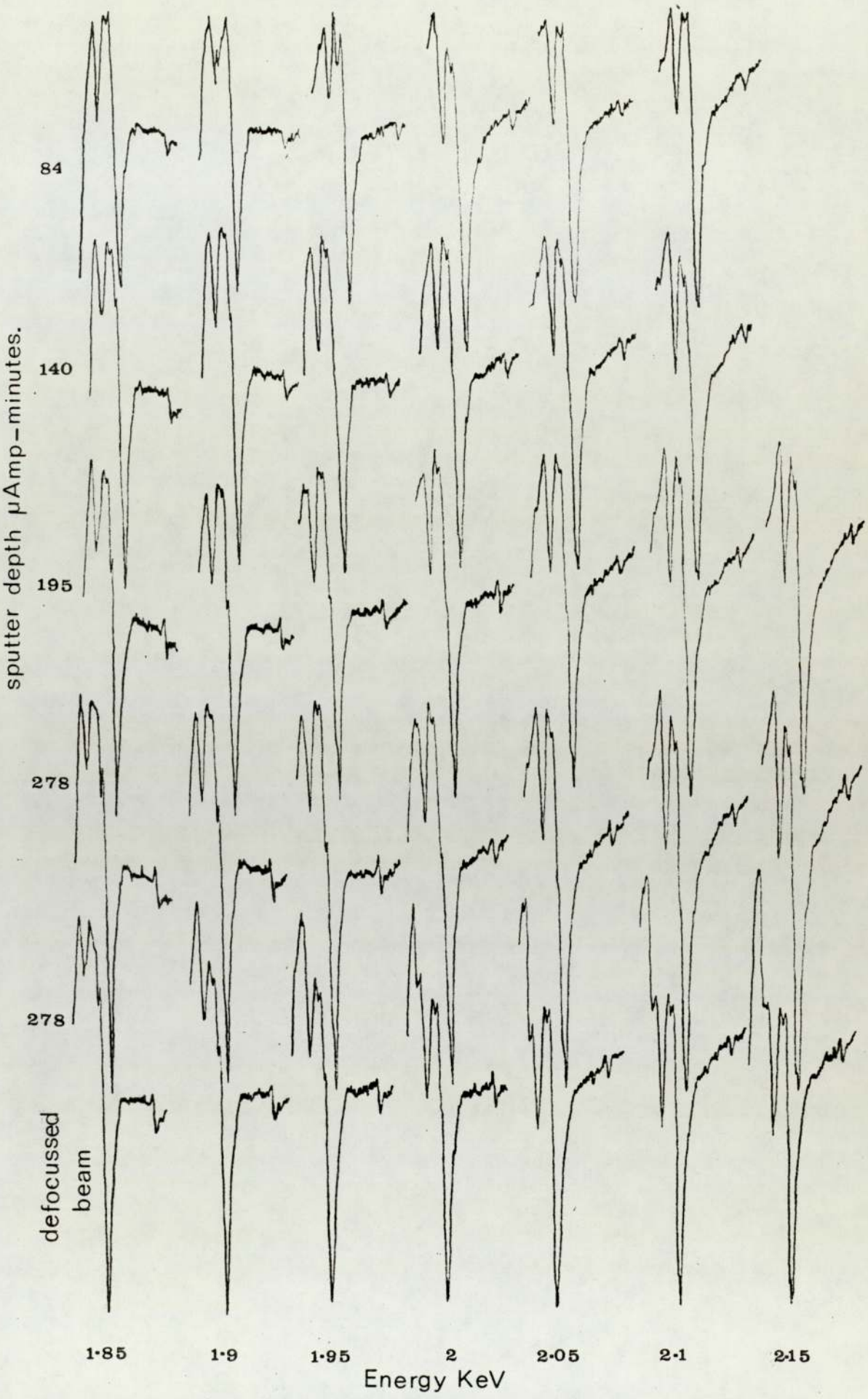
sputter depth μAmp-minutes.
84
140
195
278
278
defocussed beam
1·85
1·9
1·95
2
2·05
2·1
2·15
Energy KeV

Figure 3.20

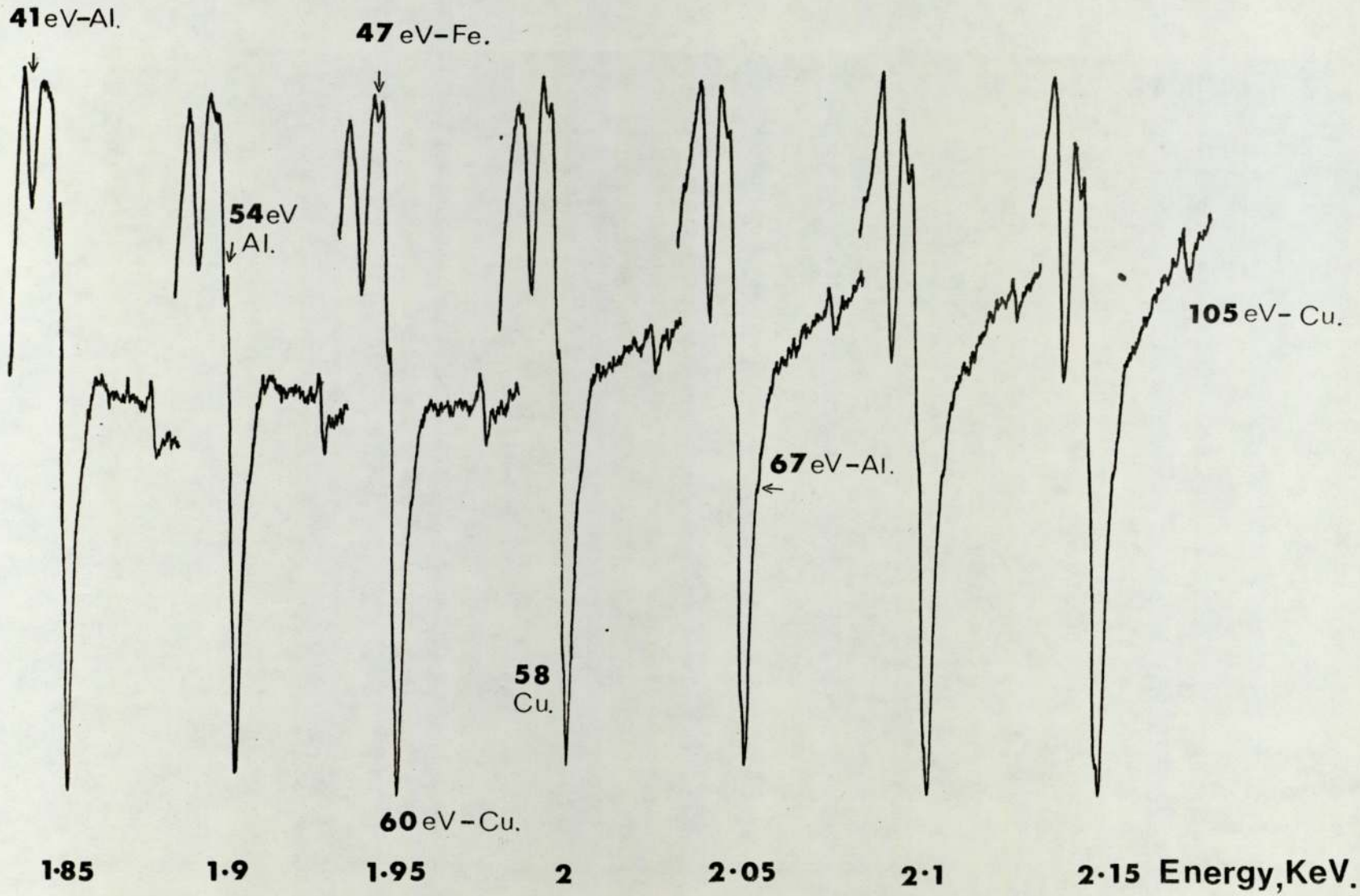
41 eV-Al.
47 eV-Fe.
54 eV
Al.
58
Cu.
67 eV-Al.
105 eV- Cu.
60 eV-Cu.
1·85
1·9
1·95
2
2·05
2·1
2·15 Energy, KeV.

Figure 3.21

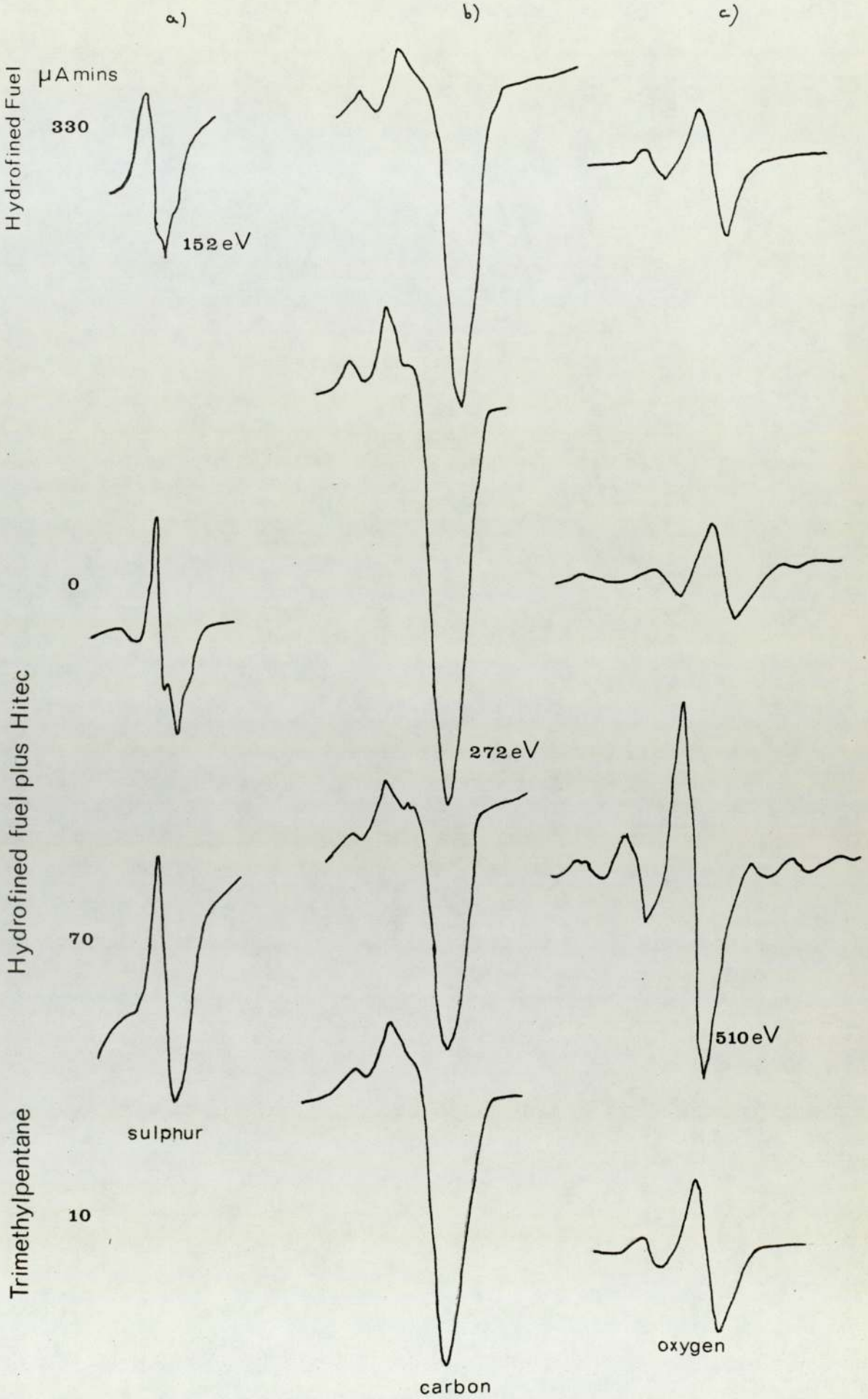

Figure 3.22 Auger peak shapes–on bronze.

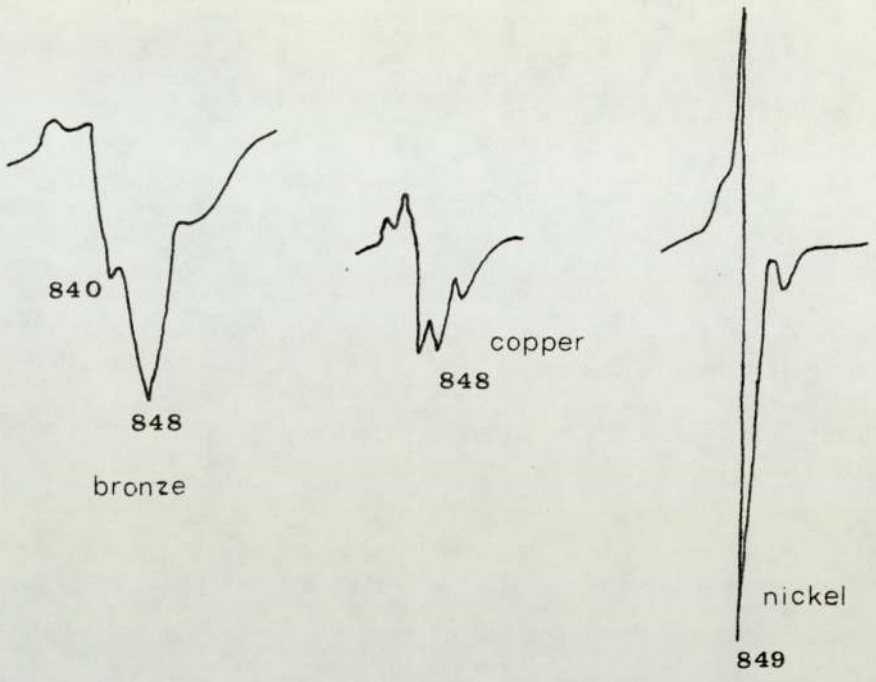

a)Identification of nickel

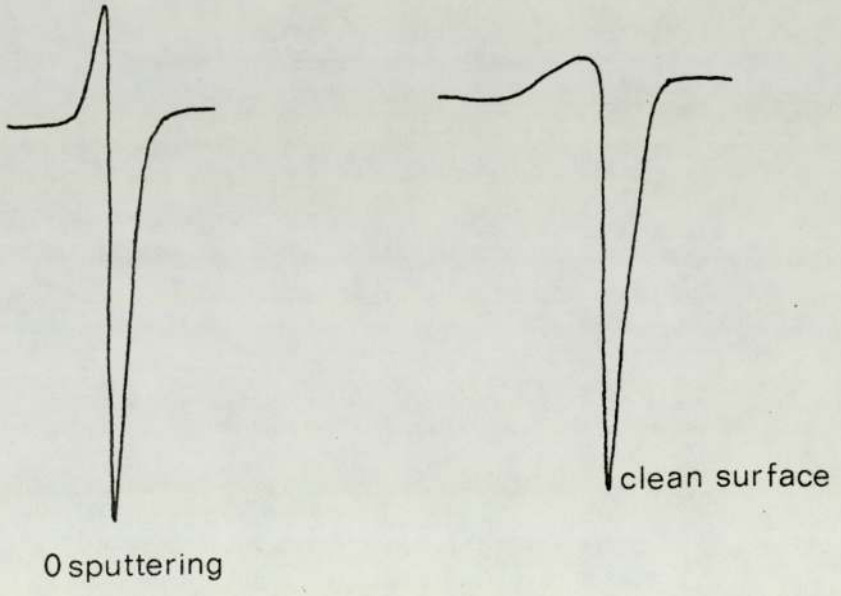

b) Elastic peak changes

Figure 3.23

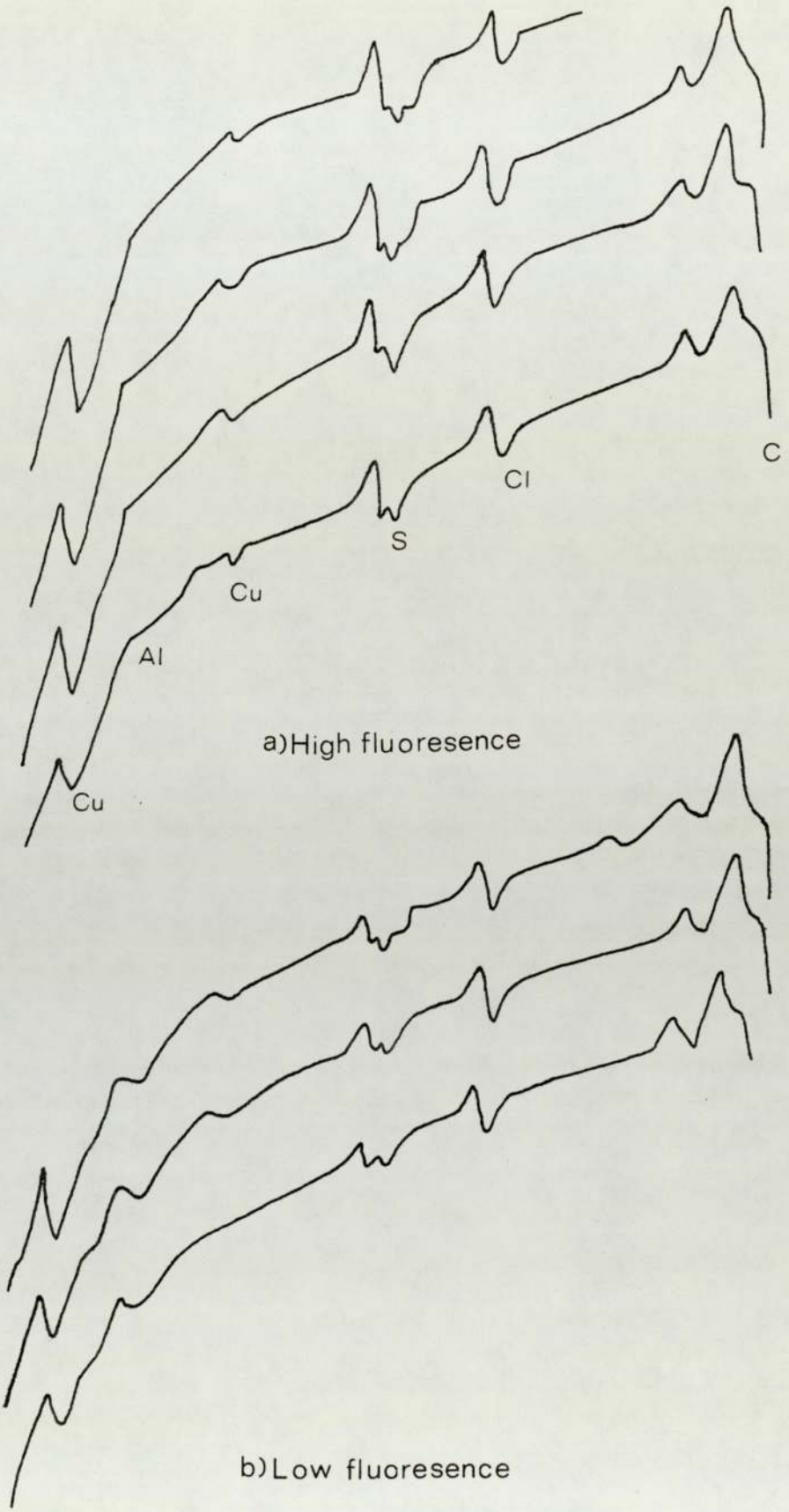

Figure 3.24.

run on kerosene, and in particular kerosene containing Hitec E515, were observed to fluoresce. This fluorescence was found to be greatly reduced on 'clean' or sputtered samples. Consequently it would seem reasonable to relate this to the change in shape of the elastic peak as shown in figure 3.23(b). The effect of this change on the Auger spectra was small. Only slight changes could be seen at the low energy end of the spectra. Successively taken spectra are shown in figure 3.24 for areas of (a) high fluorescence and (b) low fluorescence. Changes can be seen to be occurring in the sulphur peak which becomes a triplet after the beam had been on the sample for some time. In the region of high fluorescence the carbon peak also changes slightly. The aluminium plasmon gain peak is more distinct for the low fluorescent clean surface. In the case of the high fluorescent region this peak affects the general slope of the spectra.

Similar changes in peak shape could be found for the carbon on the steel, which had worn in the presence of hydrofined fuel with additive, as on the bronze wear pin in a similar fuel. Chromium peaks were identified at 482, 520 and 536 eV which suggests that an oxide of this element exists on the surface. This was particularly found on the darkened regions of the steel. Figure 3.25 shows the chromium, oxygen and some of the iron peaks obtained from this sample.

The result of depth profiling allows more obvious comparisons to be made between the samples. The profile for a steel surface run in the presence of Hitec shows an initial contaminant layer of carbon between 0 and about 10 μA minutes of sputtering (see figure 3.26(a)). A layer of carbon then exists between about 10 and 50 μA minutes. The carbon layer is attached to an oxide layer as shown by the shape of the oxygen profile. Above the carbon layer

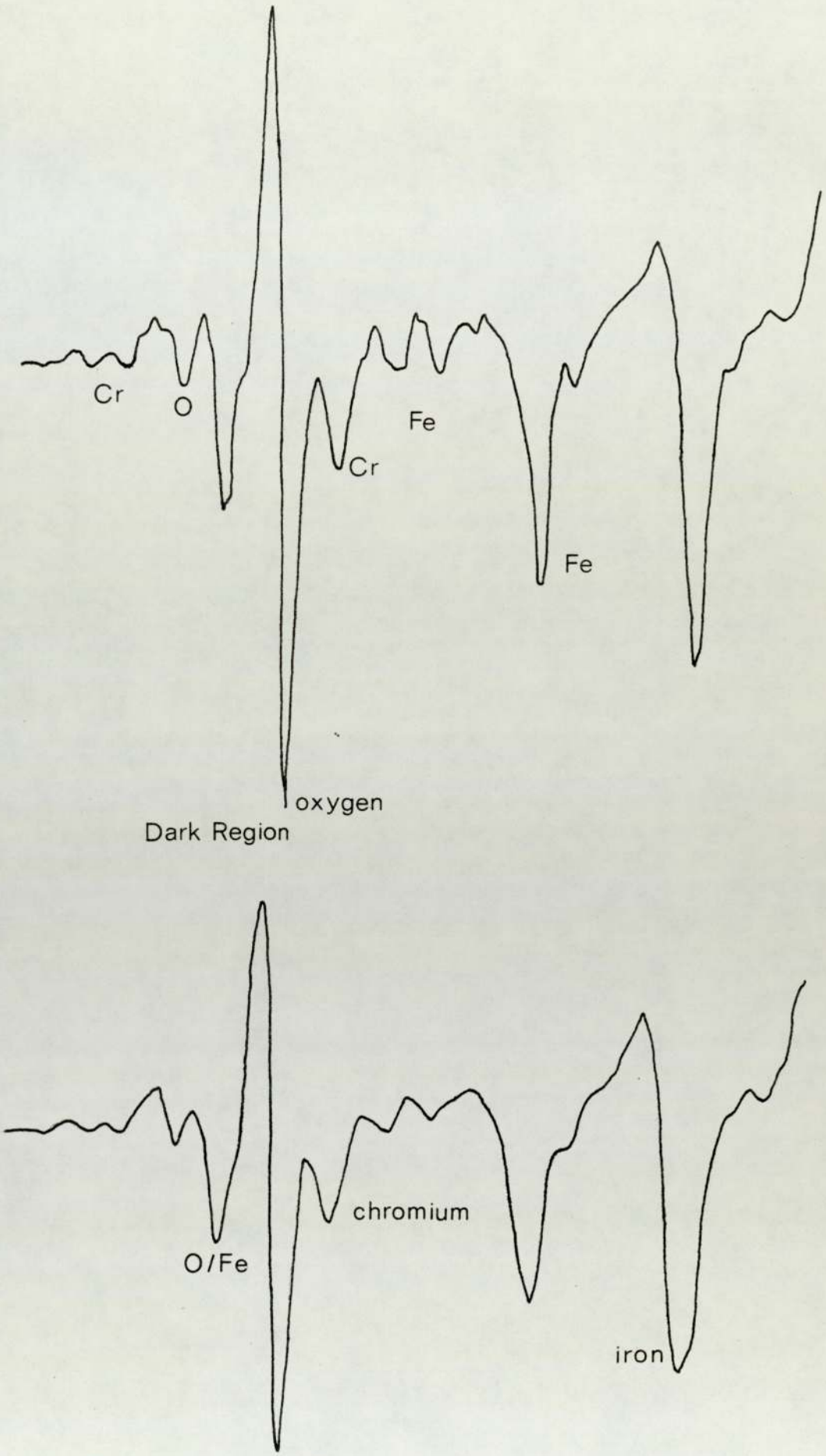

Figure 3.25, KE961 steel run in kerosene plus Hitec.

there is also evidence of an increase in the concentration of sulphur and chlorine. The profiles for the bronze surface worn in the presence of Hitec E515 are very similar to those of the steel (figure 3.27(b). A carbon layer exists between about 50 and 200 μA minutes. Again above this is an enriched sulphur layer and contaminant layer of carbon. The oxygen profile also suggests an oxide layer. The iron content rises to quite a large quantity after 800 μA minutes of sputtering compared to what might be expected from the aluminium bronze specification. It must be noted, however, that nickel and aluminium were not included on these profiles since peaks for these elements were not fully resolved. The bronze worn in the presence of alumina filtered fuel and 2, 2, 4 trimethylpentane (iso-octane) show no signs of an oxide or sulphur layer (figures 3.26(c) and (d)). The curve from the 2, 2, 4 trimethylpentane shows no sign of a carbon layer and in the case of the hydrofined kerosene the carbon profile flattens out but does not increase. These profiles were obtained using sensitivity factors calculated using the peak-to-peak height of the Auger signal.

The effect of the analytical treatment of the results, on the depth profiles, is shown in figure 3.27. The peak-to-peak heights are plotted in figure 3.27(a) and for convenience the sulphur peak-to-peak heights have been divided by two. It can be seen that the magnitude of the sulphur and oxygen initially rise above the other elements. Figure 3.27(b) shows the profiles obtained using sensitivity factors calculated from the peak-to-peak heights. The sulphur and oxygen are now much reduced in magnitude. Note that the same basic shape of all the curves has been retained. Finally the profiles obtained using sensitivity factors calculated from the product of the peak-to-peak height and half width is shown in figure 3.27(c). In this case the sulphur, oxygen and iron profiles

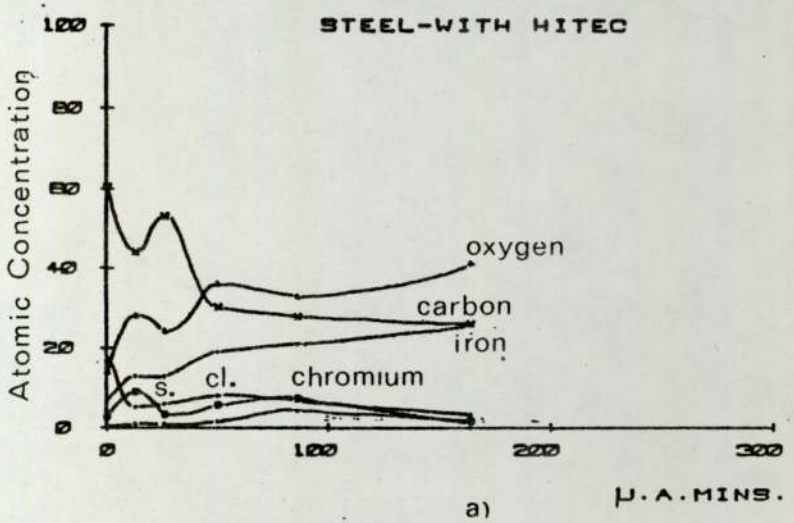

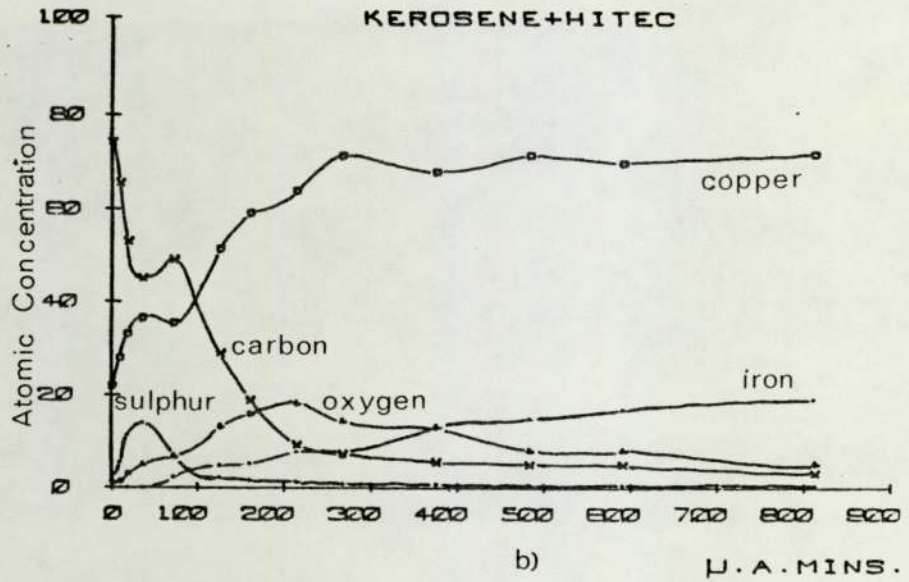

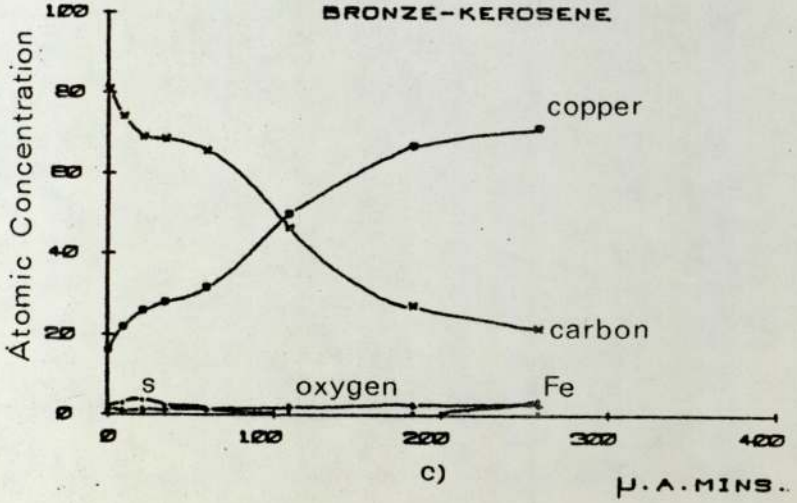

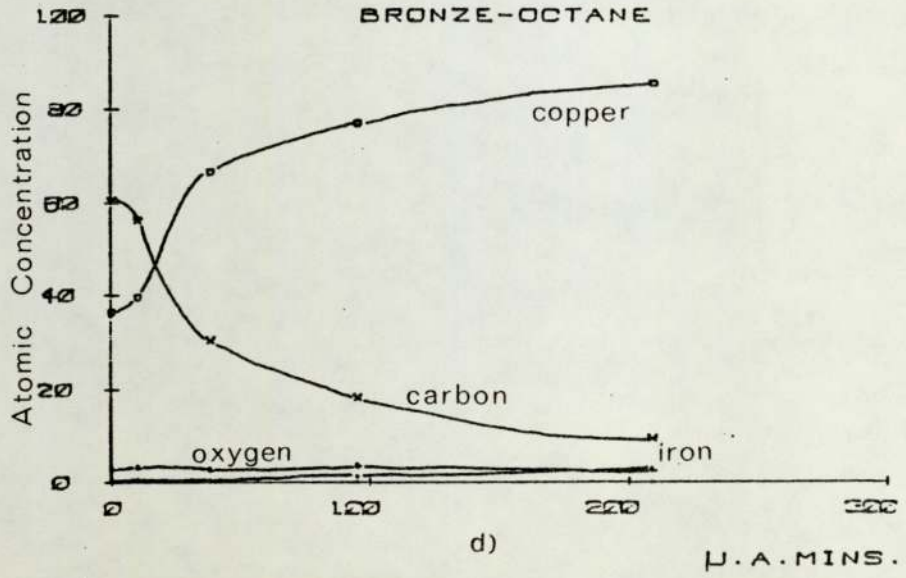

Figure 3.26 Auger depth profiles.

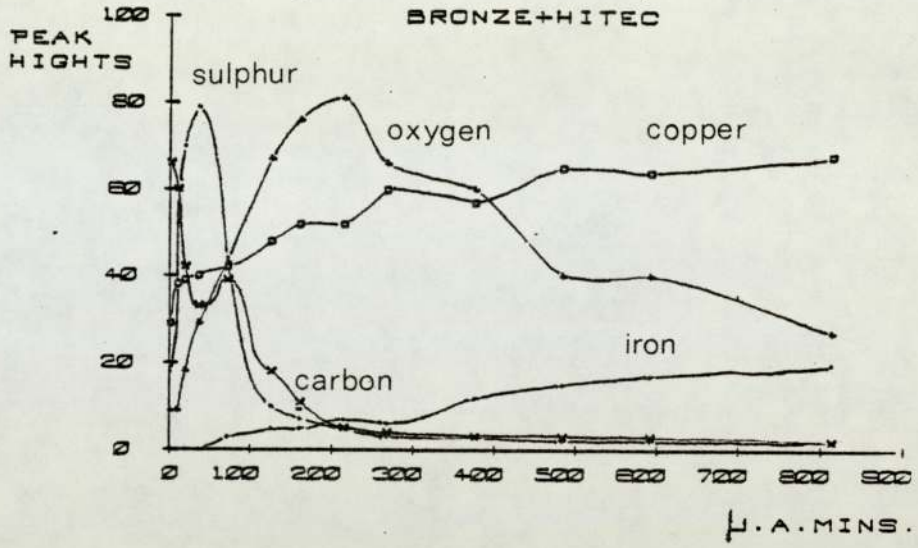

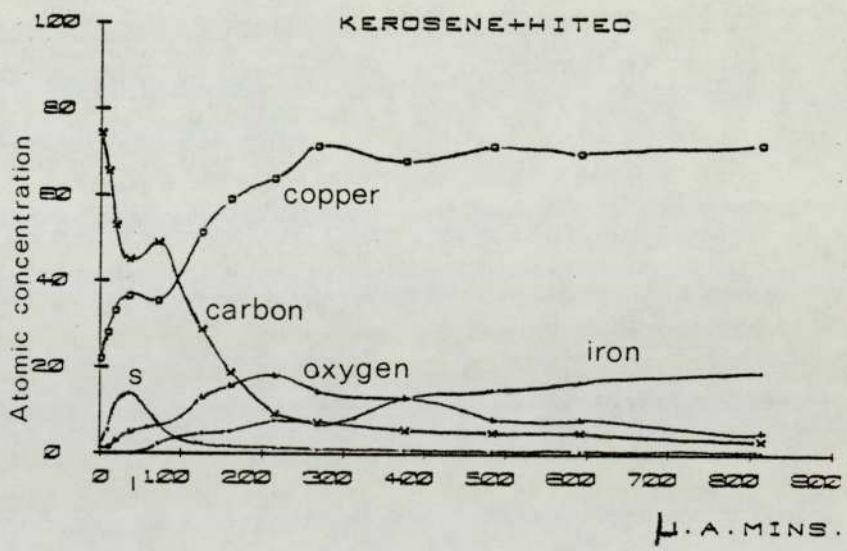

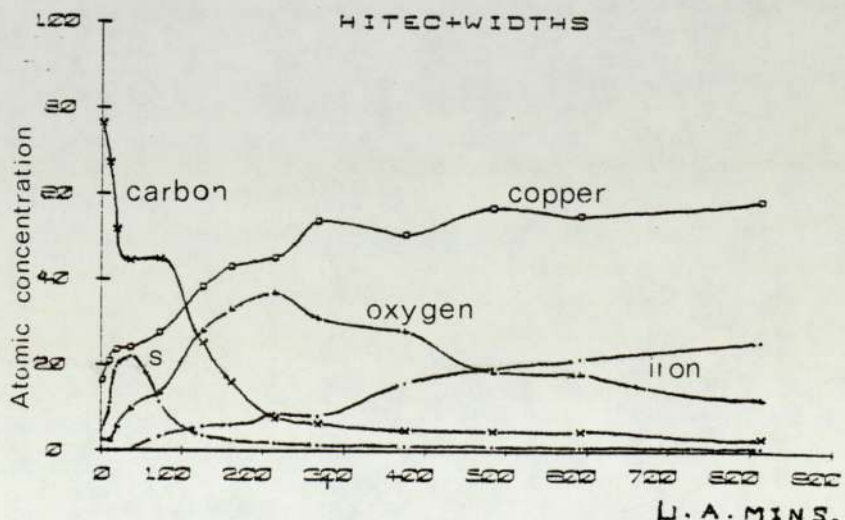

Figure 3.27 Auger depth profiles.

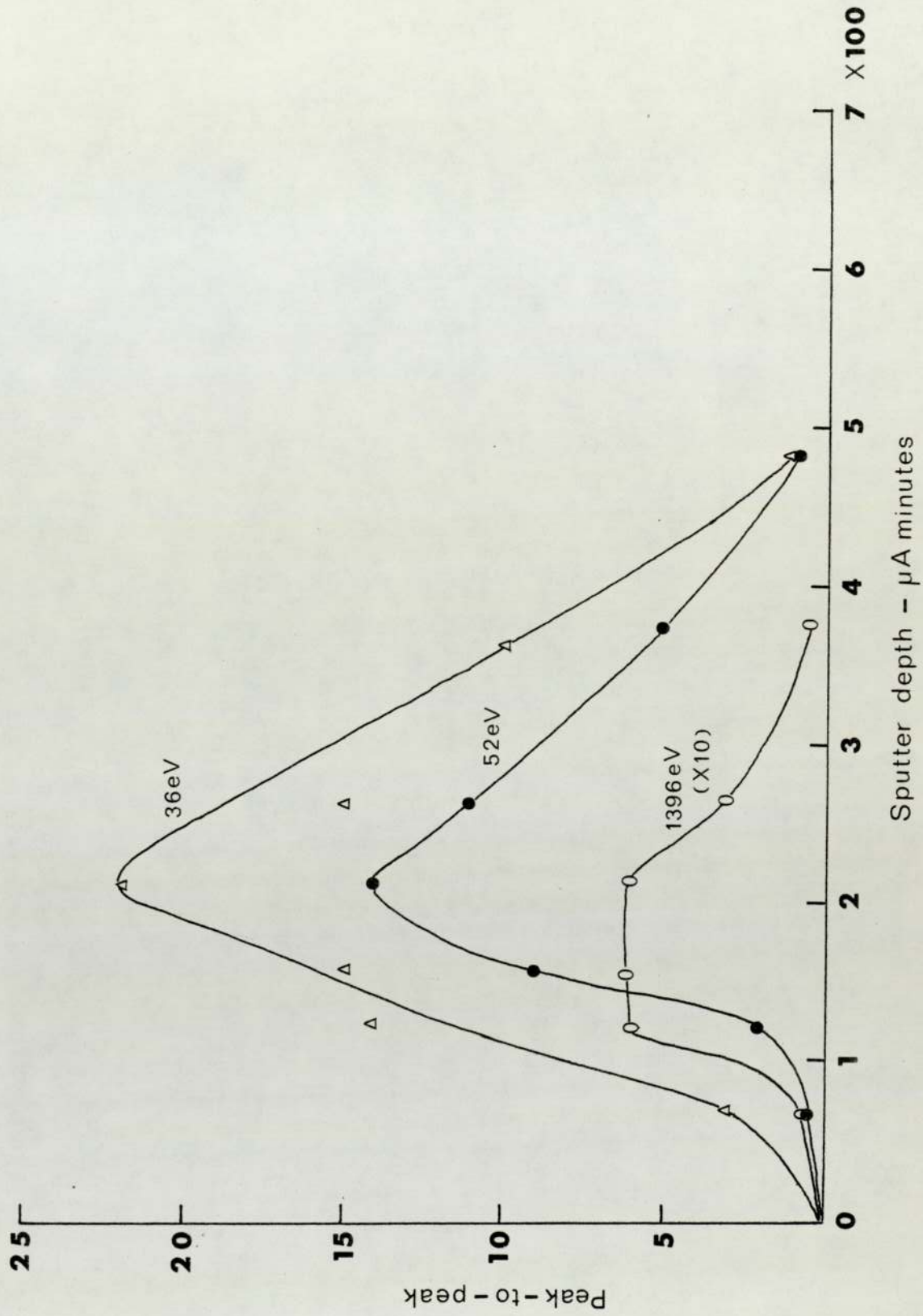

Figure 3.28, Aluminium Auger profiles.

have increased, whilst the copper profile has reduced, in magnitude at each sputter time. The carbon profile has remained essentially the same apart from a flattening, rather than an increase, at about 50 μA minutes.

Aluminium has not been plotted on these profiles because there was no reasonable peak available to measure. A plot of the plasmon loss, and gain, peaks along with the aluminium 1396 eV peak is shown in figure 3.28. This plot is for a pin worn in the presence of Hitec and suggests that there may be a surface film of aluminium oxide. The peak-to-peak heights plotted here will not be the true peak-to-peak heights since these peaks were not fully resolved. Calculating the film thickness by the method shown in Appendix II suggests the film would be about 350×10^{-10} M.

3.3.3 Electron Probe Microanalysis

The photographs of figure 3.29 show (a) part of a wear surface which had been tapered to a 10° angle to leave clean aluminium bronze, (b) the copper X-ray distribution over this region and (c) the aluminium X-ray distribution. The wear surface had been generated in the presence of Hitec E515 and appeared to be entirely copper rich when viewed optically. It can be seen from the X-ray photographs that this is the case and the elemental intensity scans confirm this evidence. Figure 3.30 shows the intensity against position of the electron beam on the surface as it was scanned across the wear surface (3.30(a)) and across the wear surface and taper (3.30(b)). Focussing the beam as a stationary spot on the tapered surface and then measuring the aluminium X-ray intensity gave a count rate of about 6,400 counts per second which is typical of that found for unworn aluminium bronze and for pins worn in the presence of hydrofined fuel. The count rate for aluminium was at about 850 counts per second on the wear surface which is

indistinguishable from the background count rate.

In the case of aluminium bronze running in the presence of Hitec E515 the surface of some of the pins had areas of copper rich appearance with surrounding areas of aluminium bronze colour. The distribution of aluminium, copper, nickel and iron X-rays for a typical region on such a surface is shown in figure 3.31. The apparent intense aluminium region gives a spot count rate of 2747 count per second with the depleted region down to 540 counts per second showing that the whole surface has in fact become depleted.

A similar set of photographs is shown for a pin, worn on a higher roughness disk, in figure 3.32. It can be seen, from these photographs, that the aluminium appears to be depleted in some regions of the surfaces. The aluminium appears to lie along the score lines on the surface.

Previously some wear results were given which showed spikes of high friction followed by periods of low friction when tests were carried out with Shellsol T. The results of an electron probe analysis for copper and aluminium on a sample from the low friction period, figure 3.33(a), and from the high friction period (3.33(b)) suggest that the distribution of these elements is important. The fluctuations in the intensity, for the two elements, are generally the mirror image of each other. The X-ray distribution photographs of aluminium, copper, iron and nickel for the high friction sample are shown in figure 3.34. The uniformity of the aluminium distribution is apparent in this case. These distributions are typical for surfaces worn in hydrofined alumina catalyst filtered fuel as well as Shellsol T. The distributions in the case of the low friction were also imilar except for the aluminium distribution which shows segregation to be occurring comparable to the fuel with Hitec results.

The sample which was stopped on the high friction period had an area which appeared to be aluminium rich. The line scan for this region is shown in figure 3.33(c) and can be compared to the unworn aluminium bronze line scan (figure 3.33(d)) for copper and aluminium. An optical micrograph of this area is shown in figure 3.35 along with the aluminium X-ray distribution. In this case the aluminium spot count rate was 9560 counts per second, for the intense region, and 5200 counts per second for the apparently depleted region. This shows aluminium enrichment at the surface when a pin is wearing in the high friction state in the presence of a hydrofined fuel.

Energy analysis of the X-rays from samples of the two-piston rig bores show that three distinct regions exist (figure 3.35(a)). A dark patch close to the area where cadmium plating still exists is shown to be aluminium. The second region was a typical aluminium bronze colour and the spectrum shows the low energy copper and aluminium peaks to be approximately the same intensity. The third region was copper rich in appearance and this is confirmed by the reduction in the intensity of the aluminium peak.

The piston which had run in the bore whilst lubricated by hydrofined fuel without Hitec is shown to have picked up aluminium (figure 3.36(b)) and where copper was present the aluminium peak is still greater in intensity than the low energy copper peak (figure 3.36(c)). These results correspond well with the failed aircraft piston, which was analysed, where aluminium is again shown to be present on the surface (figure 3.36(d)).

3.3.4 Electron Microscopy

Scanning electron micrographs were obtained for the surfaces of wear pins worn in the presence of kerosene containing 15 p.p.m. of Hitec E515. For cases where copper rich areas could be seen the

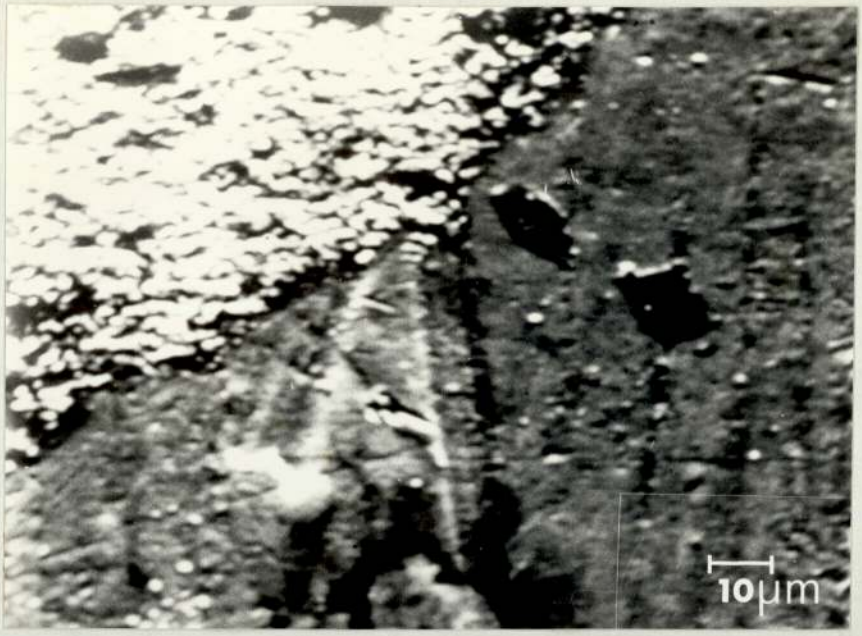

wear region.

taper section.
Top L.H.S.

Reflected electron image of surface scanned.

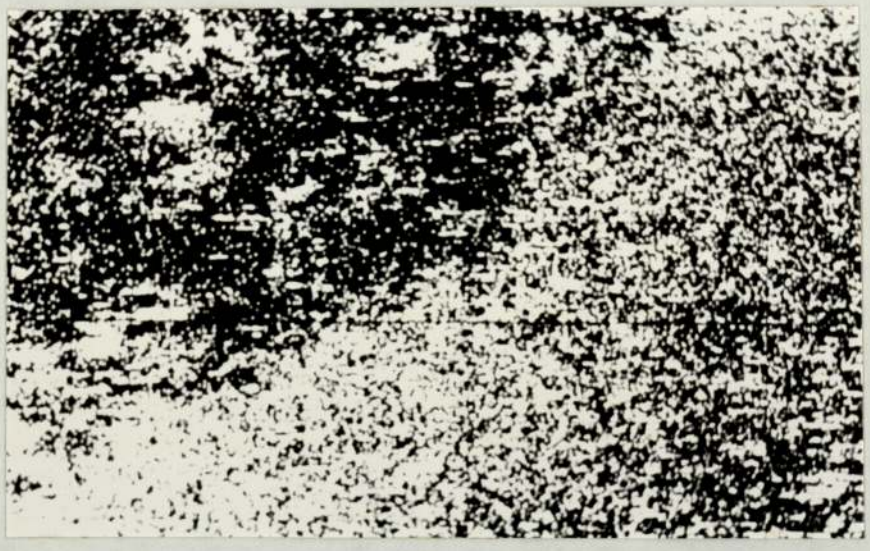

Copper X-ray distribution.

Aluminium X-ray distribution.

FIGURE 3.29 E.P.M.A SCANS OF A TAPER SECTION OF ALUMINIUM BRONZE WORN IN KEROSENE PLUS HITEC.

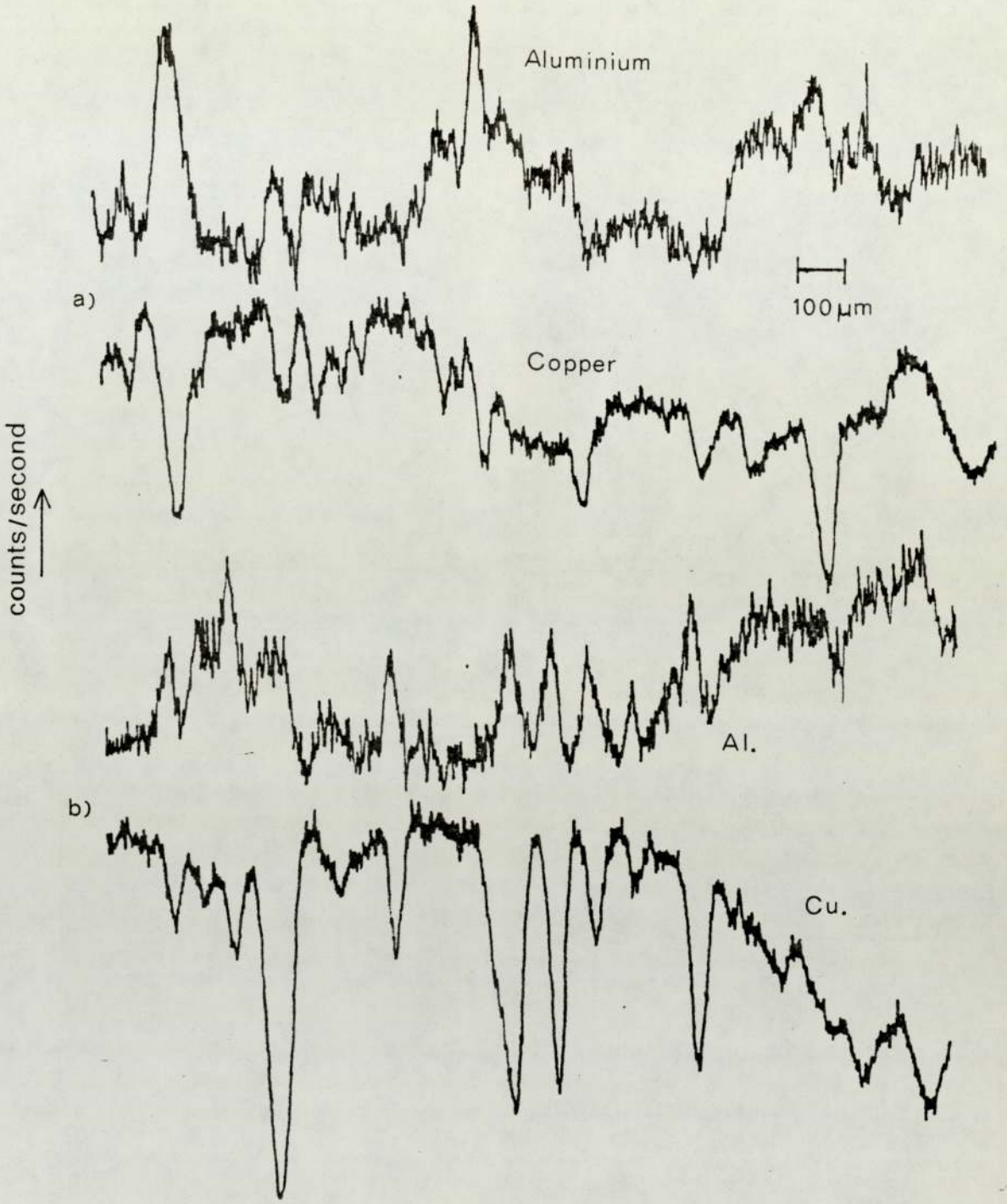

Figure 3.30 Electron probe profiles

a) Bronze wear surface.
b) Surface over taper section.

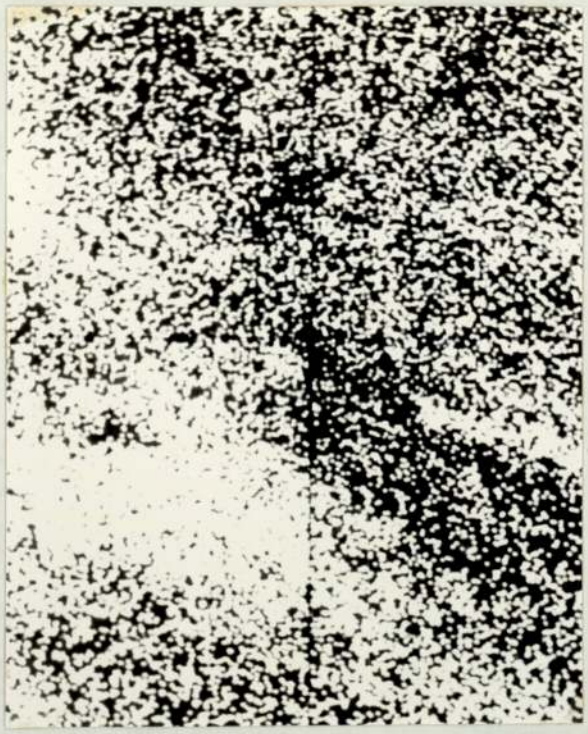

Aluminium X-rays.

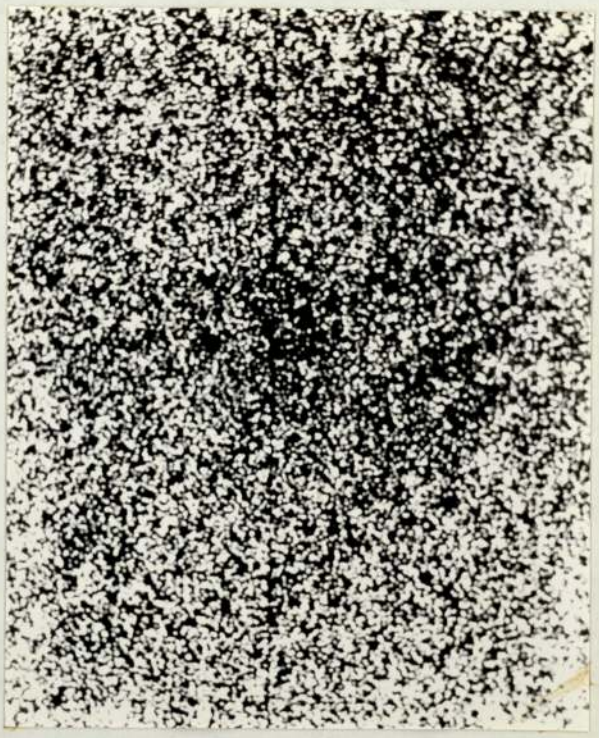

Copper X-rays.

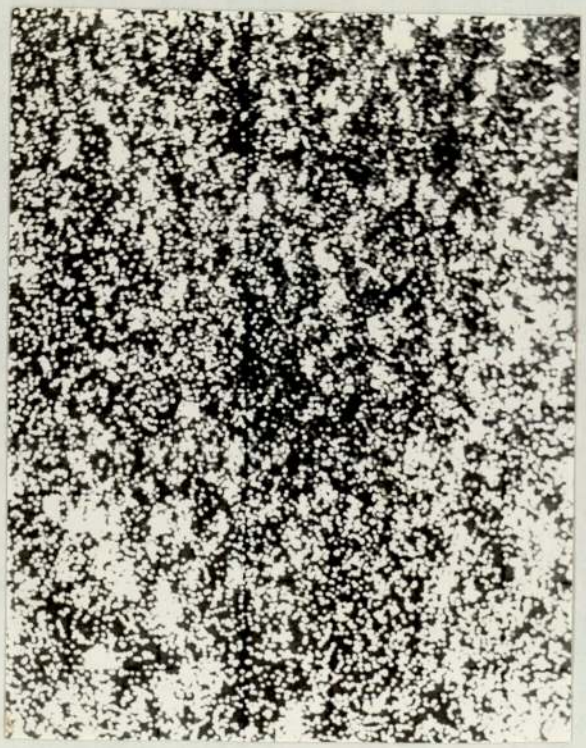

Iron X-rays.

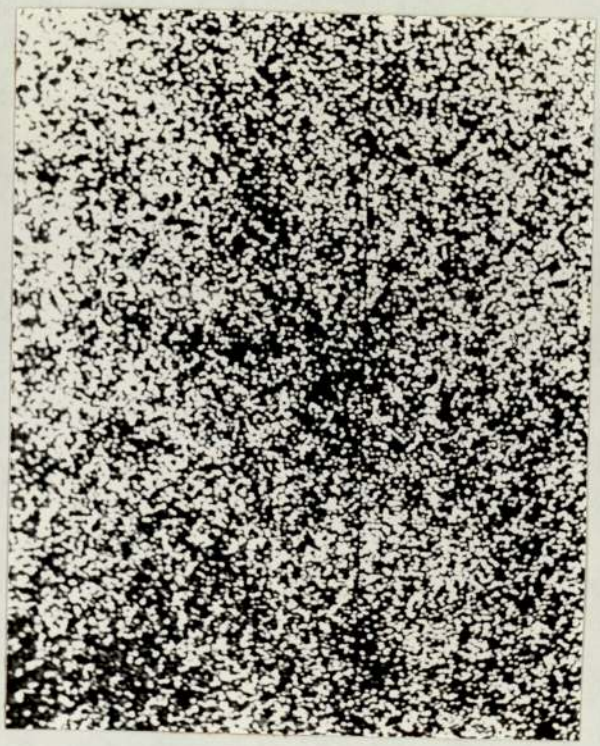

Nickel X-rays.

FIGURE 3.31 E.P.M.A SCANS OF BRONZE SURFACE WORN IN THE PRESENCE OF KEROSENE PLUS HITEC.

Aluminium X-rays.

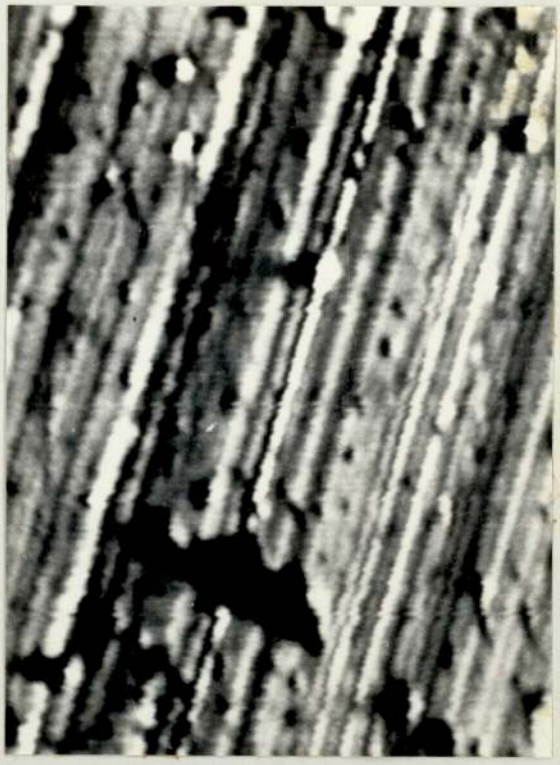

Reflected electron image.

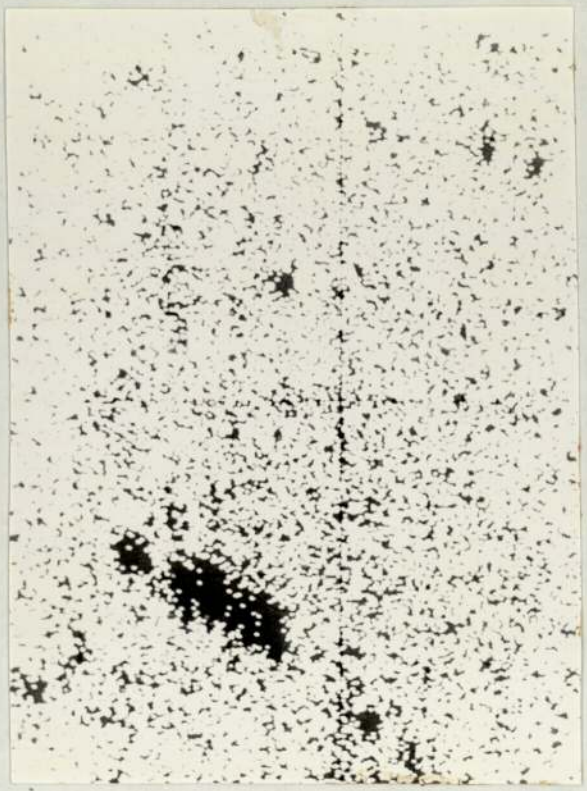

Copper X-rays

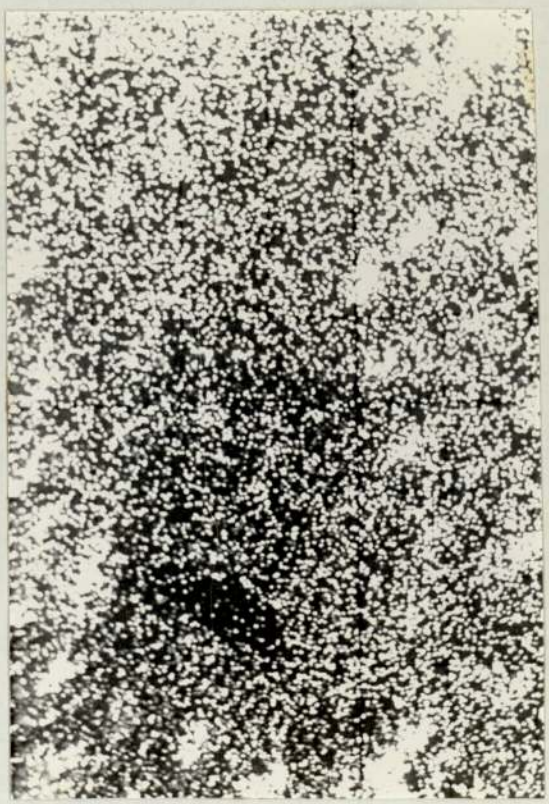

Iron X-rays.

FIGURE 3.32 E.P.M.A SCANS OF BRONZE WORN IN THE PRESENCE OF KEROSENE PLUS HITEC (HIGH ROUGHNESS DISC).

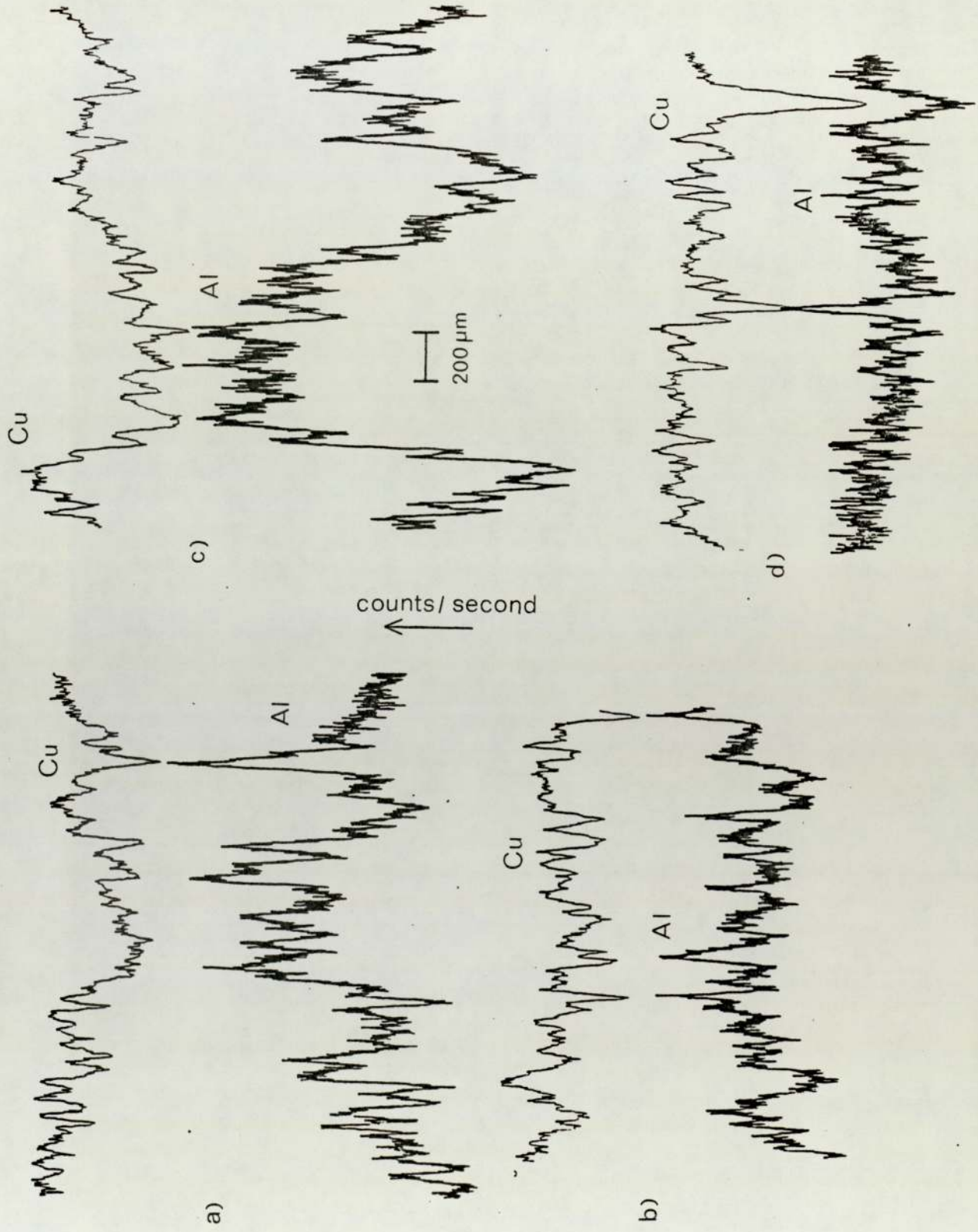

Figure 3.33 a) Low friction b) high friction c) aluminium rich region and d) unworn – a b, and c all worn in shellsol T.

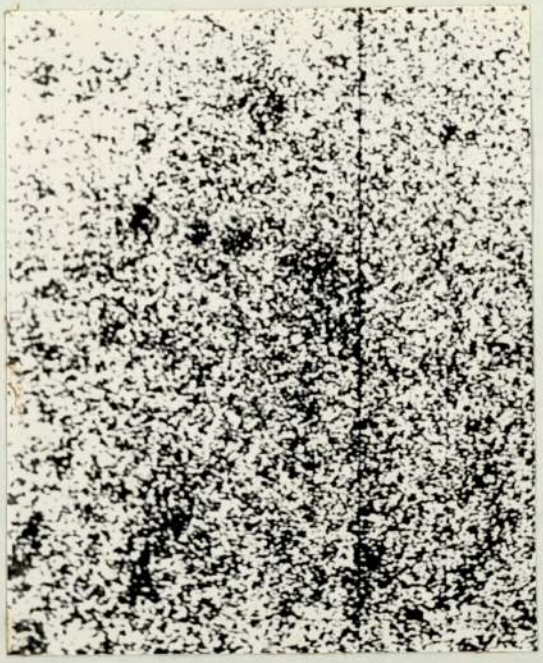

Copper X-rays.

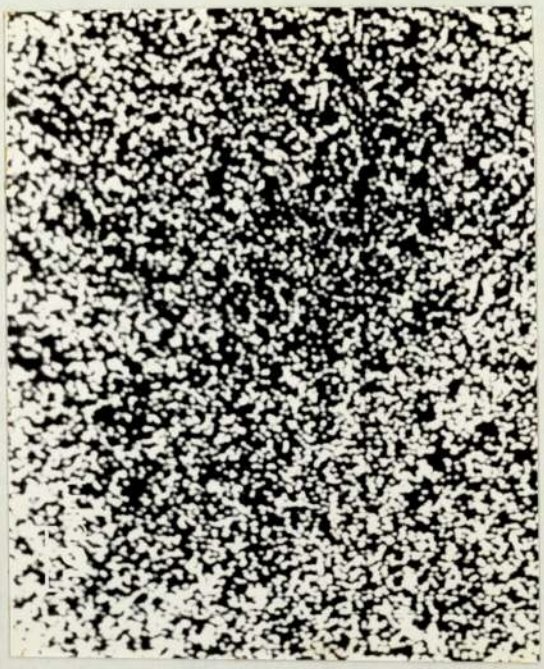

Aluminium X-rays.

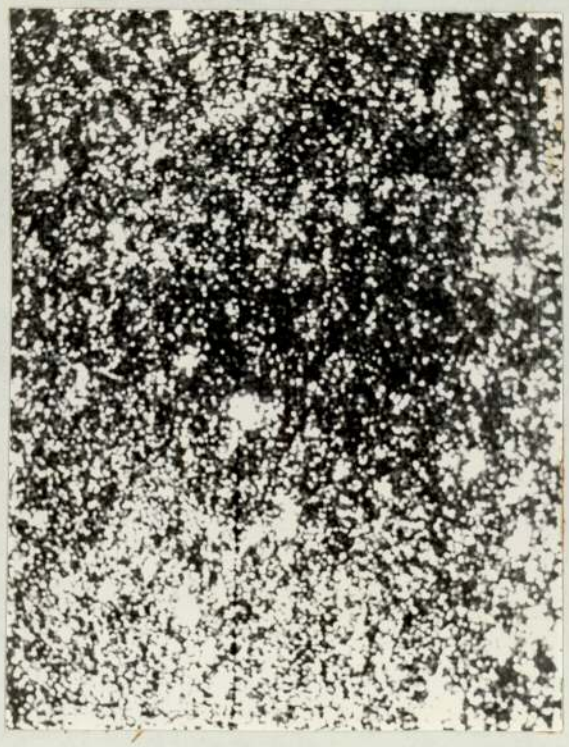

Iron X-rays.

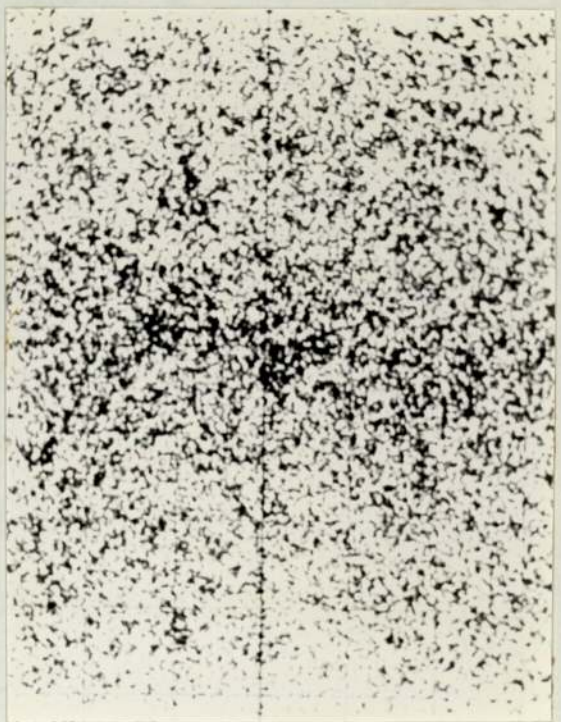

Nickel X-rays.

FIGURE 3.34 E.P.M.A SCANS OF BRONZE SURFACE WORN IN SHELLSOL-T, HIGH FRICTION PERIOD.

Optical micrograph.

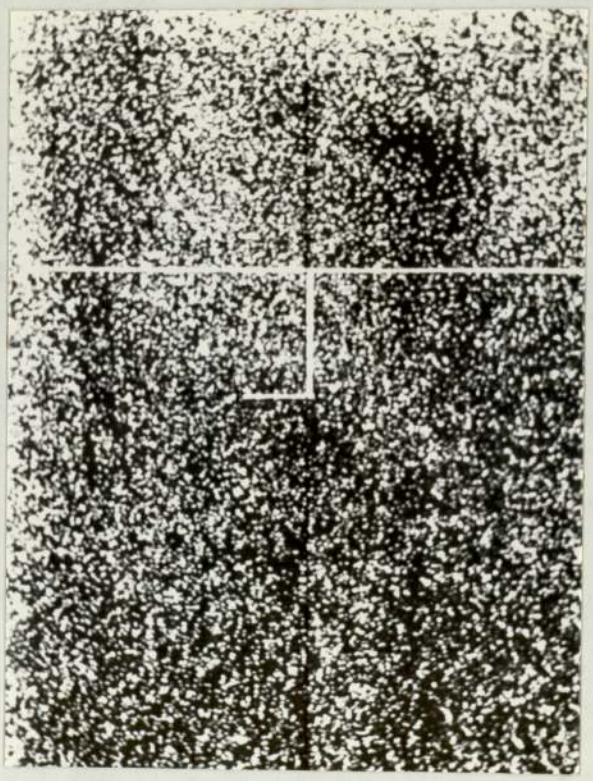

Aluminium X-ray distribution.

FIGURE 3.35 APPEARENCE OF AN ALUMINIUM RICH AREA ON A BRONZE SAMPLE WORN IN SHELLSOL-T.

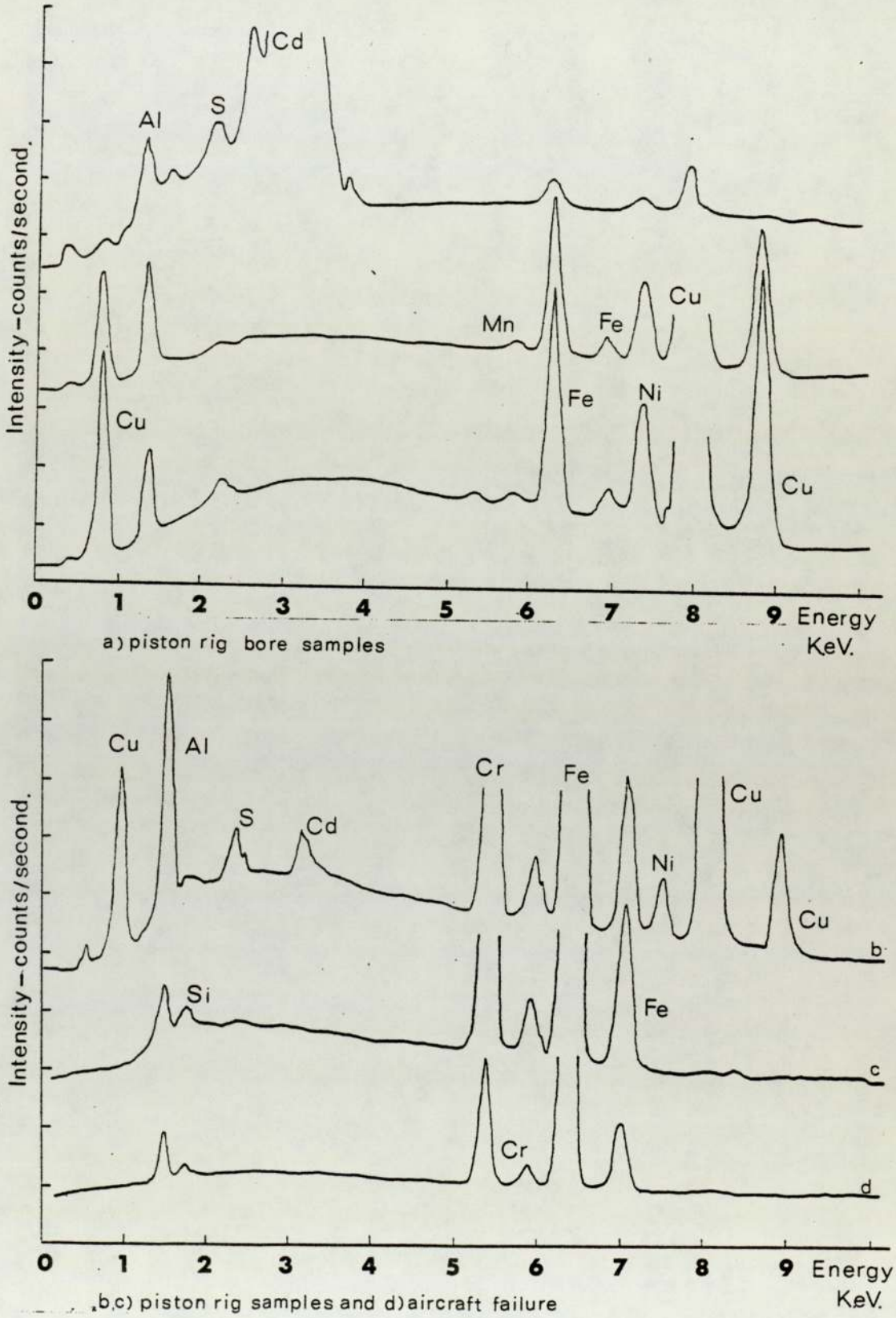

Figure 3.36, SEM Elemental Scans.

S.E.M. shows three contrasting regions. The very dark areas in figure 3.37 would appear to be the copper rich regions, the grey background would be the normal aluminium bronze whilst the white areas aluminium rich (comparable with the electron probe work in figure 3.32). Figure 3.38 shows a different area of the same sample where there appears to be plateaux of unidentified material. Another sample showed large areas of copper rich material with sections broken away (the bright areas of figure 3.39).

A sample from the high roughness disk experiments show a highly pitted surface similar to corrosion pitting (figure 3.40). There were regions on this sample similar to those found on the sample illustrated in figure 3.39.

Surfaces generated by wearing in the presence of hydrofined kerosene are shown in figure 3.41. The samples from the two piston rig bores (3.41(a) show a strong resemblance to the wear pin surfaces (3.41(b)). There is no evidence of plateau regions and no pitting on these samples. Both samples show a lot more evidence of scoring occurring.

Finally for the bronze surfaces figure 3.42 shows the effect of running under dry wear conditions. Obviously the surface is much rougher and there is evidence of large flakes breaking off the surface.

Areas of transferred material are similar in appearance for both the aircraft failed piston sample (figure 3.43(a)) and the two piston rig sample (figure 3.43(b)). An unworn surface is shown for comparison and illustrates the lapping marks (figure 3.43(c)) whilst a piston run in the presence of fuel kerosene with Hitec has a very smooth appearance (figure 3.43(d)).

Replicas of wear track surfaces produced the results shown in figure 3.44 and 3.45. Figure 3.44 shows successive photographs of

x200

x500

x1000

x2000

FIGURE 3.37 S.E.M MICROGRAPHS OF ALUMINIUM BRONZE WEAR SURFACE FROM KEROSENE PLUS HITEC TESTS.

X 2000

X 2000

X 5000

X 5000

FIGURE 3.38 S.E.M MICROGRAPHS OF A DIFFERENT AREA OF THE SAMPLE SHOWN IN FIGURE 3.37.

X500

X1000

X 2000

X5000.

FIGURE 3.39 S.E.M MICROGRAPHS OF BRONZE SURFACE WORN IN THE PRESENCE OF KEROSENE PLUS HITEC.

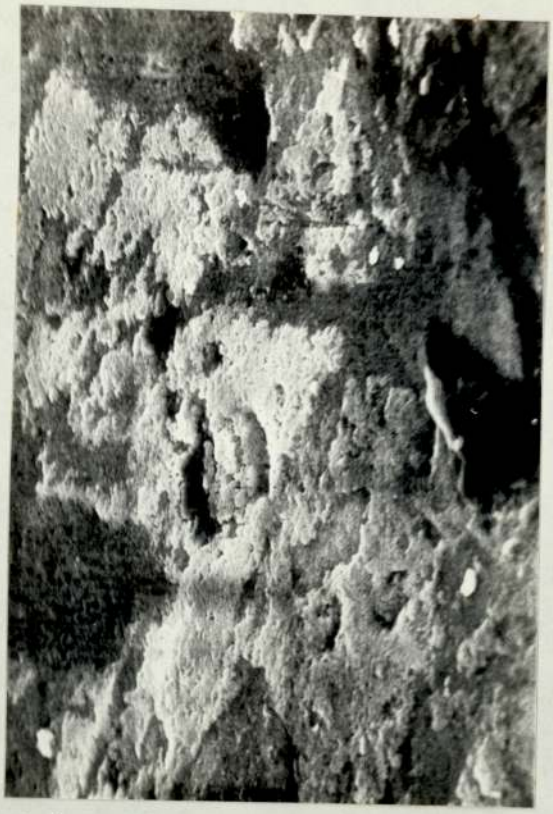

X 1250

X 2500

X 6250

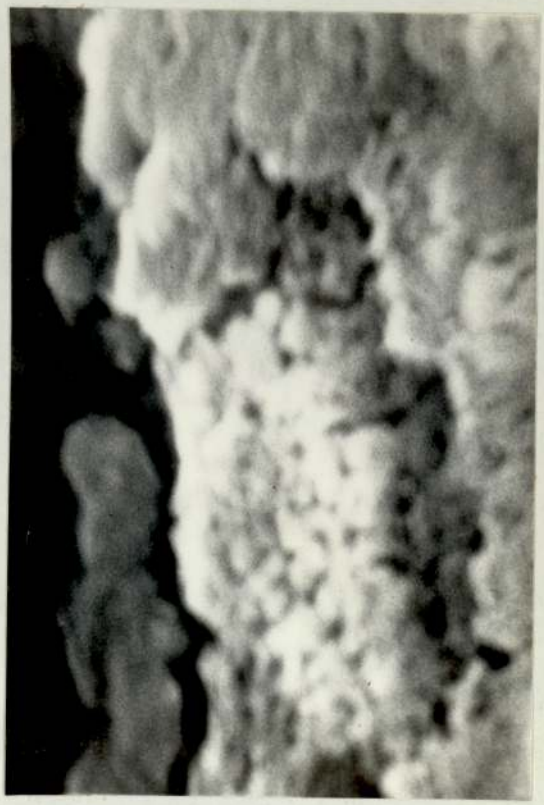

X 10000.

FIGURE 3.40 S.E.M MICROGRAPHS OF BRONZE WEAR SURFACE FROM TESTS WITH FUEL PLUS HITEC (HIGH ROUGHNESS DISC).

X 200

X 500

X 1200

Piston rig bore.

X 200

Wear pins.

FIGURE 3.41 S.E.M MICROGRAPHS OF WEAR SURFACES TAKEN FROM TESTS WITH HYDROFINED KEROSENE.

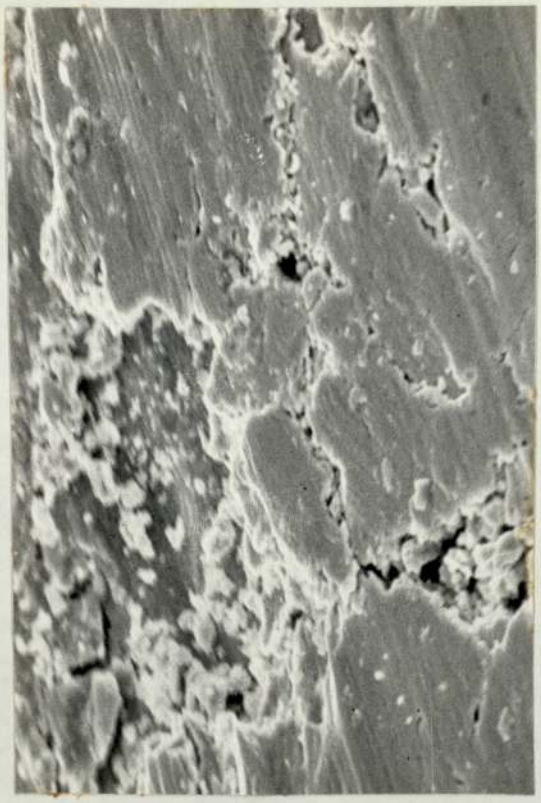

x 1150

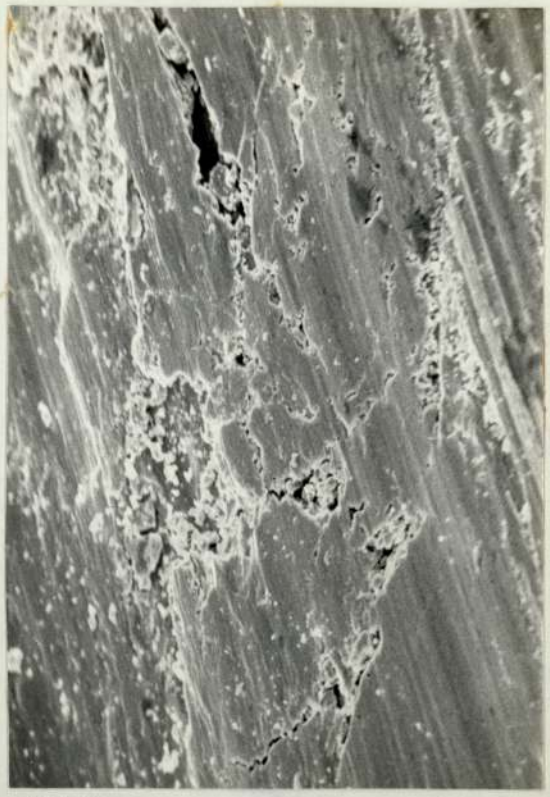

x 500

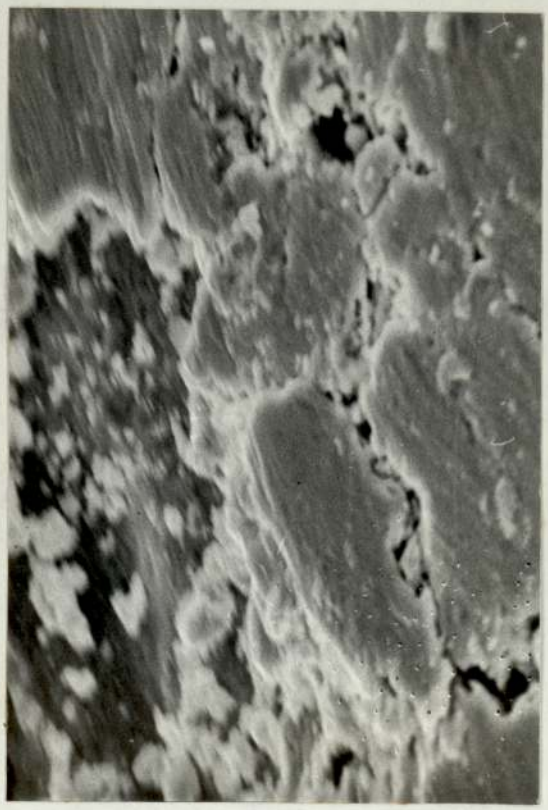

x 2350

x 1150

FIGURE 3.42 S.E.M MICROGRAPHS OF BRONZE WEAR SURFACES TAKEN FROM DRY WEAR TESTS.

Aircraft failure x 1100

Unworn x 500

Piston rig failure
(hydrofined fuel) x 500

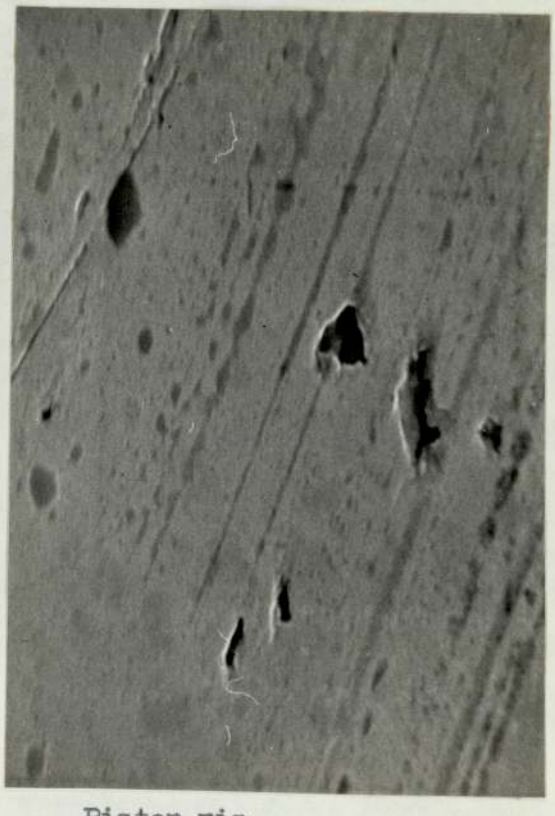

Piston rig
(fuel+hitec) x 1000

FIGURE 3.43 S.E.M MICROGRAPHS OF PISTON SURFACES TAKEN FROM VARIOUS SOURCES.

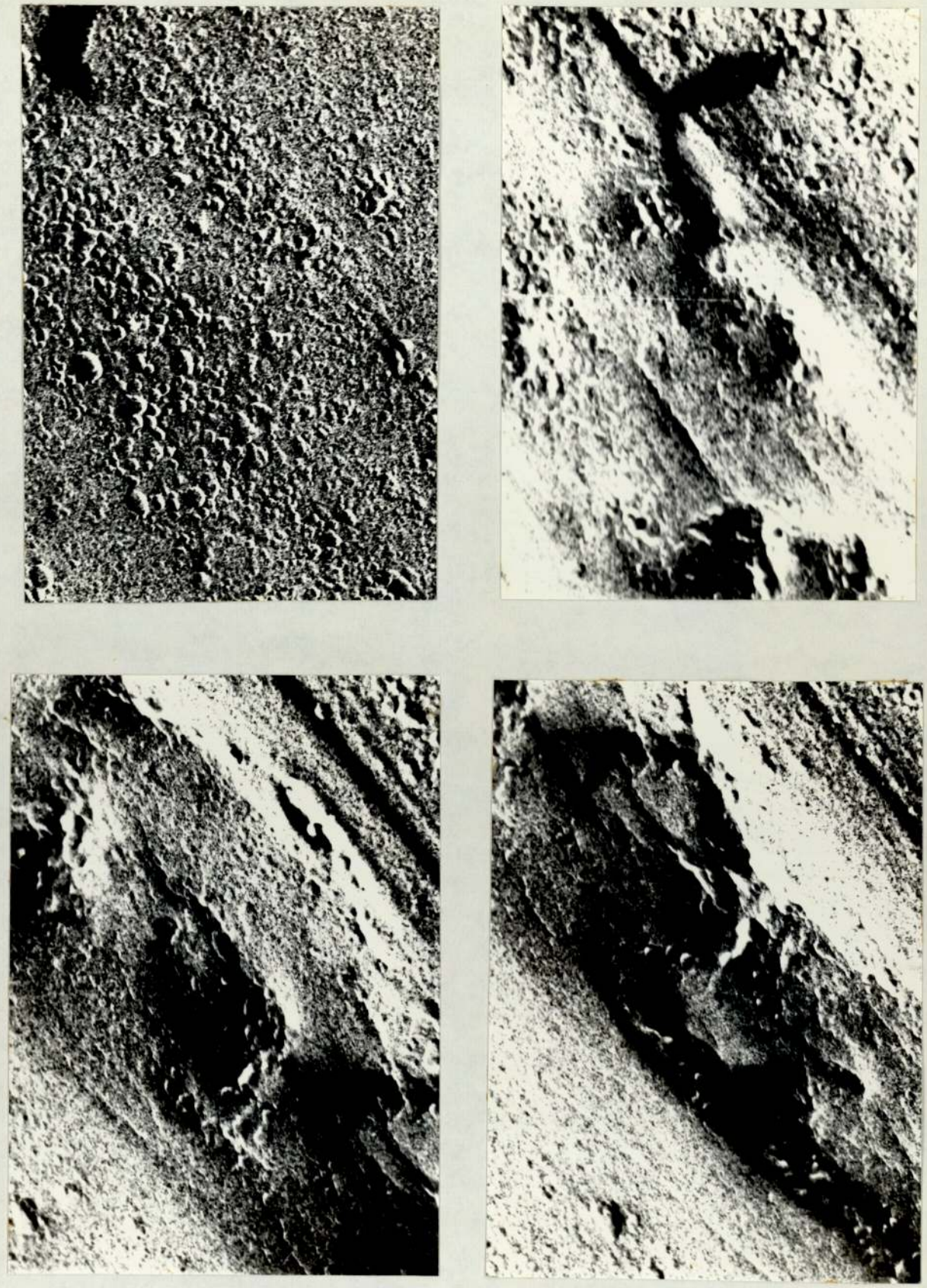

FIGURE 3.44 CARBON REPLICA OF A BRONZE WEAR TRACK ON STEEL FROM KEROSENE PLUS HITEC TESTS. (×6400).

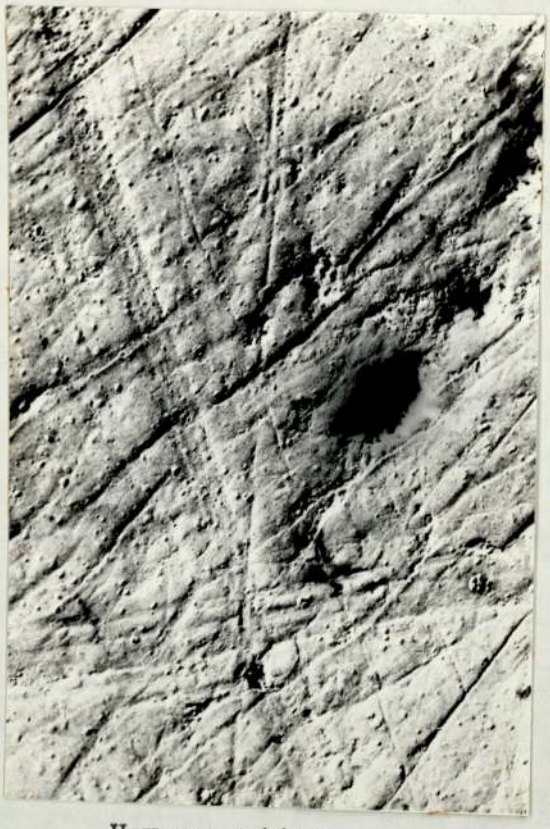

Unworn. x 6400

Hydrofined kerosene. x 6400

Kerosene + Hitec. x1200

Kerosene + Hitec. x 6400.

FIGURE 3.45 CARBON REPLICAS OF A DISC AND VARIOUS WEAR TRACKS.

a score mark on a wear track. This shows a very pitted wear track and in this respect is similar to the wear pins produced by wearing in kerosene with Hitec. Figure 3.45(a) shows the lapping marks on an unworn wear track whilst figure 3.45(b) shows a similar surface with transferred aluminium bronze from wear in hydrofined kerosene. Further pitting can be seen on plateau regions on a wear track formed in the presence of kerosene and 15 p.p.m. Hitec E515 (figures 3.45(c) (d)).

3.3.5 Wear Debris Analysis

Table 3.4 lists the results of the X-ray analysis of most of the wear detrius. The measured 'd' spacings are given for each test in decending order and results are also given for a reference sample of aluminium bronze. The hydrofined fuel debris gave 'd' spacings which were very little different from those found for the bronze. A 'd' spacing of 2.46 was found but none of the other copper oxide peaks were present. Consequently this debris appears to be aluminium bronze.

A large number of diffraction lines were found, when the additive was present in the fuel, some of which were quite broad (in particular lines at 'd' spacings of 2.09 and 2.03). The indications at 6 kg load is that phosphates are present along with copper oxide. Aluminium ortho-phosphate and copper phosphate would seem to be the most reasonable compounds to fit the measured 'd' spacings.

At the higher loads (10 kg and 12.5 kg) a change to aluminium phosphide occurs in the debris. This is particularly true at 12.5 kg load where 'd' spacings of 3.11, 1.93 and 1.65 are observed. As with the lower load, copper oxide can be identified and also pure copper lines appear. It is possible that copper

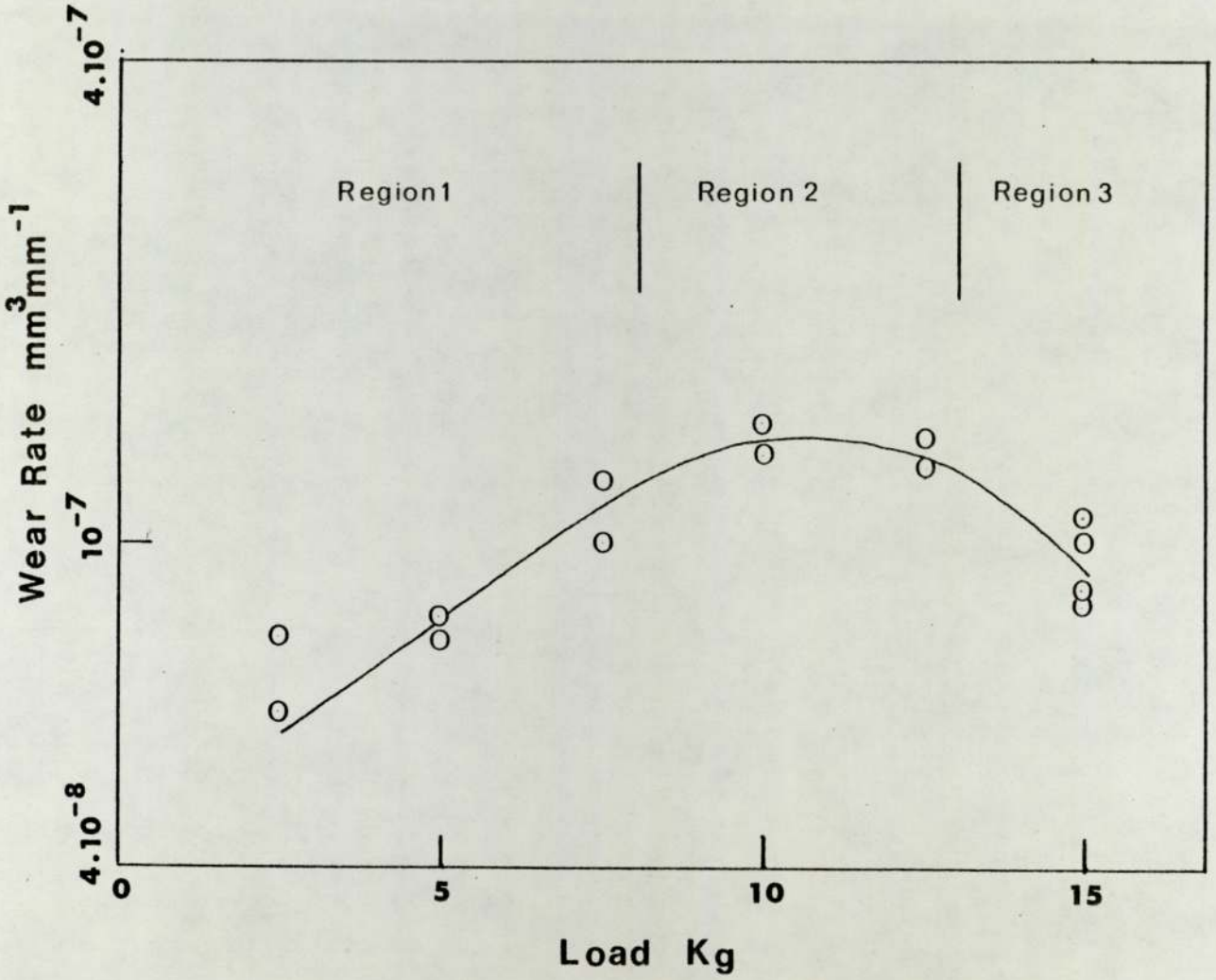

Figure 3.46, Regions of wear from which X-ray samples were taken.

phosphides are also present. Note that these last three samples are taken from the three regions of the curve in figure 3.46.

In the case of the sample taken from the two-piston rig bore failure the results were similar to the hydrofined fuel wear tests. The cadmium found in this sample (Table 3.5) arises from the cadmium plating on the bores. A sample from wear tests using 2, 3, 4 trimethylpentane as the lubricant produced the expected result of aluminium bronze wear debris. These results are given in Table 3.6.

3.3.6 Fuel Analysis

No significant differences were found between the fuel samples when analysed using mass spectrometry or gas-liquid chromatography. The chromatograms show no differences between samples with and without 15 p.p.m. Hitec (figure 3.47(a)). The sample which had become discoloured during storage shows fewer peaks at the initial stage just after injection (figure 3.47(b).

Ellipsometry measurements showed that the corrosion inhibitor Hitec E515 desorbs from silver at about 80°C when heated in a solvent. Table 3.7 shows the measurements taken when slides were dipped into Hitec, fuel plus Hitec and hydrofined fuel. The hydrofined kerosene did not leave any film on the surface as expected. Results for various concentrations of additive in hydrofined kerosene are shown in Table 3.8. A film could be detected down to the 1% by weight level and below this no film could be detected.

Changing the metallurgy to aluminium bronze and KE961 steel and leaving them in the additive for a week produced thick films on the surface which were out of the range of measurement of the ellipsometer. At least some of this film was made up of phorphorus as shown by X-ray analysis as shown in figure 3.48(a) for aluminium bronze and 3.48(b) for KE961 steel.

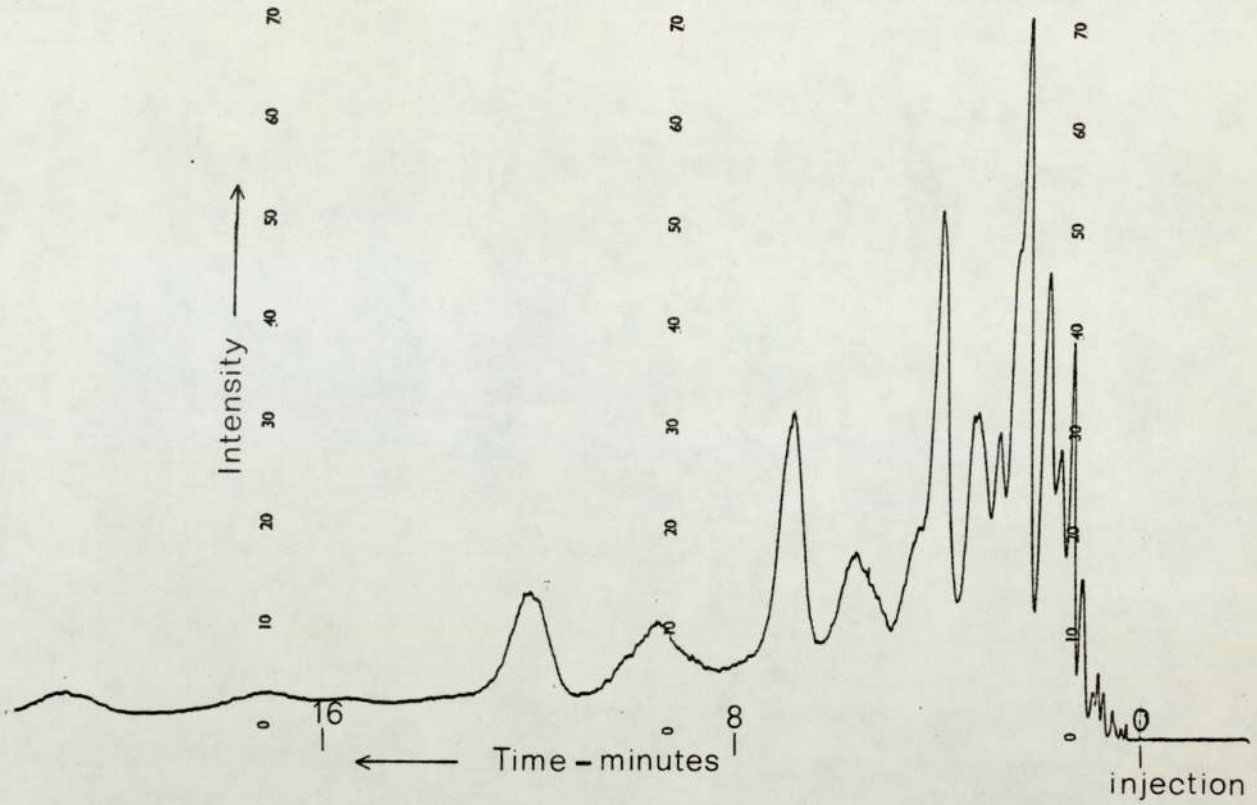

a)Kerosene - with and without Hitec.

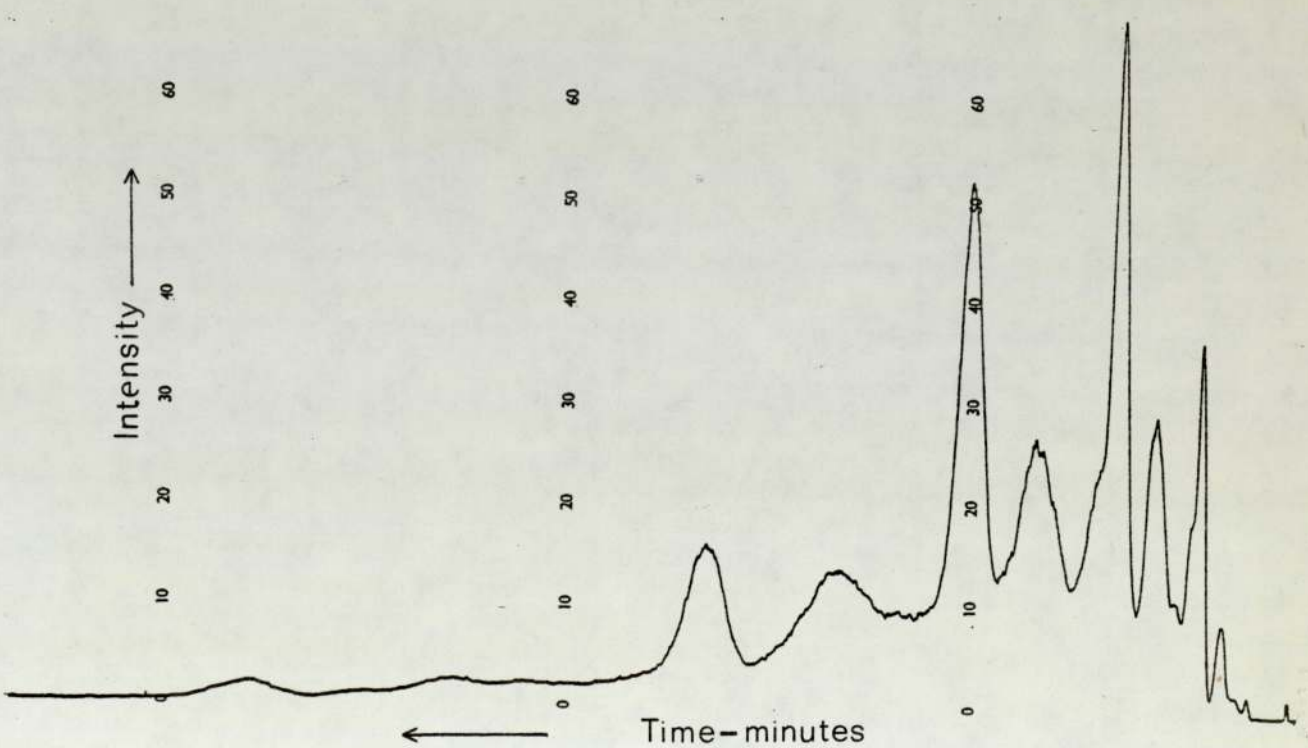

b)Discoloured kerosene.

Figure 3.47, Gas - Liquid Chomatography.

TABLE 3.4 X-RAY ANALYSIS OF WEAR DEBRIS

	d spacings							
	File Values			Al. Bronze	Fuel	Fuel + Additive		
						6Kg	10Kg	12.5Kg
Aluminium	2.34	2.02	1.22	2.92	2.48	4.05	3.19	4.94
Aluminium Ozide	2.55	2.09	1.6	2.52	2.24	3.37	3.04	3.11
Al. Ortho-Phosphate	4.08	2.51	3.16	2.33	2.04	3.14	2.49	2.63
Al. Phosphate (Berlinite)	3.37	4.28	1.84	2.22	2.02	3.04	2.29	2.48
Aluminium Phosphide	3.14	1.93	1.64	2.09	1.81	2.92	2.10	2.17
Copper	2.09	1.81	1.28	2.03	1.31	2.83	2.02	2.09
Copper Oxide (Cu_2O)	2.47	2.14	1.51	1.83	1.28	2.57	1.93	1.93
Copper (II) Phosphate	2.96	2.80	2.58	1.28	1.19	2.48	1.81	1.81
Copper Phosphide	2.01	1.95	2.49	1.22		2.33	1.52	1.65
Iron	2.03	1.71	1.43	1.17		2.13	1.45	1.31
Nickel	2.03	1.76	1.25			2.03	1.31	1.28
						1.75	1.28	1.25
						1.6	1.20	1.21
						1.51		
						1.35		
						1.28		
						1.19		

TABLE 3.5 "d" VALUES FOUND FOR DEBRIS FROM TWO-PISTON RIG BORE FAILURE

ELEMENT/COMPOUND	"d" VALUES				
		File		Measured	Assigned
Aluminium	2.34	2.02	1.22	2.80	2.80/1
Aluminium oxide	2.55	2.09	1.6	2.57	2.58
Copper	2.09	1.81	1.28	2.34	2.34/5
Copper oxide Cu_2O	2.47	2.14	1.51	2.10	2.09
Cu phosphate	2.96	2.80	2.58	2.01	2.0/3
Iron	2.03	1.71	1.43	1.9	1.90/3
Nickel	2.03	1.76	1.25	1.52	1.51
Cadmium	2.35	2.81	2.58	1.49	
				1.32	
				1.25	1.25
				1.19	1.17
				1.28	1.28
				1.43	1.43
				1.40	
				4.82	
				5.53	
				8.70	

TABLE 3.6 "d" SPACINGS FOR ALUMINIUM BRONZE WEAR DEBRIS FROM 2,2, 4 TRIMETHYLPENTANE WEAR TESTS

	File	"d"	Values	Measured "d's"	Assigned "d's"
Aluminium	2.34	2.02	1.22	2.32	2.34
Aluminium oxide	2.55	2.09	1.6	2.10	2.09
Copper	2.09	1.81	1.28	2.03	2.02/3
Iron	2.03	1.71	1.43	1.82	1.81
Nickel	2.03	1.76	1.25	1.42	1.43
				1.28	1.28
				1.22	1.22
				1.19	1.17

TABLE 3.7 FILM THICKNESS AT 20°C AND 80°C

	TEMP °C	POLARISER ANGLE	INITIAL ANALYZER	FINAL ANGLES	THICKNESS Å
Hitec	20	84.5	153.5	164.7	260
Fuel + Hitec	20	87	153	158.5	110
Kerosene	20	95.5	131.1	131	0
Hitec	80	87.25	153.5	153.5	0
Fuel + Hitec	80	84.4	153.4	153.4	0
Kerosene	80	95.1	131	131.1	0

TABLE 3.8 FILM THICKNESS - CONCENTRATION AT ROOM TEMPERATURE

CONCENTRATION HITEC - % WT	POLARISER ANGLE	INITIAL ANALYZER	FINAL ANGLES	THICKNESS Å
100	1.82	64	77	260
10	1.82	62	75.3	260
1	1.84	65.5	77	260
0.1	1.81	58.3	59.45	0
0.01	1.62	60	60.45	0

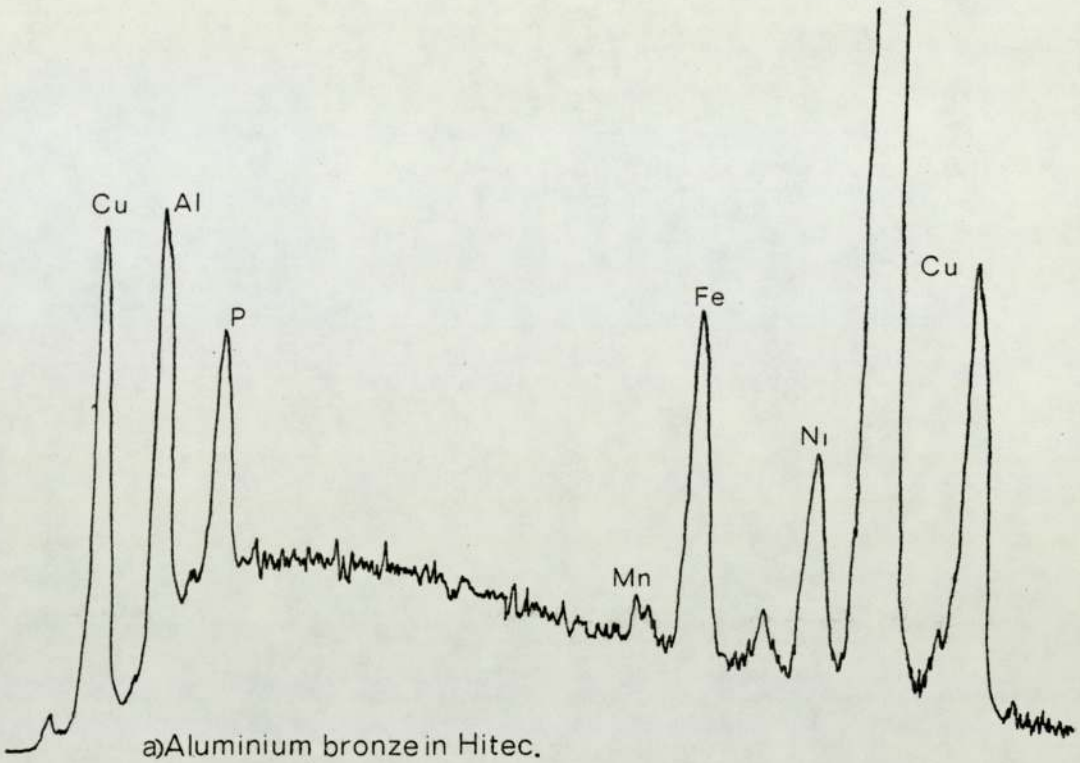

a)Aluminium bronze in Hitec.

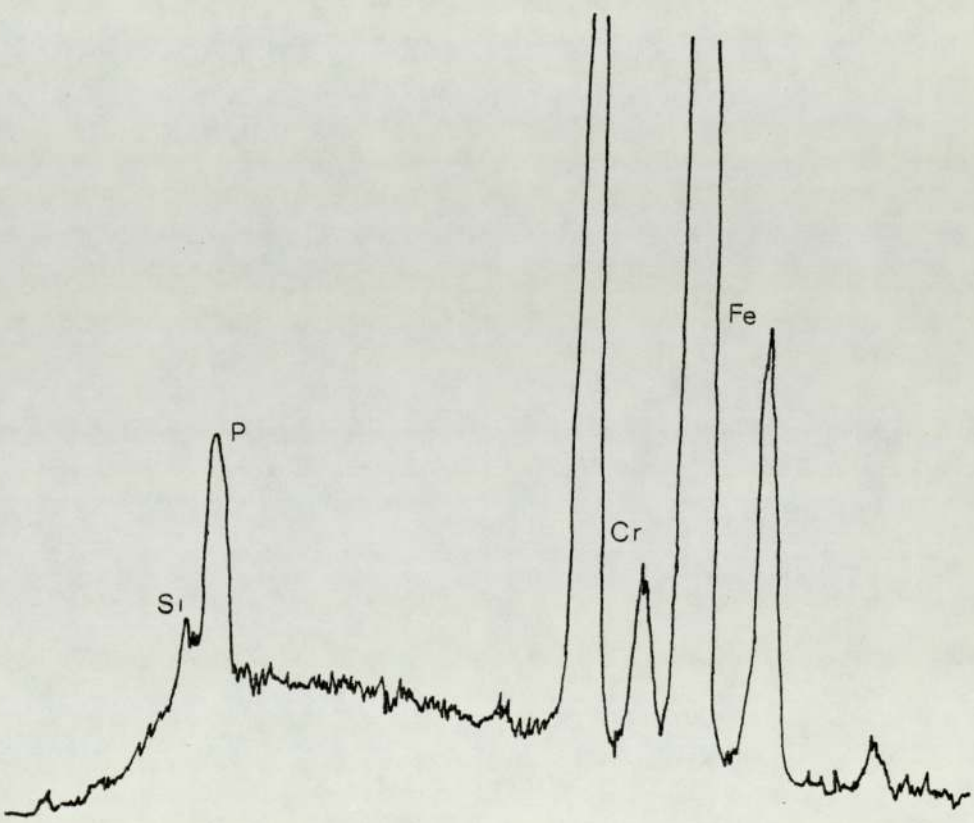

b)KE961 Steel in Hitec.

Figure 3.48, S.E.M. Energy Scans – Ellipsometry Samples.

CHAPTER 4

THEORETICAL CONSIDERATIONS

4.1 Introduction

Any theory for boundary lubrication must take into account the action of the lubricant and the state of the metal surfaces.

The results of the experiments with aluminium bronze sliding against steel in the presence of kerosene, have shown that an oxide layer exists at the surface of the bronze, which is the major wearing component. This occurs, in particular, when the complex additive Hitec E515 is present. The additive contains a dimeric acid which acts as a boundary lubricant in this system.

In a normal dry wear situation the real area of contact occurs at small areas, termed asperities, as shown in figure 4.1(a). These areas can reach quite high temperatures because of frictional heating thus accelerating the rate of oxidation. The effect of a boundary lubricant is to separate most of these contact regions by the adsorption of polar molecules onto the surface (figure 4.1(b)). This means that oxidation and wear is reduced or prevented.

However some contacts will still be sufficiently loaded for this protective film to be broken down so that the real area of contact is reduced by some fraction from the dry wear case. Once the film is broken down oxidation and wear can take place as in the dry wear situation. This is illustrated in figure 4.1(c) and (d). The film is unlikely to be complete, as in the idealised case presented so far, because of adsorption-desorption effects and the presence of the base solvent (kerosene in this case). A consequence of this is that contact between the two surfaces will

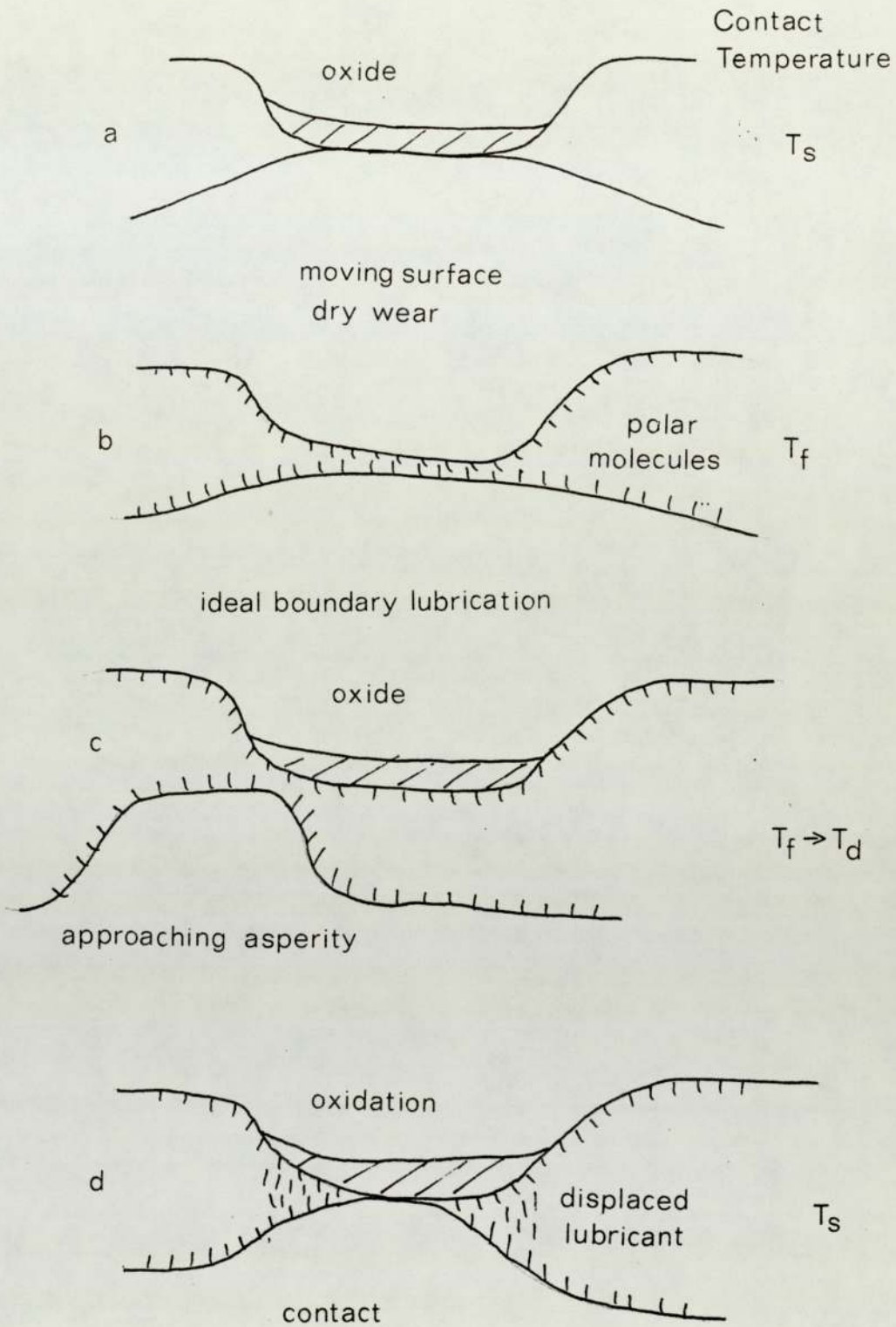

Figure 4.1, Wear Processes.

occur more readily in poorly lubricated regions.

A theory will now be developed which takes into account the oxidation of the surface and the reduction of the real area of contact by the presence of a boundary lubricant.

4.2 Oxidational Wear

Consider Archards wear equation as expressed for the dry wear situation:

$$\frac{V}{d} = K A_r \qquad \ldots (1)$$

where V is the volume of material removed, d is the total sliding distance, A_r the real area of contact and K the probability of forming a wear particle.

Following the method used by Quinn (52) to find a value for the K factor we assume a parabolic dependence of the oxide film thickness with time. The mass per unit area of oxide formed at the surface, M, is then given by:

$$\Delta M = k_p t \qquad \ldots (2)$$

where p is the parabolic rate constant and t the time for which asperity contact occurs. This time can be expressed as:

$$t = \frac{a}{uK} \qquad \ldots (3)$$

where 'a' is the Hertzian diameter associated with circular contacing asperities, u the linear speed between the two asperities and K as defined above.

Combining equations (2) and (3) it can be shown that:

$$\Delta M^2 = \frac{k_p a}{uK} \qquad \ldots (4)$$

further $$\Delta M = \rho g h \qquad \ldots (5)$$

where g is the fraction of oxide which is oxygen, ρ the density of the oxide and h the oxide thickness. Hence from equations (4) and (5):

$$K = \frac{k_p a}{Ug^2 \rho^2 h^2} \qquad \ldots (6)$$

The accepted relationship between the rate constant and activation energy, Qp, is given by the expression:

$$k_p = Ap \exp (Qp/RT_s) \qquad \ldots (7)$$

where A_p is the Arrhenius constant, T_s the temperature of the surface at which the reaction is taking place and R, the universal gas constant.

Equations (6) and (7) are combined to give:

$$K = \frac{a A_p \exp (Q_p/RT_s)}{ug^2 \rho^2 h^2} \qquad \ldots (8)$$

This expression and suitable substitution for the real area of contact leads to the oxidational wear equation for the dry wear situation.

$$\frac{V}{d} = \frac{2 Ap \exp (- Q_p/RT)}{ug^2 \rho^2 h^2 \sqrt{n\pi}} \left(\frac{W}{Pm}\right)^{3/2} \qquad \ldots (9)$$

where n is the number of contacting asperities and Pm the hardness.

4.3 Boundary Lubrication

Previously, it was stated that when a boundary lubricant was present a fraction of the real area of contact (under dry wear conditions) was prevented from coming into contact by the lubricant. The real area of contact can now be expressed as:

Real area of contact = αA_r

where A_r is the real area of contact under dry wear conditions and α the fractional film defect. The wear equation for boundary lubrication can now be written as:

$$\frac{V}{d} = K \alpha A_r \qquad \ldots (10)$$

The fractional film defect has been defined by Kingsbury (42) as:

$$\alpha = \frac{N_s - N}{N_s} \qquad \ldots (11)$$

where N_s is the total number of sites available for a molecule to absorb onto the surface and N is the number of occupied sites.

Frenkel (67) has shown that the average time that a molecule stays at a particular site is:

$$t_r = t_o \exp (E/RT_s) \qquad \ldots (12)$$

where t_r is the time of vibration of the molecule, E the heat of adsorption of the boundary molecule and T_s again is the temperature of the surface film.

The time required for an asperity to move a distance, x, at a speed u ms^{-1} is given by:

$$t_x = \frac{x}{u} \qquad \ldots (13)$$

where x is the metal lattice spacing or the diameter of an absorbed molecule.

The following conditions now apply by the use of equations (11), (12) and (13). If $t_x \gg t_r$ then $\alpha \rightarrow 1.0$ and the molecules have plenty of time to move and $N \rightarrow 0$. If $t_x \ll t_r$ then $\alpha \rightarrow 0$, the molecules have little time to detach and $N \rightarrow N_s$.

The equation,

$$1 - \alpha = \exp(-t_x/t_r) \qquad \ldots (14)$$

relates α, t_x and t_r and satisfies the above conditions. Substituting for t_x and t_r from equations (12) and (13) in this equation (14) results in the relationship:

$$1 - \alpha = \exp - \frac{x}{ut_o \exp(E/RT_s)} \qquad \ldots (15)$$

Taking logarithms to the base 'e' for equation (15) gives

$$\ln(1 - \alpha) = \frac{- x}{ut_o \exp(E/RT_s)} \qquad \ldots (16)$$

Experimentally, provided $u > 0.1$ ms^{-1}, $\alpha \leq 0.01$ even for a poor lubricant. Consequently the term $\ln(1 - \alpha)$ is approximately equal to $-\alpha$ and equation (16) becomes:

$$\alpha = \frac{x}{ut_o \exp(E/RT_s)} \qquad \ldots (17)$$

Returning to the wear equation (equation 10) that is $\frac{v}{d} = K\alpha A_r$ we now have an expression for α which accounts for boundary lubrication. In section 4.2 it was shown that the K factor was related to the oxidation rate through the equation:

$$K = \frac{a A_p \exp(-Qp/RT_s)}{ug^2 \rho^2 h^2} \quad \ldots (18)$$

The real area of contact and Hertzian diameter are interrelated and can be expressed in terms of the load W, hardness P_m, and the number of contacts n through the equations:

$$A_r = \frac{W}{P_m} \quad \ldots (19)$$

and $$A_r = \frac{n\pi a^2}{4} \quad \ldots (20)$$

substitution for K, α, A_r and 'a' from equation (17), (18), (19) and (20) in equation (10) leaves us with the result for the wear rate as:

$$\frac{V}{d} = \frac{2 A_p x}{u^2 g^2 \rho^2 h^2 t_o \sqrt{n\pi}} \operatorname{Exp}\left(-\frac{(Qp + E)}{RT_s}\right) \left(\frac{W}{P_m}\right)^{3/2} \quad \ldots (21)$$

This equation has assumed that the temperature of the surface film is equal to the oxidation temperature at the contact. A significant increase in the rate of oxidation will only occur if the molecules at the surface desorb allowing contact to occur. This can only happen if the temperature of the surface film, T_f, is increased to the desorption temperature, T_d, of the boundary lubricant. This can occur by increased shearing of the surface film in the highly loaded contact regions. Generally speaking polar molecules from the additive will be continuously adsorbing and desorbing from sites on the surface even at temperatures below the desorption temperatures. Once a high enough temperature is reached there will be sufficient energy at the surface to desorb the majority of the polar molecules. This then allows the metallic surfaces to interact producing a sharp rise in temperature at the

surface and allowing rapid oxidation to occur. As the asperities come out of contact the lubricant will rapidly cool the surface allowing polar molecules to readsorb onto the worn region. To take into account the protection afforded by the polar molecules up to desorption temperature, the wear equation (21) can be modified by dividing the exponential term up into two components to give:

$$\exp\left(-\frac{E}{RT_d}\right) \times \text{Exp}\left(-\frac{Qp}{RT_s}\right)$$

where the first exponent represents the additive term and the second the oxidation term.

The wear equation can now be written as:

$$\frac{V}{d} = \frac{2\,Ap\,x}{u^2\,g^2\,p^2\,h^2\,t_o}\;\frac{1}{\sqrt{n\,\pi}}\;\text{Exp}\left(-\frac{Qp}{RT_s}\right)\text{Exp}\left(-\frac{E}{RT_d}\right)\left(\frac{W}{P_m}\right)^{3/2} \ldots (22)$$

4.4 Solutions of the boundary lubrication oxidational wear equation

Initial calculations were made with equation (21) assuming the temperature of the surface film was the same as the temperature of oxidation.

$$\frac{V}{d} = \frac{2\,Ap\,x}{u^2\,g^2\,p^2\,h^2\,t_o}\;\frac{1}{\sqrt{n\,\pi}}\;\text{Exp}\left(-\frac{(Qp+E)}{RT_s}\right)\left(\frac{W}{P_m}\right)^{3/2}$$

Values were found for most of the parameters in this equation as follows.

4.4.1 Arrhenius constant Ap and Activation Energy Qp

The value for the Arrhenius constant was initially taken as that found from static oxidation experiments. Tylecote (68) quotes a value of 1.5×10^{-3} $Kg^2\,M^{-4}\,S\text{-}1$ for the oxidation of oxygen free copper in air in the temperature range 300°C to 550° C. Since this temperature was close to what might be expected in the wear

situation, this value of Ap was used. The associated value for the activation energy was given as 20 Kilo calories.

4.4.2 Lattice spacing or molecular diameter, X

The value of X was fixed by consideration of the size of the fatty acid in the additive Hitec E515, and of the lattice spacing of copper oxide, Cu_2O. The lattice structure of Cu_2O is a primitive cubic structure with a lattice spacing of 4.2696×10^{-10}M.

A first estimate of the molecular diameter must be, at least, the width of the ring structure of the dimer acid. Assuming that the ring exists in one plane only the maximum size would be 6.85×10^{-10} M. This is greater than the lattice spacing of Cu_2O so X must be at least two lattice spacings which is approximately 10^{-9}M. Dacre et al (41) quote values for the dimer acid size depending on the molecules orientation on the surface.

4.4.3 Time of Vibration, t_o

This parameter has again been measured, by various workers, for molecules on surfaces under static conditions. The relationship $t_o = h/kT$, where h is Plank's constant, k is Boltzmann's constant and T the absolute temperature, is given by de Boer (69) for the case of strong binding to the surface. In this work t_o was taken to be 10^{-13} seconds. Another problem with this is that most measurements have been made with gases rather than liquids so it has to be assumed that the value used is the correct order of magnitude.

4.4.4 Other fixed parameters

The values of A_p, Q_p, x and t_o have been assumed to be constants in the wear equation with the values assigned in the preceding sections. A number of other parameters are also taken to be constant. The fraction of oxide, g, which is oxygen was

calculated to be 16/144 for copper oxide. The density of this oxide is about 6×10^3 Kg M^{-3}. An oxide film thickness was estimated, from replicas and scanning microscope photographs of the surface, to be about 3×10^{-8}M on average with a hardness of 10^9 NM^{-2}.

The value for the heat of adsorption for a dimer acid is given at 13 K calories by Allen and Drauglis (62). The remaining parameters were fixed as representative of the wear tests carried out. This gives the speed as 0.62 MS^{-1} and loads of 2.5 Kg to 15 Kg in steps of 2.5 Kg. Initially a load of 10 Kg with a surface temperature T_s of 500°K was used to check that the above values were correct.

This leaves the value of n, the number of contacts, to be fixed. Taking a load of 10 Kg and a value for the wear rate from the experimental data an estimate of the value of n could be found. The estimate of n, using the above data turned out to be much less than one indicating that one or more of the values chosen was incorrect.

4.4.5 Re-evaluation of the Arrhenius constant

It was decided at this stage that a better approach might be to assume that the number of contacts lay in the range from three up to one hundred and then calculate the value for the Arrhenius constant. These values of n would appear to be reasonable from dry wear tests. Previously we used a value of Ap obtained from metallic oxidation under static conditions. However, the rate of oxidation may be affected by the dynamical nature of the wearing system. The rate constant will be determined by the time for which any two wearing asperities are in contact, the temperature and the oxygen pressure. It is also known that where fresh metal is continuously being exposed that the oxidation rate is extremely fast. Consequently the value of the Arrhenius constant may be much

higher than 1.5×10^{-3} Kg^2 M^{-4} S^1. Note that the activation energy would not be expected to change under dynamic conditions and so the rate constant is the only parameter that can change in the parabolic rate equation (apart from temperature which we have fixed).

4.4.6 Surface Temperatures

The calculation of the Arrhenius constant depends on the temperature that is assumed to be at the contacts. In the above calculation a value of $T_s = 500^oK$ was used as representative of metal-to-metal contact. However in the lubricated case the cooling effects of the lubricant must be considered. Further, in this theory, the assumption, that the dimer acid is the major lubricity agent is being made in order to simplify the problem. This component is known to desorb at about 350^oK (80^oC).

Taking T_s to be 353^oK and the number of contacts to be 100 the value of Ap was found to be 1.84×10^6 Kg M^{-4} S^{-1} for a load of 10 Kg and wear rate of 1.35×10^{-12} M^3 M^{-1}.

4.4.7 Calculations

Computer programs were written to calculate the wear rate against variations in Arrhenius constant, number of contacts and surface temperature. A program was also written in which only the number of contacts and the Arrhenius constant was varied. This was done so that the number of results of wear rate in the range 10^{-9} to 10^{-6} mm^3 mm^{-1} against Arrhenius constant could be plotted. For this program the temperature was fixed at 350^oK and load at 10 Kg.

Finally a program was written so that computed values of wear rate could be compared to the experimental values. If the computed value was close to the experimental value then values of Ap, n and T_s along with computed and experimental wear rates and the load were printed out. This program was run for equations (21) and (22).

4.4.8 Results of the Theoretical Calculations

The plot of the number of results of wear rate in the range 10^{-9} mm^3 mm^{-1} to 10^{-6} mm^3 mm^{-1} against Arrhenius constant for a load of 10 Kg is shown in figure 4.2. This shows that an optimum value exists for the value of the Arrhenius constant of 1.3×10^6 Kg M^{-4} S^{-1}. The distribution of results about this value is not a normal distribution over the range considered. The exponential nature of the wear equation would be expected to have a large influence and this is seen in the results.

The variations of wear rate against temperature, number of contacts and Arrhenius constant are shown in figure 4.3. Wear rate is seen to be very sensitive to temperature (figure 4.3(a)). An increase of 30^oK changes the wear rate from 1.55×10^{-9} mm^3 mm^{-1} to 2.9×10^{-7} $mm^3 mm^{-1}$ for a constant number of contacts and a constant Arrhenius constant.

The wear rate increases with increasing Arrhenius constant for a given temperature and number of contacts (figure 4.3(b)), whilst the converse is true for the variation of wear rate with number of contacts (figure 4.3(c)) at a given temperature and Arrhenius constant. All three sets of curves suggest an infinite number of solutions exist with the range considered.

If the effect of the boundary lubrication is removed from the equation, that is the α term is removed, then the same basic curves are maintained but at much higher values of wear rate. This is provided Ap, n, T_s etc. are kept at the same values (figure 4.4).

The computer search program which compared theoretically calculated wear rates with experimental data predicted an increase in the number of contacts with increasing load for a constant temperature. The tendency was for temperature to remain constant or, if anything, fall slightly with increasing load. These differences

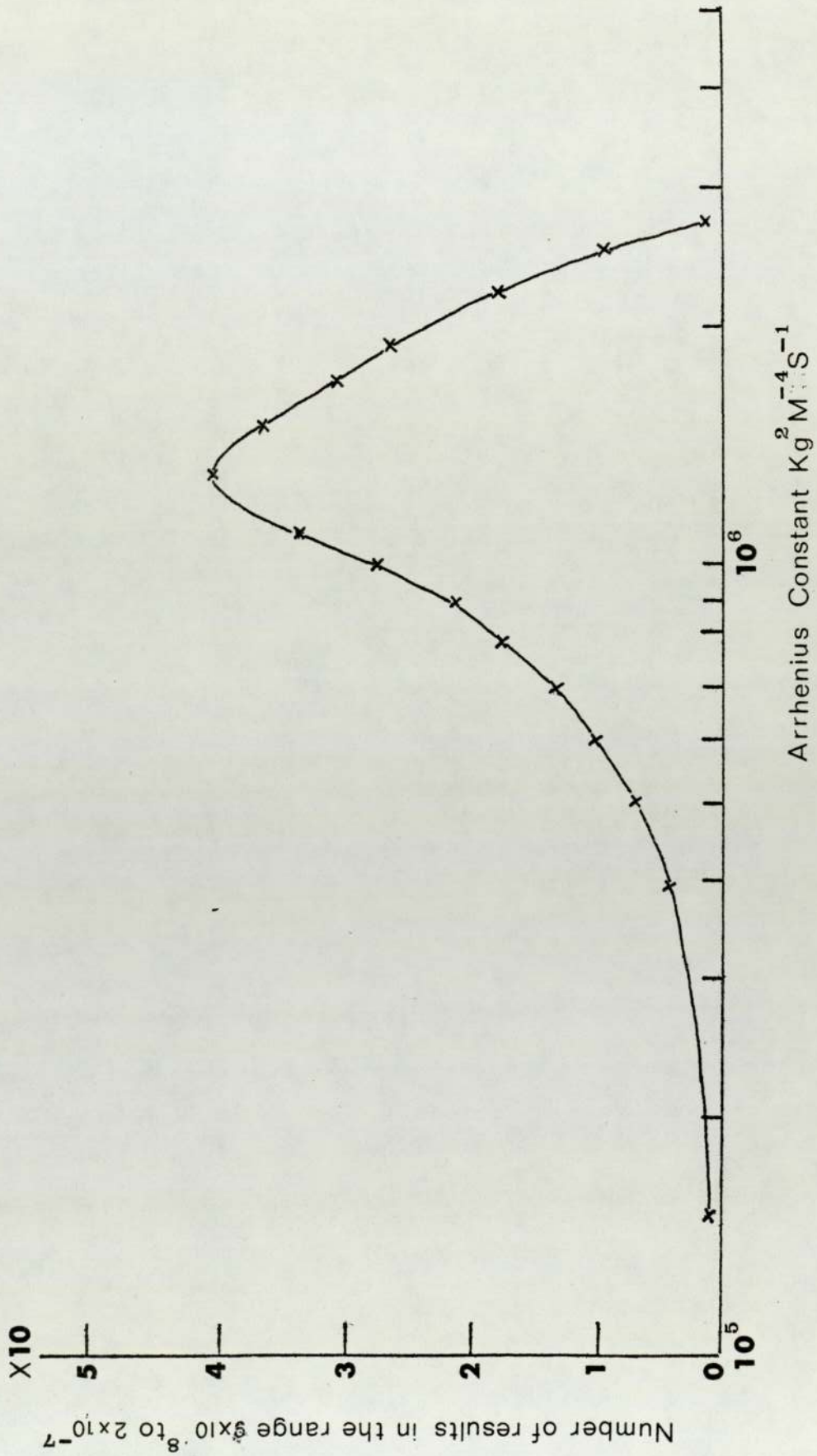

Figure 4.2. Variation of number of wear results with Arrhenius constant.

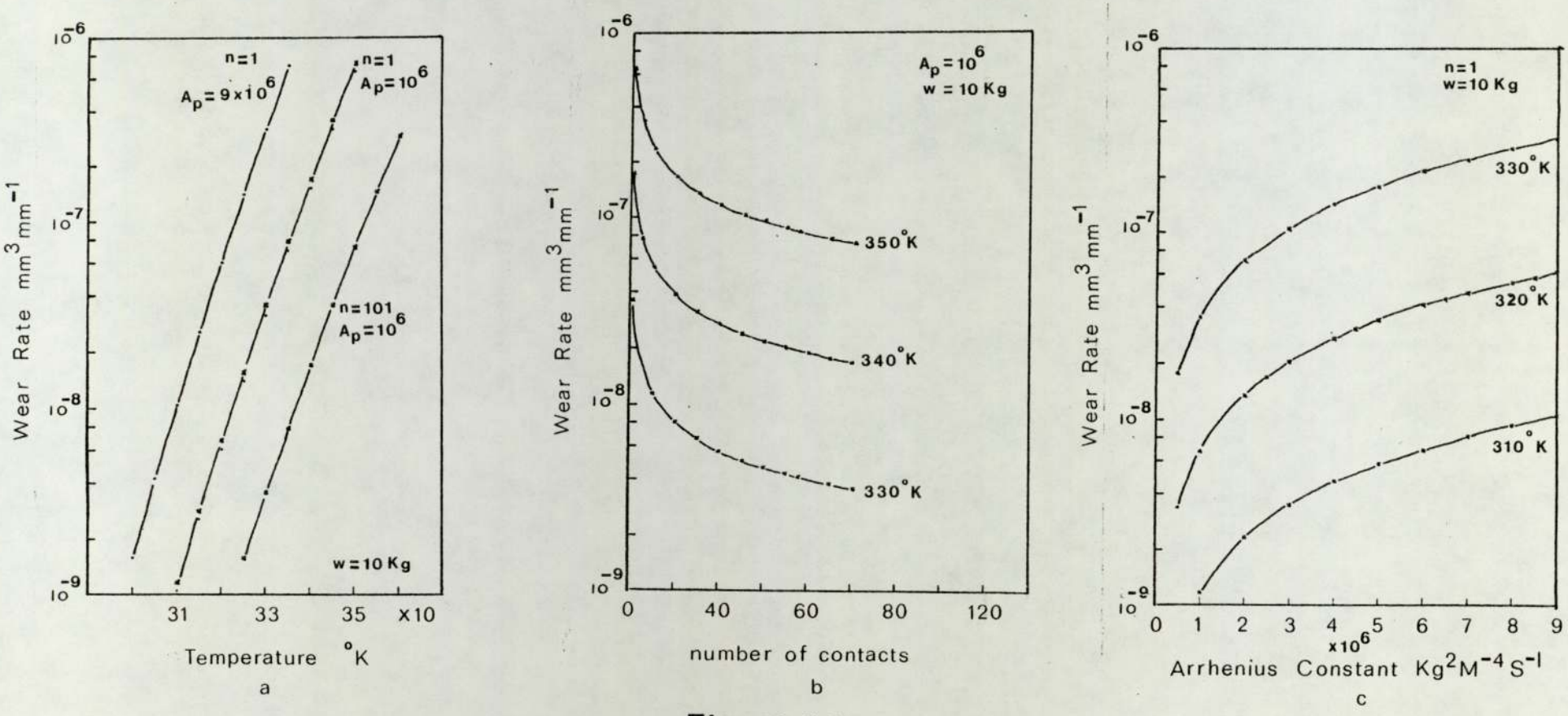

Figure 4.3

Boundary lubricated oxidational wear predictions

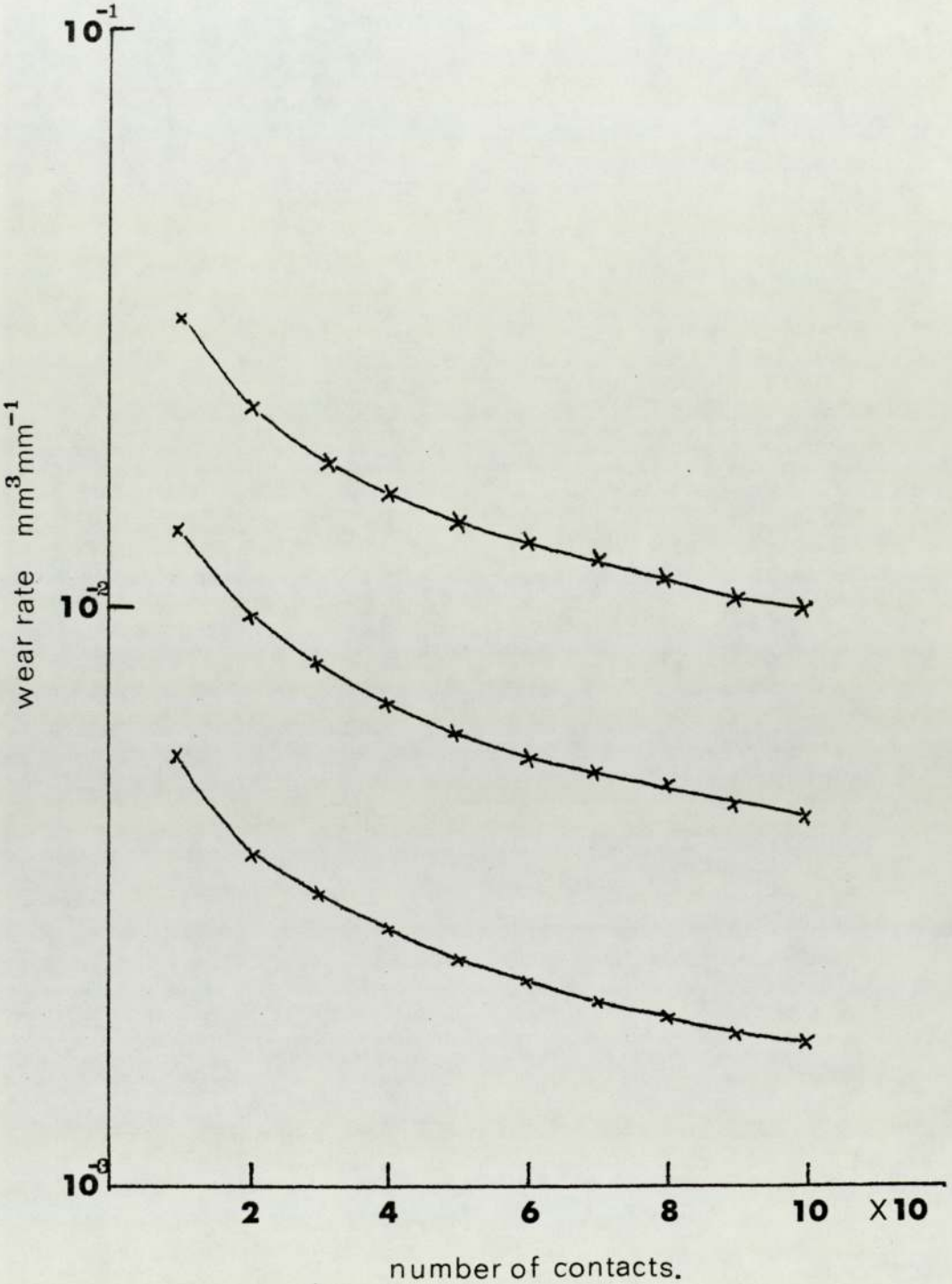

Figure 4.4. Predictions for dry wear.

are shown in figure 4.5(a). Again it can be seen that a number of curves exist. A similar result was found for the modified wear equation (equation 12) where the desorption temperature of the boundary lubricant is taken into account. These results are seen in figure 4.5(b). The main effect of the modification was to increase the number of contacts at a given load and temperature to produce the required wear rate. An example of this can be seen at a load of 10 Kg and 350°K where, for the modified equation, the predicted number of contacts is between 54 and 62 whilst for the original equation (equation 21) the prediction was 40 contacts.

4.5 The Delamination wear theory applied to Boundary Lubricated Wear

4.5.1 Introduction

Suh (70) has objected to the adhesive theory of wear on which the preceding theory is based. His main critisms of Archard's theory are (a) that it ignores the physics and physical metallurgy of metal deformation (b) the assumptions used and (c) the fact that the theory does not provide any insight into the wear of metals under different sliding conditions.

4.5.2 Suh's delamination wear theory

This theory is based on the following assumptions (a) the metals wear layer by layer, each layer consisting of N wear sheets, (b) the number of wear sheets per layer is proportional to the average number of asperities in contact at any instant between the two surfaces and (c) the rate of void and crack nucleation and the critical degree of shear deformation for loose particle formation can be expressed in terms of a critical sliding distance, d_o, for a given sliding situation.

From these assumptions it can be seen that the theory depends on dislocation theory, plastic deformation and fracture of metals

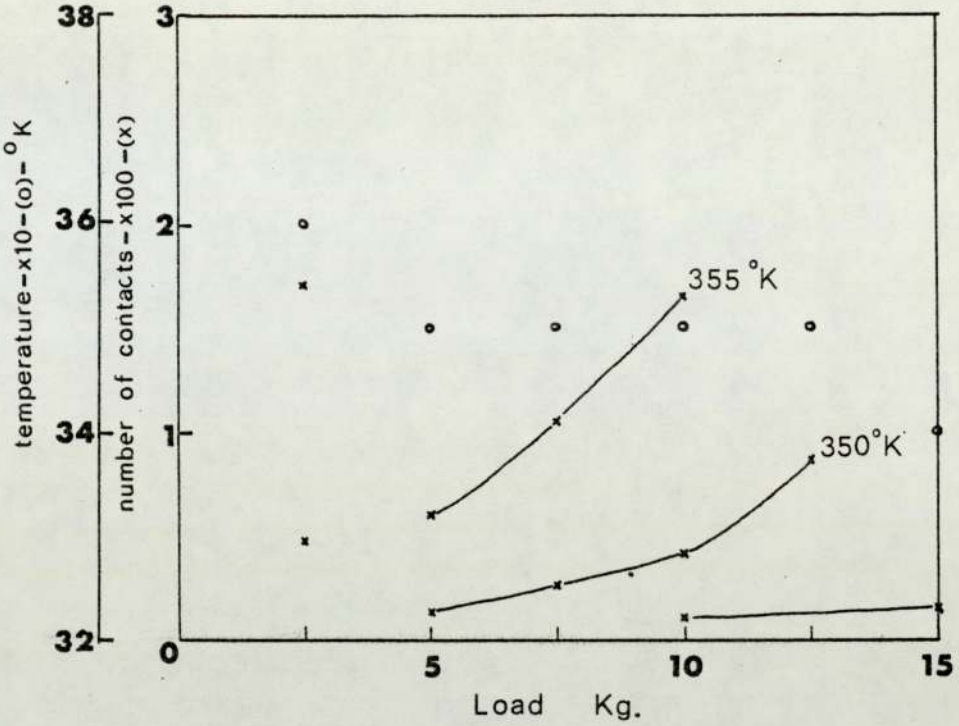

a) Boundary lubricated oxidational wear.

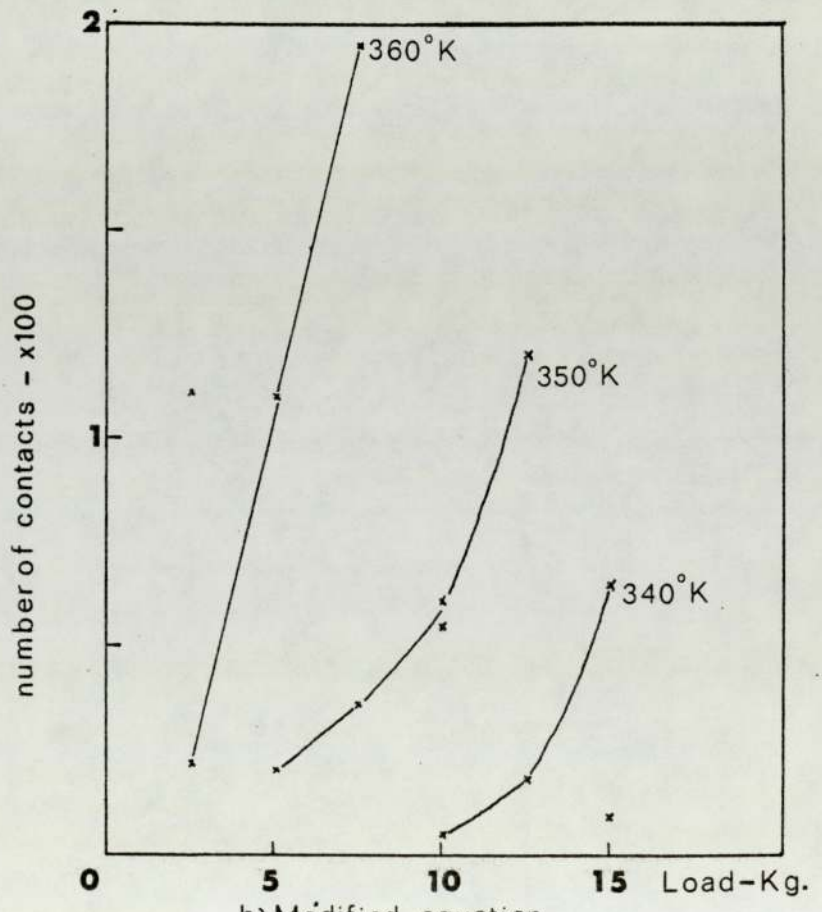

b) Modified equation.

Figure 4 5, Computer predictions.

near a surface.

The total wear of a hard - soft combination was expressed by Suh as a volume removed, V.

$$V = N_1 (d/d_{o1}) A_1 h_1 + N_2 (d/d_{o2}) A_2 h_2 \quad \ldots (1)$$

where the subscripts refer to the hard (1) and soft (2) materials, N is the number of delaminated wear sheets, A is their average area and d_o is defined as the critical sliding distance required for the removal of a complete layer.

The wear sheet thickness is given by:

$$h = \frac{G\, b}{4\,(1-\nu)\ \sigma_f} \quad \ldots (2)$$

where G is the bulk modulus, σ_f the friction stress, b the Burger's vector and ν Poisson's ratio.

Assuming that the area of these sheets is given by $A = CA_r$ where C is a constant of proportionality and A_r the rea area of contact it can be shown that:

$$V = kWd \quad \ldots (3)$$

In this wear equation the constant k is given by the expression:

$$k = \frac{b}{4\pi} \left[\frac{K_1 G_1}{\sigma_{f1} (1-\nu_1)\, d_{o1}} + \frac{K_2 G_2}{\sigma_{f2} (1-\nu_2)\, d_{o2}} \right] \quad \ldots (4)$$

with K_1 and K_2 constants depending on the surface topography.

4.5.3 Boundary Lubrication

Suh's wear equation (3) can be modified, in the same way in which Archard's equation was modified, by the introduction of the

fractional film defect. This will then introduce the effect of lubrication into the equation. To simplify the problem it will be assumed that only the soft surface wears. The wear equation can then be written as:

$$\frac{V}{d} = \alpha_2 N_2 \frac{A_2 h_2}{d_{o2}} \qquad \ldots (5)$$

where α_2 is the fractional film defect. Substituting for values of α_2, N_2, A_2 and h_2. This results in the equation:

$$\frac{V}{d} = \frac{b}{4\pi u t_o} \frac{K_2 G_2 X_2}{d_{o2} (1-\nu_2)\sigma_{f2}} \text{Exp } (-E_2/RT_2)W \qquad \ldots (6)$$

The delamination wear theory is based on metallic contact with assumption that any oxide layer is thin compared to the thickness of the delamination wear sheets. Consequently solutions have not been sought for this equation. More will be said about this, and other theories, in the discussion.

CHAPTER 5

DISCUSSION

5.1 Introduction

The wear results will be compared to those obtained by other workers and a comparison made between the fuels analysed.

A review will be given of the metallurgy found at the wearing surfaces under various conditions of friction, wear and type of lubricant. From this, physical and chemical processes such as the Kirkendall effect and oxidation, involved with seizure, in the case of a hydrofined fuel, and prevention of wear, in the case of a fuel containing Hitec, will be elucidated. Correlation between "in-service" failures and laboratory testing will be illustrated. Further it will be shown how these results effect the interpretation of those from tests, such as the dwell test, used to rank fuels.

Finally the relevance of the theory developed in Chapter Four will be discussed with respect to the results and other existing theories.

5.2 Wear Tests

5.2.1 Comparison with past work

The use of Stribeck curves was found satisfactory as a means of determining conditions for boundary lubricated wear. Three distinct regions were observed when the additive was present (figure 3.1) which enabled the boundary region to be easily identified. Surface roughness was found to affect the result obtained in that the transition from boundary to fluid film conditions was not so pronounced. The objection raised by Fein (61) about the whole curve being generated by elastohydrodynamic conditions has been avoided by

monitoring contact resistance between the two surfaces (figure 3.2).

The results from the Stribeck curve tests suggest that this may be a fairly rapid way of ranking fuels with respect to lubricity. Response at high speed depended on the concentration of Hitec (figure 3.4) with seizure occurring at the zero and 15 p.p.m. levels. However friction has been shown to be dependent on surface roughness of the pins and disks used and to the mode of wear.

Work carried out previously has been concentrated at the boundary lubrication region of the Stribeck curve, but the evidence from these tests suggest that an investigation at high speeds may be worthwhile. This is illustrated by figure 3.4 showing film breakdown and seizure with increase in speed.

The present results are the first to systematically record wear rate against load for a given speed with the aluminium bronze-steel metallurgical combination. Most of the work prior to this investigation has been carried out by companies directly involved with kerosene lubricity problems. They have, out of necessity, been intent on finding a rapid solution rather, than isolating the fundamental mechanisms. This has meant that research was aimed at ranking fuels according to their lubricating ability. Emphasis has been placed on the chemistry of the fuels (4, 10, 23) with little attention being paid to metallurgical changes occurring during the tests. However, to understand the problem in its entirety, it is also necessary to consider what happens to the metal surfaces rather than to investigate the fuels in isolation.

Commercial requirements have meant that a short duration test for the calibration of fuels has been sought. Consequently many of the tests have been run for 15 to 30 minutes meaning that little time has been allowed for any mode of wear to be established. Another reason for the short duration of the tests carried out by

many workers is that they have been trying to find seizure conditions with hydrofined fuel (four-ball tests).

The present tests have been run for periods which have allowed wear to become stabilised in a particular mode and then, after the tests, the surfaces have been analysed to determine what has occurred during wear. Further, these tests have been carried out over a wide range of loads which thus covered the possibility of seizure conditions.

Vere (4) is one of the few workers to publish wear data for the silver plated steel-on-steel system. An estimate of wear rate from his wear against time graph, for a production hydrotreated kerosene (figure 1.4), gives a value of 6×10^{-7} mm^3 mm^{-1}. These results are similar to those found in the present work.

Since the wear results given by other workers have been measurement of wear scar diameter and friction no further comparisons between this work and published wear data will be given at this stage. These results will be more easily discussed in the light of the surface analysis results obtained in the present work.

The shapes of the curves obtained with the various roughnesses are interesting. Sharma and Cameron (71) have shown that the heat adsorption of boundary lubricants is dependent on surface roughness. They found that surfaces have an optimum roughness of 0.4064 μm c.l.a. for maximum heat of adsorption. Bjerk (72) points to some results which are the reverse of those found by Sharma (71). The problems of relating the effect of surface roughness as found by Sharma, Bjerk and the work carried out here would appear to be one of the different conditions under which results were obtained. In particular the results of this work were obtained with a flat-faced aluminium bronze pin on a flat steel disk whilst Sharma used a steel ball-on-plate and Bjerk used steel rollers. Note also in figure 3.10

the maximum roughness used was 0.00254 μm c.l.a. for the bronze wear pins. Further the work of Sharma was not concerned with situations in which chemical reactions are occurring but was restricted to the reversibly physically adsorbed layers on steels. Having made the above comments it is still appreciated that Sharma's (71) results and those of Sharma, Malhotra and Cameron (73) may still be significant in the results found with the pin-on-disk machine. More will be said about the shape of the curves obtained in this work in terms of the surface metallurgy. For the present it will be noted that the minimum wear rate, found when varying surface roughness, may be indicative of a maximum heat of adsorption as found by Sharma et al and that the transition on the wear rate against load curve (with the additive present) may also be due, in part, to this effect.

Furey (59) has shown the problems of measuring contact temperatures for dry wear situations. From his work it can be seen that the experimental results are generally an under estimate of the real contact temperatures. In this work no high temperature spikes were observed for the lubricated case. Reasons for this will be those associated with dry wear, plus the fact that a thick wear track rapidly builds up, that oxides form and the effect of the lubricant is to make the contact time very small. The latter point probably means that the response time of the amplifier was not great enough. The dry wear measurements produced temperatures similar to those measured by Furey and would consequently appear to be reasonable although lower than expected.

5.2.2 The effect of Hitec E515 on wear

Comment has already been passed on the desire of the companies involved with the lubricity problem requiring a test to

rank the fuel according to their lubricating ability. In addition the test is also required to detect the presence or otherwise of lubricity improvers such as Hitec E515. Most of the results obtained and given in Chapter 3 enable a direct comparison to be made between fuels with and without the addition of Hitec E515. The comparison is illustrated in figure 3.9 for 2 mm diameter pins. It can be seen that there was very little difference between the wear rates for the two samples over most of the load range. Seizure did occur with the hydrofined fuel at a load of 15 Kg. A similar comparison can be made for the 3 mm diameter wear pins (figure 5.1). It can be seen that the additive has an apparent pro-wear effect up to a load of about 12.5 Kg. This apparent pro-wear effect was again observed in tests varying the concentration (Table 3.1). However if the test was allowed to run for sufficient time then zero wear was observed. Other workers have found this pro-wear effect of Hitec and arrived at the conclusion that their tests have failed to rank fuels. It can now be seen that the ranking of a fuel depends on both the test conditions and on the duration of the test.

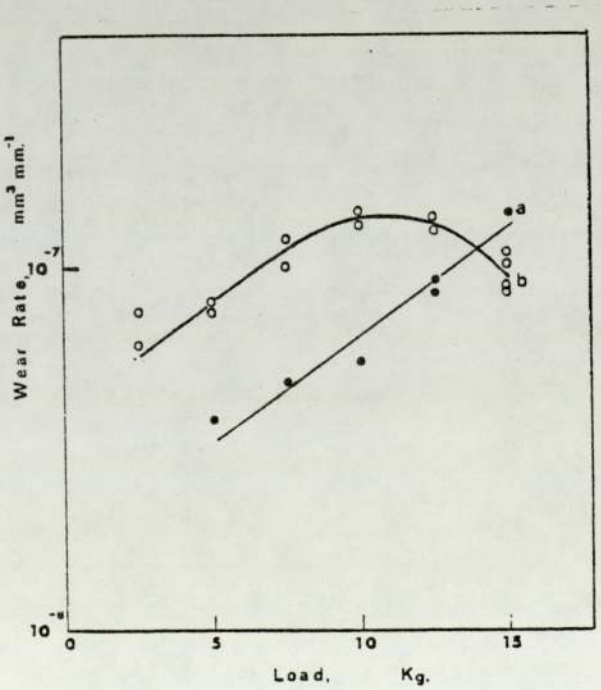

Figure 5.1. Comparison between fuel (a) with and (b) without Hitec E515 - 3 mm diameter wear pins @ 0.62 ms^{-1}.

A standard statistical analysis on thirteen wear results gave the mean wear rate for the fuel with Hitec greater than that for Hydrofined fuel at a load of 10 Kg and 0.62 ms^{-1} again suggesting the additive has an initial pro-wear effect. However the spread of results was quite large hence reducing the significance of this result. Non-parametric statistics (74) suggested that the two samples could not be ranked with respect to wear rate at this particular load and speed. A more significant analysis may be obtained at 15 Kg load and 0.62 ms^{-1} but at present there is insufficient data to carry out this analysis.

Surface roughness of the pins and disks has been shown to influence the magnitude of results obtained. This is one of the factors which produced the spread on the results (see figure 3.10). A significant set of results was found for different disk surface roughnesses (figure 3.8) using hydrofined fuel containing Hitec E515. The normal roughness disk (c.l.a. better than 0.0254 μm) produced a wear curve with a definite transition point when using fuel with Hitec. A similar transition point was observed for a higher surface roughness disk (figure 3.8) An estimate of the frictional heating from the frictional force and speed, gives the same value at each transition point. At the higher roughness two wear rates could be measured giving rise to the two curves shown in figure 3.8b. This can be explained in terms of surface segregation of aluminium and will be left until later in this Chapter. For a hydrofined fuel no transition point was observed (figure 3.7) and seizure occurs at high loads.

The surface analysis has shown that the aluminium content of the bronze was having an effect on the wear rate. For hydrofined fuels aluminium enrichment was observed in some cases (figure 3.35) and when Hitec was present aluminium depletion occurred (figure 3.29)

resulting in low wear. It was for this reason that some wear tests were carried out with duralumin wear pins. Fuels without Hitec again produced seizure at high loads whereas when Hitec was present this was prevented. The effect of additive concentration in this case was to produce a steady decline in wear with increasing concentration until about 40 p.p.m. At the 40 p.p.m. level the additive was again seen to be pro-wear, an effect which persisted on dilution of the fuel. It will be quite important to bear this result in mind when the evidence from the surface analysis is discussed. It may also be noted that these concentration results were much more stable than those found with the bronze where there was a dramatic reduction in wear as the concentration was increased.

Finally the results from the dry wear tests show a steady increase of wear with load, as in the case of additive free fuels. The wear rates were much higher for these tests compared to tests with hydrofined fuel and seizure occurred at a load of 5 Kg.

5.3 Sample analysis

5.3.1 Auger electron spectroscopy

Auger electron spectroscopy was found useful for detecting thin surface layers on worn samples. A thin layer of carbon was found for surfaces worn in the presence of kerosene and Hitec. Some surface decomposition of this thin film may be occurring because of the electron beam. This is apparent from the modifications found in the Auger spectra (figure 3.24) and is confirmed by the work of Pepper (75) in which modifications to transferred polymer on steel spectra were observed. This will be important if Auger peak shapes are used to indicate the chemical state of the surface. Any change of chemical state of the surface film can present a number of difficulties. The interpretation of the spectra is one problem but

chemical reaction can also have an effect on the sputtering rate of the elements concerned. If a film is loosely bound to the surface before the beam is applied then afterwards, when chemical changes have occurred because of the beam, then the remaining products will be tightly bound to the surface and consequently take longer to remove by sputtering. Sputtering itself can cause changes to occur at the surface and ion implantation also has an effect (76). These factors determined the operating conditions selected for the Auger analysis and for the sputtering. A 2 KeV electron beam was chosen as a reasonable energy to minimise surface reactions and at the same time give a reasonable high energy spectrum (around 1 KeV). Similarly 400 eV Xenon ions produces reasonable sputter yields with low implantation and tolerable surface chemical changes (77).

One of the problems associated with the above working conditions was the resolution of the aluminium Auger peak. However aluminium was identified by plasmon loss and plasmon gain peaks. Durfour et al (78) found peaks at 34 and 52 eV with oxidised aluminium. Suleman and Pattinson (63) found that as aluminium was oxidised a peak appeared at 57 eV. Under saturation oxidation conditions the 57 eV peak shifted to 54 eV with new peaks at 45 eV and 36 eV. All these peaks were observed on the surfaces analysed in this work. This does not mean that aluminium oxide was involved in the wear process. If free aluminium comes to the surface during wear then as soon as wear is stopped, and the surface exposed to laboratory atmosphere, then oxidation will occur.

A similar problem was found with the chromium Auger peak when analysing the steel surfaces. In this case the main chromium peak is masked by the oxygen Auger peak. Peaks were found at energies 481/482 eV, 520 eV and 536 eV which were assigned to chromium oxide. This is in agreement with the work of Ekelund and Leygraf (79) who

studied the oxidation of single crystals of chromium. Stoddart and Hondros (80) found similar results when working with stainless steel thus giving more support to this interpretation of these Auger peaks.

The above factors along with the masking of the nickel by copper Auger peaks makes it difficult to obtain complete depth profiles of the elements present on the surface. Treatment of results to obtain profiles has, in any case, problems. Calculation of relative atomic concentration involves cross-section data for the particular transitions analysed. The cross-section data available is sparse and obtained using gaseous samples (81, 82). However a plot of peak-to-peak heights against depth can be misleading so it was considered that some treatment of results was necessary. Provided this treatment is applied to each sample then comparisons can be made between profiles and this does in fact produce reasonable results as shown in figures 3.26 and 3.27. The profiles are plotted with concentration against the product of sputter current and time. The latter is proportional to depth, but the proportionality is different for each element because of different sputtering yields. Conversion to depth in micrometers requires the assumption that the surface is uniform and that it consists entirely of the element under consideration (so that the published sputter yield values can be used). This gives a removal rate of 0.7×10^{-10} metres per microamp minute for copper (see Appendix II). Since no other method of determining the depth removed was available on the spectrometer, it was thought preferable to plot the profiles as given in Chapter Three.

5.3.2 Electron Probe Microanalysis

The Auger technique is useful for studying the first few

surface atomic layers but for thick oxide layers the sputtering time required becomes excessive under the conditions used for these experiments. Element distributions over the surface were not obtainable with the present instrument. The electron probe gives X-ray elemntal scans for all the elements concerned except carbon and oxygen and so the results from the two instruments become complimentary. Taper sectioning the samples proved to be useful in identifying the difference between the surface layer and bulk material. These surface layers were often thin enough for the probe beam to penetrate and for a contribution to the X-ray count to be made from the bulk. This makes quantitative analysis difficult. However, as with the Auger work, comparisons between samples were easily made. Another problem with this instrument was the analysis of curved samples, in particular piston rig bore samples, which could not be accurately positioned in the sample chamber for analysis. This arose because of the design of the chamber which could not be readily modified. These samples could be more readily analysed using energy dispersive analysis of X-rays on a scanning electron microscope.

5.3.3 Fuel Analysis

The main aim of the fuel analysis was to obtain a rapid assessment of the differences between samples by a relatively simple method. Gas chromatography was thought to be one possible method of doing this with the added advantage of requiring only very small sample volumes. Blok et al (37) and Hillman et al (36) have developed methods of dimer acid extraction and chromatographic analysis to detect Hitec in fuels. In the present work it was only intended to "finger print" the fuels consequently the complicated procedures used by Blok and Hillman would be avoided. Monitoring

the fuels in this way it was hoped that any significant changes in wear between two fuels of the same batch might be correlated to changes in the fuel. Further it was hoped that Hitec might be detected in hydrofined fuels. Unfortunately only large changes in fuel composition (recognised by a change from a clear transparent fuel to a yellowish fuel) could be detected (figures 3.37(a) and (b)). The detector used, a flame ionisation device, was insensitive to the small quantities of Hitec in the fuels. A better detector for this work might be the flame photometric device developed by Brady and Charney (83) but this might prove to be over sensitive since it can detect one part in 10^9 of phosphorus. This in fact would give a means of detecting Hitec in fuels but would be poor for detecting other lubricity improving agents such as aromatics.

Ellipsometry was found useful for determining the temperature at which adsorbed Hitec dissociated from a silver surface but could not be used as a method of detection, for the additive, at the levels found in aviation fuels. Film thickness measurements, by this technique, would have been useful on the bronze and steel surface for depth calibration of the Auger profiles. Solutions are available for the equation of ellipsometry providing a sharp transition exists between the film and substrate (84). In cases where chemical reaction occurs (as with Hitec on aluminium bronze or steel) it becomes difficult to select a value for the refractive index of the film which is necessary for calculations of film thickness. Consequently experiments carried out in this work were primarily to determine the desorption temperature of Hitec.

5.4 Influence of Surface Metallurgy on the Friction and Wear Results

In section 5.5.2 it was suggested that aluminium segregation was having an effect on the magnitude of friction and wear. The

particular case of a series of tests with fuel containing Hitec gave a wear rate against load curve which split depending on whether the test gave a high wear rate or low wear rate (figure 3.8(b)). Other tests have produced periods of high friction and wear (figure 3.36) interspersed between periods of low friction and wear. Generally the surfaces from high friction and wear periods have been a bright aluminium bronze colour (figure 3.15) and analysis has shown them to be free from oxides (figure 3.26(c) and (d)). This applies particularly to tests carried out with hydrofined fuels.

The presence of Hitec produced surfaces which are partially or entirely copper rich (figure 3.15 and figure 3.29). This has been in the form of an oxide layer as shown by wear debris analysis and the presence of oxygen in the Auger depth profiles (figure 3.26(b)). A copper rich oxide layer results in low friction and wear. The formation of this layer occurs when the additive is present and in that case a pro-wear effect is observed because of an increased rate of removal of aluminium. This is shown by the presence of aluminium phosphates and phosphides in the wear debris (Table 3.4). The formation and removal of such a layer can lead to periods of high friction and wear with periods of low friction and wear interspersed.

These findings now give an explanation for the scatter of results. The same pin is used in the dwell test technique for both hydrofined fuel with and without Hitec and is used for many tests. A great deal of work has gone into cleaning methods, particularly for the disk, but little attention has been paid to what is happening to the wear surfaces during the tests (10). It is now obvious that the segregation of aluminium at the wear pin surface has an important influence on the results obtained and so this should be carefully monitored.

Work carried out at the British Petroleum Research Centre (10) resulted in the conclusion that the phosphate component of Hitec E515 was unlikely to play any part in protecting the surfaces against wear. It was suggested that there was a chemical reaction between the dimer acid and the metal surfaces. Although the latter is true the present work shows that the phosphate ester reacts with the aluminium content of the bronze and acts as an extreme pressure agent at high loads. The extreme pressure affect contributes to the reduction in wear rate at high loads as shown in figure 3.8. This reaction between phosphorus and aluminium would appear to be the cause of the pro-wear period seen when Hitec is present in the fuel. Phosphorus has been shown to be present on bronze and steel surfaces under static conditions (figure 3.48).

Changes in the distribution of aluminium in the bronze during wear may also be a contributing factor in the incorrect ranking of fuels (10).

5.5 Correlation between laboratory and "in service" results

The samples analysed, using various physical techniques, have shown the same general trends. A failed aircraft fuel pump piston had a relatively large amount of aluminium on the surface (figure 3.36). A similar situation was found in the case of a piston failure produced in a simulation rig. The bore from this test was also analysed and three distinct regions were found (figure 3.36) one of which was normal bronze, another aluminium depleted and one region aluminium rich (figure 3.36(a)).

Wear pins showed a depletion of aluminium when the additive was present (figure 3.29) and a normal aluminium bronze appearance when a hydrofined fuel was used to lubricate the system. From these results it can be seen that field experience, simulation rig

and pin-on-disk systems have shown that migration of aluminium occurs and that this is important in the wear and seizure mechanisms.

Hydrofined fuels produced high wear or seizure in both the pin-on-disk wear tests and in the pump simulation rig. The presence of Hitec E515 was found to reduce wear in both the simulation rig and the pin-on-disk machine. In the latter case there was a pro-wear effect before the benefit of using Hitec was observed.

5.6 Surface Metallurgy

5.6.1 The Structure of Aluminium Bronze and KEA961 Steel

In order to understand how seizure occurs in the aircraft fuel pump it is necessary to appreciate the structure of the metallurgy concerned, and how the components of these structures may interact with one another.

Figure 5.2 shows the phase diagrams for the aluminium bronzes according to Cook et al (85). The bronze used in this work contained 11% aluminium so the structures present are seen to be essentially α and K phases with δ phase at temperatures below 600°C. Süry and Oswald (86) have described and can contain up to 55% by weight of iron. If the tungsten is present then this will be incorporated into the carbide by direct substitution of the iron or chromium (87).

The structures found in complex iron-nickel-copper-aluminium alloys α, β and δ are used to describe the random face-centred cubic, random body centred cubic and δ -brass structures. The K phase is believed, by Cook et al, to be an ordered body-centred cubic structure. Süry and Oswald state that a structure of the CrCl form (figure 5.3) is found, it being a compound of Fe, Ni, Cu and Al. The δ -brass structure has a complex unit cell containing some 54 atoms (this is illustrated by Hume-Rothery and Raynor (87)).

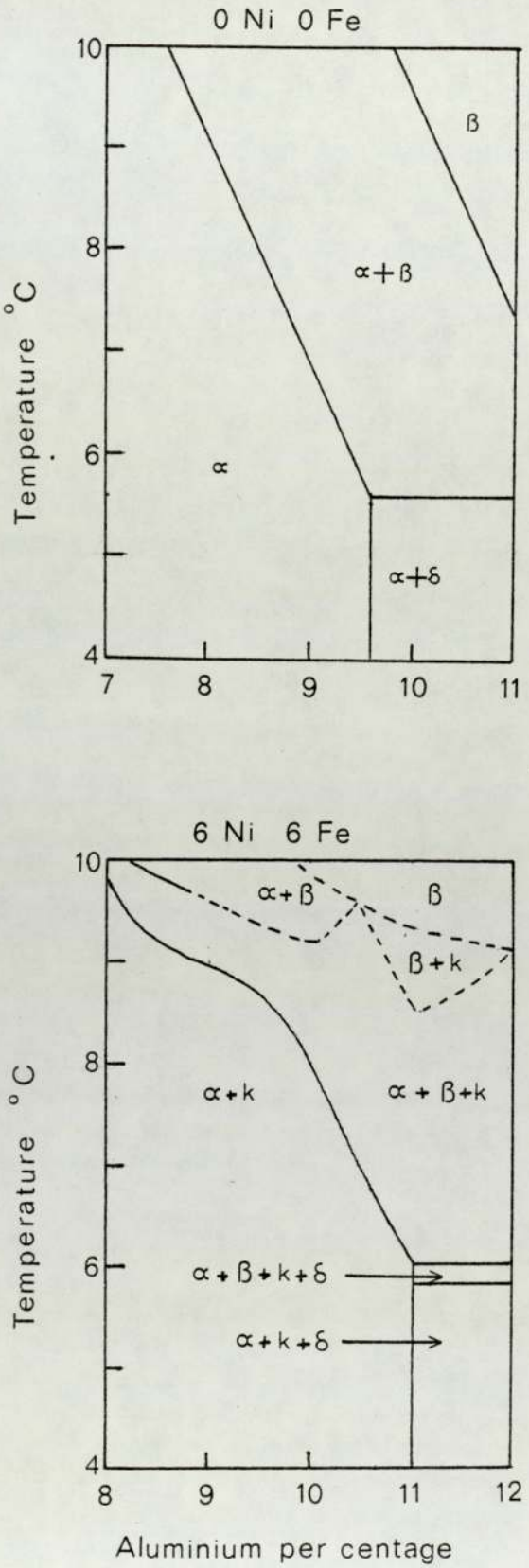

Figure 5.2, Aluminium Bronze Phase Diagrams.
After Cook et al (Ref 85)

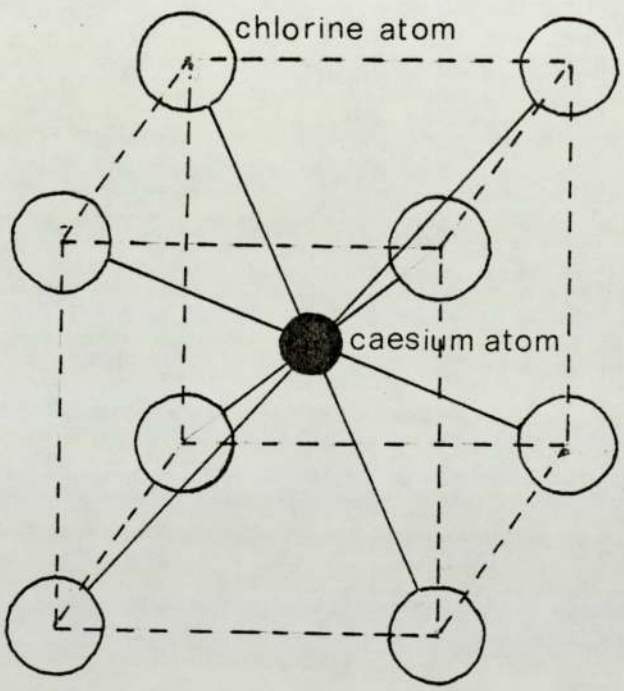

Figure 5.3. The Caesium Chloride Structure.

The KE 961 steel is a complex mixture of iron, carbon (1.5%), chromium (12.5 to 13.5%) with other trace quantities of silicate, manganese and tungsten (all about 0.5%). The tungsten is absent in the KE180 steel used for the disk. At the 1.5% carbon and 13% chromium levels carbides are formed in the alloys (88). A ternary alloy of iron chromium and carbon consist of a body centred cubic structure of chromium and iron in solid solution and a carbide of the form Cr_7C_3 which is trigonal (89).

5.6.2 Wear Mechanism in the absence of Hitec E515

The results have shown that when the aluminium bronze is worn against steel in the presence of a hydrofined fuel then a wearing surface is maintained which is not oxidised, has no boundary lubricant film on it and in some cases aluminium enrichment occurs at that surface. This enrichment is associated with high friction values. Aluminium was also observed on the steel surfaces in quantities that occur in the bronze. This suggests a preferential transfer of the aluminium from the bronze to the steel. A similar situation has been found by Dzhevaga and Lebedev (90) when welding aluminium bronze to carbon steels. They found that copper and aluminium became alloyed with iron in the steel. After annealing for 50 hours at 900°C they found that, in certain regions, the concentrations of aluminium was 14 to 17%. With the steel they used they found that the iron and carbon had diffused towards the bronze. After annealing they suggest an intermetallic compound of the type Fe_3Al forms.

In the present work the steel also contains chromium with which the aluminium and copper can react to form an intermetallic compound or primary solid solution. A number of factors determine which elements will preferentially combine with which to form these

compounds or solutions. The diffusion of a given element through any other element depends on the size of the atoms, and the rate of diffusion on the Kirkendall effect (91). Considering each of these parameters in turn, it has been found empirically that when the atomic diameters of the solvent and solute are within 15% of each other the elements will go into solution (87). Smigelskas and Kirkendall (91) electroplated alpha brass with copper and at the interface between the copper and brass had a series of molybdenum wires. In this way they showed that the diffusion rate of zinc is much greater than that of copper in alpha brass. Further they demonstrated that the interface shifts, to compensate at least partially for the difference in diffusion rate.

Another factor which measures the ability of elements to combine is the electronegativity, which expresses the power of an element to attract electrons to itself when present in a molecule or aggregate of unlike atoms. Large differences between the electro electronegative values of atoms normally means that a stable compound forms in preference to a solid solution. In these compounds each atom forms more bonds with the other element than with its own kind. The difference in electronegativity is about 0.5 units on the electronegativity scale for an intermetallic compound to form at the expense of a primary solid solution (92). Taking the above parameters into account the processes by which wear, and seizure, occur can now be investigated.

Consider what happens when two asperities interact, as they approach there will be some fluid in the space between the metals (figure 5.4(a). The kerosene is squeezed out from between the two surfaces as the asperities get closer, because shearing of the weakly bound molecules occurs, resulting in contact of the asperities (figure 5.4(b)). During contact frictional heating

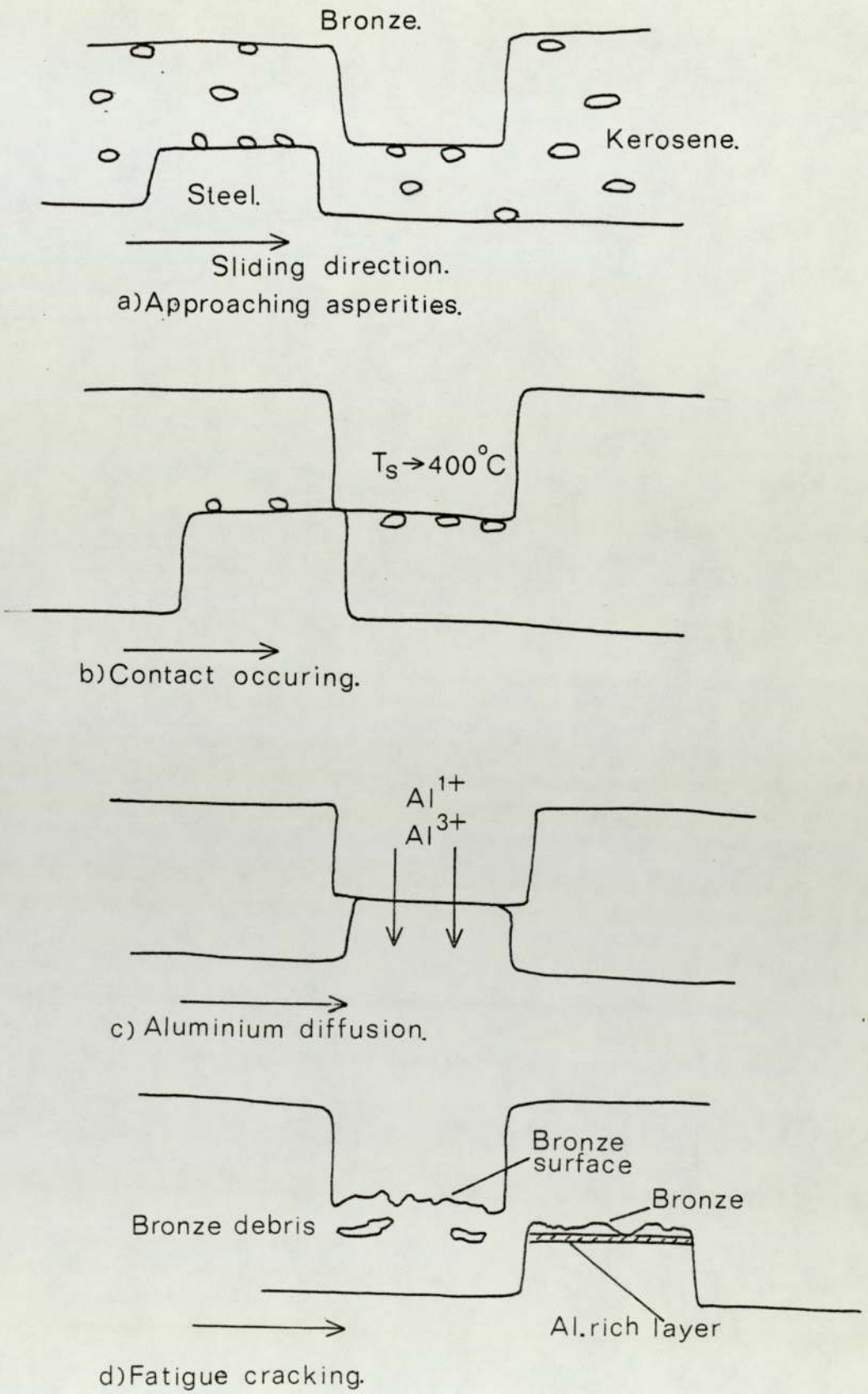

Figure 5.4, Wéar with hydrofined kerosene.

occurs and the temperature rises sharply as in the dry wear case. Temperatures in the range 180°C to 400°C, were found under dry wear conditions, are similar to those measured by Furey (59). Since the cooling effect of the fuel is negligible the same temperatures would be expected in this lubricated situation. It is noted that the same difficulties of interpretation of the output, from the present thermal junction, exist as for those measured by Furey. However such a temperature gradient would be sufficient to enhance diffusion of the aluminium content of the bronze. Transfer of free aluminium to the steel could occur, by the Kirkendall effect, at the interface (figure 5.4(c)). Even if the temperature was not as high as suggested adhesion would occur at the interface due to bonding between the atoms at the clean metal surface. Obviously when bonding occurs over sufficiently large areas seizure of the two surfaces takes place. The fact that the aluminium content of the bronze changes has been shown by examination using the electron probe and Auger spectrometer.

The question now arises as to the most likely interaction of elements present at the interface. Electronegativity and the atomic size factor determine the type of interface formed. Table 5.1 shows the difference in these parameters for combinations of the various elements present at the surfaces. The atomic size requirement for the formation of a solid solution are met, but in cases involving aluminium the tendency is for large percentage differences to exist.

Most of the electronegativity values suggest that primary solid solutions would be formed by the various combinations considered except for aluminium with copper, iron and chromium. The latter cases have electronegativity differences which suggest intermetallic compound formation would be more likely with these elements. Dzhevaga et al suggest that an Fe_3Al type compound may

TABLE 5.1 FACTORS DETERMINING BONDING OF ELEMENTS

COMBINATION	DIFFERENCE IN ELECTRONEGATIVITY	% DIFFERENCE IN ATOMIC DIAMETER
Al - Cu	1.6	9.8
Al - Fe	1.7	13.4
Al - Cr	1.9	11.97
Al - Ni	0.3	12.7
Cu - Fe	0.1	3.9
Cu - Cr	0.2	2.3
Cu - Ni	0.2	3.1
Fe - Cr	0.2	1.6
Fe - Ni	0	0.8
Cr - Ni	0.2	0.8

form in the interlayer region of a welded joint but only after a prolonged annealing at 600 to 700°C. A similar process can be considered to be occurring at the wear surface because during contact high temperatures are reached which produces a modification in the crystal structure (in this case by diffusion of aluminium) resulting in a softening of the surfaces. The values in Table 5.1 suggest that Cr_3Al and Fe_3Al type compounds will be formed at the interface, whilst any transferred copper may form a solid solution with the ferrite structure, or iron and chromium carbides in the steel. Copper has been observed on the piston surface (figure 3.36(b)).

Once the two surfaces have bonded together a number of alternatives arise. Firstly the bond will break due to the driving force being sufficiently large. However, repeated contacts will cause sub-surface fatigue cracking and wear debris will eventually be produced. This will then leave transferred bronze on

the steel with bronze debris appearing in the fuel (figure 5.4(d)). The latter has been shown to occur by the use of X-ray powder analysis (Table 3.4). Alternatively the driving force will be insufficient and seizure will occur.

Note that the above processes will apply to only a limited number of asperities since the fuel will provide some lubrication between some of the asperities which would otherwise contact under dry wear conditions.

5.6.3 General Wear Mechanism in the presence of Hitec E515

Physical methods of analysis have revealed that, in the case where Hitec E515 is present, aluminium is removed from the bronze surface. In this case no seizure occurs and the wear debris is no longer aluminium bronze.

Consider two asperities approaching each other with components of Hitec present on each surface. The Auger spectroscopy has shown that a carbon layer exists on the surfaces, and X-ray analysis revealed phosphides and phosphates in the wear debris, when Hitec is present. This suggests that both the dimer acid (long chain polar molecules of dilinoleic acid) and the phosphate ester component have an effect on the wear process. Figure 5.5(a) illustrates this initial situation with one layer of dimer acid been shown for clarity, although there may be multilayers on the surface as proposed by Allen and Drauglis (62) and by Fuks (93, 94). As the asperities approach the boundary film experiences increased shear and when contact occurs the surface temperature increases. If the increase in temperature due to shear or contact exceeds 80°C then the dilinoleic acid will desorb from the surface, as indicated by ellipsometry, allowing contact. Contact may also occur, in regions where the base kerosene is present rather than

the additive, in a manner similar to that described in the previous section on hydrofined fuels (figure 5.5(b)). Fuks (94) points out the influence of the base solvent in boundary lubrication films. If the temperature remains relatively low the situation would be that the asperities would be prevented from coming into contact, there being effective boundary lubrication. The contact produces a further increase in temperature which brings about dimer acid desorption, aluminium diffusion to the surface and reaction of the phosphorus component of the additive with the surfaces.

That the aluminium content of aluminium bronze is attacked by acids has been shown by Schussler and Napolitan (95). Sürry and Oswald (86) have shown that a sodium chloride solution will preferentially corrode the aluminium phases in the bronze. It is thus reasonable to suggest that a similar process is occurring here, through the action of the ester of ortho-phosphoric acid on the surface. The difference in electronegativity between aluminium and phosphorus is 0.6, suggesting compound formation occurs more readily between aluminium and phosphorus than with any other combination of phosphorus with the other elements present. The presence of phosphates and phosphides in the wear debris supports this hypothesis (Table 3.4).

The ester of ortho-phosphoric acid may break up, in the contact, by mechanical shearing or due to an increase in temperature. This releases the phosphorus which can then react with the aluminium preventing its transfer to the steel surface. That temperature has an influence on this mechanism is supported by the increased presence of phosphorus on the rougher surfaces (figure 3.16) where higher temperatures might be expected. The diffusion of aluminium and its reaction with phosphorus is illustrated in figure 5.5(c).

The bronze surface will now have a copper rich layer (figure

5.5(d) because of the diffusion of the aluminium and corrosion effects of the ortho-phosphoric acid. This layer can be oxidised to form cuprite as shown by the wear debris analysis and indicated by the Auger results. Oxidation may arise from, free oxygen in the fuel, residual products from the breakdown of the ortho-phosphoric acid and from reaction with the COOH group of the dimer acid. As this oxide layer builds up copper oxide will be observed in the debris along with the phosphates and phosphides (figure 5.5(d)).

Finally as the asperities come out of contact they will be cooled and dimer acid can re-adsorb onto the surface giving protection once again (figure 5.5(e)).

This simple model can be used to explain some of the friction and wear measurements. The pro-wear effect of the additive is seen as the corrosive removal of the aluminium content of the bronze. Ultimately a sufficiently thick copper oxide layer is built up and this, combined with protection afforded by the dimer acid, results in low wear. If the oxide layer is removed then periods of low friction and wear will be interspersed between high friction and wear.

The above model explains the wear processes occurring for the wear curve, up to and including, the transition point (figure 3.8). Beyond this point the wear debris contains some copper suggesting that the loads are high enough for the depleted layer to be removed before oxidation. Further only phosphides are present in the wear debris, particularly aluminium phosphides. In this case it would appear that chemical reaction, of the phosphorus with the surface, prevails resulting in a reduction in wear rate. This is typical of an extreme pressure action.

Two wear rates could be measured in the same test, or separately in different tests under the same conditions, when the disk surface roughness was increased to 0.6 μm c.l.a. (figure 3.8).

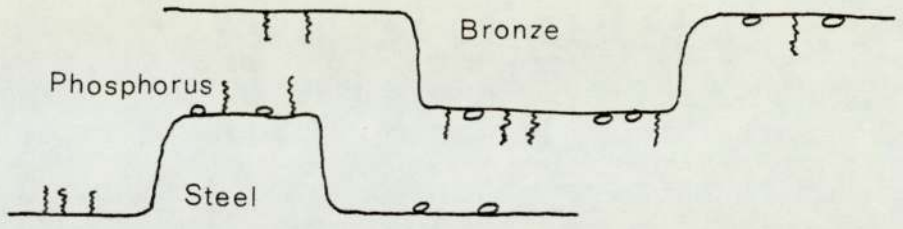

a) Approaching Asperities.

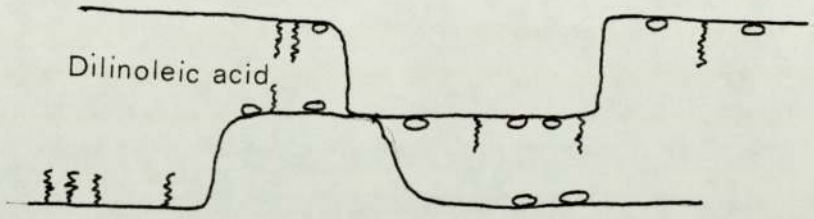

b) Desorption.

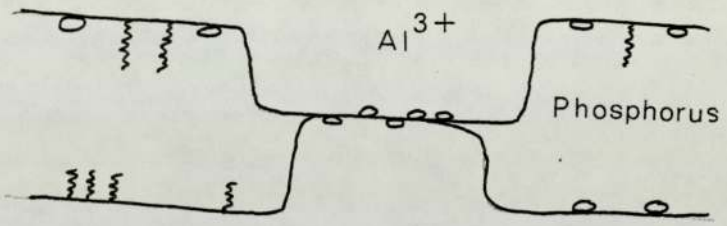

c) Diffusion and reaction.

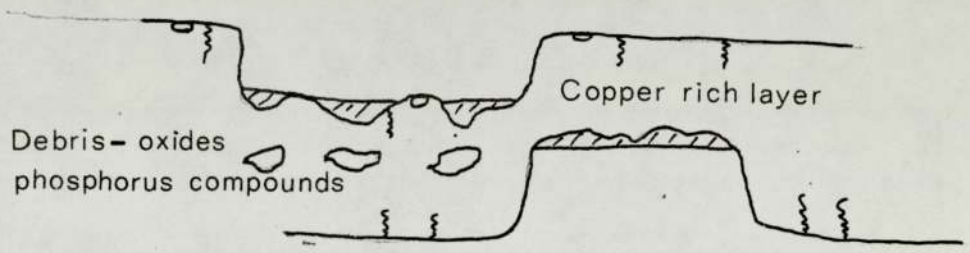

d) Wear

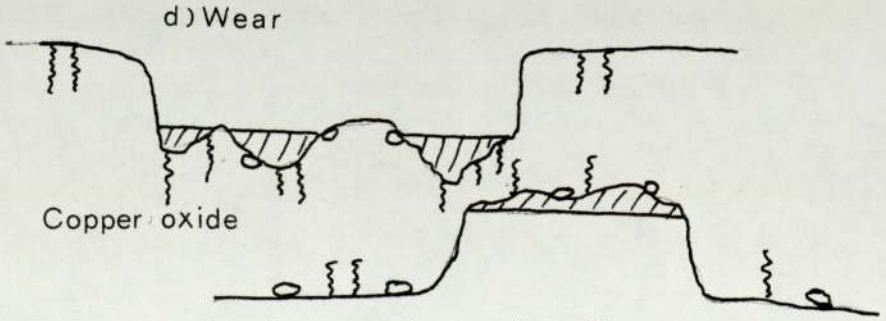

e) Oxidation and re-adsorption.

Figure 5.5, Wear with hydrofined kerosene plus Hitec.

This would appear to be a result of the concentration of aluminium at the surface as shown by the electron probe microanalysis.

5.7 Theoretical Considerations

Various theories for boundary lubrication were reviewed in Chapter One. To briefly reiterate, it was noted that most of the workers had tended to concentrate on one aspect of boundary lubricated wear (42, 43, 44, 53, 54, 55). Kingsbury and Rowe (42, 44) have looked at the protection of the surface, by the adsorbed molecules, in terms of the fraction of the surface prevented from coming into contact. Gupta et al (55) developed a theory based on the relationship between hydrocarbon chain length and wear rate. Their theory has been shown to work for the specific case of a steel-on-steel system and, like the theories of Kingsbury and Rowe, takes no account of oxidation of the surfaces. The model proposed by Sakurai et al (54) was based on the assumption that the load was supported partly by metal-to-metal contact and partly by a hydrodynamic film and so appears to ignore boundary lubrication.

In view of the shortcomings and specific applications of the above theories an attempt was made to develope a new theory for the current work. Oxidation, which has been shown to play an important role in the wear of aluminium bronze on steel, has been taken into account in the new theory along with a term for the fraction of surface protected by the additive. A large number of variables are incorporated into the wear equation so derived, some of which are interdependent. This means that in order to produce a manageable equation assumptions had to be made about a number of parameters so that they could be assigned constant values. Oxide film thickness was one parameter which was assumed to remain constant. Quinn (96) gives evidence for this for the dry wear case of steel-on-steel

provided a single type of oxide is present on the surface. The latter is true for the present work where only copper oxide (Cu_2O) was observed in the wear debris. An average value of this thickness was estimated from electron micrographs and then used as the constant value in the wear equation.

The time of vibration of a molecule on the surface was assumed to be the same as that measured in gaseous samples under static conditions, which may not be true for the dynamic wear situation. It was assumed that the lattice spacing or molecular diameter was dependent on the size and orientation of the ring structure in the dimer acid. Assuming a circular molecule, an estimate of the molecular diameter was made from the data of Dacre et al (41). This gave a value of 10^{-9} M for the molecular diameter for a molecule orientated perpendicular to the surface. Consequently this value was taken to be constant in the wear equation.

Other parameters could be more easily assigned values leaving the number of contacts, the surface temperature and Arrhenius constant to be varied in order to find solutions for the equation. These three variables are unfortunately interdependant. It was found that a reasonable solution to the wear equation could only be obtained if the Arrhenius constant was very different than that measured for copper under static conditions. Considering the nature of the sliding system, where fresh metal is continually being exposed for oxidation, this may not be as bad as it first appears.

Quinn, Sullivan and Rowson (97) have proposed reasons for retaining the static value of the activation energy for oxidation, and changing the value of the Arrhenius constant, for dynamic wear systems. Justification for keeping the activation energy constant the same, for the dynamic as the static case, is made with respect

to the theory of Cabera and Mott (98). Quinn et al suggest that the oxidation process consists of two stages. The first depends on electron transfer followed by electron tunnelling of the potential barriers of the surface and sub-surface atoms. This affects about ten molecular layers because the probability of tunnelling decays exponentially with oxide film thickness. The proposed second stage is one of thermal diffusion of metal or oxygen atoms or both. This means the rate of oxidation is dependent on the Arrhenius constant through the diffusion coefficients of the metal and oxygen atoms in the oxide. Kubaschewski and Hopkins (99) show that the value of the Arrhenius constant is influenced by many factors such as the number of voids and dislocations present, surface conditioning and partial oxygen pressure. Consequently, since these factors are subject to change under wearing conditions it is reasonable to assume that the value of the Arrhenius constant will change. Variations from 10^{3} to 10^{16} M^{-4} S^{-1} were found for the Arrhenius constant for the various dry wear conditions studied by Quinn et al (97).

An optimum value of 1.3×10^{6} Kg M^{-4} S^{-1} was found for the Arrhenius constant when using a load of 10 Kg for the wear tests in this work. The use of this value enabled the number of variables to be reduced to two in the wear equation. If, as with the dry wear case (100), a value, or series of values, of the number of contacts could be determined experimentally then improved solutions could be found for this wear equation.

The present work leaves us with the situation that there are an infinite number of alternative values of number of contacts and surface temperature, within a narrow range, which are possible solutions to the equation. The above values can be obtained from a computer programme which compares the calculated wear rates with experimental data. In this way the range of possible values can be

reduced making predictions of number of contacts and surface temperature more acceptable.

The theory as developed so far can be criticised in that it takes no account of the segregation of the aluminium from the bronze or of the corrosion due to the ortho-phosphoric acid. However, it is difficult to incorporate these effects at this stage in view of the problems of solving the present equation. If the behaviour of the phosphate ester was assumed to be similar to that of the dimer acid, then another exponential term could be added to the equation. The heat of adsorption term would take a value for phosphorus adsorbed onto the surface in this new term. Similarly yet another exponential term would have to be introduced for the diffusion of aluminium to the surface. These terms would obviously make the equation unmanageable.

Although a theory could be developed for boundary lubrication, using Suh's theory (70) as a starting point, as shown in section 4.5.3 of Chapter 4, it could not be easily solved. Most of the work carried out relating to Suh's theory has been experimental verification that delamination type wear sheets exist. Nothing however has been published so far on the numerical solution of the delamination wear equation. In particular no values are available for the constants K_1 and K_2 which depend on the surface topography according to Suh and the form of this dependence is not stated in the original publication of the theory.

Oxide film thickness is assumed to be negligable for the delamination wear theory and like the other theories discussed does not take into account any corrosion or diffusion processes. Consequently although the theory might be applicable to the hydrofined fuel situation it cannot be used for the fuel with additive and even in the case of hydrofined fuel the problem of numerical values for the constants still remains.

CHAPTER 6

CONCLUSIONS AND RECOMMENDATIONS

Conclusions can be drawn from the present work which has been carried out in three main areas. These areas are (i) the wear tests (including piston rig tests and field experience), (ii) the analytical tests used in studying the surfaces, fuel and wear debris and (iii) the development of the boundary lubricated oxidational wear theory.

6.1 Wear Tests

Stribeck curves are useful for determining the conditions under which the wear test machine should be run to obtain boundary lubricated conditions. Experiments have indicated (figures 3.3,34) that they might prove to be a means of ranking fuels and show where the fluid film breaks down at high speeds.

It has been found that extended wear tests (greater than 90 minutes duration), were necessary to establish a wear mode and to reveal the beneficial aspects of the addition of Hitec E515. These runs have been longer than those used by other workers who may have, in view of the present results with Hitec, been mislead by the apparent pro-wear effect when the additive is present. A correct ranking of fuels can thus only be obtained if tests are carried out for a sufficient length of time.

Although the scatter of wear results is quite large, for a given fuel, differences between fuels with and without additive can be observed if a wear rate against load curve is plotted. The plotting of this type of curve also serves a useful purpose in that selection can be made of a small number of samples for detailed analysis. Further, any transitions in the wear curve can be observed which can

assist in determining the processes occurring at the surface, by sample analysis from the different regions of the curve. It is concluded that although surface roughness contributes to the scatter in results this was not the major cause of the scatter.

Correlation, with respect to wear measurement, between "in service" pumps, the two-piston rig and the pin on disk machine was not entirely satisfactory. This can be attributed to the absence of cadmium plating on the wear pins in the pin-on-disk tests. However the fact that problems only arise in the pump when the camium is worn away and the difficulties in obtaining the expected type of wear with cadmium plated pins justify the use of bronze in these tests.

Anomalies found in the results obtained from the dwell tester have been investigated by the continued use of aluminium bronze in this work. Consequently the present results can also assist in the understanding of commercial tests like the dwell test.

6.2 Analysis of Samples

Optical microscopy proved to be useful for giving an overall impression of what was happening to the surfaces during a given series of wear tests. This applies particularly to the wear on bronze in the present work and is not necessarily generally applicable.

Comparisons between samples can be made using Auger spectroscopy. The high surface sensitivity makes the instrument useful for detecting surface films. Problems of quantification arise due to incomplete resolution of low energy peaks but much information can still be obtained from energy shifts in incompletely resolved differential peaks. In general information about the surfaces can be obtained from peak shape and from energy shifts. Other problems arise in quantification because of incomplete knowledge about the energy levels involved with the Auger transitions. Difficulties are also

found in determining the area under the differentiated Auger peaks since the peaks are sometimes asymmetric. Despite these problems quantification does give more realistic depth profiles and the inclusion of thepeak widths into the analysis only modified the profiles slightly. The depth profiling is a useful technique which permits comparisons, for example of the oxygen levels in the surface layers, between samples.

Difficulties were experienced in detecting aluminium with the Auger technique. The low energy peaks were masked by copper whilst operating conditions restricted the detection of the high energy aluminium peaks. Alternatively the electron probe, although of no use for detecting elements below fluorine in the periodic table (oxygen and carbon can be obtained with careful adjustment of the instrument), was useful for observing the distribution of aluminium on the surfaces. Further the probe analyses a relatively large volume compared to the Auger so was useful for anlysing the oxide layers on some of the surfaces. With the Auger technique the sputtering times required to remove these oxide layers became excessive. Samples for the probe could be taper sectioned allowing rapid analysis of these layers for aluminium and copper content. In this way electron probe microanalysis was complementary to the Auger work.

X-ray facilities on the scanning electron microscope proved useful for analysis of curved surfaces where difficulty occurred in focusing the probe. The S.E.M. and replicas from the transmission microscope also revealed features on some surfaces which could be related to the wear mode.

Although the above techniques indicated that an oxide might be present at the worn surfaces it was necessary to use X-ray analysis to confirm this suggestion. The fact that oxides were present on

the surfaces worn in the presence of Hitec was confirmed by powder X-ray analysis of wear debris.

Taken in isolation each of the above techniques tells us a little about the state of the surface analysed, but together they provide a wealth of information which can be pieced together to give a better picture of that surface. Consequently it is suggested that it is always beneficial to use as many techniques as are available for this type of work.

Fuel analysis was generally unsuccessful with the present equipment. A different detector, sensitive to phosphorus, on the gas-liquid chromatography column may prove useful in detecting Hitec through the phosphate ester component. However the latter could prove to be over-sensitive. Ellipsometry did show that non-chemically adsorbed additive desorbs from silver at 80°C but is of no use for measuring thick (greater than 1000 Å) films which were chemically reacted to the surface.

6.3 Surface Models

The use of the above techniques enabled surface models for the wear of the bronze, in the presence of fuel with and without Hitec, to be built up. This lead to an insight of the wear mechanisms for the two cases investigated.

Hydrofine fuels allow metal-to-metal contact to occur with consequent high temperatures at the contact regions. These high temperatures lead to preferential transfer of aluminium to the steel by diffusion (Kirkendall effect). This results in formation of an interlayer rich in aluminium which can lead to seizure if conditions are sufficiently severe. Wear occurs at a rate which is rapid enough to prevent the formation of protective oxide layers.

Presence of an additive introduces a corrosive mechanism which

preferentially removes aluminium from the surface leaving the resultant copper rich surface to become oxidised. This removal of aluminium prevents the transfer to the steel occurring and hence seizure is avoided. Apparent pro-wear effects can be attributed to this removal of aluminium but anti-wear effects are observed if the tests are carried out for periods of 90 minutes or longer.

6.4 Recommendations for experimental work

The present work has been carried out, in general, over a range of loads at one speed. More information may be obtained if the load range is extended to higher loads particularly in the case where the additive is present. Variation in speed and ambient temperature could also be made, the latter to relatively high values (greater than 80°C). Consideration of the temperature effect is important in view of some of the temperatures attained in fuel systems, and it would be interesting to determine at what temperature protection from the additive film breaks down under wearing conditions.

Another parameter worthwhile investigating would be the speed at which tests were carried out. Tests at both low speed, as in this work, and at higher speeds, where the Stribeck curve indicates film breakdown, would be of value. Although these tests could be carried out with and without Hitec present it would be beneficial to study other additives, particularly those without phosphorus components, since (a) many others are being approved for use as alternatives to Hitec and (b) the phosphate ester appears to be of prime importance in the wear mechanism for this particular additive.

Wear testing or the plotting of Stribeck curves may prove to be a better alternative, for ranking fuels, than monitoring the friction as is done, for example, in the dwell test. Further work needs to be carried out, to show if this is so, with fuels of suspected different

lubricity. The use of different metallic combinations would also be interesting in this case and in studying the effects of Hitec E515. A copper wear pin would enable results to be obtained which might more easily be matched with the theory developed because of the absence of the aluminium content. In other words a reduction in the number of variable parameters for testing the theory is recommended.

The use of a number of physical methods of analysis have proved to provide useful information for building up a model of the surface. Alone, each technique gives part of the information but combined they provide a more complete picture of the wearing surface. It is recommended that this approach can be used for the study of low lubricity fluids in general. Other techniques, not used in this work, may also prove invaluable for this purpose. Nuclear magnetic resonance (N.M.R.), infra-red and ultra violet techniques could be used for the study of the fluids after wear has taken place. X-ray photoelectron spectroscopy (X.P.S.) combined with Auger electron spectroscopy would give more information on the type of oxide formation on the surface. This would be extremely useful in the work with kerosene and additives, since the Auger work showed oxygen to be present on the surfaces but not how it was combined with other elements.

6.5 Theory

Difficulties have been encountered in developing a theory for boundary lubricated wear which covers all the variable parameters found in the present work. Segregation of aluminium from the bronze makes the problem unmanageable at the present time. The theory strictly deals with the lubrication afforded by the fatty acid component of Hitec E515 (standard boundary lubrication) and takes no account of the complex reactions taking place between the metal

surfaces and the phosphate ester component of the additive. However the theory does take account of the oxidation which has been shown to take place at the surfaces. In this respect the new theory is better than previous ones which only deal with the lubrication provided by fatty acids. If more data was available for the delamination wear theory it is possible that a theory for boundary lubricated oxidative wear could be developed. However the delamination wear theory is still in its infancy even for the dry wear case so it would seem some time before this could be attempted.

As suggested in the recommendations for further experimental work a simpler system, of a copper wear pin-on-disk, could be used to test the theory. This task would be made even easier if standard boundary lubricants, such as stearic or palmitic acid, were used as the test additives. If either measurement of number of contacts or contact temperature (under lubricated conditions) could be made then a large step forward would be achieved in solving the equation. Again these parameters are difficult to measure (even under dry wear conditions).

REFERENCES

1. Dowson, D., "Transition to Boundary Lubrication from Elastohydrodynamic Lubrication", Boundary Lubrication - An appraisal of World Literature, Ed. F.F. Ling, E.E.Klaus and R.S. Fein, A.S.M.E., 1969, pp. 229-240.

2. Dukek, W.G., and Vere, R.A., "Fuel Lubricity", International Air Transport Association Aviation Fuel Symposium, Geneva, May 4-6, 1971.

3. Appeldoorn, J.K., and Dukek, W.G., "Lubricity of Jet Fuels", SAE Transactions, Vol. 75, 1967, pp. 428-440.

4. Vere, R.A., "Aviation Fuel Lubricity", Report to AGARD Meeting, The Hague, May 1971.

5. Johnson, R.K., and Shamblin, J.E., "Jet Fuel Thermal Stability Studies by Electron Microscopy", J.Inst.Petroleum, Vol. 47, number 451, 1961, pp. 241.

6. Unzelman, G.H., and Wolf, C.J., "Processes", Petroleum Processing Handbook, Eds. Bland, W.F., and Davidson, R.L., McGraw-Hill, 1967, Section 3, 3.38-3.39, 3.118-3.119 and 3.128-3.129.

7. "F.D/11 Viscosity-Temperature Characteristics", Issued by The Royal Aeronautical Society and the Institute of Petroleum, Second Issue, 1956.

8. "Specification D.Eng.R.D. 2494", (P.E.) M.O.D., Sept. 1974, REF AX/403/02 (for example).

9. Aird, R.T., and Forgham, S.L., "The Lubricating Quality of Aviation Fuels", Wear, 18, pp.361-380 (1971).

10. "Lubricity of Aviation TurbineFuels", Editors: Vere, R.A., Askwith, T.C., and Hardy, P.J., Second Report of the work and findings of the M.O.D.(P.E.) Fuel Lubricity Panel, 1976, REF AX/395/014.

11. "Aviation Turbine Fuel Lubricity, Evaluation of Corrosion Inhibitors", Wright-Patterson Air Force (OHIO), Technical Report AFAPL-TR-75-47, Sept.1975.

12. Dukek, W.G., and Vere, R.A., "Fuel Lubricity", International Air Transport Association Aviation Fuel Symposium, Geneva, May 4-6, 1971.

13. Patent Specification, 790, 231, London, 1958.

14. Vos, P., "Low Lubricity of Aviation TurbineFuels", Paper presented at the P and W.A. JT-9D overhaul and maintenance conference, 1973 (Sabena-Belgian World Airlines Publication).

15. Agnihotri, R.K., Narang, J.R., Metha, K.C., and Nandy, A.N., "Study of the effect of dilution on the Lubricity of Hydrotreated Jet Engine Fuels", Wear, 28, pp.392-394, (1974).

16. Vere, R.A., and Watts, F.W., "The Dwell Tester as an Evaluator of Fuel Lubricity", Esso Research Centre, Abingdon, Report No: 2PE-I.75.

17. Bishop, G.J., and Howells, H.E., Letter to the Editor, Wear, 18, pp.488-489, (1971).

18. Aird, R.T., and Forgham, S.L., Letter to the Editor, Wear, 18, pp. 489-491, (1971).

19. Johnston, R.K., Discussion on "Lubricity of Jet Fuels, S.A.E. Trans., 75, pp.438-439, (1967).

20. Kichkin, G.I., Rozhkov, I.V., Vilenkin, A.V., and Kornilova, E.N., "Effect of Additives on Anti-wear Properties of Fuels", Khim. i Tekhnol. Topliv i Masel, No. 6, pp. 60-65 (1963).

21. Tao, F.F., and Appeldoorn, J.K., "The ball-on-cylinder Test for Evaluating Jet Fuel Lubricity", A.S.L.E. Trans., 11, pp. 345-351, (1968).

22. Shayeson, M.W., Discussion on "The ball-on-cylinder Test for Evaluating Jet Fuel Lubricity", ibid, pp.351.

23. Appeldoorn, J.K., and Tao, F.F., "The Lubricity Characteristics of Heavy Aromatics", Wear, 12, pp.117-130, (1968).

24. Podolsky, Yu. Ya., Letter to the Editor, Wear, 13, pp.61-62, (1969).

25. Appeldoorn, J.K., and Tao, F.F., Letter to the Editor, ibid, page 446.

26. Suresh, N., Tuteja, A.D., and Goel, P.K., "Assessment of the Anti-Wear Property of Fuels under Point Contact Conditions", Ind.J.Technology, 9, pp.110-115, (March 1971).

27. Nandy, A.N., Mehta, K.C., Narang, J.R., and Agnihotri, R.K., "Lubricity of Jet Fuels and Lubricity Additives", Labdev J.Sci.Tech., 11-A, No. 1-2, (Jan-April 1973).

28. Bowden, F.P., and Tabor, D., "The Friction and Lubrication of Solids", Oxford University Press, London, pp. 185-189 (1958).

29. Agnihotri, R.K. Narang, J.R., Metha, K.C., and Nandy, A.N., "Study of the effect of dilution on the lubricity of hydrotreated jet engine fuels", Short communication, Wear, 28, pp. 392-394, (1974).

30. Vere, R.A., "Dilution Restores Lubricity to Hydrotreated Jet Fuels", S.A.E. Journal, 78, pp. 42-43, (April 1970).

31. Vere, R.A., "Lubricity of Aviation Turbine-Fuels", S.A.E. 690667 - S.A.E. Aeronautics Meeting, Los Angeles, October 1969.

32. Appeldoorn, J.K., Goldman, I.B., and Tao, F.F., "Corrosive Wear by Atmospheric Oxygen and Moisture", ASLE Trans., 12, pp. 140-150, (1969).

33. Klaus, E.E., and Bieber, H.E., "Effect of some Physical and Chemical Properties of Lubricants on Boundary Lubrication", ASLE Trans., 7, pp. 1-10, (1964).

34. McHugh, K.L., Discussion on "Lubricity of Jet Fuels", S.A.E. Trans., 75, pp.438-439, (1967).

35. Mitra, G.D., Mohan, G, and Sinha, A., "Gas chromatographic Analysis of Complex Hydrocarbon Mixtures", Journal of chromatography, 91, pp. 633-648, (1974).

36. Hillman, D.E., Paul, J.I., and Cobbold, D.G., "Determination of Pipeline Corrosion Inhibitor (Hitec E515 in Aviation Fuels by Gel Permeation Chromatography", Recent Analytical Developments in the Petroleum Industry, Ed. Hodges, D.R., pub. Applied Sciences (Galhard), G.T. Yarmouth, pp. 47-58, (1974).

37. Blok, A.P., Dahmen, E.A.M.F., and Verjaal, A.J., "Determination of Santolene C in Jet Fuels", J.Inst. of Petroleum, 51, No.502, pp. 348-353, (October 1965).

38. Groszek, A.J., "Heat of preferential adsorption of surfactants on porous solids and its relation to wear of sliding steel surfaces", Trans. ASLE, 5, pp. 105-114, 1962.

39. Smith, J.D., "The Lubricity of Turbine Fuels - An Enthalpimetric Approach", Shell Research Ltd., Report Number K.191, M.O.D. contract K 12A/33/CB12A.

40. Chertkov, Ya. B., and Piskunov, V.A., "Polyfunctional Additives for Jet Fuels", Chemistry and Technology of Fuel and Oils, No. 5/6, pp. 377-380, (1969).

41. Dacre, B., Savory, B., and Wheeler, P.A., "Adsorption of Lubricity Additives", Part I, Technical Report AC/R/13 Royal Military College of Science, Shrivingham, M.O.D. Contract AT/2160/025, ENG., D., (1977).

42. Kingsbury, E.P., "Some Aspects of Thermal Desorption of a Boundary Lubricant", J.Appl.Phys., 29, No.6, pp. 888-891 (1958).

43. Kingsbury, E.P., "The Heat of Adsorption of a Boundary Lubricant", ASLE TRANS., 3, pp.30-33, (1960).

44. Rowe, C.N., "Some Aspects of the Heat of Adsorption in the Function of a Boundary Lubricant", ASLE TRANS., 9, pp. 100-110, (1966).

45. Holm, R., Electric Contacts Handbook, 4th Edition, Springer-Verlag (Berlin), pp. 199, f.f. (1967).

46. Burwell, J.T., and Strang, C.D., "On the Empirical Law of Adhesive Wear", J.Appl.Phys., 23, pp.18-28, (1952).

47. Bowden, F.P., and Leben, L., "The Nature of Sliding and the Analysis of Friction", Proc.Roy.Soc., 169A, pp.371-391 (1939).

48. Bowden, F.P., and Tabor, D., "The Area of Contact between Stationary and between Moving Surfaces", ibid, pp.391-(1939).

49. Archard, J.F., "Contact and Rubbing of Flat Surfaces", J.Appl. Phys., 24, pp.981-988 (1953).

50. Archard, J.F., "Single contacts and multiple encounters", ibid, 32, pp.1420-1425, (1961).

51. Archard, J.F., and Hirst, W., "The Wear of Metals under Unlubricated Conditions", Proc.Roy.Soc. (London), Ser.A 236, pp. 397-410, (1956).

52. Quinn, T.F.J., "The Effect of 'Hot-Spot' Temperatures on the unlubricated wear of Steel", ASLE Trans. 10, pp.158-168 (1967)

53. Rowe, C.N., "Role of Additive Adsorption in the Mitigation of Wear", ibid, 13, pp.179-188 (1970).

54. Toshio Sakurai, Heihachiro Okabe and Keiji Nakayama, "The Mechanism of Adhesive wear of copper under Boundary Lubrication", ibid, 16, pp.91-96, (1973).

55. Gupta, P.L., Krishna, M.G. and Ramakrishna, V., "Wear Characteristics - Hydrocarbons", Proc.International Conf. on Wear and Materials, St. Louis, Missouri, April 25-28, 1977.

56. Beerbower, A., "A Critical Survey of Mathematical Models for Boundary Lubrication", ASLE Trans. 14, pp. 90-104, (1971).

57. Wilson, F., and Eyre, T.S., "Metallographic Aspects of Wear", Metals and Matls, 3, No. 3, pp 86-91, (1969).

58. Phillips, M.R., Dewey, M., Hall, D.D., Quinn, T.F.J., and Southworth, H., "The Application of Auger Electron Spectroscopy to Tribology", Vacuum, 26, p.451, (1977).

59. Furey, M.J., "Surface Temperatures in Sliding Contact", ASLE Trans., 7, pp.133-146, (1964).

60. Czichos, H., Grimmer, W., and Mittmann, H.U., "Rapid Measuring Techniques for Electrical Contact Resistance applied to Lubricant Additive Studies", Short Communication, Wear, 40, pp.265-271, (1976).

61. Fein, R.S., and Villforth, F.J. Jr., "Lubrication Fundamentals", Lubrication, 59, pp. 77-88, Oct-Dec. 1973, Pub. Texaco Services (Europe) Ltd.

62. Allen, C.M., and Drauglis, E., "Boundary Layer Lubrication: Monolayer or Multilayer", Wear, 14, pp. 363-384 (1969).

63. Suleman, M., and Pattinson, E.B., "Observation of a plasmon-gain in the fine structure of the Aluminium Auger Spectrum", Letter to the Editor, J.Phys. F: Metal Phys., Vol.1, pp.L21-L24, (1971)

64. Chang, C.C., "General Formalism for Quantitative Auger Analysis", Surface Science, 48, pp.9-21, (1975).

65. Birks, L.S., "Electron Probe Microanalysis", Second Edition, page 107, Wiley-Interscience (New York), 1971.

66. Quinn, T.F.J., "The Application of Modern Physical Techniques to Tribology", pp.40-69, Newnes-Butterworths, London, (1971).

67. Frenkel, J., "Theorie der Adsorption und Verwandter Erscheinungen", Z.Physik, 26, pp.117-138, (1924).

68. Tylecote, R.F., "Review of Published Information on the Oxidation and Scaling of Copper and Copper Base Alloys", J.Inst.Metals., 78, pp.259-300, (1950-51).

69. de Boer, J.H., Molecular Processes on Solid Surfaces", page 234, Pub. McGraw-Hill, New York, (1968).

70. Suh, N.P., "The Delamination Theory of Wear", Wear, 25, pp. 111-124, (1973).

71. Sharma, J.P., and Cameron, A., "Surface Roughness and Load in Boundary Lubrication", ASLE Trans. 16, pp.258-266, (1973).

72. Bjerk, R.O., "Discussion", ibid, p.264.

73. Sharma, J.P., Malhotra, R.C., and Cameron, A., "Heat of Adsorption and Critical Temperature Studies of Boundary Lubricants on Steel Surfaces", Wear, 25, pp. 281-297, (1973).

74. Alder, H.L., and Roessler, E.B., "Introduction to Probability and Statistics", 5th Edition, pub. W.H.Freeman (San Francisco) (1972).

75. Pepper, S.V., "Auger Analysis of Films formed on Metals in Sliding Contact with Halogenated Polymers", J.Appl.Phys., 45, No.7, pp.2947-2956, (1974).

76. Wehner, G.K. Chapter 1 in "Methods of Surface Analysis", Ed. Czanderna, A.W., pub., Elesevier Scientific, (1975).

77. Rosenberg, D., and Wehner, G.K., "Sputtering Yields for Low Energy H_e^+ -, K_r^+-, and X_e^+- Ion Bombardment", J.Appl.Phys., 33, No.5, pp.1842-1845, (1962).

78. Dufour, G., Guennou, H., and Bonnelle, C., "Auger Spectra of Magnesium and Aluminium", Surface Science, 32, pp.731-734, (1972).

79. Ekelund, S., and Leygraf, C., "A LEED-AES Study of the oxidation of Cr (110) and Cr (100), "Surface Science, 40, pp.179-199, (1973).

80. Stoddart, C.T.H., and Hondros, E.D., "Element Profiles across Thin Oxide Films", Nature Phys.Sci., 237, pp.90-91, (1972).

81. Glupe, G., and Mehlhorn, W., "A new method for measuring electron impact ionization cross-sections of inner shells", Phys.Letters, 25A, No. 3, pp. 274-275, (1967).

82. Vrakking, J.J., and Meyer, F., "Electron Impact Ionization Cross-sections of Inner Shells Measured by Auger Electron Spectroscopy", Phys.Rev., A9, pp.1932-1937, (1974).

83. Brody, S.S., and Chaney, J.E., "Flame Photometric Detector", J. of Gas Chromatography, pp.42-46, (1966).

84. Kruger, J., and Hayfield, P.C.S., "Ellipsometry in Corrosion Testing", Handbook on Corrosion Testing and Evaluation Pub. Wiley and Son, (1971).

85. Cook, M., Fentiman, W.P., and Davis, E., "Observations on the Structure and Properties of Wrought Copper-Aluminium-Nickel-Iron Alloys", J.Inst.Metals, 80, pp.419-429, (1951-52).

86. Sury, P., and Oswald, H.R., "On the Corrosion Behaviour of Individual Phases Present in Aluminium Bronze", Corrosion Science, 12, pp.77-90, (1972).

87. Hume-Rothery, W., and Raynor, G.V., "The Structure of Metals and Alloys", Pub. Inst. of Metals, (1962).

88. Greaves, R.H., "Chromium Steels", page 73, pub. H.M.S.O. (1935)

89. "Metals Handbook", Vol.8, 8th edition, pub. American Society for Metals, (1973).

90. Dzhevaga, I.I., and Lebedev, Yu. M., "Research into the Fusion Zones of Welded Joints between Carbon Steel and Aluminium Bronze", Avt. Svarka, No. 8, pp. 11-14, (1970).

91. Smigelskas, A.D., and Kirkendall, E.O., "Zinc Diffusion in Alpha Brass", Trans.A.I.M.E., 171, pp.130-135, (1947).

92. Darken, L. and Gurry, R., "Physical Chemistry of Metals", page 84, McGraw-Hill, New York, (1953).

93. Fuks, G.I., "The Properties of Solutions of Organic Acids in Liquid Hydrocarbons at Solid Surfaces", in B.V. Deryagin (ed.), "Research in Surfaces Forces", Vol.1, pp. 79-88, (1960); Translation by Consultants Bureau, New York, (1964).

94. Fuks, G.I., "The Polymolecular component of the lubricating boundary layer", ibid, Vol.2, (1964): Translation, pp. 159-167, (1966).

95. Schussler, M., and Napolitan, D.S., "Dealuminization of Aluminium Bronze", Corrosion, 12, pp.25-30, (1955).

96. Quinn, T.F.J., "The Division of Heat and Surface Temperatures at Sliding Steel Interfaces and their Relation to Oxidational Wear, ASLE Trans., 21, No.1, pp.78-86, (1978).

97. Quinn, T.F.J., Sullivan, J.L., and Rowson, D.M., "New Developments in the Oxidational Theory of Mild Wear of Metals", To be published, A.S.M.E. Wear of Materials Conference, (Dearborn), 1979.

98. Cabrera, N. and Mott, N.F., "Theory of Oxidation of Metals", Reports Prog.Phys., 12, Page 163, (1949).

99. Kubaschewski, O. and Hopkins, B.E., "Oxidation of Metals and Alloys", Butterworths, London, (1962).

100. Quinn, T.F.J., and Sullivan, J.L., "A Review of Oxidational Wear", Proc. A.S.M.E. Conf. on Wear of Materials, St. Louis, pp. 110-115, (1977).

APPENDIX 1

Calculation of piston-bore side loads in an axial piston pump

The main force acting in the fuel pump is the normal reaction between the slipper and camplate. This is produced by the pressure of the fuel being pumped. To calculate the forces acting in the system the following assumptions were made:

(1) The slipper-camplate frictional force is small. This will be so provided that the interface is lubricated by the fuel.

(2) The slipper-piston ball frictional force is small provided that there is adequate lubrication. However during running there may be a phase during which the slipper is found to stick against the piston ball. This has been noted when pumps have been stripped down after a period of running.

(3) The piston spring force is small. Note that the spring rate is 2×10^{-2} Kg M^{-2} for a 0.7M long spring.

(4) The centrifugal force experienced by the pistons is small.

(5) The problem is assumed to be one of rigid contact.

(6) The points of contact are assumed to be starved of lubricant.

(7) All forces have been assumed to act at a point.

(8) In order that the slipper face conforms to the camplate surface at all angular positions it is assumed that the slipper follows a conical path over the piston ball surface rather than the piston rotating about its axis in the bore.

The co-ordinate system was set up as shown in figure A1(a). The X direction was taken to be radially inwards along the camplate surface, the Y direction as tangential to the locus circle along the

camplate surface in the direction of motion, while the Z direction was taken normal to the camplate angle. The angle α is the camplate angle, θ the angle from the radius through the outer dead centre (O.D.C) to the point C on the camplate and β the angle between the normal to the camplate surface and the line of action of the piston.

The diagram (figure A1(b)) shows the forces acting on the system. F_1 is the normal reaction force between the slipper and camplate produced by the hydraulic piston force, P, acting along the centre line of the piston. F_1 and F_2 are the reaction forces between the piston skirt and bore and their directions are fixed by the friction angle ϕ_2.

Summing forces along the piston axis

$$F \cos\beta = P + (F_1 + F_2) \cos \phi_2 \qquad \ldots (1)$$

and normal to the piston axis

$$F \sin\beta = (F_1 - F_2) \cos \phi \qquad \ldots (2)$$

Taking moments about A

$$F_1 (b - c) \cos \phi_2 = F_2 (b + a - c) \cos \phi_2 \qquad \ldots (3)$$

From (1) and (2)

$$\tan\beta = \frac{(F_1 - F_2) \cos \phi_2}{P + (F_1 + F_2) \sin \phi_2} \qquad \ldots (4)$$

and from (3)

$$F_1 = \frac{(b + a - c)}{(b - c)} F_2$$

substituting for F_1 in (4) from (5) and re-arranging it can be shown that:

$$F_2 = \frac{P (b - c) \tan\beta}{(b + a - c)(1 - \tan\beta) - (b - c)(\cos \phi_2 + \sin \phi_2 \tan\beta)}$$

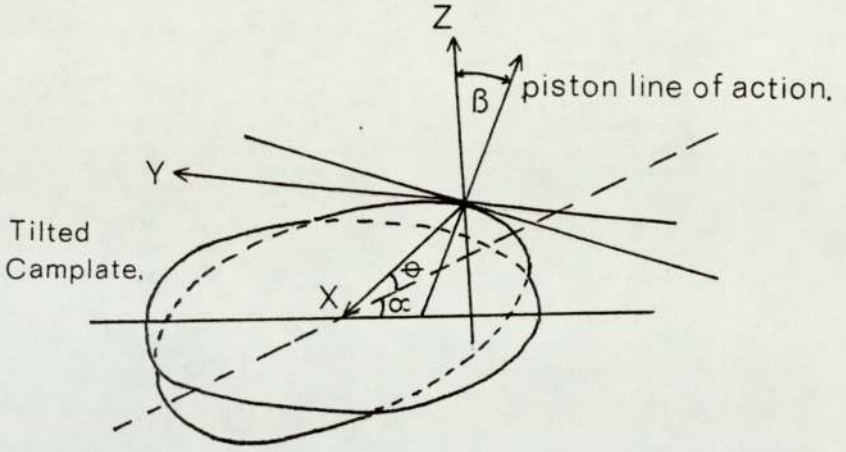

a)Co-ordinate system.

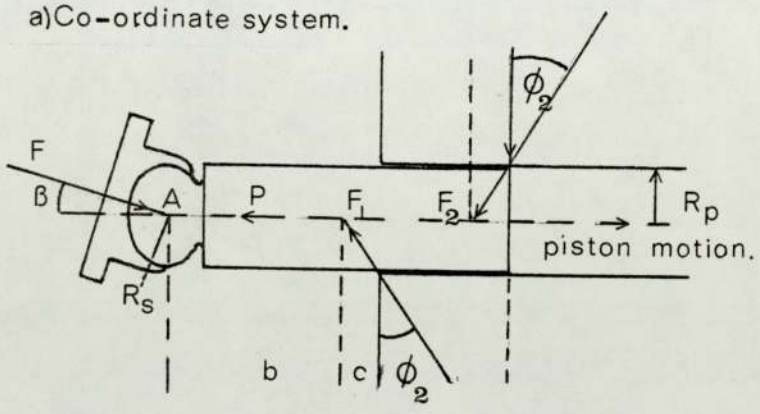

b)Pumping Stroke Forces.

Figure. A1.

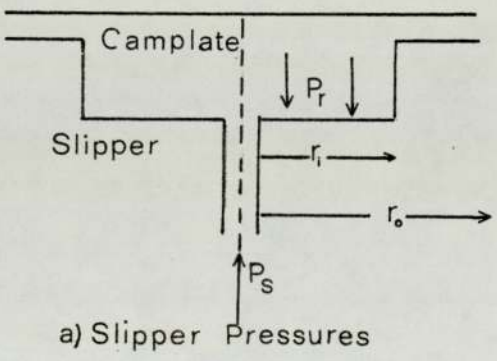

a) Slipper Pressures

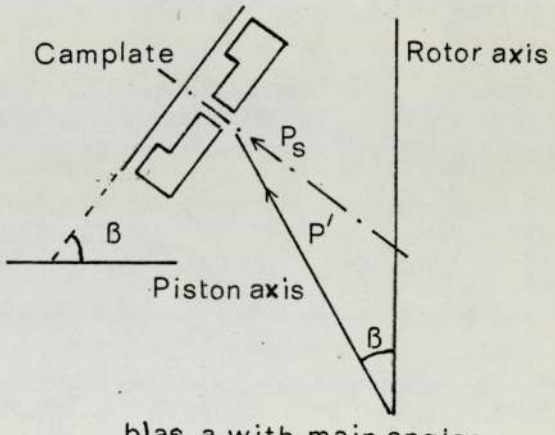

b)as a with main angles

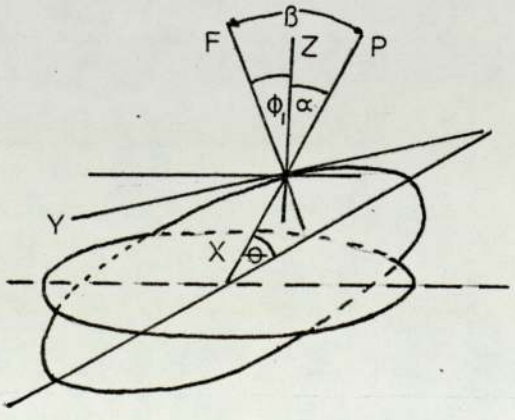

c) Redrawn a es.

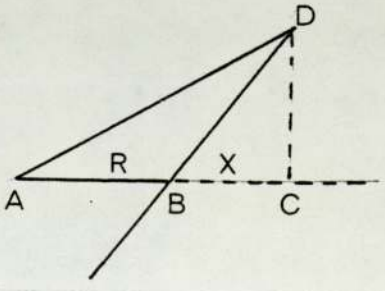

d)piston hangover.

Figure A2.

where b is the amount of overhang of the piston and a the length of piston remaining in the bore. Futher $P = \pi p' R_p^2$ where P' is the pressure of the fuel and R the radius of the piston orifice plate. Also $c = \mu_2 R_p$ where μ_2 is the coefficent of friction between the piston and bore and R_p is the piston radius.

A similar expression can be obtained for F_1.

If $R = 0.0127$ M, $P^1 = 12.5$ MN M^{-2}, $b = 0.0254$,

$\mu_2 = 0.1$ (assumed), $Rp = 0.01$ M, $\beta = 15^\circ$, $a \doteqdot 0.0254$,

$\phi_2 = \tan^{-1} \mu_2 = 5.711^\circ$.

$F_1 = 1895$ N

$F_2 = 916$ N

One of the assumptions made in these calculations was that the frictional force between the piston slipper and the camplate is small. If the slipper does not "lift off" from the camplate into full fluid film conditions then the coefficient of friction rises to 0.08 (carbon against steel).

The condition for the slipper to "lift off" is given by:-

Maximum pressure available $x\pi r_i^2 > W$, the load capacity where r_i is the radius of the slipper recess (figure A2 (a)). In figure A2(b) the pressure P_s acting to produce slipper lift off is shown along with the important angles.

The system is equivalent to a hydrostatic bearing for which the load capacity is given by:

$$W = \frac{\pi P_s (r_o^2 - r_i^2)}{2 \ln (r_o/r_i)}$$

where r_o is the radius of the slipper.

Now $A_\epsilon P_r \geq W$ for lift off conditions where A_ϵ is the effective area supporting the load and P_r the recess pressure.

$$\text{So} \quad \pi Rp^2 \cos \quad Pr \geqslant \frac{P'\pi(r_o^2 - r_i^2)}{2 \ln (r_o/r_i)}$$

using the previously quoted values for Rp, ß and P' with $r_o = 6 \times 10^{-3}$M and $r_i = 1.3 \times 10^{-3}$M gives

$$Pr = 13.15 \text{ MN M}^{-2}$$

Now the supply pressure is given by

$$P_s = P \cos ß$$

$$= 13.32 \text{ MN M}^{-2}$$

The effect, of this added force, on the calculation of F_1 and F_2 is to change the value of ß in the expressions giving these forces.

Including this force we can redraw the axes of figure A1(a) as shown in figure A2(c). In this case OP represents the hydraulic piston force acting along the line of action of the piston and OF represents the resultant of the normal reaction at the slipper-camplate interface and the frictional force in the direction of motion. Thus OF acts at the friction angle ϕ_1 to the Z axis in the Y-Z plane.

Let $|OF| = |OP| = 1$ i.e. unit vectors

$$Fp^2 = OF^2 + OP^2 - 2OF\ OP \cos ß$$

$$= 2 - 2 \cos ß$$

$$Fp^2 = (Fx - Px)^2 + (Fy - Py)^2 + (F_z - P_z)^2$$

where Px, Py, P_z are the component pressures and Fx, Fy, F_z the component forces in the X, Y, Z directions.

$$Fp^2 = 2 + 2 \sin \phi_1 \sin \alpha \sin \theta - 2 \cos \alpha \cos \phi$$

$$\cos ß = \cos \phi_1 \cos \alpha - \sin \phi_1 \sin \alpha \sin \theta$$

where θ is the rotor angular position. For the case of maximum overhang of the pistons $\theta = 0^\circ$ and $\sin \theta = 0$.

$$\text{Cos } \beta = \text{Cos } \phi_1 \text{ Cos } \alpha$$

Given the coefficient of friction for the slipper camplate is 0.08, tan ϕ_1 = 0.08 so Cos ϕ_1 = 0.9968.

$$\text{Cos } \beta = 0.9628$$

$$\text{and tan } \beta = 0.2805$$

This gives F_1 = 2095N

and F_2 = 1014N

These results are then about 10% higher than the original solution. Consequently this force should be included in the calculation.

An estimate was also made for the centrifugal force acting on the pistons since this had also been assumed to be small. Assume that the whole mass, M, of the piston acts at a point of contact on the lip of the bore. Let R be the radius of the point of contact from the rotor axis and w the rotor angular speed in radians per second.

$$\text{Centrifugal force} = MRW^2$$

For the two-piston rig w = 4100 r.p.m. M = 8.0×10^{-2} Kg and we need to find R.

Figure A2(d) shows the radius, R to the point of contact with a piston at maximum overhang. The length AD is the radius of the camplate from the rotor axis. Note that the camplate angle is 15° and the angle of the bores to the rotor axis is 15.13°.

Therefore from ΔADC, $x + R = AD \text{ Cos } 15^\circ$

and from ΔBDC, $x = BD \text{ Cos } 74.87^\circ$

where BD is the amount of overhang of the piston. Now BD = 0.026M and AD = 0.043M. Thus the centrifugal force is about 510N. This will be reduced by the action of the rotor on the piston in the bore. Consequently a force of about 50N would be reasonable to assume and can be neglected.

APPENDIX II

1. Quantitative Auger Analysis

Chang (64) has shown that the relative concentration X_i of the i^{th} element in a matrix of j elements is given by:

$$X_i = \frac{\alpha_i I_i}{\sum_j \alpha_j I_j}$$

where I_i and I_j are the Auger currents for the i^{th} elements and the sum over j elements. The α_i, α_j are inverse sensitivity factors defined by:-

$$\alpha_i \times I_i^{o} = I_s^{o}$$

where I is the Auger current, the subscript 's' represents a chosen standard element and the super script 'o' represents a pure element.

The α_i and α_j are evaluated empirically from known standards. In this work the spectra obtained on the Birmingham instrument were compared to standards from the Handbook of Auger Electron spectroscopy by Palmberg et al (A1).

$$\text{Define} \quad \alpha_i^{OB} I_i^{OB} = I_s^{OB}$$

where the superscript B refers to the Birmingham instrument and the other terms as previously defined. Similarly

$$\alpha_i^{OH} I_i^{OH} = I_s^{OH}$$

where H refers to the handbook.

$$\text{Also} \quad \alpha_i^{B} = \frac{I_s^{B}}{I_i^{B}}$$

The problem is to find the relationship between I_s^B, I_i^B and I_s^H and I_i^H. Now the Auger current is given by:

$$I_i = G\ Ip\ N_i\ D\ (E_i)\ r\ (Ep) \quad \sigma\ (E_i/p)$$

where G is an instrument factor, Ip the primary beam current, N the number of surface atoms, D the electron escape depth, r a backscattering factor and σ the cross-section for a given Auger transitition. Chang[64] has simplified this equation by letting T, r and G be constant terms.

$$\text{So } I_i \propto Ip\ \sigma\ (E_i/p)$$

For the Birmingham system we can now write:

$$\alpha_i^B = \frac{I_s^B}{I_i^B} = \frac{\sigma_s^B}{\sigma_i^B}$$

and for the Handbook

$$\alpha_i^H = \frac{I_s^H}{I_i^H} = \frac{\sigma_s^H}{\sigma_i^H}$$

so

$$\frac{\alpha_i^H}{\alpha_i^B} = \left(\frac{\sigma_s}{\sigma_i}\right)^H \Big/ \left(\frac{\sigma_s}{\sigma_i}\right)^B$$

rearranging and substituting for α_i^H

$$\alpha_i^B = \frac{\sigma_s^B}{\sigma_s^H} \times \frac{\sigma_i^H}{\sigma_i^B} \times \frac{I_s^H}{I_i^H}$$

The maximum normalised cross-sections can be used directly in this equation since terms involving cross-sections are dimensionless. This gives

$$\alpha_i^B = \beta_s \times \frac{\sigma_i^H}{\sigma_i^B} \times \frac{1}{I_i^H}$$

where $\beta_s = \sigma_{ns}^{B} I_{cs}^{H} / \sigma_{ns}^{H}$ and σ_{ns}^{B} refers to the normalised cross-section for an arbitarily chosen standard using the Birmingham instrument, σ_{ns}^{H} a similar cross-section derived using the handbook and I_{cs}^{H} a corrected peak intensity for the selected standard element.

Direct comparison, between the Birmingham instrument and the instrument used to obtain the handbook spectra, is not possible without first correcting for a number of factors. These corrections will now be shown in the derivation of the inverse sensitivity factors.

Table I shows the corrected peak-to-peak heights of elements taken from the handbook. The corrections are for the scale factor used and for the cases where compounds have been used to obtain the spectra. The latter includes oxygen, sulphur, phosphorus and chlorine. Correction for compounds is made on the assumption that the material analysed contains a 50%:50% ratio of the component elements. A linear relationshipe between concentration and peak-to-peak height is assumed and the height consequently doubled. This is a particularly course assumption which can be seen from consideration of the case of oxygen. The handbook achieves the oxygen spectrum from a compound of magnesium oxide. Oxidation has two main effects. The first is that the magnitude of one peak may increase whilst another decrease. Secondly an energy shift occurs.

The change in peak size for magnesium and magnesium oxide is shown in Table II.

Unfortunately what happens to the magnitude of the oxygen peak cannot be determined so the above approximation has to be used. The third correction that has to be made is for the electron multiplier gain which varies, as shown in figure 1, for the handbook instrument. At this stage it was also necessary to use some normalisation procedure since this would help to account for variations in gain with time. Since the major component of aluminium bronze is copper

Table I Corrected peak-to-peak heights from the Handbook of Auger electron spectroscopy					
Element	Energy	Scale Factor	Height	Corrected Height	
	eV		mm	Scale Corrections	Compound
Nickel	848	2.5	87	34.8	-
Aluminium	1396	2.0	133	6.65	-
Iron	651	2.5	68	27.2	-
Copper	920	2.5	81	32.4	-
Carbon	272	5	75	15	-
Oxygen	510	2.5	174	69.6	139.2
Sulphur	152	1	89	89	178
Phosphorus	120	2.5	81	32.4	64.8
Chromium	529	2.5	105	42	-
Cadmium	376	1	130	130	-
Chlorine	181	2	73	36.5	73

Table II Effect of compounds on P-P Heights				
Element/Compound	Peak energy		Magnitude	
Mg	45	1186	56.8	13.7
Mgo (Mg Component)	45	1186	19.2	22

it was decided to normalise with respect to that element. Table III shows the corrected peak-to-peak heights when electron multiplier gain is taken into account.

To calculate sensitivity factors it is necessary to know the corrected peak-to-peak heights and the cross-section value for the particular Auger transitions under consideration. Palmberg et al used a 3KeV beam whereas a 2KeV beam energy was used for this work so this has to be taken into account when determining the cross-sections. Normalised cross-sections are plotted against the reduced energy

Table III Corrected Peak-to-Peak Heights for Electron Multiplier Gain

Element	Energy eV	Gain	Normalised Gain	Corrected Height
Nickel	848	1945	0.94	32.7
Aluminium	1396	1865	0.98	6.5
Iron	651	2022	0.91	24.7
Copper	920	1835	1.00	27.6
Carbon	272	2050	0.89	13.35
Oxygen	510	2119	0.87	121.1
Sulphur	152	1780	1.03	183.34
Phosphorus	120	1610	1.14	73.87
Chromium	529	2110	0.87	36.54
Cadmium	376	2125	0.86	111.8
Chlorine	181	1890	0.97	70.81

Ep/E_i where Ep is the primary beam energy and E_i the energy for the transition. Table IV shows the reduced energies for a 3KeV and 2KeV beam. The transition energies listed in this table were obtained from the X-ray data of Bearden & Burr[42] which is the most accurate data so far available. Also given in the table are the maximum cross-sections for the transitions listed.

For M shell transitions Vrakking and Meyer[82] give the relationshipe $\sigma = AE_i - 0.8$ and then show that for Bromine $\sigma = 1.4 \times 10^{-19}$ in which case since E_i for Bromine is 70.1 eV then $A = 4.19 \times 10^{-18}$ and $\sigma = 4.19 \times 10^{-18} E_i^{-0.8}$ for M shell transitions at least for Bromine. The equation $\sigma = 8.3 \times 10^{-16} E^{-1.56}$ was quoted by the same workers for L_{III} transitions. Figure 2 shows a graph of normalised cross-section against reduced energy for K shell transition as given by Vrakking and Meyer. This graph was used to determine the normalised cross-sections for the calculation

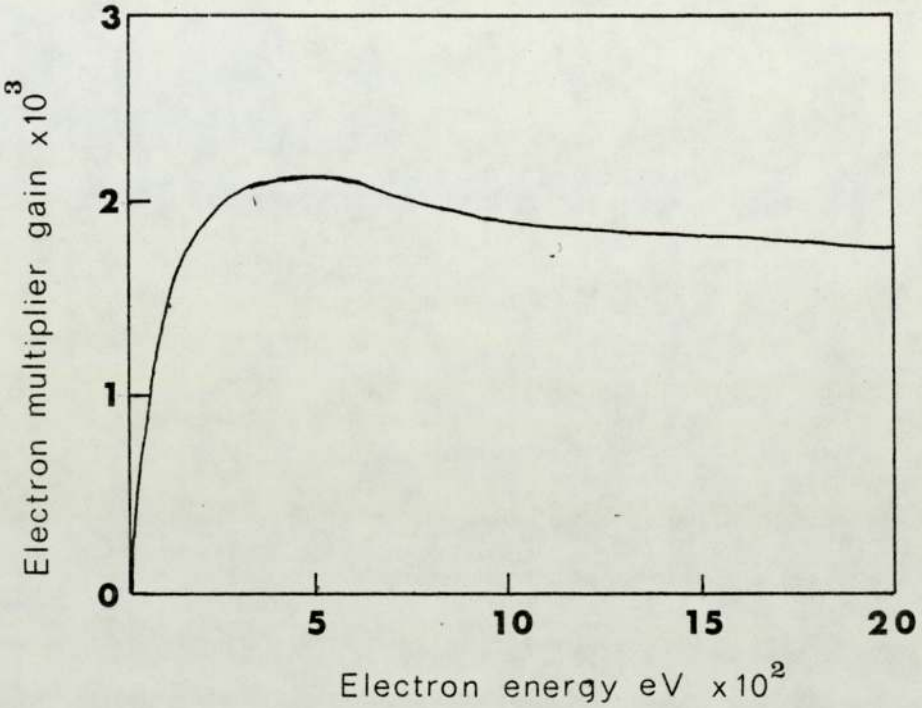

Figure 1 after Palmberg (RefA1)

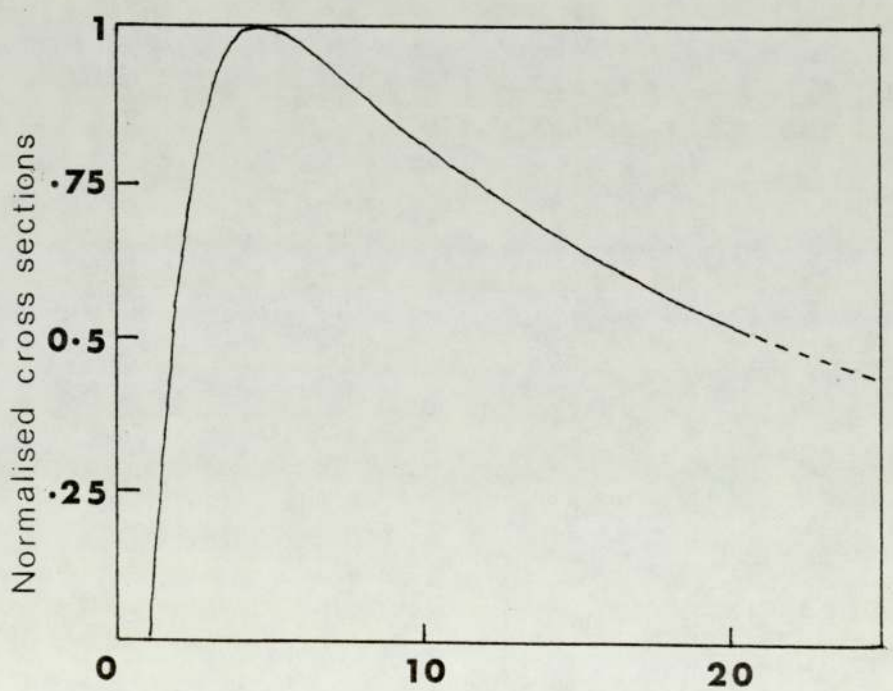

Figure 2 after Glupe & Mehlhorn (Ref. 81)

Table IV Reduced Energies and Maximum Cross-sections

Element	E_i	Type of Transition	Ep/E_i(3KeV)	Max($Ep/E_i=4x10^{-20}$)	Ep/E_i(2KeV)
Nickel	854.7	L	9.51	2.2	2.34
Aluminium	1559.6	K	1.92	0.7	1.28
Iron	708.1	L	4.24	2.97	2.83
Copper	931.1	L	3.22	1.94	2.15
Carbon	283.8	K	10.57	16.4	7.05
Oxygen	532	K	5.64	7.5	3.76
Sulphur	164.8	L	18.2	27.5	12.13
Phosphorus	1322	L	22.69	39	15.13
Chromium	5745	L	5.22	4.1	3.48
Cadmium	403.7	M_v	7.43	3.45	4.95
Chlorine	200.0	L	15.0	22	10.0

of the inverse sensitivity factors. Values for the cross-sections quoted for carbon and oxygen, were determined by Glupe and Mehlhorn[71]. One problem with these results is that Glupe and Mehlhorn used gaseous samples but do not say whether they measured their cross-sections relative to any particular element. Vrakking and Meyer however again used gaseous samples and measured relative to carbon and chlorine. The fact that gaseous samples were used is a further complication when trying to apply the data to solid specimens.

Table V shows the normalised cross-section data obtained from Vrakking and Meyers graph (figure 2).

Table V Normalised cross-section values

Element	Ep/E_i (mm)	σ_n(mm) 2KeV	σ_n	Ep/E_i (mm)	σ_n(mm) 3KeV	σ_n
Nickel	168.5	90	0.84	2527	106.75	0.99
Aluminium	92.2	51.25	0.30	138.2	75.5	0.7
Iron	203.8	104	0.97	318.2	105.25	0.98
Copper	154.8	84.25	0.78	231.8	104.25	0.97
Carbon	507.6	94	0.87	761.0	83.75	0.78
Oxygen	207.7	107	0.99	406.1	103	0.96
Sulphur	873.4	78	0.72	1310.4	61	0.57
Phosphorus	1089.4	68.75	0.64	1633.7	53.25	0.49
Chromium	250.6	106.5	0.99	357.8	105.5	0.98
Cadmium	356.5	105.5	0.98	535.0	94.25	0.88
Chlorine	720	86.25	0.80	1080.0	69	0.64

Note that in this case normalisation has been with respect to the maximum cross-section at $Ep/E_i = 4 \times 10^{-20}$. There is some justification for taking σ values for L_{23} transitions from this graph since the data for sulphur, phosphorus and chlorine, obtained by Vrakking and Meyer, fit this curve.

Previously we had the equation

$$\alpha_i^B = \beta_s \times \frac{\sigma_i^H}{\sigma_i^B} \times \frac{1}{I_i^H}$$

Where

$$\beta_s = \frac{\sigma_s^B \times I_s^H}{\sigma_s^H}$$

Therefore $\beta_s = 22.2$ by using values for the table of normalised cross-sections with copper as the standard.

$$\alpha_i^B = 22.2 \frac{\sigma_{in}^H}{\sigma_{in}^B} \times \frac{I}{I_{ic}^H}$$

The α_i^B's could then be calculated and again normalisation carried out with respect to copper.

The use of peak-to-peak height in the above analysis was an approximation to the Auger current as suggested by Southworth (A3). A better measure is the area under the peak. Taking this into account with the corrections applied as given for the simple peak-to-peak height calculations the β_s is given by:

$$\beta_s' = \frac{\sigma_s^B}{I_s^H} I_s^H$$

Where $I_s'^H = \frac{I_s^H \times I_w}{2}$

and I_w is the peak width.

For copper $\beta_s' = 91.2$ and α_i^B is given by:

$$\alpha_i'^B = 91.2 \frac{\sigma_{in}^H}{\sigma_{in}^B} \frac{1}{I_{ic}'^H}$$

and

$$I_{ic}'^H = I_{ic}^H \times I_w$$

Table VI shows the calculated sensitivity factors (a) using peak-to-peak heights, α_i^B, (b) using peak-to-peak heights multiplied by half the peak width, $\alpha_i'^B$ and (c) the sensitivity factors normalised to iron using peak-to-peak heights, $\alpha_i''^B$.

Table VI Sensitivity Factors							
Element	in^H	in^B	I_{ic}^H	$I_H w/2$	α_i^B	$\alpha_i^{/B}$	$\alpha_i^{//B}$
Nickel	0.99	0.84	32.7	3.5	0.8	0.94	0.943
Aluminium	0.7	0.3	6.5	3.5	7.97	9.33	10.24
Iron	0.98	0.97	24.7	2.5	0.91	1.49	1.0
Copper	0.97	0.78	27.5	3.5	1.0	1.0	1.14
Oxygen	0.96	0.99	121.1	2	0.18	0.365	0.358
Sulphur	0.57	0.72	183.3	2	0.096	0.197	0.272
Phosphorus	0.49	0.64	73.9	2	0.23	0.473	0.799
Chromium	0.98	0.99	36.5	2.5	0.6	0.988	0.61
Cadmium	0.88	0.98	111.8	1	0.18	0.732	0.177
Chlorine	0.64	0.8	70.8	1	0.25	0.686	0.7
Carbon	0.78	0.87	13.3	5	1.49	1.22	1.586

2. The relationship between the product of sputter current and sputter time to depth of surface removed

Assume that each atom is singly ionised so that the number of ions per second per square metre corresponding to one microamp per square metre can be obtained from the following:

$$\text{current} = \frac{\text{charge}}{\text{time}}$$

$$1\ \mu A = 10^{-6}\ \frac{q}{t}\ \frac{\text{coulombs}}{\text{seconds}}$$

If one electron flows per second for each singly ionised atom then the current flowing is 1.6×10^{-19} atoms. So 1 electron/second gives 1.6×10^{-13} A.

$$1\ \mu A = \frac{10^{13}}{1.6}\ \frac{\text{electrons}}{\text{sec}}$$

Since we assume single ionisation

$$1\ \mu A = \frac{10^{13}}{1.6}\ \frac{\text{ions}}{\text{sec}}$$

$$= 6 \times 10^{12}\ \text{ions/sec}$$

$$1\ \mu A/\text{sq m} = 6 \times 10^{12}\ \text{ions/sec/sq M}$$

Let the size of the atomic spacing on the sample be, $a \times 10^{-10}$ M. The number of atoms per sq M on the surface will then be $10^{20}/a^2$.

A particular element will have a sputter yield s, so the number of atoms removed /sq M/sec

$$= S \times 6 \times 10^{12}$$

Therefore the number of monolayers removed/sec

$$= \frac{a^2 \times s \times 6 \times 10^{12}}{10^{20}}$$

The number of metres removed per minute of a simple cubic lattice is $\frac{36Sa^3}{10^{17}}$ for a Xe^+ ion flux of 1 $\mu A\ M^{-2}$.

i.e. number of metres removed /μA minute $\frac{36Sa^3}{10^{17}}$

For a face centred cubic lattice such as copper the nearest neighbour distance is $\frac{9}{2} \times 10^{-10}$ M.

number of metres removed /μA minute is $\frac{18Sa^3}{10^{17}}$

The 400 eV Xenon ions give a flux of approximately $\frac{0.5\ \mu A/\text{sq.M}}{10^{-4}}$ at the sample in the Birmingham spectrometer.

$$M/\mu A \text{ min} = \frac{18Sa^3}{10^{17}} \times \frac{0.5}{10^{-4}}$$

$$= \frac{9Sa^3}{10^{13}}$$

Rosenberg and Wehner[77] have measured sputtering yields for a number of elements. Their yield curve for copper sputtered by Xenon is reproduced in figure 4. This gives a yield of 1.7 atoms/ion at an ion energy of 400 eV. Assuming the aluminium bronze to be pure copper at the surface the lattice spacing a = 3.6 Å.

$$a\ M/\mu A \text{ min} = \frac{9 \times 1.7 \times (3.6)^3}{10^{+13}}$$

$$= \underline{0.7 \times 10^{-10}}$$

References

A1. Palmberg, P.W., Riach, G.E., Weber, R.E., and MacDonald, N.C., "Handbook of Auger Electron Spectroscopy", Pub.Physical Electronics Industries (1972).

A2. Bearden, J.A., and Burr, A.F., "Reevaluation of X-ray Atomic Energy Levels", Rev.Mod.Phys., 39, No.1, pp. 125-142 (1967).

A3. Southworth, H.N., "Surface Studies using Auger Electron Spectroscopy", Vac. News., pp. 10-21 (1976).

APPENDIX III

Ellipsometry

This technique has been described in detail elsewhere (84) so a brief review of some of the physical principles involved, with an indication of the theory will be given here.

To understand the operation of the ellipsometer a number of optical terms and ideas need to be introduced. First, the components of the electric vector of a light beam undergo different phase changes when reflected by an absorbing medium. The difference between these phase changes, δ , is 90° at the principal angle of incidence Ip. Suppose a plane polarised light beam is incident at the principal angle of incidence with its electric vector at 45° to the plane of incidence then elliptically polarised light results. The elliptically polarised light will have one of its axes in the plane of incidence and will have unequal reflected components which are $\pi/2$ out of phase. In the analysis of elliptically polarised light this phase difference is compensated to give plane polarised light and the plane of vibration of this light is determined with an analyser.

Secondly, consider what happens to light in anisotropic mediums, in which there are two refraction paths 'O' and 'E'. The 'O' path in these birefrunent materials is the path taken by ordinary waves and rays. These waves and rays obey the normal laws of optics and the rays are normal to the waves. Similarly the E path is the path taken by extra-ordinary waves and rays which do not obey Snell's law of refraction and the waves and rays are not normal to each other. In this type of material the 'O' and 'E' waves have different velocities and the privileged directions are the two directions of vibration of the incident light which correspond to a single plane

polarised emurgent beam. Longhurst (A4) has dealt with the detection and compensation of polarised light in his book.

It can be shown that the equation of ellipsometry is given by:

$$\frac{r_{13}(P)}{r_{13}(S)} = \tan\Psi\, e^{-i\Delta}$$

Where $r_{13}(P)$ is the Fresnel coefficient, for the component of light whose wave vector is parallel to the plane of incidence, as it travels from medium (1) to medium (3). Similarly $r_{13}(S)$ is for light with the wave vector perpendicular to the plane of incidence. The relative amplitude reduction is given by $\tan\Psi$ and Δ the difference in phase changes for the (P) and (S) components. Δ is a function of the complex refractive index, the thickness and the angle of refraction through the Fresnel coefficients.

The experimental arrangement for the compensator method of ellipsometry is shown in figure (1). Plane polarised light is produced by the polariser P with the plane of polarisation inclined at an angle γ to the plane of incidence. Reflection at the sample produced an ellipse whole major axis aziminth is γ and has ellipticity δ . The quarter wave plate compensator is arranged so that its privileged directions are parallel to the axes of the ellipse.

This produces plane polarised light with its aziminth at δ to the ellipse major axis. The analysing polaroid is rotated until the transmission axis is 90° to the plane of polarisation. The ellipticity is related to the phase difference between the (P) and (S) components by the following expression:

$$\tan\Delta = \frac{\tan 2\delta}{\sin 2\gamma}$$

but $\chi = 45^{\circ}$ since this is the quarter wave plating setting.

$$\tan \Delta = \tan 2\delta$$

$$\therefore \Delta = 2\delta$$

The ellipticity determined from the analyser aziminth. The aziminth of the compensated light and of the anlyser in the extinction position is $45^{\circ} + \delta$ with respect to the perpendicular to the plane of incidence. If x is measured experimentally,

$x = 45 + \delta$

$$x + 45 + \frac{\Delta}{2}$$

giving $\Delta = 2x - 90^{\circ}$

A4 Longhurst, R.S., "Geometrical and Physical Optics" (2nd Ed.), Pub. Longman 1967.

The effect of the addition of corrosion inhibitors on the wear of aluminium bronze on steel in the presence of aviation fuels

W. Poole and J.L. Sullivan, University of Aston.

The absence of saturated hetrocyclic compounds and other polar impurities in modern hydrotreated aviation kerosenes can lead to high wear and siezure in jet aircraft pumps. It was found that the addition of commercially available corrosion inhibitors reduces wear and eliminates seizure, but although the effects of the additive have been known since the 1960's the mechanism responsible for protection was not understood. The purpose of the study was to isolate these mechanisms. The additive used in the experiments consisted of 45% dilinoleic acid and 5% phosphate ester in 50% fuel oil base. This was added to the kerosene at 12 p.p.m. by weight.

The test rig was a 3mm diameter aluminium bronze pin running on K.E. 180 steel disks of 700 HV. Surface finishes of the disks varied from 0.1 to 0.6 microns c.l.a. All components were cleaned in an additive free petrol vapour bath prior to use. Fuel was pumped on to the disk at a constant rate of 30 $ml.min^{-1}$ and was recirculated and filtered to remove debris.

In order to select the boundary lubrication region Sribek curves were plotted. Using this information samples were generated for surface investigations and load versus speed characteristics plotted for kerosene plus additive and an inert control fluid (isooctane). In order to identify surface elements present during wear Auger electron spectroscopy was used. Depth profiles of the elements being measured using xenon ion bombardment. The thickness of the boundary film formed was found from ellipsometry.

The Stribek curves and wear v. velocity curves are shown below

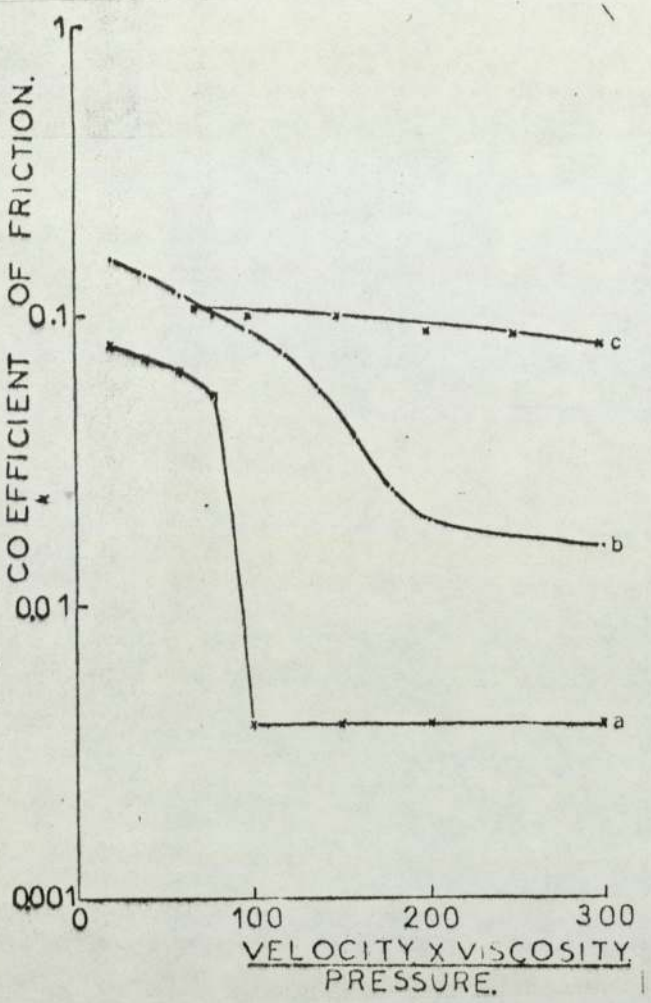

Fig.1. Stribek curves;
(a) Fuel with additive, disk 0.2µm c.l.a.
(b) Same disk 0.6µm c.l.a.
(c) Iso octane, disk 0.2µm c.l.a.

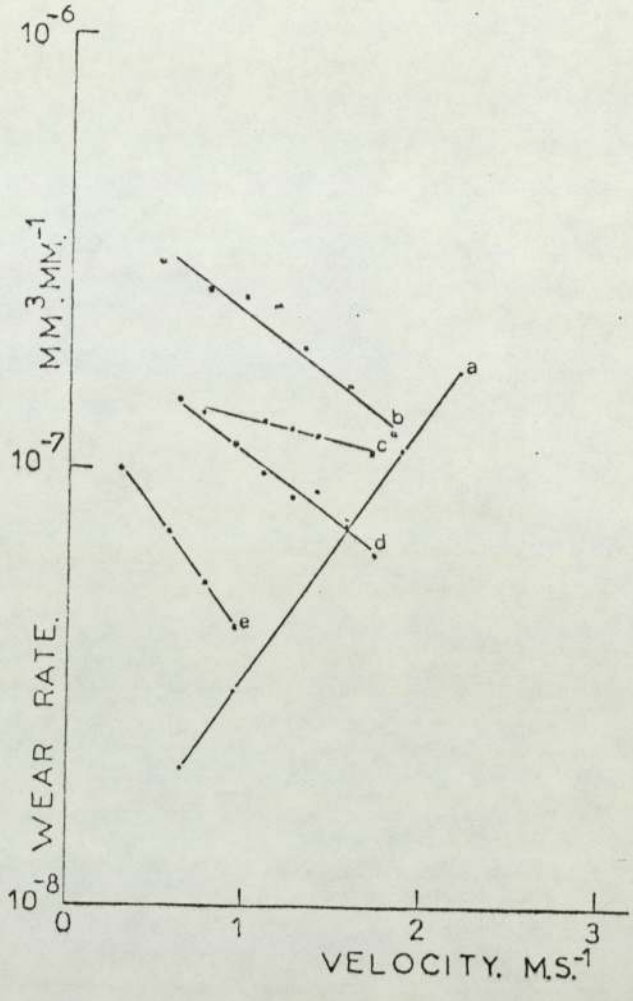

Fig. 2. Wear rate v.velocity curves;
(a) Iso-octane 2 Kg.load disk 0.2µm c.l.a.
(b) Fuel plus additive 5 Kg, disk 0.6µm c.l.a;
(c) (d) (e) Same disk, 0.2µm 12.5 Kg, 10 Kg and 5 Kg loads resp.

Fig. 3 is a typical wear rate v. load curve. The transistion from increasing to decreasing wear rates occurs at the same value of frictional heating at the surface. This indicates that the reduction in wear rate is due either to oxidation or increased surface activity of the additive with heat.

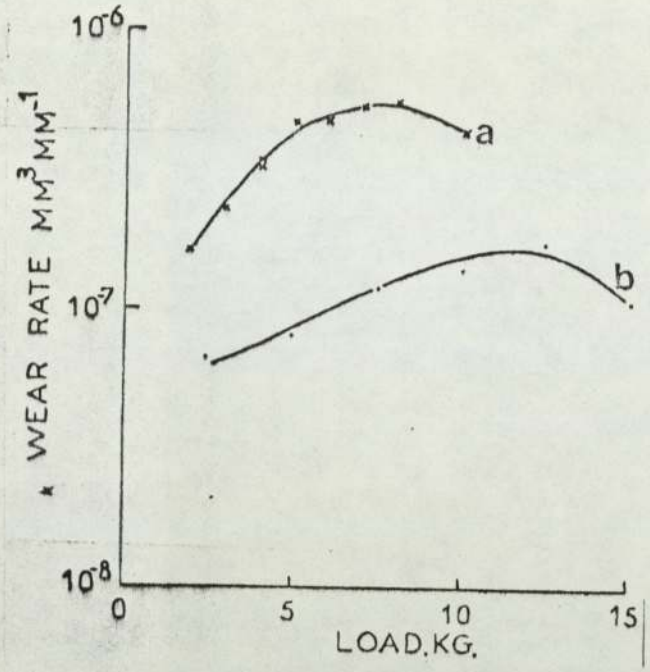

Fig. 3. Wear rate v. load for 0.6ms^{-1} velocity and fuel with additive
(a) 0.6μm c.l.a.
(b) 0.2μm c.l.a.

Typical Auger Spectra are shown in Figs. 4 and 5.
The appearance of P and Cl in the samples for high temperatures, high surface roughnesses and high loads indicates that the phosphate ester might have an important role as an e.p. additive. X-ray analysis of certain wear debris from fuels indicates the presence of phosphorus compounds so supporting the argument.

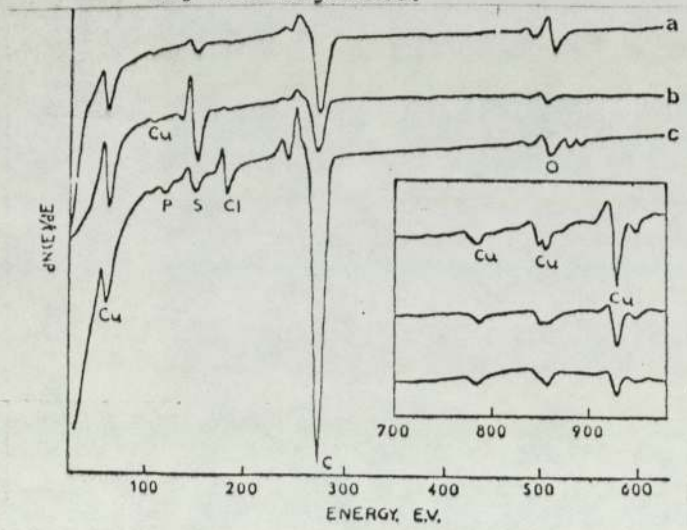

Fig. 4. Auger spectra of pin surface run in
(a) Iso octane
(b) Fuel with additive, disk 0.2μm c.l.a.
(c) Same, disk 0.6μm c.l.a.

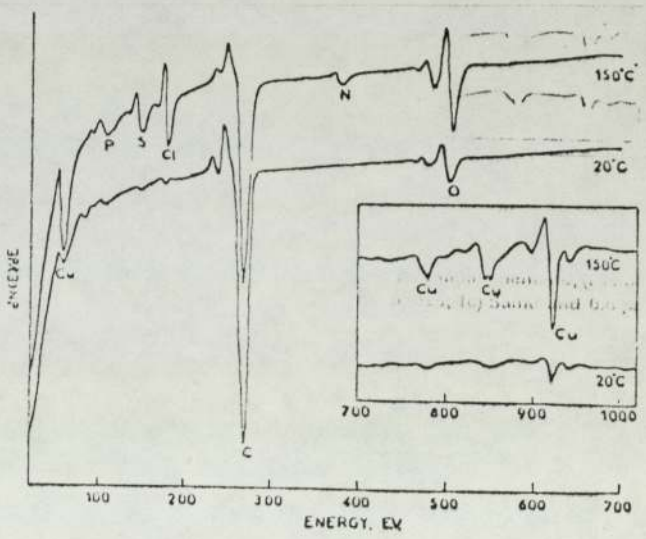

Fig. 5. Auger spectra of unworn pins immersed in additive.

Figs. 6, 7 and 8 show the calculated depth profiles of the important elements present on the surface.

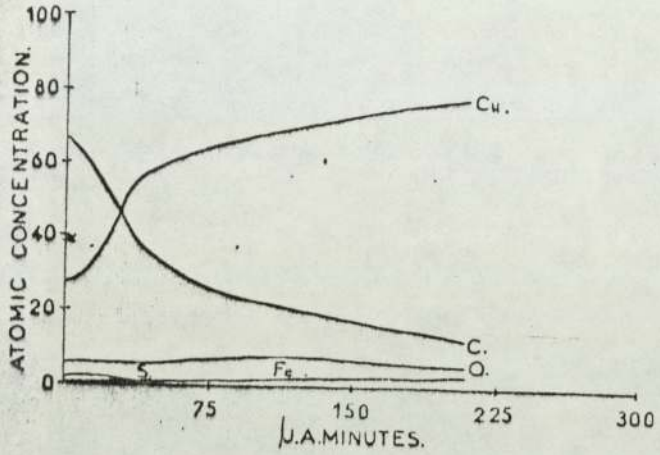

Fig. 6. Depth profiles for pin worn in presence of iso octane

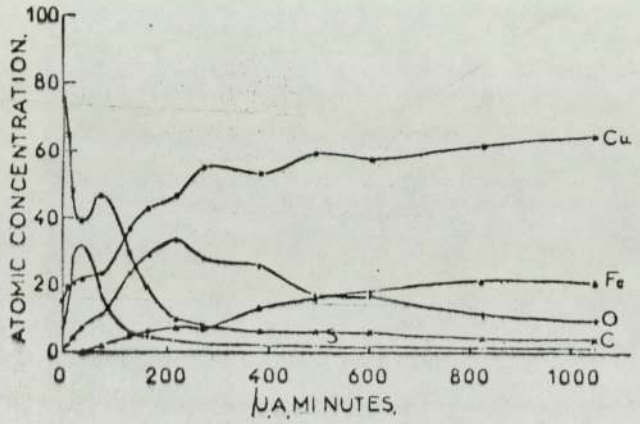

Fig. 7. Depth profiles for pin worn in fuel plus additive

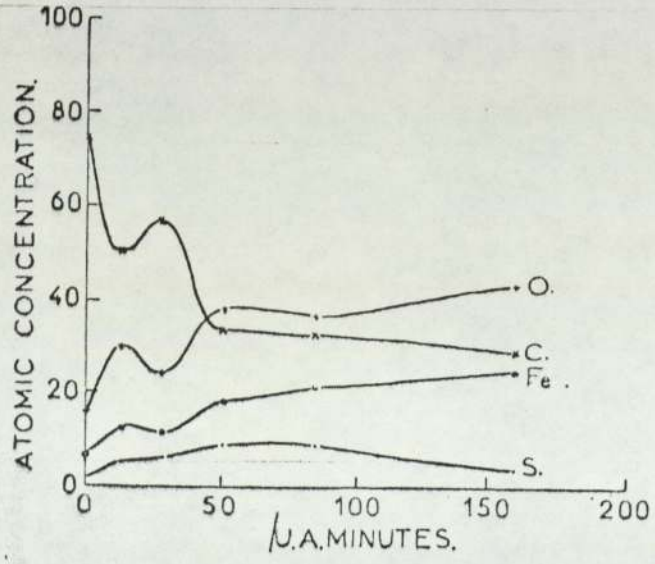

Fig. 8. Depth profiles of elements present on worn steel surface

It would appear that the surface consists of a very thin layer (a few Angstroms thick) of atmospheric contamination, shown by the initial high concentration of carbon. The carbon peaks indicate a boundary layer (the dimeric acid) with either sulphur or sulphur compounds present in or adhering to the surface. This layer is formed on a copper rich oxide layer. The ellipsometric measurements show the boundary layer to be 130Å thick, and this corresponds very closely to one molecular chain length of the dimeric acid. The sulphur present on the surface is due to the additive fuel oil carrier.

This surface, resulting from the addition of the corrosion inhibitor, is responsible for protection of contacting components in aircraft fuel systems.

PREPRINT NO. 79-AM-5E-1
ASLE PREPRINT

The Role of Aluminum Segregation in the Wear of Aluminum/Bronze-Steel Interfaces Under Conditions of Boundary Lubrication

W. POOLE and J. L. SULLIVAN
University of Aston in Birmingham
Birmingham B4 7ET, England

An interest in the wear of steel nonsteel systems, currently in use in aircraft fuel systems, has led to a study of aluminum bronze sliding on KE961 steel in the presence of kerosene with, and without, the addition of a commercial boundary lubricant. Experiments were conducted to determine wear rates with change of load together with an extensive investigation of the contacting surfaces using physical techniques such as EPMA, SEM and Auger spectroscopy.

It was found that the additive had an initial pro-wear effect on the bronze followed by a sharp reduction in wear. The results of the measurements, and of the surface analysis, indicate that the mechanism responsible for this wear is due to preferential segregation of the aluminum to the surface. In the absence of the additive, aluminum is transferred to the steel and forms a solid solution which can cause seizure to occur.

INTRODUCTION

Modern jet aircraft require fuels of high thermal stability (*1*). This, together with the cost of producing traditional, chemically treated fuels, resulted in the introduction of hydrotreated kerosenes (*2*). While hydrotreating has some beneficial effects, it removes many of the polar impurities present in fuels refined using traditional techniques. This, in turn, leads to a reduction in the fuels' lubricating ability (*3*).

Hydrotreated fuels have, it is claimed, produced a number of problems in fuel systems, but the one of particular interest to the authors and the subject of this investigation relates to a piston pump (KE961 steel pistons running in cadmium plated A1-Bronze bores. This pump suffered high wear and, in some cases, seizure when run for prolonged periods in this type of fuel (*4*). The addition of a commercial corrosion inhibitor (consisting of a dimeric acid plus phosphate ester) eliminated the problem and previous work by the authors (*5*) has indicated the action of the additive in producing a surface layer helping to reduce wear and prevent seizure. Their work with Auger electron spectroscopy showed the presence of a surface hydrocarbon protective layer produced by the additive overlying a copper rich oxide. It was found difficult to detect the presence of aluminum in the study.

There were two basic aims in the work presented in this paper. The first was to determine differences in wear mechanisms in the presence of hydrotreated fuels with and without additive and, hence, more fully investigate the role of the additive as a surface protective agent. It is obvious that the effects of the fuels cannot be studied in isolation from their interactions with the wearing surfaces; hence, the second aim was to gain knowledge of the role of the surface metallurgical combination in the wear mechanisms.

An understanding of these mechanisms was sought through the use of surface sensitive techniques such as electron probe microanalysis (EPMA), scanning and transmission electron microscopy (SEM and TEM) and Auger electron spectroscopy (AES) together with extensive X-ray analysis of wear debris samples taken from different parts of the wear rate against load curves.

EXPERIMENTAL

Wear Tests

Friction and wear measurements have been made, at room temperature (20°C), using a pin-on-disk machine for a system lubricated with hydrotreated aviation kerosene and a similar fuel with the addition of a commercially available corrosion inhibitor. The kerosene was filtered through a 13 percent alumina catalyst to remove polar compounds formed, or taken up, by the fuel during storage. Addition of 15 ppm of the corrosion inhibitor was made to a similarly treated batch of fuel.

The flat-faced, 2-mm and 3-mm diameter, wear pins were an aluminum bronze of 10-percent aluminum, 4-percent nickel, 4-percent iron with the remainder copper. The disk was a 13-percent chrome steel of 0.2 μm cla surface finish. Tests were carried out, in laboratory atmo-

Presented at the 34th Annual Meeting
In St. Louis, Missouri,
April 30-May 3, 1979

sphere, for a constant speed of 0.6 m.s^{-1} and loads between 2.5 and 15 kg inclusive. These operating conditions were such that boundary lubrication was maintained throughout the test period.

Details of friction and wear machine, test procedure and continuous friction and wear monitoring have been given previously (5).

Debris Analysis

Wear debris has been analyzed using an X-ray powder technique. Samples were prepared by washing with acetone and centrifuging before drying and being placed in a thin-walled capillary of 0.3-mm diameter. These samples were irradiated, for 20 minutes at the center of a 114.6-mm diameter powder camera. The measured "d" values were compared to powder diffraction file values for various elements and compounds.

Surface Analysis

Samples of the pin-and-disk surfaces were analyzed after wear by using EPMA and AES surface topography was investigated using SEM and two-stage carbon replicas for TEM.

The electron probe was operated at a beam energy of 15 keV with 80 μA beam current for an 0.03 micron spot size. X-ray distribution photographs were obtained for elements of interest on the surface, the area scanned being 125 (microns)^2. Some samples were polished to give a ten-degree taper before analysis so that the wear surface could be directly compared to the bulk with respect to element concentration.

Details of the AES technique and sample preparation have been given previously (5), so only the important operating conditions will be given here. The primary beam energy was 2 keV giving 10 μA current in a 1-mm diameter spot at the sample. By selecting a 2-keV beam energy, it was hoped that the high-energy, aluminum Auger transitions could be observed without causing too much damage, from beam effects, to the surface layers. Spectra were obtained at a pressure better than 10^{-10} torr with ion beam etching being carried out, using 400 eV xenon ions, at 10^{-4} torr xenon pressure.

RESULTS

Figure 1 shows the wear rate against load curves obtained for the 3-mm diameter wear pins. Curve (a) for the hydrofined fuel shows a steady increase in wear with load. Addition of the corrosion inhibitor [curve (b)] produced a pro wear effect over most of the load range but, at 15 kg, the wear rate was reduced. A definite transition point is observed for this series of tests at about 10 kg.

Similar trends in wear against load were found for the 2-mm diameter wear pins (Fig. 2). For the hydrofined fuel, wear increases with load until at 12.5 kg, a seizure occurred. The test carried out at 12.5 kg produced a wear rate for a short time (15 minutes) and then seizure occurred between the pin and disk. The results for the hydrofined fuel [Fig. 2(b)] are similar to the 3-mm diameter pins except

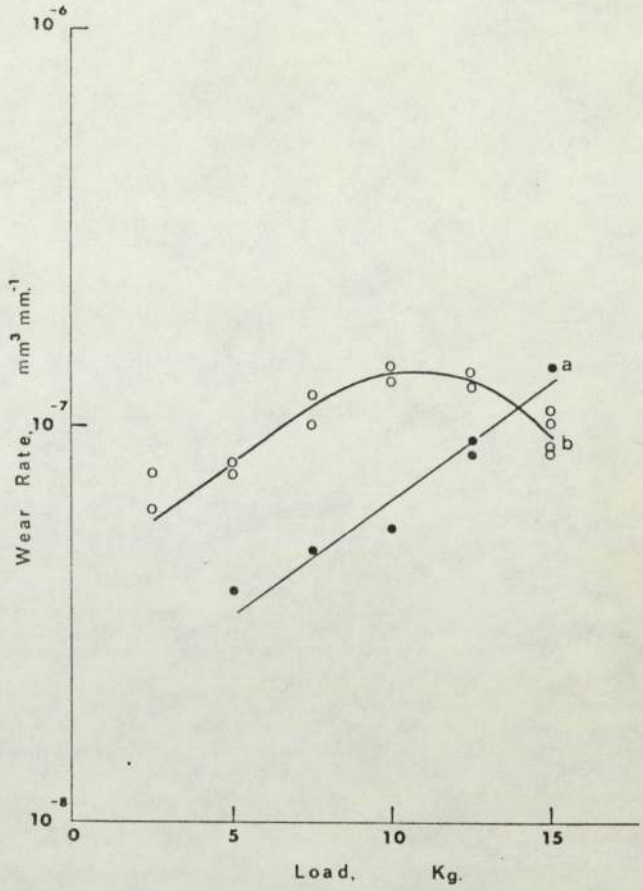

Fig. 1—Wear rate v load for 3-mm diameter wear pins at 0.6 m.s^{-1} (a) Without additive, (b) with additive.

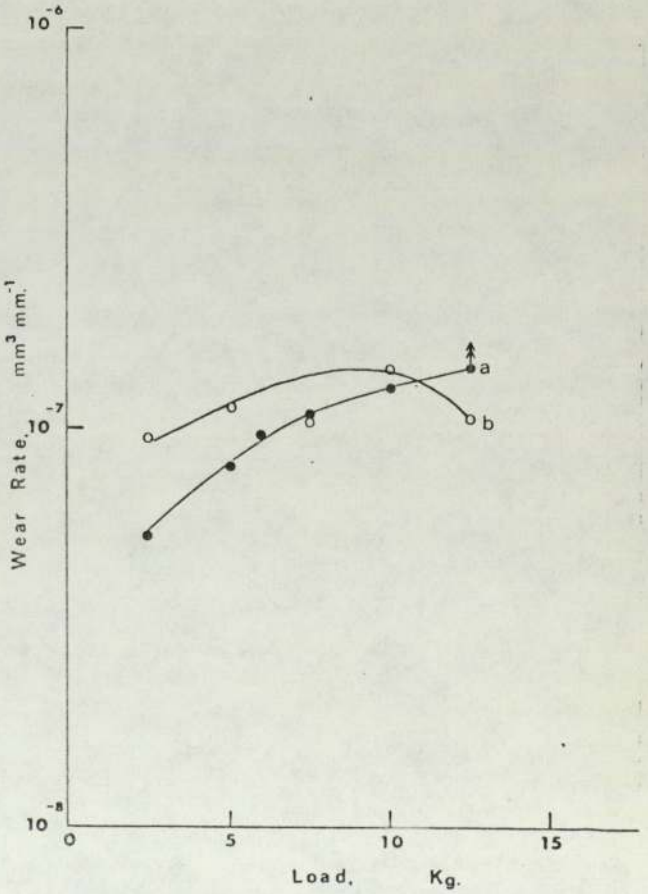

Fig. 2—Wear rate v load for 2-mm diameter wear pins at 0.6 m.s^{-1} (a) Without additive, (b) with additive.

that, at 7.5 kg, a lower than expected wear rate was recorded. Again, a transition point was observed and no seizure occurred at 12.5 kg.

Friction behavior was generally variable for both fuels but the coefficient of friction for hydrofined fuels was normally higher than that for fuel with additive (0.12 compared to 0.09). The coefficient of friction remained constant at about 0.12 for hydrofined fuels in most cases but, on some occasions, friction "spikes" were obtained (Fig. 3) when the coefficient varied between 0.02 and 0.17 and occasionally seizure occurred. The "spikes" lasted for about 40 seconds with intervals of about 10 to 15 minutes between spikes. At the start and towards the end of the spike, large variations in the coefficient indicate the stick-slip that was occurring during the test. A period of very stable friction can be seen soon after the friction rises to its maximum. The effect of the additive was to produce a steady friction value during wear with no spikes. However, periods of low friction were still observed and, after about 1.5 hours, wear many tests produced low friction and wear.

Table 1 shows the results of the X-ray analysis of the wear debris. The measured "d" spacings are given for each test in descending order. Results are also given for a reference sample of aluminum bronze. The hydrofined fuel debris was very little different to that of the bronze. A "d" spacing of 2.48 was found but none of the other copper oxide peaks were present. Consequently, this debris appears to be aluminum bronze.

A large number of diffraction lines were found when the additive was present in the fuel, some of which were quite broad (in particular lines at "d" spacings of 2.09 and 2.03). The indications at 6 kg load is that phosphates are present, along with copper oxide. Aluminum ortho-phosphate and copper (II) phosphate would seem to be the most reasonable compounds to fit the measured "d" spacings.

At the higher loads (10 kg and 12.5 kg), a change to aluminum phosphides occurs. This is particularly true at 12.5 kg load where "d" spacings of 3.11, 1.93 and 1.65 were found. As with lower load, copper oxide can be identified and also pure copper lines appear.

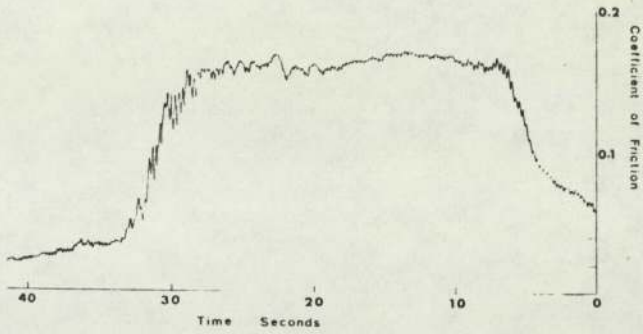

Fig. 3—Variation of coefficient of friction with time for a hydrofined fuel test.

The X-ray distributions of aluminum for a pin worn in the presence of kerosene and additive and in the presence of hydrofined fuel are shown in Figs. 4(a) and (b), respectively. Unworn bronze gives an aluminum distribution similar to that obtained with hydrofined fuel with an X-ray intensity of about 6400 counts per second in both cases. The distribution of aluminum when additive is present shows segregation to be occurring. The apparent intense region gives a count rate of 2747 counts per second with the depleted region down to 540 counts per second showing the whole surface is in fact becoming depleted. A similar X-ray distribution to Fig. 4(a) was obtained for pin which had been stopped wearing at the maximum coefficient of friction on one of the "spikes" in a hydrofined fuel test. In this case, the aluminum count rate was 9560 counts per second, for the intense region, and 5200 counts per second for the apparently depleted region. This shows aluminum enrich-

TABLE 1—X-RAY ANALYSIS OF WEAR DEBRIS

	"d" SPACINGS							
	FILE VALUES			AL. BRONZE	FUEL	FUEL + ADDITIVE		
						6 kg	10 kg	12.5 kg
Aluminum	2.34	2.02	1.22	2.92	2.48	4.05	3.19	4.94
Aluminum Oxide	2.55	2.09	1.6	2.52	2.24	3.37	3.04	3.11
Al. Ortho-Phosphate	4.08	2.51	3.16	2.33	2.04	3.14	2.49	2.63
Al. Phosphate (Berlinite)	3.37	4.28	1.84	2.22	2.02	3.04	2.29	2.48
Aluminum Phosphide	3.14	1.93	1.64	2.09	1.81	2.92	2.10	2.17
Copper	2.09	1.81	1.28	2.03	1.31	2.83	2.02	2.09
Copper Oxide (Cu_2O)	2.47	2.14	1.51	1.83	1.28	2.57	1.93	1.93
Copper (II) Phosphate	2.96	2.80	2.58	1.28	1.19	2.48	1.81	1.81
Copper Phosphide	2.01	1.95	2.49	1.22		2.33	1.52	1.65
Iron	2.03	1.71	1.43	1.17		2.13	1.45	1.31
Nickel	2.03	1.76	1.25			2.03	1.31	1.28
						1.75	1.28	1.25
						1.6	1.20	1.21
						1.51		
						1.35		
						1.28		
						1.19		

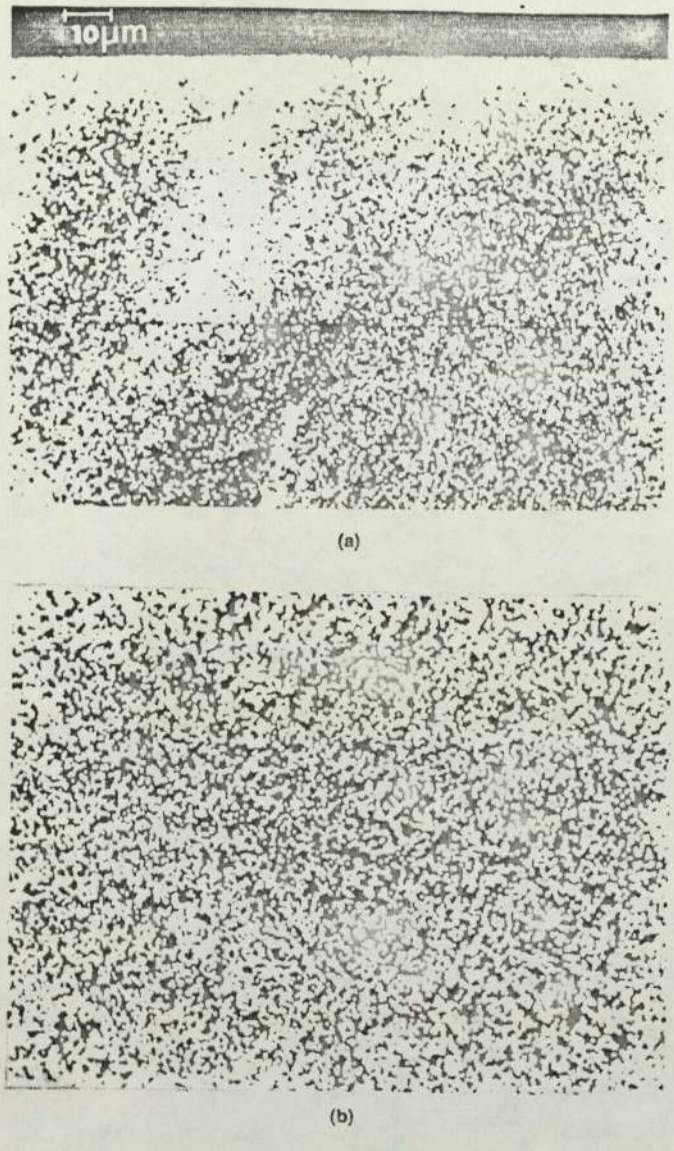

Fig. 4—Aluminum X-ray distribution (a) for a wear pin from tests with fuel plus additive, (b) from tests without additive.

ment at the surface when a pin is wearing in the high friction (on a friction "spike") state in the presence of hydrofined fuel.

Figures 5(a), (b) and (c) show the copper and aluminum X-ray distributions over a tapered section of a pin surface which had been worn in the presence of fuel and additive for a long period (approximately 2 hours). In this case, the test had terminated with low friction and wear. The wear surface is obviously depleted of aluminum, whereas the taper section (top left-hand corner on the photographs), shows a normal concentration.

The results of an Auger analysis had previously shown an oxide layer to be present on the surface of a pin worn in the presence of fuel and additive (5). The depth profile from that analysis is reproduced in Fig. 6 so that a direct comparison can be made with a similar profile obtained for a pin worn in hydrofined fuel (Fig. 7). This shows that in the latter case there is no oxide layer.

Micrographs of aluminum bronze wear pin surfaces are shown in Figs. 8(a) and (c). Figure 8(a) shows the buildup of

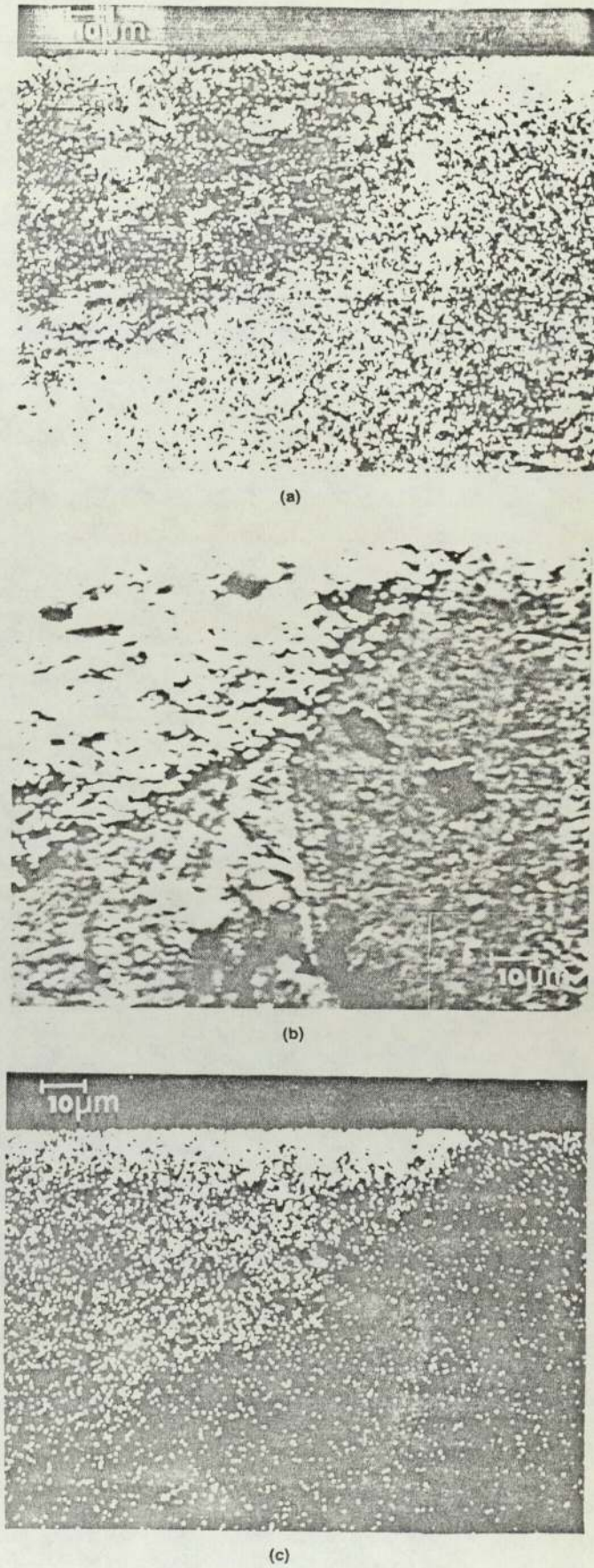

Fig. 5—(a) copper X-ray distribution, (b) reflected electron image of surface analyzed (tapered surface in top left hand corner and (c) aluminum X-ray distribution.

copper rich areas to be occurring (the dark areas on the micrograph) on a pin surface from tests with fuel. The largest copper rich area is over 460 microns long and reaches 80 microns in width. This area also appears to be quite rough compared to the surrounding bronze. In contrast, no such areas were observed on a pin worn in the presence of hydrofined fuel [Fig. 8(c)].

A two-stage carbon replica of a wear track formed on the disk when wearing in the presence of hydrofined fuel with additive suggests that microcorrosion pitting is occurring. The pits are between 1 and 2 microns in diameter and small spherical particles can be seen in them [Fig. 8(b)].

Finally, Fig. 9 shows an energy dispersive analysis of X-rays obtained from a steel surface having transferred material on it. This shows that aluminum is the main element transferred when wear occurs in the presence of a hydrofined fuel.

DISCUSSION

The results for the fuel with additive suggest that a corrosion mechanism is responsible for the wear of the bronze [Fig. 8(b)]. Sury and Oswald (*6*) have shown that the aluminum content of this type of bronze is preferentially

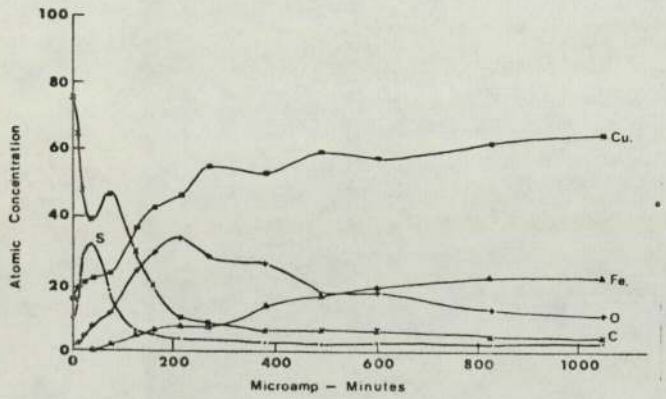

Fig. 6—Auger depth profile for a pin worn in the presence of fuel and additive.

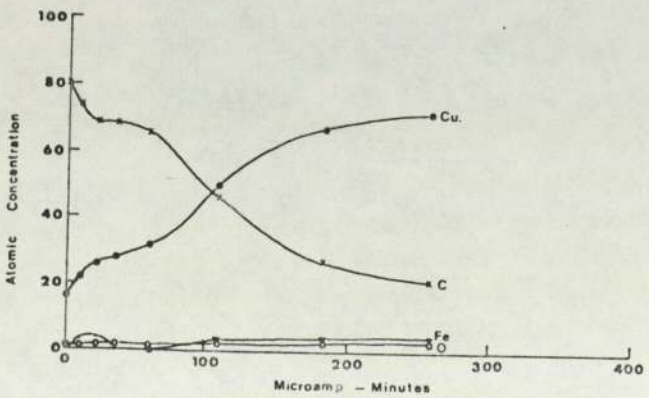

Fig. 7—Auger depth profile for a pin worn in the presence of hydrofined kerosene.

(a)

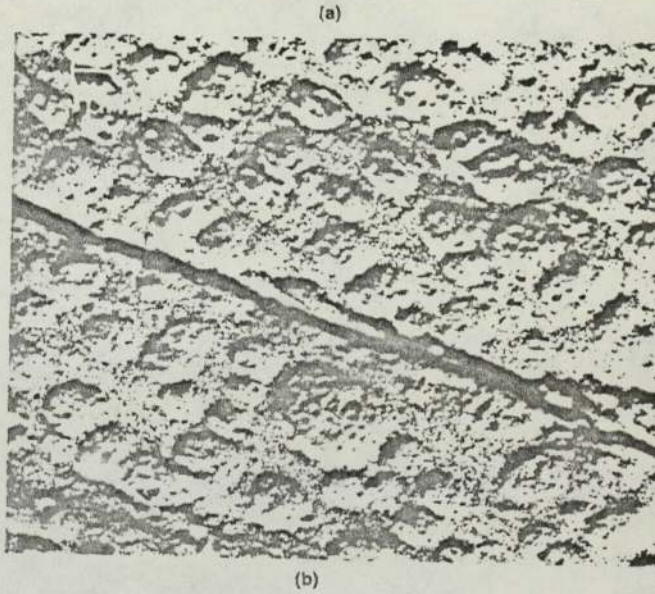

(b)

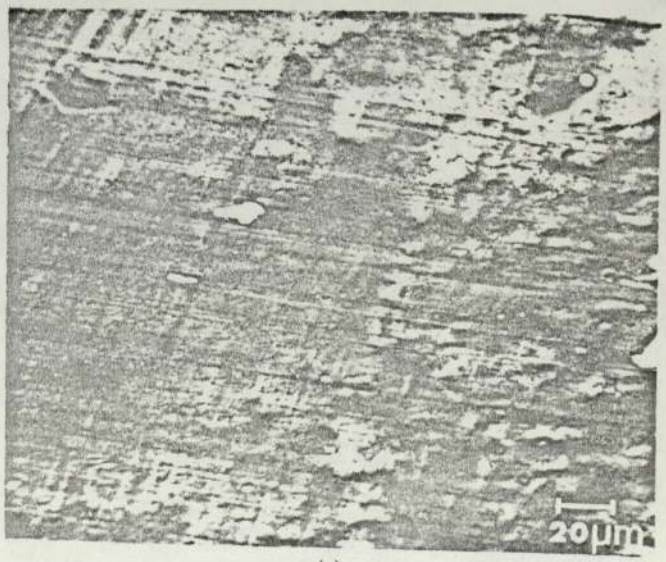

(c)

Fig. 8—(a) Wear pin surface from a fuel with additive test (b) carbon replica of wear track surface from a fuel with additive test, (c) bronze wear pin surface from a hydrofined fuel test.

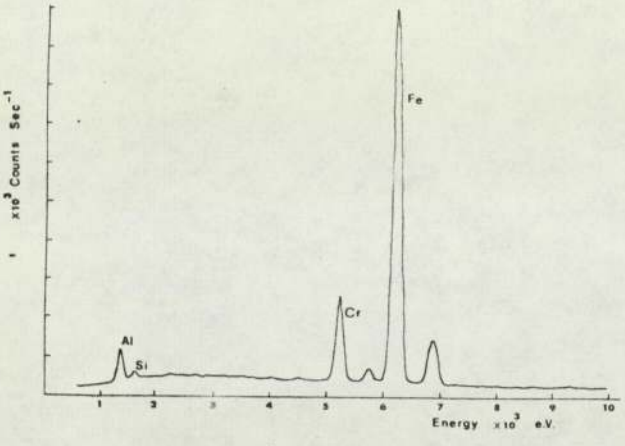

Fig. 9—Energy dispersive spectrum of elements present on a steel surface after wear in the presence of hydrofined fuel.

removed in the presence of sodium chloride solutions. They also found that Cu_2O forms the primary oxide and that a separate oxide of aluminum could not be detected, even though the latter is often supposed to be responsible for the improved corrosion resistance of copper-aluminum alloys with respect to pure copper.

Further evidence of selective corrosion of aluminum has been found by Schussler and Napolitan (7). In this case, an aluminum-silicon bronze was exposed to an aqueous solution of hydrofluoric acid.

The present work suggests that similar mechanism is involved, particularly since Cu_2O was found in the wear debris. This implies that the copper rich surfaces (Fig. 5) are copper oxide. The wear debris analysis has shown that phosphorus is involved in the wear mechanism. Phosphorus has also been detected on wear surfaces in previous experiments by the authors (5). The origin of the phosphorus must be the additive which contains an ester of orthophosphoric acid. The fact that phosphates were detected at low loads (6 kg) and phosphides at higher loads (10 and 12.5 kg) suggest that chemical breakdown of the ester is occurring at the higher loads. It seems reasonable to assume that this breakdown occurs by reaction with free aluminum at the surface. Chemically, this reaction seems favorable since the difference in electronegativity (8) between aluminum and phosphorus is large at a value of 0.6. This is supported by the fact that aluminum phosphide was found to be present in the wear debris.

Once aluminum is removed from the surface, the copper-rich layer is free to be oxidized and the dimer component of the additive can adsorb to the surface giving added protection and resulting in low friction and wear. This is supported by the observation of a carbon layer on the oxide surface on the Auger depth profile (Fig. 6).

Absence of the additive permits high friction and wear to occur. This can be attributed directly to the presence of aluminum. In particular, aluminum enrichment was found on a pin which had reached the high friction state on a friction spike. Further, aluminum has been found to be transferred to the steel when lubricated by hydrotreated kerosene (Fig. 9). No oxidation of the surface was observed for the wear pins in these tests (Fig. 7) and the debris was aluminum bronze. The correlation between increased adhesion and excess aluminum at the surface found in these experiments is consistent with the work of Ferrante and Buckley (9). In this case, free aluminum comes to the surface by diffusion, at the hot spots, and goes into solution with the steel resulting in welding of the asperities. This hypothesis is supported by the work of Dzhavaga and Lebedev (10). They investigated the welding properties of aluminum bronze to carbon steel and found that, on the steel side of the weld, the concentration of aluminum was as high as 14–17 percent.

In severe cases, sufficient welding occurs between the wear surfaces resulting in a seizure, whereas, in other cases, welding of asperities occurs between the pin and disk resulting in fatigue cracking and consequent production of bronze debris.

The difference in wear rates between the two fuels can now be explained in terms of the wear mechanisms described above. The role of the additive is to prevent the transfer of aluminum to the steel by removing it from the bronze surface through preferential corrosion. Thus this gives an apparent initial pro-wear effect under laboratory conditions, but it must be noted that effective protection of the surfaces is provided by the additive once a sufficiently thick oxide layer is built up on the surface.

CONCLUSIONS

The use of several physical methods of analysis has enabled sufficient information to be obtained on the metallurgical changes occurring, when aluminum bronze wears against steel in the presence of aviation fuel, to propose wear mechanisms for fuel with and without additive. In the case of hydrofined fuel being used as the lubricant, cold welding occurs with the diffusion of aluminum being an important factor. The presence of a corrosion inhibitor changes the wear to a corrosive mechanism in which aluminum transfer is prevented by the action of the additive. The corrosion gives an apparent increase in wear compared to the fatigue cracking in the presence of hydrofined fuel. At high loads (15 kg on a 3-mm diameter wear pin) an extreme-pressure effect reduces wear when the additive is present.

ACKNOWLEDGMENTS

The authors would like to thank Prof. Smallman (Birmingham University, England) for the use of the Auger spectrometer and J. F. Smith for his help advice in using the instrument. Thanks are extended to K. Palmer of Lucas Aerospace for his advice and for providing materials.

Finally, W. Poole should like to acknowledge SRC, The University of Aston in Birmingham and Lucas Aerospace for financial assistance.

REFERENCES

(1) Johnson, R. K. and Shamblin, J. E., "Jet Fuel Thermal Stability by Electron Microscopy," *J. Inst. Petroleum*, **47**, 451, pp 241–250.

(2) Unzelman, G. H. and Wolf, C. J., "Processes," Section 3, *Petroleum Processing Handbook*, McGraw-Hill Book Company, New York (1967), Eds. Bland W. F. and Davidson, R. L., pp 3–38 to 3–39.

(3) Appeldoorn, J. K. and Dukek, W. G., "Lubricity of Jet Fuels," *SAE Trans.*, **75**, pp 426–440 (1967).

(4) Aird, R. T. and Forgham, S. L., "The Lubricating Quality of Aviation Fuels," *Wear*, **18**, pp 361–380 (1971).

(5) Poole, W. and Sullivan, J. L., "The Wear of Aluminum-bronze on Steel in the Presence of Aviation Fuel," presented at the ASLE/ASME Lubrication Conference in Kansas City, Missouri, October 3–5, 1977, ASLE Preprint number 77-LC-5C-1.

(6) Sury, P. and Oswald, H. R., "On the Corrosion Behaviour of Individual Phases Present in Aluminum Bronzes," *Corrosion Sic.*, **12**, pp 77–90 (1972).

(7) Schussler, M. and Napolitan, D. S., "Dealuminization of Aluminum Bronze," *Corrosion*, **12**, pp 25–30 (1955).

(8) Eggins, B. R., *Chemical Structure and Reactivity*, Macmillan Press, London, pp 27–31, (1972).

(9) Ferrante, J. and Buckley, D. H., "A Review of Surface Segregation, Adhesion and Friction Studies Performed on Copper-Aluminum, Copper-Tin and Iron-Aluminum Alloys," *ASLE Trans.*, **15**, 1, pp 18–24 (1971).

(10) Dzhevaga, I. I., and Lebedev, Yu. M., "Research into the Fusion Zones of Welded Joints Between Carbon Steel and Aluminum Bronze," *Avt. Svarka*, **8**, pp 11–14, (1970).

77-LC-5C-1
ASLE PREPRINT

The Wear of Aluminum-Bronze on Steel in the Presence of Aviation Fuel

W. POOLE and J. L. SULLIVAN
University of Aston
Gosta Green, Birmingham, England

A study has been made of the action of a commercially available corrosion inhibitor added to hydrofined aviation fuels in reducing the wear of aluminum bronze sliding on KE180, 13 percent chromium steel.

From measurements of friction and wear and an extensive examination of surfaces using Auger electron spectroscopy, a surface model has been proposed which elucidates the mechanism of wear protection.

INTRODUCTION

The absence of saturated hetrocyclic compounds and other polar impurities in modern hydrotreated aviation fuels reduces their effect as a lubricant and can lead to high wear and eventual seizure in aircraft fuel systems (*1*). The problem first appeared when Lucas Aerospace piston pumps (KE961 steel running in cadmium plated aluminium bronze bores) exhibited a much reduced life when operating on certain fuels. It was found that the addition of about 12 ppm of a commercially available corrosion inhibitor cured the problem. It has now been completely eliminated in the case of the Lucas pump by the use of carbon lined bores, but still remains in many fuel systems (*2*). For this reason, corrosion inhibitors of the original type are still added to fuels. The additive used in the experiments to be described consists of 45 percent of a dimeric acid of the type:

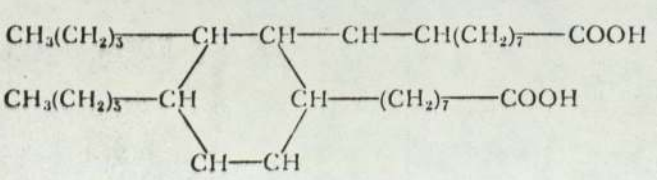

plus 5 percent of a phosphate ester in kerosene or fuel oil.

Although the effects of the additive have been known since the 1960's, the mechanisms responsible for the reduction in wear rates are not understood. The purpose of the study was, therefore, to take the particular metallurgical combination (aluminum bronze on 13 percent chromium KE180 steel) and to produce a model to explain the mechanism of protection. The pump manufacturers suggest that the cadmium coat is removed by the wear-in process.

Measurements of wear and friction were made with variation in load and speed and these results were correlated with those from an extensive physical analysis of the contacting surfaces using Auger electron spectroscopy (AES), ellipsometry and X-ray analysis.

The experiments were carried out using commercially available fuels containing the additive, and for pure 2,2,4 trimethylpentane (isooctane) containing no polar impurities. The study would have benefited from measurements for a pure hydrofined fuel, but since the additive package is introduced during, or soon after manufacture, no such fuel was available at the time of the experiments.

EXPERIMENTAL DETAILS

Wear Tests

The main aims of the wear tests were:

(1) to measure the wear characteristics of the metals in combination with different fuels

(2) to generate samples for analysis by AES

The wear test rig was a conventional pin-on-disk machine shown in Fig. 1. The movable loading arm allowed a number of tests to be carried out at various radii on the face of the KE180 (KE961 equivalent) steel disk. The disk was hardened and tempered to a minimum of 700 HV. A surface finish in the range of 0.1 to 0.6 microns was produced by lapping the 100 mm disk with diamond paste and kerosene.

The flat faced aluminum bronze pin was 3 mm diameter. This size was selected to give reasonable loads for the wear tests and sufficient area for analysis using AES.

Presented as an American Society of Lubrication Engineers paper at the ASLE/ASME Lubrication Conference in Kansas City, Missouri, October 3-5, 1977

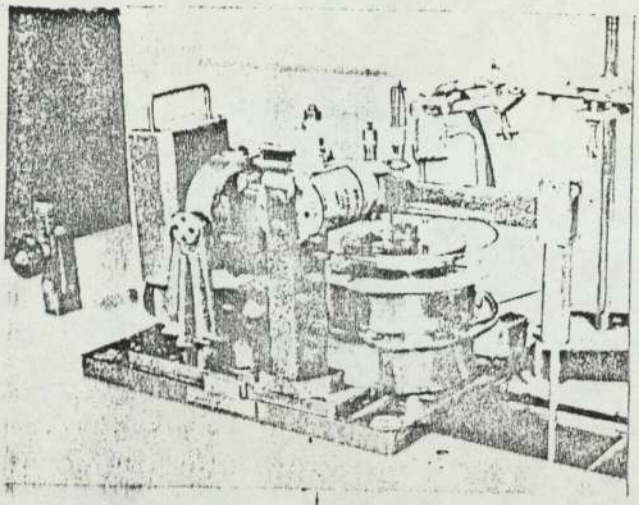

Fig. 1—Pin-on-disk wear machine

It was important to avoid contamination of the test fuel because small amounts of polar impurities, including water, could significantly improve its lubricating properties. Consequently, the pin, disk, all retaining nuts and washers and tubing supplying fuel were cleaned with an additive-free petrol (Shell SBP2) in a vapor bath. Cleaning was carried out at 80°C for approximately 30 minutes. Surface composition of a pin was investigated using AES to determine if the cleaning had been effective. Fuel was pumped onto the disk through a constant head tank at a rate of 30 ml.min^{-1} and was recirculated. During recirculation it was filtered to remove wear debris.

Frictional force was measured using a strain gauge load cell and wear rate using an inductance transducer and by measurement of weight loss.

To select the conditions of load and speed for the wear tests, a curve of friction coefficient vs speed × viscosity/pressure was obtained by measuring the frictional force for a given load and fuel at various speeds. Loads and speeds which gave friction coefficients greater than 0.07 were selected for the wear tests since this value indicated the onset of boundary lubrication.

When load and speed had been selected, tests were carried out at room temperature (approximately 22°C) to determine wear rate as a function of linear velocity and load for the two fluids. To reduce error in measurements caused by misalignment of the disk, the results were only accepted if the wear track was uniform. The main wear process investigated was adhesive wear.

The test fluids used were aviation kerosene with the addition of a corrosion inhibitor and 2,2,4 trimethylpentane (isooctane). The wear-in sliding distance was found to be of the order of 10^3m. This was determined from the point at which the friction fell to a steady value of about 0.07 and the wear rate became a constant. Typically, for a load of 12.5 kg and speed 0.6 ms^{-1}, the run-in wear rate was 3.35×10^{-7} mm^3 mm^{-1}, compared with a steady condition of 1.4×10^{-7} mm^3 mm^{-1}, for aviation fuel on a 0.2 μm cla disk.

Auger Electron Spectroscopy

In order to identify surface elements present during wear, the pins were analyzed using Auger electron spectroscopy. The instrument has been described elsewhere (*3*). Differentiation of the secondary electron spectrum enables the Auger peaks to be resolved (*4*). Thus, low atomic number elements such as carbon, oxygen, sulfur and phosphorus can be detected.

This technique was used because of its ability to detect the elements of interest in this wear process and because Auger electron spectroscopy is a low energy technique and consequently very surface sensitive.

Pin samples were selected from the wear tests carried out using each fluid. Some samples were also prepared by immersing unworn pins in the additive at room temperature (20°C) and 150°C. It was hoped that these samples would give an indication of the elements to be expected on the pin surface due to the additive. Samples of steel worn in the presence of the fuel with additive were also analyzed. Samples were cleaned in the same vapor bath used for the machine parts for 5 minutes at a temperature not greater than 50°C to avoid desorption.

Having mounted the samples, the system ws evacuated to a pressure of 10^{-8} torr and the initial Auger spectra recorded. The primary beam energy was 2 KeV with a beam spot of about 1 mm at the sample. These conditions gave a beam current of approximately 10 μA. The energy was scanned over a range of 30 to 1400 eV.

The sample surfaces were depth profiled by bombarding with 400 eV xenon ions at normal incidence at a pressure of 10^{-4} torr. The area sputtered was small compared to the ion beam so removal should have been uniform over the entire area of the pin. After each sputtering, the Auger spectra was recorded.

Identification of the elements was made using the Handbook of Auger Electron Spectroscopy (*5*). For calibration purposes, it was assumed that the electron transition energies for the copper peaks occurred in the same place as for the pure element as given by the handbook. This was checked by recording the elastic peak at various energies.

It has been shown that the peak-to-peak heights of the differential Auger signals is a good approximation to the Auger current (*6*). After normalization, the peak-to-peak heights were used to calculate the relative atomic concentration of the elements present on the surface.

Film Thickness Measurements

The measurement of thin boundary films of the order of 100 Å has been attempted using various methods (*7*). These techniques involve either displacement or capacitance measurements where the major problem is calibration. An alternative method of measuring these film thicknesses is by the optical technique of ellipsometry. On reflection at an optically transparent or absorbing medium, such as a surface film, amplitude and phase changes are produced in a beam of light. The ellipsometer (*8*) measures these changes. The changes in amplitude and phase are related to film thickness by the equation:

$$\frac{R_p}{R_s} = \tan \psi \, e^{-i\Delta}$$

where R_p and R_s are the Fresnel reflection coefficients

parallel and perpendicular to the plane of incidence, ψ is the ratio of the amplitude coefficients and Δ is the difference in the phase changes on reflection.

In order to establish if the technique could detect small amounts of the additive, mixtures of 100, 10, 1, 0.1, 0.01 percent concentration by volume were made and films of these formed on silver-plated glass slides. Silver was used because it could be easily evaporated onto an optically flat surface and its optical constants are well known. It would be difficult to produce a suitable surface of KE961 and the thickness of the adsorbed film should not be greatly effected by the substrate. A film was formed by immersing a slide into one of the mixtures and withdrawing it at right angles to the solution surface. It was then gently heated to drive off the nonpolar components. Changes in Δ and ψ between a clean silver glass plate and the same plate with an additive film were measured and the film thickness was calculated. Samples which had been immersed in the 100 and 0.1 percent solutions were heated to a temperature of 85°C in isopropyl alcohol and the film thickness measured in order to investigate temperature effects.

RESULTS AND DISCUSSION

Figure 2 shows the Stribeck curves for the fuel with additive at the two surface roughnesses and for isooctane. Curve (a) obtained for the 0.2 μm cla surface shows the three distinct regions of boundary, mixed and full fluid film lubrication (9) but in curve (b) obtained with the 0.6 μm cla surface the transitions are not so pronounced. In the latter case, the surface roughness would be expected to be of the order of the film thickness and so a mixed regime would persist. In the case of isooctane, curve (c) was obtained for a surface roughness of 0.2 μm cla and shows that no fluid film action is present. The viscosity is so low that the film thickness is not sufficient to keep the metal surfaces completely separated and high friction and wear result. These curves gave an indication of the loads and speeds required to operate the wear rig under boundary conditions.

Reasonable agreement was found between the two methods of measuring wear rate. The wear rate measured by weight loss was higher than that by transducer measurement because no account of wear-in could be made for the latter. Repeatability was better than 10 percent for both methods.

Figure 3 shows wear rate as a function of velocity for various loads. The experiments using fuel with additive show a reduction in wear rate with increasing speed due to an in-

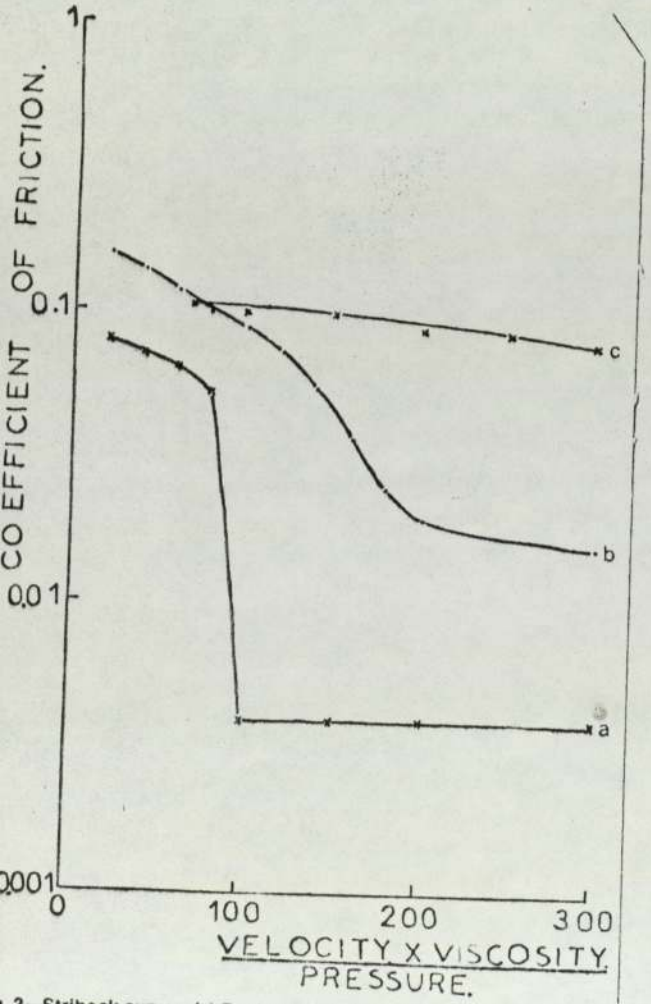

Fig. 2—Stribeck curves; (a) Fuel with additive with a disk surface roughness of 0.2 μm cla; (b) Fuel with additive with a disk surface roughness of 0.6 μm cla; (c) Trimethylpentane with a disk surface roughness of 0.2 μm cla.

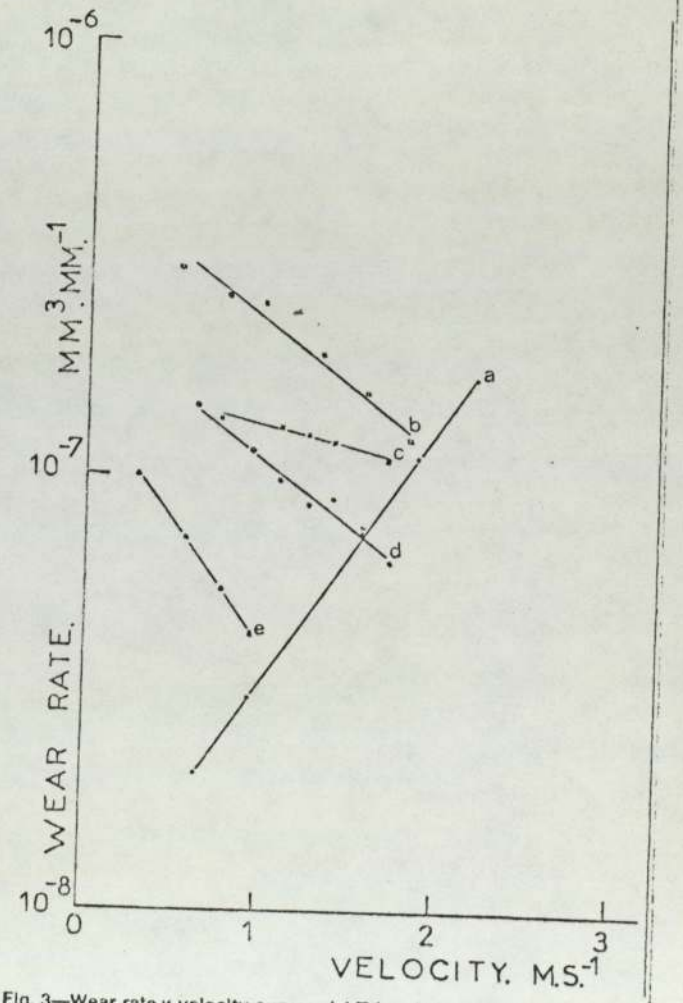

Fig. 3—Wear rate v velocity curves; (a) Trimethylpentane for a 2 kg load and a disk surface roughness of 0.2 μm cla; (b) Fuel with additive with a disk surface roughness of 0.6 μm cla and 5 kg load; (c), (d), (e) Fuel with additive with a disk surface roughness of 0.2 μm cla and 12.5 kg, 10 kg and 5 Kf loads, respectively.

crease in fluid film thickness. The temperature rise associated with increased speed may also increase the activity of the additive. The onset of full fluid film lubrication results in a sudden drop in the wear rate which then became too low to measure. The isooctane shows an increased wear rate with increased sliding velocity. Due to the low viscosity of isooctane (4×10^{-4} NSM^{-2} compared with 10^{-3} NSM^{-2} for the fuel) metal-to-metal contact occurs producing higher temperatures thus further reducing the viscosity and increasing the contact. Curves (3a, c, d) and (e) were for 0.2 μm cla and (3b) for 0.6 μm cla. Figure 4 is a typical wear rate versus load curve at a velocity of 0.6 ms^{-1} for 0.2 μm (4b) and 0.6 μm (4a) surface roughnesses. Both curves show an initial increase in wear rate with load up to about 8 kg for the high surface roughness and 12.5 kg for the low surface roughness. Frictional heating produced at the surface, estimated from the frictional force and speed, was found to be the same at each transition point. Thus, it appears that the reduction in wear rate was a heating effect either due to oxidation of the surface or to increased surface activity of the additive. The system was boundary lubricated over the entire load and speed range.

Figure 5 shows Auger spectra for worn aluminum bronze pin surfaces. Samples were worn on a 0.2 μm cla disk at a speed of 0.6 ms^{-1} and loads of 2 kg and 12.5 kg, respectively. The spectra (5a,b) are similar in that the same elements were present on the surfaces. In the sample run on the 0.6 μm cla disk with 10 kg load at a speed of 0.6 ms^{-1}, the spectra reveals the presence of phosphorus and chlorine on the surface (5c). Since the surface temperatures (estimated from friction measurements) must be similar to those of the isooctane samples, but higher than those for the 0.2 μm cla samples, the phosphorus must be preferentially adsorbed at these higher temperatures. The coefficients of friction were 0.125 for isooctane and the high surface roughness sample and 0.075 for the sample obtained using the 0.2 μm cla disk. It appears that phosphorus might be important as an extreme pressure additive at high surface temperatures. An X-ray analysis of the wear debris for the fuel indicated that some phosphorous compounds were present while the isooctane gave only aluminum bronze wear debris.

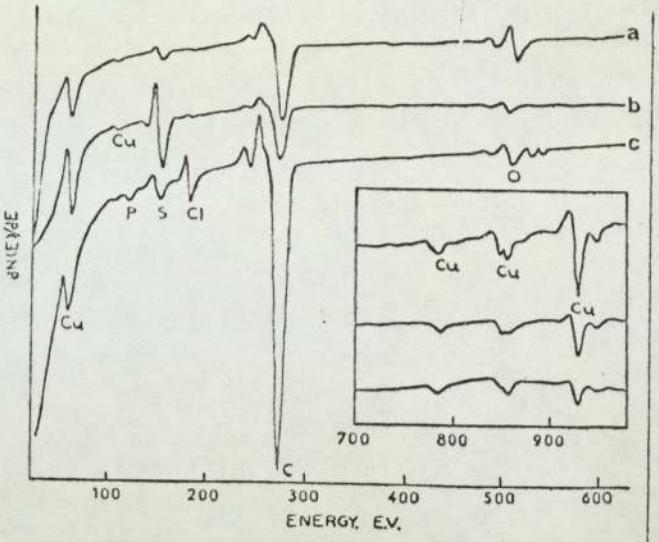

Fig. 5—Auger spectra of pin surface run in (a) Trimethylpentane; (b) Fuel with additive and 0.2 μm cla surface roughness; (c) Same and 0.6 μm cla surface roughness.

The spectra for the two unworn pins immersed in the additive at 20°C and 150°C are shown in Fig. 6. In general, it is not desirable to compare spectra quantitatively since the magnitude of the peaks may vary. Consequently, these spectra only indicate the presence of elements (in particular sulfur, phosphorus, chlorine, and carbon) which may originate from the additive. The phosphorus must come from the additive.

To obtain a semi-quantitative comparison between samples, the calculated relative atomic concentrations were plotted versus sputter rate in microamp minutes (μA, minutes) for isooctane samples, the samples run in fuel on the low surface-roughness disk and for a steel sample are

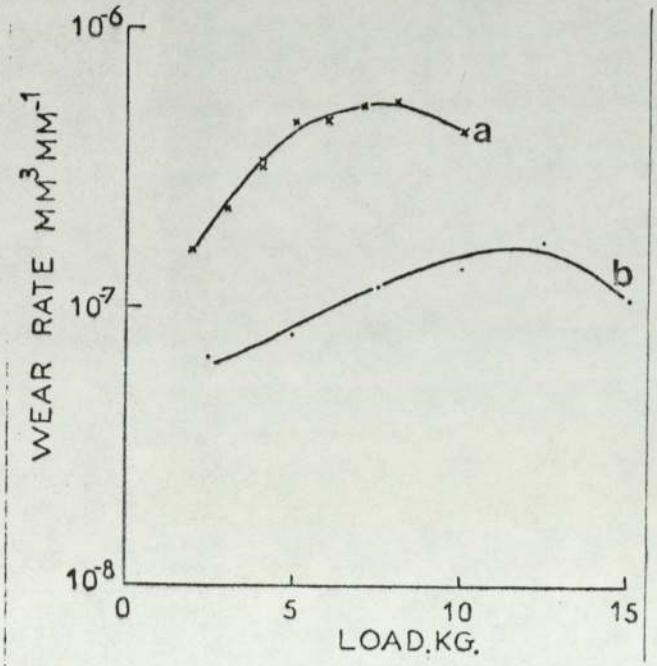

Fig. 4—Wear rate vs load for 0.6 ms^{-1} velocity and fuel with additive (a) 0.6 μm cla roughness; (b) 0.2 μm cla roughness.

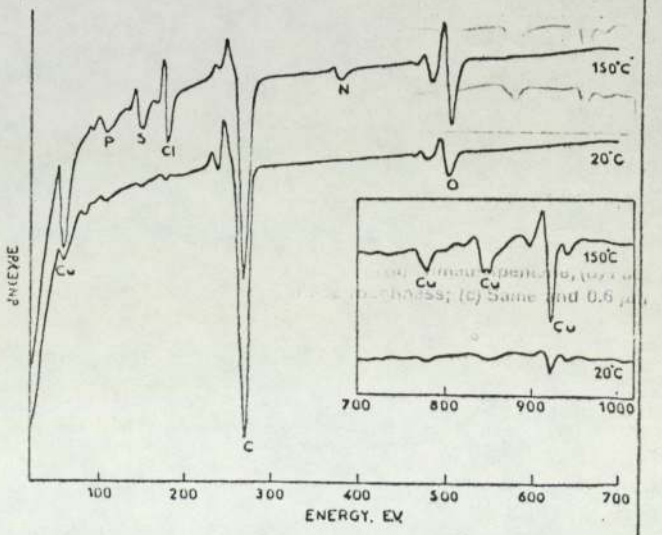

Fig. 6—Auger spectra for unworn pins dipped in additive

shown in Figs. 7, 8 and 9. As a guide to the relationship of the product of sputter current and time to layer thickness, a pure copper layer is removed at a rate of 0.7 Å per microamp minute. It is difficult to calculate the depth removed for complex compounds. This is a point which many authors fail to appreciate when presenting data calculated from elemental sputtering rates. The ellipsometer measurements show an adsorbed layer thickness for the dimeric acid of 130 Å. This would correspond to a value of 75-μA.minutes in Fig. 8. The sample worn in isooctane shows a relatively clean surface, the fall-off in carbon concentration is typical of the contaminant curves expected for pure mineral oil (*10*), (*11*) with low quantities of sulfur and oxygen (oxides) present on the surface. The pin worn in the fuel with additive shows quite a different profile, significant levels of sulfur are present due to the additive carrier, and a carbon peak occurs in all similar samples examined at about 75 μA. minutes. At 200 μA. minutes, oxygen reaches a peak indicating the presence of an oxide film beneath the boundary layer. No phosphorus profile could be obtained. The curves for the steel surface indicate a similar surface layer with the carbon peak present. Ellipsometer measurements showed the thickness of the boundary layer to be 130 Å and that the films desorbed at about 80°C.

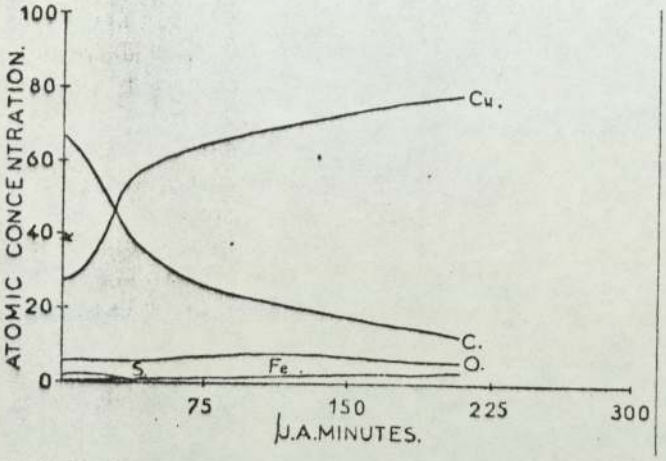

Fig. 7—Depth profile of elements present on a pin worn in the presence of trimethylpentane.

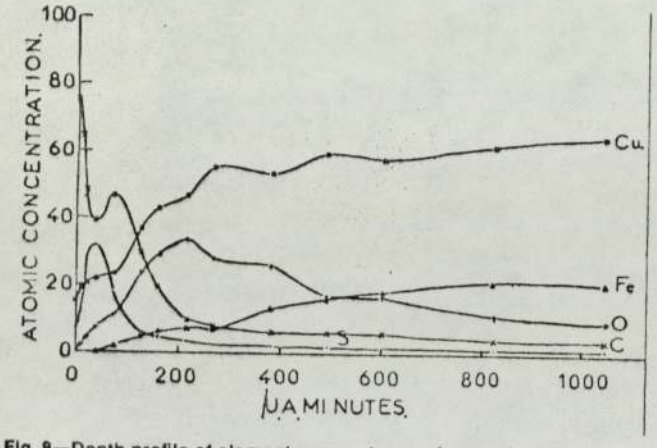

Fig. 8—Depth profile of elements present on a pin worn in the presence of fuel with additive.

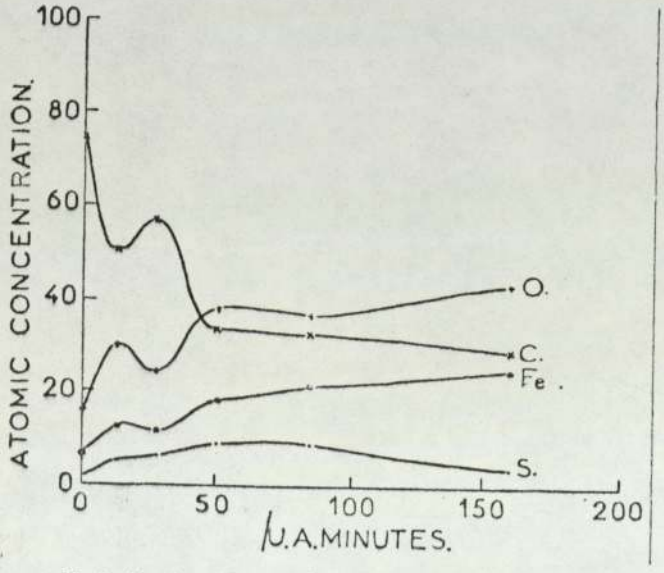

Fig. 9—Depth profile of element present on KE961 steel

It would appear, therefore, that the surface consists of a very thin layer (no more than a few Angstroms thick) of surface contamination shown by the initially high concentration of carbon. The carbon peaks indicate a boundary layer, with sulfur or sulfur compounds present either in or adhering to its surface. The layer is formed on a metal oxide substrate in a manner similar to that proposed by Allen and Drauglis (*12*). This boundary layer of long chain carbon molecules (dimeric acid) was about 130 Å. This thickness, measured using the ellipsometer, for the film formed on silver, corresponds to the calculated value of one molecular chain length of the acid and, therefore, should not be different from that formed on aluminum bronze. The effect of pressure on the film at the contacting surfaces will be negligible (*13*). No aluminum could be detected. This indicates a copper-rich oxide. The high levels of iron present are probably a result of transfer from the disk surface. Thus, the surface model is as shown in Fig. 10. The steel surface has a similar structure with the boundary layer on an iron oxide substrate.

The evidence further suggests that at the highest temperatures (above 80°C) when the dimeric acid desorbs from the surface, the phosphate ester present in the additive acts as an extreme-pressure lubricant protecting the surfaces when metal to metal contact occurs.

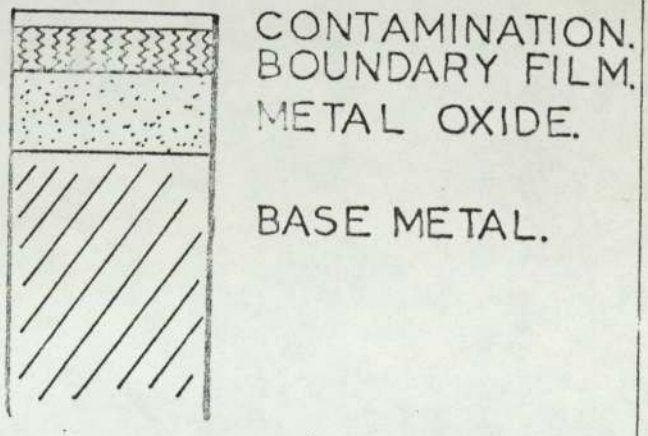

Fig. 10—Conjected surface

CONCLUSION

For isooctane containing no polar impurities, the surfaces examined by Auger spectroscopy were found to be relatively clean. No boundary layer was found to exist and very little oxide.

With the aviation fuel with corrosion inhibitor, a boundary layer of long chain hydrocarbon molecules exists on the surface. As the conditions were made more severe by an increase in surface roughness, phosphorus or phosphorus compounds appeared on the surface indicating the breakdown of the ester giving some extreme-pressure action. The ellipsometer measurements showed that the dimeric acid desorbs at 80°C where the extreme-pressure component of the additive might become important.

The action of the corrosion inhibitor in reducing wear was found to be primarily due to the adsorption of the dimeric acid on the metal surface forming a boundary layer. The oxide film thickness in the presence of the additive was found to be thicker than it was without it. This could be important in reducing metallic contact and hence wear.

ACKNOWLEDGMENTS

The authors would like to thank H. Southworth (Birmingham University, England) for the use of the Auger spectrometer and D. D. Hall for his help and advice in using the instrument. Also thanks are extended to K. Palmer of Lucas Aerospace for providing materials and advice.

Finally, Mr. W. Poole would like to acknowledge SRC and Lucas Aerospace Limited for financial assistance.

REFERENCES

(1) Vere, R. A. Aircraft Fuels Lubricity and Safety Conference (The Hague) AGARD May (1971).
(2) "Lubricity of Aviation Fuels," Editors Vere, Askwith and Hardy, P.E., Ministry of Defence (G. B.). Second Report on the Working party p x 1395/014 January 1976.
(3) Ignatiev, A. and Rhodin, T.N., "Secondary Electron Spectroscopy—a surface sensitive tool," *International Laboratory*, February 18-25 (1973).
(4) Southworth, H. "The Auger Electron Comes into Its Own," *New Scientist*, November (1973).
(5) Palmberg, P. W., et al, "Handbook of Auger Electron Spectroscopy" published by Physical Electronics Industries, Inc. (1972).
(6) Chang, C.C., "Analytical Auger Spectroscopy," Ch. 20, Characterization of Solid Surfaces. Published by Plenum Press, New York (1974).
(7) Needs, S. J., "Boundary Film Investigations," *Trans ASME* 62, 331 (1940).
(8) Kruger, J. and Hayfield, P. C. S., "Ellipsometry in Corrosion Testing," Handbook on Corrosion Testing and Evaluation. Pub. by Wiley and Son (1971).
(9) "Lubrication Theory and its Applications," p. 57 P. O. Trading Ltd., published by Harrison and Sons Ltd (1969).
(10) Jones, H. M., "Element Concentration Analysis of Films Generated on Phosphor Bronze on Steel under Boundary Lubrication," *Proc. ASLE/ASME Lubrication Conference*, October (1976).
(11) Phillips, M. R. et al, "The Application of Auger Electron Spectroscopy to Tribology," *Vacuum*, 26, 451, January (1977).
(12) Allen, C. M. and Drauglis, E., "Boundary Layer Lubrication," Wear, 14, 363 (1969).
(13) Fuks, G. I., "The Polymolecular Compound of the Lubricating Boundary Layer," *Research in Surface Forces*, 2, 159 (1964).

Presented at the ASLE/ASME Lubrication Conference, Kansas City, Missouri, October 3-5, 1977: